ION DYNAMICS IN COLLISIONLESS SHOCK WAVES

David Sherwell

A Thesis Submitted for the Degree of PhD
at the
University of St Andrews

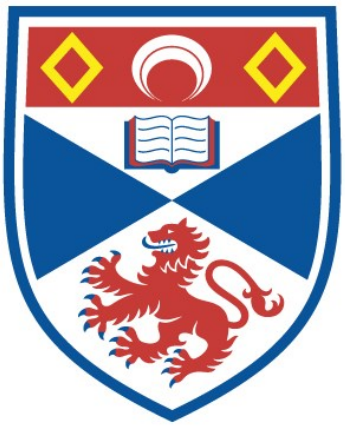

1976

ION DYNAMICS IN COLLISIONLESS SHOCK WAVES

DAVID SHERWELL

Thesis submitted for the Degree of Doctor of Philosophy of the University of St. Andrews.

April 1976

ProQuest LLC.
789 East Eisenhower Parkway
P.O. Box 1346
Ann Arbor, MI 48106 – 1346

Th

8812

TO MY

PARENTS

DECLARATION

I declare that the following thesis is a record of research work carried out by me, that the thesis is my own composition, and that it has not been previously presented in application for a higher degree.

D. Sherwell

POSTGRADUATE CAREER

I was admitted into the University of St. Andrews as a research student under Ordinance General No. 12 in October 1972, to work on ion dynamics in collisionless plasma shock waves under the supervision of Dr. R. A. Cairns. I was admitted under the above resolution as a candidate for the degree of Ph.D. in April 1973.

CERTIFICATE

I certify that David Sherwell has satisfied the conditions of the Ordinance and Regulations and is thus qualified to submit the accompanying application for the degree of Doctor of Philosophy.

ABSTRACT

In a laminar model of a collisionless magnetosonic shock wave, ion equations of motion are integrated through shock-like profiles. Conservation relations and Maxwell's equations allow a self-consistent determination of unknown downstream ion distribution functions f_i, ion temperature T_i, and electric potential jump ϕ.

Favourable comparison of model T_i, ϕ, with experiment establishes (at low $\beta \lesssim 0.3$, $\beta = 8\pi N_1 k(T_{e2}+T_{i1})/B_1^2$) the importance of laminar ion dynamics. Heating is due to distortion of Maxwellian distributions when entropy is conserved; in particular shock dynamics is dominated by a fast "tail" of reflected ions.

The solutions for f_i are considered. The "stability" of the model to its assumptions (linear profiles, shock thickness (L_s)) is shown. When reflections occur a self-consistent length emerges.

The solutions T_i, ϕ are extensively studied at various Mach numbers for different values of β. Laminar ion heating is very efficient and at high β can exceed proper conservation levels due to ion reflections; at high β ($\geq \beta^*$) the electric potential is unable to slow the ions to conservation levels. The model predicts significant reflected ion currents in the plane of the shock.

The boundary β^* is determined. Then laminar ion dynamics on the scale of the electron heating length ($\sim 10\ c/\omega_{pe}$) cannot occur for $\beta > \beta^*$. Dependence on L_s and T_{el}/T_{il} is considered.

The nature of non-laminar $\beta > \beta^*$ shocks is considered. Collisions are found to be important in laboratory shocks, and are efficient in slowing the reflected ions. In the absence of collisions, ion instabilities must be considered. It is shown that turbulent slowing of the fast ions cannot take place in L_s alone. Further it is shown possible to construct a shock so that non-laminar mechanisms cannot occur significantly. Then the laminar model is re-instated. A decoupling of ion and electron heating lengths is proposed. Reflection heating in the Earth's Bow Shock ($\beta > \beta^*$) is modelled, and is comparable with experiment.

ACKNOWLEDGEMENT

I wish to express my most sincere thanks to my supervisor, Dr. R. A. Cairns, for his encouragement and considerable patience.

I would like to thank Prof. S. N. Curle for obtaining for me the University Research Scholarship which made this thesis possible, and the Computing Laboratory in the person of Dr. R. Erskine for making a large amount of computer time available. The typing of the thesis has been cheerfully and accurately performed by Miss. Seonaid McCallum, to whom go my thanks.

I acknowledge receipt of a University Research Scholarship from October, 1972 to 1975.

CONTENTS

1 INTRODUCTION

This thesis will be concerned with the behaviour of the ion component of a plane, perpendicular, collisionless shock wave. Such shocks are important in the understanding of many physical events. They arise first as a curiosity in about 1964 with satellite observations of a shock beyond the Earth's magnetosphere which showed a thickness very much less than the mean free path for collisions in the solar wind. As Sageev reports (in 1964)[22], there was some difference of opinion as to the reasons for this phenomenon. He found three groups believing, first, that the shock was a laminar event maintained by ordered non-linear oscillations in the observed field profiles; second, that they were non-laminar, or turbulent; while a third opinion was that they did not exist at all, for while collisions might be infrequent in the shock, they might yet explain downstream conditions and shock thickness.

In 1965 the first laboratory shocks were produced. The work of Paul et al.[1] is typical. They found reproducible, well-defined, steady-state (in a macroscopic sense) shocks, where again shock thickness, L_s, was less than the mean free path for collisions. But now they were further able to show by computer calculations[15] that collisions could not explain electron heating. Thus it was suggested in the 1965 paper that ion acoustic turbulence in L_s would be the cause of an "anomalous" resistive heating of electrons - resistivity had to be two orders of magnitude greater than the collisional level!

Collisionless shock waves existed then in that heating had to be explained by the interaction of one charge with all others, via the self-consistent fields, and not by binary collisions. Thus Sagdeev's third group was proved wrong, while, at least for the electrons, the shock was non-laminar with electron density fluctuations above the thermal level. The ions in these early shocks are found to be about adiabatically heated, merely being slowed without increase in thermal energy, by the fields. Theoretical research has then concentrated on the electrons in the past, and in all but perhaps one experiment,[7,9] they seem to be understood.

Shocks are of further importance. The laboratory shocks are generated (for example) in θ and z-pinches, and so might be expected naturally in magnetic containment devices in the thermonuclear program. It was initially hoped that collisionless shocks could be used to heat ions to ignition temperatures which are so high that collisions are infrequent. (They have also been used in explanation of solar flare events, as well as being of close geophysical interest in the Earth's Bow Shock).

In 1970, Kornherr[8] published the first significant deductions of ion heating. In his strong, hot, shock non-adiabatic ion heating $T_{i2}/T_{iad} \sim 7$ occurred in two degrees of freedom. This heating, and that found by Paul et al. is as yet unexplained. Encouraged by the success of the turbulent electron heating studies, most work has gone into demonstrating ion turbulence via instabilities. As will be shown below, ion heating occurs only for quite well-known shock types, and typical of hot ion shocks is the presence of two-ion-beam instability. But as Biskamp reports in his review of 1973[9], this has not been a success.

Evidence will be given below, that even when ion heating occurs, turbulence does not appear to play an important part. Thus the possibility of some laminar ion heating mechanism is naturally suggested. Needless to say, there is collisionless ion heating in experiments, when non-adiabatic heating is found.

In this work, the ions are considered in an approximation in which neither turbulence, nor collisions, are present. In the rest frame of a plane, perpendicular shock, the ions move in time-independent, averaged fields. A non-adiabatic heating will be shown possible, which is of the magnitude of the observed experimental results - a result not obtained by turbulence theories.

In highly collisional shocks, a species is heated by an entropy increase while collisions maintain Maxwellian particle distributions. If in some system there is no entropy rise, then the species is adiabatically heated and does not increase its "non-flow" energy. On the other hand, in a laminar, collisionless plasma, it is well-known that entropy is conserved. It is shown below that if, now, the ion distributions are allowed to be non-Maxwellian downstream, their energy must exceed adiabatic levels. Such heating is only accessible to a kinetic theory study - in a fluid model, the collisionless ions must go unheated if entropy is conserved.

It will be shown that the laminar shock does indeed suggest that distributions are non-Maxwellian. A model of a laminar perpendicular shock is then constructed. This is built on the following properties. Profile shapes for magnetic field and electric potential in the shock are not calculated self-consistently, but chosen by comparison with experiment and the aid of available physics. Thus shock thickness is taken from experiment, while short,

steep, profiles can to a first approximation, be modelled as linear. The physics, in the form of Maxwell's equations and the conservation relations, makes it possible to find self-consistent jumps from the upstream to the downstream for all parameters. The effect is that the electrons may be ignored, and attention is concentrated specifically on ion dynamics in laminar fields.

The observed geometrical set up of the plane perpendicular shock is shown in Fig. 1.1. In the rest frame of the shock, plasma drifts from $x = -\infty$ in crossed E_y and B_z fields. It's equilibrium conditions are specified. These are N_1, V_1, B_1, $T_1 = T_e + T_i$, and T_e/T_i, say. The electric field E_y must be compatible with V_1, B_1, so that for a proper upstream drift,

$$E_y = \frac{1}{c} V_1 B_1 = \text{const.} \qquad (1.1)$$

This is constant in the whole space by Maxwell's equation, $\nabla \wedge \underline{E} = 0$

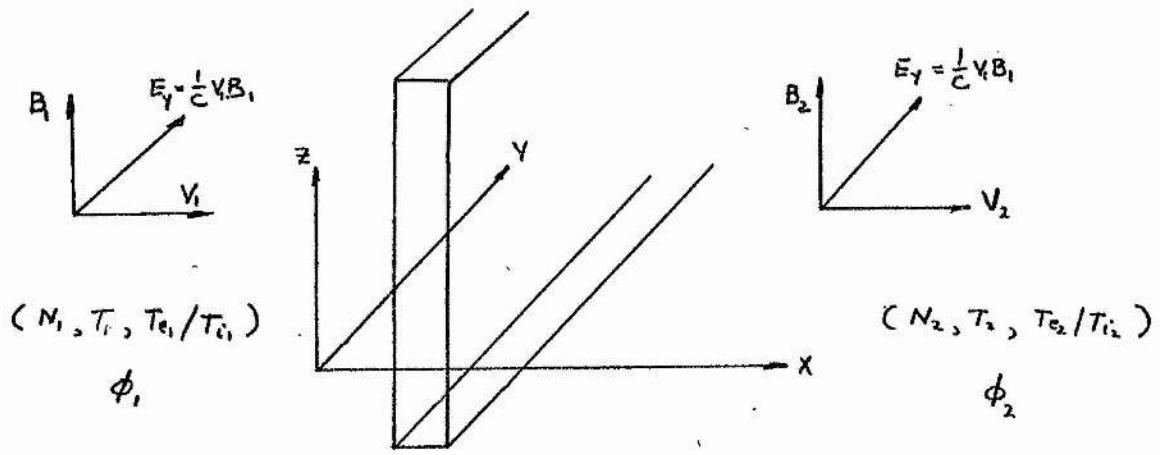

FIG 1.1

An electric potential, $\phi(x)$, is experimentally observed to appear in the shock, increasing to ϕ_2 in the downstream. Then ion dynamics requires the modelling of $\phi(x)$, $B(x)$, in L_s. The absence of currents outside of L_s gives

$$\left[\underline{E} \mp \frac{1}{c}\, \underline{v} \wedge \underline{B}\right]_{\mp \infty} = 0$$

and the y-component gives, since E_y=const,

$$v_1 B_1 = v_2 B_2 \qquad (1.2)$$

Both ions and electrons must be slowed to v_2, to conserve overall charge neutrality.

If there is no time dependence anywhere, then the shock parameters are x-dependent only, giving the conservation relations

$$\left[\int \underline{v}\, f_s\, (\underline{v})\, d^3v\right] = 0 \qquad (1.3)$$

$$\left[\sum_s M_s \int \underline{v}\, v_x\, f_s\, (\underline{v})\, d^3v + \frac{1}{8\pi}\, (\underline{E}^2 + \underline{B}^2).\hat{\underline{x}}\right] = 0 \qquad (1.4)$$

$$\left[\sum_s \tfrac{1}{2} M_s \int v^2 v_x\, f_s\, (\underline{v})\, d^3v + \frac{c}{4\pi}\, \hat{\underline{x}} \cdot \underline{E} \wedge \underline{B}\right] = 0 \qquad (1.5)$$

The square brackets are interpreted as $[A] = A_2 - A_1$. It is noted that the total of all species, s, and not of individual species occurs, for momentum and energy flux. Electromagnetic momentum and energy flux are included.

The initial upstream distributions may be chosen as Maxwellian. At $x = \mp\infty$, collisions will ensure that distributions are once again thermalized. If Maxwellians are substituted in 1.3 - 1.5, then the plasma equivalent of the Rankine-Hugoniot relations[36] results. These may be written to order m/M and v_1^2/c^2,

$$\frac{N_1}{N_2} = \frac{1}{8}\left\{ \frac{5K(T_{e1} + T_{i1})}{MV_1^2} + 1 + \frac{5B_1^2}{8\pi MN_1V_1^2} + \right.$$

(1.6)

$$\left. \sqrt{\left(\left(\frac{5K(T_{e1} + T_{i1})}{MV_1^2}\right) + 1 + \frac{5B_1^2}{8\pi MN_1V_1^2}\right)^2 + \frac{2B_1^2}{\pi MN_1V_1^2}} \right\}$$

$$\frac{N_1}{N_2} = \frac{V_2}{V_1} = \frac{B_1}{B_2} \qquad (B_x = 0 \text{ everywhere}). \tag{1.7}$$

$$\frac{5K(T_{e2} + T_{i2})}{MV_1^2} = \frac{5K(T_{e1} + T_{i1})}{MV_1^2} + 1 + \frac{B_1^2}{2\pi MN_1V_1^2} - \frac{V_2^2}{V_1^2} - \frac{B_1^2}{2\pi MN_1V_2V_1}$$

The condition $V_2/V_1 < 1$ for the existence of a shock, gives

$$M = \frac{V_1}{\frac{5K(T_{e1} + T_{i1})}{3M} + \frac{B_1^2}{4\pi MN_1}} > 1$$

This is the magnetosonic Mach number, relevant to propagation perpendicular to the magnetic field. The quantities $K(T_{e1} + T_{i1})/M$, $B_1^2/4\pi MN$, may be identified as the squared acoustic and Alfvén velocities. Their ratio is twice

$$\beta = \frac{N_1 K(T_{e1} + T_{i1})}{(B_1^2/8\pi)}$$

, and it

is an important measure of the relative dominance of fields and particles. It gives the ratio of particle to magnetic pressure. The non-dimensionalized quantities M,β are in common use as initial shock parameters for they are useful for comparison purposes. The R-H relations (1.6)-(1.8) may be written in terms of M and β. A further property is that $V_{2y} = V_{2z} = 0$.

Now if the (ion) distributions are non-Maxwellian immediately downstream, these relations might still apply. Thus, in the constant laminar fields extending from the rear of the shock to $x=+\infty$, if temperature is defined as

$$T_s = \frac{M_s}{N_2} \int (\underline{v} - \underline{v}_2)^2 \; f_{s2} \; (\underline{v}) \; d^3v \qquad (1.11)$$

they still hold,

and are used in this form in the shock model, for the ions. It has been suggested above that even with conservation of entropy , downstream non-flow energy may increase above adiabatic. Thus it must be shown that T_s as defined here, under the constraint Entropy=const., can be super-adiabatic. While the conservation relations apply even for collisional shocks, they must now be restricted to collisionless plasmas.

It is noticeable that no determination of ϕ_2 occurs in the conservation relations while ϕ is required by the model for the ion dynamics. Also, no jump for T_e/T_i is given so that the energy partition between species downstream is unknown. It is the solutions of these quantities which emerge as the most valuable information given by the model, when a technique is developed for finding self-consistent ϕ. A kinetic theory approach, yielding solutions for the downstream ion distribution functions, will give valuable information on

the nature of ion instabilities, and the consequences of unfreezing the time component. All these will be compared with experiment.

It is first necessary to review the evidence in favour of a laminar ion approach.

2. The Thesis and the Experimental Problem

Two principal sets of experiments will be quoted. The first, chronologically, has been the stimulus for a great deal of shock research, demonstrating in 1965 most of the known behaviour of plasma shock waves. These are experiments performed at the Culham Laboratory by Paul et al., and reported in a series of papers [1,2,3] between 1965 and 1970. They showed perpendicular shocks where pure collisions could not explain downstream parameters - they could then justifiably be called collisionless shock waves. This work has been conveniently summarized by Paul in reference [4]. These experiments were restricted to the domain $T_e >> T_i$.

The second set of experiments were specially conceived to investigate the domain $T_e \lesssim T_i$, which has the effect of amplifying the role of the ions in the shock dynamics. Thus they are of interest in this thesis. They are due to a team at Garching [5,6,7,8] and are published between 1968 and 1972, these later dates reflecting a slow shift of interest to the role of hot ions in a shock. Of importance is reference [8], due to Kornherr, where the nature of ion heating in the shock is considered explicitly, and reference [7] where first direct measurement of ion temperature downstream of the shock is reported. Few experiments have been reported since then. The goal of nuclear fusion has become more realistic, and thus justifiable from the point of view of expense. Further, some degree of theoretical stagnation seems to have occurred, Biskamp, in his review of

1973 [9], is quoted on a shock problem - the explanation of an electron turbulence: "All theoretical attempts to find an efficient instability for $T_e >> T_i$, $V_d >> V_e$ [V_d is the drift of ions relative to electrons] .... have failed, and there is little room left for further research." Problems seem either too complicated to justify their theoretical investigation (say of turbulent collision frequencies), or no appropriate mechanism could be proposed to explain the unusual events. Again, fusion research seems to offer greater attractions to the theoretician.

This thesis examines some phenomena unexplained since 1965, and the first Culham experiments. No absolute conclusions can be drawn for as indicated above, a (hypothetical) model is used. The existance of a firmly defined theoretical behaviour for ion heating is conclusively demonstrated, however, so that only the dominance of the model's explanation of ion heating need be considered in the future. A mechanism to solve Biskamp's problem is suggested, among other ideas.

The experiments will be examined below under headings. Each heading will become relevant to the properties of the model which is finally constructed.

The following observations, principally at the Culham and Garching Laboratories, have been made.

i/ Steady State Shocks. There is observed in the experiments above, a well-defined region in the life-time of the shock, when no evolution of the profiles occurs. There is a well-defined, sharp, transition between two regions that are themselves well defined, and accessible to measurement. (It is a recurring problem of shock experiments, that while a stable initial plasma can easily be achieved, the shock and its generating magnetic "piston" are not clearly separated to expose a "shocked" flow. The Culham and Garching experiments are z- and θ- pinches respectively, where the shock is formed as a disturbance propagating ahead of the imploding cylindrical surface current sheet. Strong magnetic field gradients in this sheet form the magnetic piston). The Culham experiments are taken at Mach numbers $M_A \sim 2.5$, 3.7, 6.3. The final shock shows no separation of piston and shock, and has further strongly oscillatory profiles, and so is accordingly ignored.

This information is taken from oscilloscope traces of electric potential and magnetic field. Thus within the resolution of the trace these "steady-state" profiles may hide very fine-scale, fast oscillations.

ii/ Profile Types Two basic profile types are observed. These are illustrated in Fig. 2.1

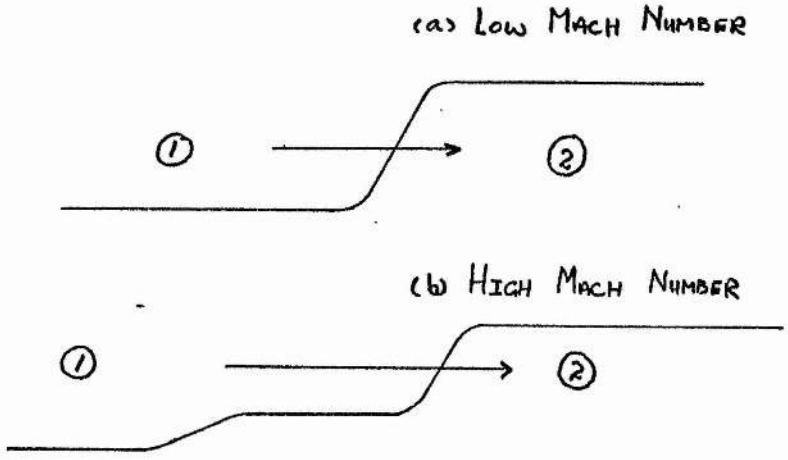

FIG. 2.1

The first is the expected smooth transition and is characteristic of low Mach number shocks only. The shock thickness, L_s, is found to be of order 7 C/ω_{pe}, for Culham $M_A \sim 2.5, \beta \sim 0.04$. For the Garching shocks of Kornherr [8], $L_s \sim 0.5\ C/\omega_{pi} \sim 20\ C/\omega_{pe}$, where $M \sim 1.7$, $\beta \sim 0.4$; further $T_e < T_i$, contrasting with Paul's work, $T_e > T_i$, and suggesting an increased shock width with ion temperature. This dependence of L_s is not clear, however. Experiments due to Hintz [10] at these low Mach numbers, but with $\beta = \beta_e + \beta_i \sim 0.1$ and ~ 1.0, claim $L_s \sim 10\ C/\omega_{pe}$; here $T_e \sim T_i$, so that the ions are very hot, thus suggesting L_s is constant with $\beta = \beta_e + \beta_i$.

The dependence on β_e/β_i is not clear. The ion Larmor radius, $r_i >> L_s$, always applies, while for electrons, $r_e << L_s$.

The individual traces of electric potential and magnetic field are found at Culham to have the same shape, but with the former rising more rapidly. No potential measurements have been made at Garching. This is unfortunate for they give valuable information on the nature of ion heating in the shock, as will be shown below. An explanation for the fast rise in electric potential may be offered by the experiments of Eselevich et. al. [11,12]. A special probe allows high resolution display of the potential profiles, which shows the appearance of an electrostatic subshock (predicted theoretically by Krall [13]). This occurs in a region quite far into the transition where flow becomes sub-Alfvénic, but remains super-ion acoustic, indicating a region of insignificant magnetic field dynamics. These electrostatic subshocks are rapidly oscillatory. However, they are not found at low Mach numbers $M_A \lesssim 2.8$, and indeed, they are observed when the second profile type of Fig. 2.1 (b) is seen.

The high Mach number shocks show a "foot" developing in front of the transition proper. An experiment due to Phillips and Robson [14], has studied the foot in some detail. Directional current probes established the presence of gyrating ions, such that they were reflecting off the shock front. The radius of gyration closely corresponds to the length of the foot. This mechanism had been noted by Sagdeev [15] in 1964 who saw that these deflecting ions gain energy. The pure resistive shocks of the low Mach number region, analysed theoretically as solitons,

show the appearance of three-valued flows (over-turning of the wave profile) at a critical Mach number, M*. Beyond this critical level, which represents the break-down of two-fluid equations to the shock (and indeed represents the possible limit of a sensible analytical shock theory), the reflection of ions is an obvious explanation of three-valued flows. The critical M* has been calculated by Kornherr, as a function of β, and falls from $M^* \sim 2.8$ at $\beta=0$ (cold plasma), to $M^* \sim 1$ as $\beta \to \infty$. As in most such low-M analyses, the ions are assumed to gain no thermal energy. Thus, almost by definition, $M>M^*$ shocks should see ion heating in a decreasingly efficient electron heating environment. Inclusion of hot ions in $M<M^*$ shock waves, does not affect the theoretical results significantly (at least at small β), as will be shown below.

The ions reflect off the electric potential, and follow an orbit given schematically in Fig. 2.2 The ion is assumed to suffer no collisions, at least in the upstream of the shock. This is supported by the observation above, that foot length corresponds to the ion radius of gyration. After bouncing off the shock, the ions are accelerated by the ambient electric field Ey, while in the upstream. They then gain large velocities, Vy, and are eventually turned by the magnetic field B_z, with sufficient kinetic energy to surmount the electric potential.

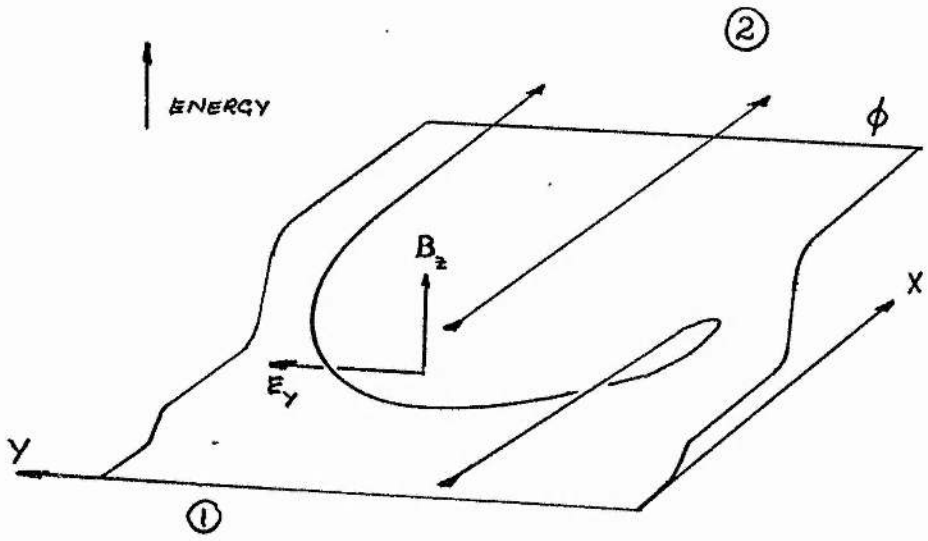

FIG. 2.2

An ion current to the positive y-direction occurs. The observed positive value of $B_z(x)$ in the foot is maintained by a current of electrons swept with the ions. In the steady-state shock,

$$\frac{dB}{dx} \propto -J_y = n\,e(V_y^{\,i} - V_y^{\,e}) \qquad (2.1)$$

where n is the density. Then sufficient electron flow $V_y^{\,e}$ may keep $\frac{dB}{dx} > 0$ [7,14], even in the foot.

It will be shown below that the energy gained by the ions is enormous; the M<M* shock waves are no longer purely resistive. It further appears that reflected ion levels depend on the shape of the ion distribution function, thus requiring a kinetic theory approach to the problem of following ion behaviour, and signalling the collapse of the M<M* fluid theories.

It is now held by most reviewers that shock thickness increases when M<M*. This is borne out by the collations of reference [4] (Table II). But no consideration is given to other variables and their possible

influence on L_s. Thus the Culham experiments progress according to $M_A \sim 2.5 < M^* > 3.7$ by fixing initial temperature, and varying the initial magnetic field; thus initial β varies. But the Alfven Mach number is not the natural one for the plasma shock wave where two "sound" modes operate. It is shown below, that the typical profile Fig. 2.1 (b) should be removed at $M>M^*$, if β is small enough. If the reasons for shock thickening at $M>M^*$ are connected with reflecting ions, then there is a possible β- dependence for L_s (there are no reflections when the initial ions are cold).

Thus the thickness L_s is not well known, but is safely taken as lying between a few C/ω_{pe} for low-β, low-M, shocks, varying up to C/ω_{pi} for $M>M^*$, and probably for high β. This problem is extensively considered below. However, for the resistive transition, $r_i >> L_s$, always, while in the foot $r_i \sim L_s$; conversely, $r_e << L_s$.

The conservation relations across the shock require that $N_1V_1 = N_2V_2$, $V_1B_1 = V_2B_2$. Thus reasonably similar profiles for density and velocity, as compared with magnetic field and electric potential, may be expected. The Garching experiments, expecially of Kornherr, are unusual. Very low ionization is effected ($\sim$50%), and ionizing collisions in the shock allow ($N_1V_1 < N_2V_2$). It is therefore necessary to derive a modified set of conservation relations. As usual the electric potential does not appear in the relations.

Much more may be said of shock profiles. It has been indicated that plasma flows in the plane of the shock are required. Their distribution across the shock is important, but is of no essential

use to this thesis. Turbulence regions in the shock are also of interest. Eselevich et al.[12] show that for shocks propagating into an initially thermalized plasma with $T_e = T_i$, fine resolution of profiles shows an initial slow increase where Coulomb collisions heat the electrons. When $T_e >> T_i$, ion-acoustic instability saturates to further heat the electrons and further modify the profile. Again the ion dynamics are of importance in this thesis and in spite of these latter properties of shock profiles, the $M<M^*$ ions are not heated across the shock, and so do not see these details (within experimental error).

The essential data is then the appearance of the foot in the magnetic field and electric potential profiles, indicating reflecting ions. Relevant shock thickness for various parameters is vaguely known. The shape of the profiles has no observed effect on ion heating at $M<M^*$.

iii/ Electron Heating. The first deductions on the nature of electron heating across a perpendicular, collisionless shock were made without a direct measurement of the electron temperature jump! The 1965, Culham experiments, measured the electric potential in the shock, and shock velocity. Conservation relations across the shock satisfied $\frac{1}{2}MV_1^2 \sim \frac{1}{2}MV_2^2 + e\phi$. Thus the ions are slowed only by the electric potential jump and are not heated. But then all dissipation must appear as electron heating downstream. It was found that while ion-ion and ion-neutral collisions did not occur in the shock, some electron-ion collisions were present. Maxwell's equations give

$dB/dx \propto - J_y$, and (to M_e/M_i) the current J_y is carried by electrons in the transition. Thus a collisional resistive heating was occuring. Estimation of this heating, even in the extreme conditions at the rear of the shock, suggested the resistivity was too small. But it was known that conditions were suitable for ion-acoustic instability, with $T_e \sim 10 T_i$ and $V_d \sim 0.1\ V_e$ (where V_d is the electron drift maintaining the current J_y, and V_e is the thermal velocity of the electrons). Electron heating via-ion-acoustic turbulence was immediately suggested. Later papers validated the deduced heating levels by direct measurement. The electron gyroradius is much smaller than shock thickness. The electrons then see the averaged shock fields as very slowly varying and will follow their drift orbits (equipotentials). They cannot gain energy from the fields (the ions are reflected by ϕ, while the electrons would be accelerated).

The measured electron temperatures agreed well with conservation relations. An MHD computer solution [15] using classical resistivity, gave a ratio of total heating to resistive heating of order 6.

These results have been the stimulus for most of the shock research to date; "anomalous" electron heating has been found over all parameter ranges - indeed such heating defines the "collisionless" shock.

The Garching experiments were such that $T_e << T_i$. While the Culham experiments quickly verified that ion-acoustic turbulence was responsible for electron heating, the condition $T_e << T_i$ at Garching implies that ion-acoustic waves are stable. However, electron-cyclotron instabilities occur in these shocks [7] with growth rates sufficiently rapid - as measured by the rate of growth of linear waves, rather than by the energy content of the resulting turbulence - to be a viable dissipation mechanism. Biskamp [9]

argues that the turbulence energy content is too low. Further in the experiments of Kornherr, the mechanism of electron heating remains unresolved. All turbulence heating theories rest on a so-called universal instability, typified by a relative drift of particles. This drift is so low in the case of Kornherr, that no waves can be unstable, again as discussed by Biskamp. Electron turbulence still persists.

At high Mach number, increasing ion heating has been deduced by Kornherr, with direct measurement of ion heating in one instance by Keilhacker et al. [7]. Since conservation relations must fix the total thermal content of the downstream, a decreasing electron heating must take place. Electron heating remains in excess of resistive (classical) levels and some instability can usually be found. There appears to be no change in the nature of electron heating at $M>M^*$.

iv/ Electron Turbulence. The above feature of turbulent electron heating is noted, for it implies the presence of turbulent shock profiles in contrast to the picture presented in i/. Thus there is a fine-scale structure within the trace of the oscilloscope. In the paper of 1970, the Culham team reported light-scattering measurements of turbulent spectra of frequency and wave number within the $M<M^*$ ($M_A \sim 2.5$) example. These are measurements of electron density fluctuations. The results were consistent with the theory of ion-acoustic turbulence of Kadomtsev [16], finally ensuring the process as

the cause of electron heating. Some inadequacy of this stochastic theory has been noted in [17], requiring a further step in the chain of events. This is mentioned below. In this shock no ion heating occurs, so they do not see the electron fluctuations.

It is noted then that the motion of the ions through the shock is apparently consistent with the oscilloscope picture of steady - state, laminar profiles.

No turbulence measurements at M>M* were made. Thus it is not certain that the ion heating which occurred there, is due to an ion-scale turbulence. Except for the appearance of the "foot", no major change of profile shape occured.

Electron-cyclotron turbulence was identified in the Garching experiments by comparison with computer simulations, and the growth rates of the linear waves. Reversal of the electron current in the shock front, $J_y^{(e)}$, reversed the direction of turbulent wave propagation, thus supporting the suggestion that the electrons generate the turbulence. This shock showed large ion heating. Biskamp [9], argues that no sensible ion instability has yet been found to give a turbulent ion heating.

v/ Ion Heating. Typical of all M<M* shock waves, then, is the absence of ion heating. Pedantically, this is not strictly true as will be indicated below, but may be taken to apply within experimental accuracy.

In the M$\sim$3.5>M* Culham experiment, an approximate 28% of total heating may be due to the ions. Experimental errors in the direct

measurement of electron temperature are about $\pm$15%, while together with errors in the determination of the initial conditions for application of the conservation relations, the evidence for ion heating is rather tentative. This low ion heating is due to low initial $\beta \sim 0.1$, and to the moderate initial $T_e/T_i \sim 1$.

A somewhat different situation is found at Garching. In the z-pinch, Culham experiments, the initial plasma is established by an oscillating axial current. This efficiently ionizes the filling gas ($\gtrsim$85%), with strong turbulent heating of the low-inertia electrons resulting. Rapid thermalization follows, and $T_e \gtrsim T_i$, upstream. The experiments at Garching are θ-pinches, but their importance lies in their heating technique. Here, a θ-prepinch strongly heats the ion component to give $T_i \gtrsim T_e$. The resulting plasma may pay the penalty of low ionization; Kornherr's shock has ~50%, Kielhacker very high, ionization.

A quick comparison of initial parameters shows

Culham: $M \sim 2.4 < M^*, \beta \sim 0.04$ $M \sim 3.5 > M^*, \beta \sim 0.1$

$T_e/T_i \sim 1$, $\gtrsim$ 85% ionization.

Garching (Kornherr) [8]: $M \sim 1.7 < M^*, \beta \sim 0.4$ $M \sim 4.9 > M^*, \beta \sim 2.6$

$T_e/T_i \sim 0.25$ $T_e/T_i \sim 0.16$

50% ionization.

(Keilhacker et al) [7] $M \sim 2.5 > M^*, \beta \sim 1$

$T_e/T_i \sim 0.23$

At Culham, the conditions are such that $T_{e2} >> T_{i2}$, allowing at some point in the shock, the non-acoustic instability. At Garching

$T_i > T_e$ everywhere. Then this instability is suppressed as mentioned earlier; the ion thermal effects should be greatly amplified. Kornherr examined the ions in the following way. Profiles of density, magnetic field and electron temperature were made. Noticeably lacking is a measure of electric potential in the shock. The shocks were in a region of sufficient time independence so that the Rankine-Hugoniot relations could be used to calculate further unknowns. The presence of ionizing collisions due to low initial ionization required extended conservation relations, and these allowed calculation of the following:

i) total temperature downstream, which immediately allowed evaluation of ion temperature;

ii) the downstream ratio of density rise due to ionization, to the total density there, may be found;

iii) this last is the most important and is the calculation of the number of degrees of freedom m_i of the ions (assuming that the electrons are heated by anomalous resistivity, in three degrees of freedom). This last point is important for if $m_i < 3$, turbulent stochastic heating is unlikely (for example), and thus the effectiveness of ion-seen turbulence as a heating mechanism can be judged.

At low Mach number $M \sim 1.7$, no ion heating was deduced, so that again the ions do not see electron turbulence (which is in this case electron-cyclotron, since $T_i > T_e$ always).

At $M \sim 4.9 > M^*$, strong ion heating is calculated with $T_{i2}/T_{i1} \sim 17$. Now compressional heating of the ions across the shock must occur. By definition, adiabatic heating measures increase in temperature without an increase in the internal energy, and is given according

to $T_{iad}/T_{il} = (N_2/N_1)^{\gamma_i - 1}$. Here $\gamma_i = (m_i + 2)/m_i$, is the ratio of specific heats for the ions. Clearly, if the non-adiabatic heating content is to be measured, a knowledge of m_i is very important, for the larger m_i, the smaller is the adiabatic heating.

In Kornherr's experiment,

$$T_{iad}/T_{il} \sim 2.3, \quad T_{i2}/T_{il} \sim 17, \quad T_{i2}/T_{iad} \sim 7.4$$

This last ratio shows very strong non-adiabatic ion heating. The source of this heating has not yet been demonstrated. The data suggests that $m_i = 2$ is very probable.

For a beam of cold ions, conservation of energy across the shock must satisfy

$$\tfrac{1}{2}MV_1^2 = \tfrac{1}{2}MV_2^2 + e\phi \tag{2.2}$$

If any shock shows ions satisfying this equation, then conversely no ion heating takes place. It is unfortunate that electric potential has not been measured in the Garching experiments. More generally, conversion of upstream ion streaming energy to non-adiabatic heating will imply

$$\tfrac{1}{2}MV_1^2 = \tfrac{1}{2}MV_2^2 + e\phi + [\text{heating}] \text{ ions}, \tag{2.3}$$

and the useful ratio

$$R_\phi = 2e\phi/M(V_1^2 - V_2^2) < 1 \tag{2.4}$$

this latter $R_\phi < 1$, has been obtained by Eselevich, in shocks where reflecting ions occur ($M > M^*$). No ion heating was deduced, so that the energy balance could not be tested. The ratio R_ϕ ranges from $R_\phi \sim 1$ for weak shock waves, to $R_\phi \sim 0.5$ at high M. These shocks are of low $\beta \lesssim 0.05$. The Culham $M > M^*$ shock gives $R_\phi \sim 1$, even in the presence

of reflecting ions, and with estimated 28% of heating due to the ions; here $\beta \sim 0.1$. It will be shown that ion heating increases strongly with increasing β; it is then to be expected that R_ϕ becomes smaller with increasing β. The experimental results do not support the simple energy balance (2.3), where the self-consistent value of ϕ is apparently too large. The model to be proposed below will cast new light on the value of ϕ. But it may be noted now that the ions acquire very large velocities, V_y by reflection. This is a source of ion energy which may account for the downstream ion temperature. But this large V_y velocity is turned into the shock front, where it must be slowed by the electric potential. It is possible then that ϕ may increase to adequately slow these ions, while temperature increases - in violation of (2.3). Some quantification is clearly necessary. None the less, R_ϕ is a useful quantity in estimating shock heating, and $R<1$ certainly implies ion heating.

vi/ Ion Turbulence. The problem immediately occurs for an explanation of non-adiabatic ion heating, as shown by the Garching experiment, and suggested by the Culham M>M* shock. The example of turbulent electron heating, via a universal instability, has led to a search for similar ion instabilities. There is only one seriously considered example, and this is due to counter-streaming of the reflected ion beam with the main bulk of ions. Since ion heating appears to be concurrent with the appearance of reflection ions at M>M*, this is a very natural suggestion. It is the nature of the conversion of upstream ion kinetic energy to downstream thermal energy that is the interest of

this thesis. All research to date has had in mind the turbulent heating of ions, while this thesis assumes the ions see no turbulence. The two ion beams are indeed unstable, and establish a turbulence which will result in a stable single ion beam downstream. It is noted now, in favour of this thesis, that the reflecting beam draws its energy from a Laminar motion. It is the conduction of energy to the downstream that must be accomplished, and this may be in the form of a fast ion beam downstream, or as a thermalized (due to ion-ion instability) ion distribution.

The reflecting ions give rise to various forms of distribution at different situations in the transition. These are shown in Fig. 2.3 as contours of constant f_{ions} over velocity space (V_x, V_y),

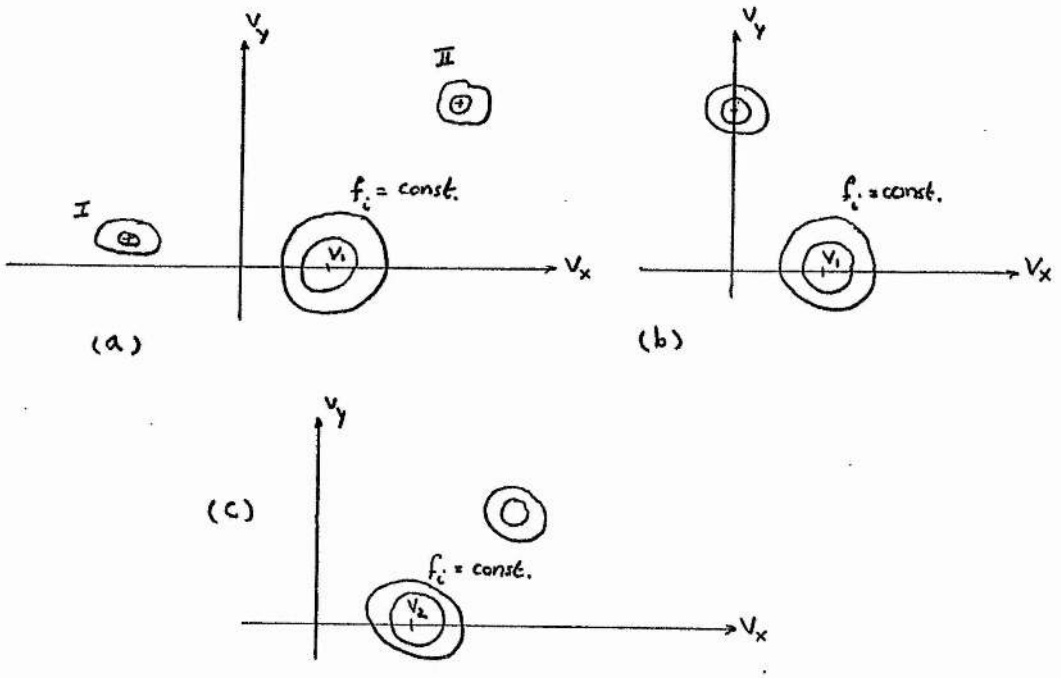

FIG. 2.3

Example (a) is a schematic representation of the situation at the front of the shock. The upstream flows into the transition with

velocity V_1. Some ions are exiting from the shock or reflection (I), while others have followed their gyration orbits and re-enter the shock with average conditions (II). The beams I,II, need not be so well defined. At the leading edge of the foot, no flow to V_x occurs as the ions reach a turning point. This is shown in example (b), and is an opportunity for an ion instability far in front of the resistive transition. Example (c) represents the situation that could occur downstream if the upstream growth - rates are too small to cause any diffusion of f_{ions} to a stable form. The energy of this last form has not been previously estimated.

A good study of the instability is due to Auer et al. [18] who analyse the linear behaviour for a hot plasma in a magnetic field. Computer solutions of the complete electromagnetic problem, show that for $T_e/T_i \gtrsim 5$ peak growth rates of the unstable modes are $\gamma \sim .1\ \omega_{pi}$. As T_e/T_i decreases this growth rate drops sharply so that at $T_e/T_i \sim 1.7$, $\gamma \sim \Omega_i$. Of use is the fact that γ_{max} occurs when the ions are cold, and when the ion beams are equal in size. A simulation shows further that the ion-ion instability cannot explain the observed thermalization of the ions; gyrating ions are observed downstream.

A non-linear analysis of the most unstable situation of equal, cold, ion beams has been discussed for the case of perpendicular propagation by Popadopoulos et al. [19]. Conditions were matched to those of laboratory shocks. Then computer solutions showed a heating of ions co-incident with the attenuation of the ion beam velocities.

Certainly, on sufficiently long time scales, the instability will yield a stable, hot, ion distribution. As to whether growth rates to saturation are sufficiently rapid to take place inside a shock thickness must be decided. If they are, then the ion heating must be examined as a turbulence phenomena. If γ is the linear growth rate, and τ is a time to saturation of the instability, then Popadopoulos finds that $\gamma\tau \sim 7 \to 5$ for $\omega_{pe}^2/\Omega_e^2 \sim \frac{1}{4} \to 100$. The latter situation is comparable with the Garching shocks where shock velocity and thickness give $\tau_s \sim L_s/V_1$ and $\gamma_{max}\,\tau_s \sim 2.6$. This is calculated at the growth rate γ_{max} of the simulation, and so τ_s is too small to allow saturation. If the same growth rate is taken for the Culham shock, then $\gamma_{max}\,\tau_s \sim 10^{-2}$, and again the plasma spends too little time in the shock.

It is unlikely then, that if even these most exaggerated forms of the instability are inadequate, that ions are heated in the space L_s. Fig. 2.3 (b) shows an unstable situation that exists over much longer times (the length of the foot is, at Culham for example, about $8L_s$). But again it is expected that γ is too small, for while τ_s increases, γ_{max} decreases when the $T_e/T_i \sim 1$ upstream conditions are met (the linear analysis of Auer et al.). The initial plasma is often in thermal equilibrium between species so that $T_e \sim T_i$ is reasonable (the Culham shock); when $T_e < T_i$, γ is further reduced (Garching) and in any case remains of order Ω_i so that $\gamma\tau_s$ is small. No fluctuations have been observed in the foot. The simulations of Auer et al. mentioned above, and those of Biskamp

and Welter [20] show evidence of fast ion beams downstream, implying that non-linear attenuation of the ion beams is at least incomplete. This latter paper [20] also suggests that damping of the magneto-sonic wave train found behind low-M shocks, occurs when reflecting ions are present [6]. They show that a fast ion beam may efficiently damp the wave train. This is indirect evidence of the fast beam surviving in the shocked plasma. The examples (b) and (c) of Fig. 2.3 are then doubtful sources of complete ion turbulent heating, in L_s. The situation (a) has not been analysed.

The Earth's bow shock gives support for a laminar ion behaviour [21]. Stable electron distributions have been shown to occur on scales $L \lesssim C/\omega_{pe}$, while dissipation of a high velocity ion component takes about 100 C/ω_{pi}. The form of the electron distributions is typical of electron instabilities seen in Laboratory shock waves; the narrow $L_s \sim C/\omega_{pe}$ is accepted as compatible with an electrostatic instability of Buneman.[34] The fast ion beam was deduced from the observation of strong variation in structure with the angle of observation. This reference [21], is important for the following reasons. It was found that the bulk of slow ions downstream is adiabatically heated if the ions have three degrees of freedom, $m_i=3$. If $m_i<3$, then non-adiabatic heating occurs. But it is found, too, that this heating is always about four times smaller that that of the whole plasma, including the fast beam. The latter has a density about 10% of the total. There is thus observed large energy in the fast component, downstream. The electron temperature is always less than that of the ions (as in the Garching experiments), so that

electrons play a decreasing role in energy dissipation in this high-M shock. These observations were made in a region where the complex Bow Shock was approximately of perpendicular type.

Other sources of ion heating have been proposed, but none have been as favourable as the ion-ion instability. The electrostatic subshock is discussed by Biskamp [9]. The strong electrostatic oscillations could cause the trapping of some slow-moving ions. But the work of Eselevich et al. has showed that the subshock is co-incident with the appearance of reflecting ions; it is just these ions that would be trapped. Further, at very high Mach numbers, the subshock disappears altogether, while the ions continue to be heated (as deduced by $R_\phi<1$). Biskamp concludes that any ion heating would be insignificant in the subshock.

The indications are that the processes above are inadequate to explain ion heating as a turbulence phenomenon. A much stronger approach is possible, when a laminar study is examined.

References [14,21] show that sufficient energy is carried by the reflecting ions to account for the ion heating. This energy is gained in the (laminar) reflection orbit upstream of the shock, in the two degrees of freedom perpendicular to the magnetic field. But it was deduced by Kornherr [8], on observations of the shocked plasma, that ion temperature levels may best be understood by $m_i=2$. For the turbulence-heated electrons, $m_e=3$. There is thus tentative support for ignoring turbulence ion heating. The absence of ion turbulence at low $M<M^*$, the similarity of the resistive profiles at both high and low Mach

number, the stability of the foot at M>M*, with its dimensions very close to those of an unimpeded ion orbit, and the absence of the downstream magnetosonic wave-train when M>M*, together with the deduction of $m_i = 2$, the generally low growth-rates of the ion-ion streaming instabilities, and the high (kinetic) energies of the fast reflected ions, make a laminar study even more viable.

The intriguing problem of a non-adiabatic heating mechanism in laminar profiles arises - a situation where ion entropy is preserved in the collisionless plasma.

vii/ Confirmation with the Rankine-Hugoniot Relations. The Culham and Garching experiments both satisfy the conservation relations. The Culham experiment at M<M* gives good comparison of total heating (calculated from the R-H relations) with electron heating. This confirms the early indirect evidence of zero ion heating, while supporting the use of the conservation relations in a form assuming Maxwellian distribution both upstream and down of the shock.

The Garching experiments[7], in measuring all unknowns (except electric potential which does not appear in the conservation relations), including ion temperature directly, satisfy the R-H relations. This confirms their use when M>M*, when gyrating ions can lead to strongly non-Maxwellian distributions in the downstream.

The R-H relations are accurate to order M_e/M_i and V^2/C^2, and require Maxwellians. Over a wide range of parameters these approximations are satisfactory - including all laboratory shocks examined here.

From the above, all explanations of observed ion heating are in some way unsatisfactory; they all insist on turbulent heating. It is this idea which marks the departure point for this thesis.

The question is asked whether ion dynamics in smooth electric and magnetic fields can raise the temperature of the ions. Such orbits will automatically conserve ion entropy. A steady-state profile for the ion motion has been noted in i/ above, and so the ion study becomes completely time independent. If the time component is switched off, then all the above mentioned ion heating mechanisms are blocked. The orbit of an ion is unperturbed and is such that the ion Larmor radius is very much greater than shock thickness, $r_i >> L_s$. The ions see a very rapid change in fields in the shock, almost a step-function change, and so are unable to follow their drift orbits. This is in contrast to the electron behaviour where $r_e << L_s$, and their unperturbed orbits are equipotentials.[1] The ions then depart from equipotentials along what might be called non-adiabatic orbits (the ion gains or loses energy). Since adiabatic flow requires Maxwellian distributions (entropy is always conserved in the collisionless plasma) it is expected that non-adiabatic heating must appear as a departure of the ion distribution function from Maxwellian. An extreme example is the bump-in-tail distribution as proposed in Fig. 2.3. This is in contrast to gas-dynamic shocks where the Maxwellian form is conserved (by collisions), and so entropy must increase.

In the next section this idea is placed on a firm theoretical footing. The relevance of the mechanism to shock waves must be judged. Accordingly, following sections will be devoted to the construction of a laminar, but kinetic theory, Model of a shock wave, and to the investigation of its properties. The model may be regarded

first of all as a solution of an arbitrary entropy-preserving ion-heating problem, to demonstrate the mechanism. But second, the Model may be sensibly compared with experimental results.

The approximation to a study of a pure laminar theory allows no simultaneous comparison with the turbulent heating mechanism proposed elsewhere. These must be assessed independently for the dominant phenomenon. But this section ends with a quote from the early 1964 review of shock waves in collisionless plasmas, by R.Z. Sagdeev [22], which reflects the attitude towards ion dynamics carried in this thesis:

"One feels that a natural and reasonable approach to the theory of collisionless shock waves should start with a laminar theory, based on the notion of regular oscillations. The stability of the solutions so obtained would be examined. Finally, in the unstable cases (and when no laminar solutions exist) the turbulence question should be examined. "

He was referring to the behaviour of plasma modes in the shock, but recognition of the shock as itself a wave with laminar and turbulent properties makes the attitude applicable. The simplest possible case should be examined first.

3. On Temperature in a Collisionless Shock

Given the species distribution function at some point in space and time, then its first, second and third moments are identified with the macroscopically observed quantities, density, momentum and pressure, of some statistical assembly. In particular, the plasma pressure is given by

$$\underline{\underline{P}}_s(\underline{x},t) = M_s \int d^3v \; (\underline{v}-\underline{v}_s)(\underline{v}-\underline{v}_s) \; f_s \; (\underline{x},\underline{v},t) \qquad (3.1)$$

where

$$\underline{v}_s(\underline{x},t) = \int d^3v \; \underline{v} \; f_s \; (\underline{x},\underline{v},t) \Big/ \int d^3v \; f_s \; (\underline{x},\underline{v},t) = \frac{(N_s V_s)}{N_s} \qquad (3.2)$$

On scales longer than the times to thermalization of the species when distributions become Maxwellian, the tensor nature of $\underline{\underline{P}}_s$ may be made to vanish, and indeed the species label as well, for equipartition of energy is implied as a few collisions are always present. By a suitable choice of co-ordinate axes, the components of $\underline{\underline{P}}_s$ are reduced to the diagonal elements only (rotation of an axis to lie along the drift direction, $\underline{v}_s$). The pressure is the same in all directions, and the internal energy is the sum of (in m_s degrees of freedom) m_s equal components. If P_s is an element of the diagonal, then temperature is defined as $T_s \; (\underline{x},t) = P_s \; (\underline{x},t) \; / \; N_s \; (\underline{x},t)$, suitable for adiabatic flow (entropy is automatically conserved).

On times of interest much shorter than thermalization time, spatial anisotropy must be considered. Again by rotation of the axes

to lie along the drift $\underline{v}_s$, of the bulk fluid, the pressure tensor can be reduced to a diagonal form. But the components of the diagonal will not be the same; in a plasma this may reflect the free flow of charges along the magnetic field direction, with motion perpendicular to the field restricted by Larmor gyration. This leads to the "two-temperature" MHD theories. In the shock wave it is possible to imagine strong x-dependence across the shock. There is no z-dependence at all in the perpendicular case. The gyration of reflection ions in the y-direction may hold different the x- and y- dependence. It is then possible that the downstream state requires a "three-temperature" study!

Quite pedantically, from the pressure tensor, a "temperature tensor" may be formed

$$\underline{\underline{T}}_s(\underline{x},t) = \underline{\underline{P}}_s(\underline{x},t) \;/\; N_s(\underline{x},t) \qquad (3.3)$$

Each component T_{ii} of $\underline{\underline{T}}_s$ is a measure of the non-flow energy of the plasma, associated with the direction i, i=x,y,z. The sum of the (scalar) diagonal components is a total non-flow energy. (It is in fact not necessary that $\underline{\underline{T}}_s$ be diagonalized, as this sum is invariant under rotations). If M_s is the degree of freedom of the species, then temperature defined as $\sum_i T_{ii}/M_s$ can be different from each component T_{ii}. Definition (3.3) follows naturally from the moment $\underline{\underline{P}}_s$, and in particular, will be relevant downstream of a laminar shock wave for the following reason. The orbits of ions will be composed of circular Larmor orbits, super-imposed on the down-

stream drift V_2. Temperature, as a measure of internal non-flow energy, then resides in the Larmor gyration, and is an ordered, kinetic energy. This is consistent with conservation of entropy in the collisionless plasma, in laminar fields. It is just the non-adiabatic nature of such orbits that must be assessed; it has been suggested above that, with entropy conserved, non-Maxwellian, anisotropic distributions must occur.

The following important question must then be considered: can a distortion from an initial Maxwellian distribution lead to an increase in non-flow energy, as defined by equation (3.1), or "temperature" as defined by (3.3), under the constraint that entropy be conserved?

Entropy is given in the laminar fields by

$$S_s(\underline{x},t) = \int f_s\ (\underline{x},\underline{v},t)\ \ln f_s\ (\underline{x},\underline{v},t)\ d^3v = \text{constant} \qquad (3.4)$$

This is the classic isoperimetric problem [23]. If $\underline{\underline{\lambda}}$ is a set of Lagrangian multipliers, then the variation $\delta \underline{\underline{F}}_s$ of $\underline{\underline{F}}_s\ (\underline{v}, f_s, \partial f_s/\partial \underline{v})$ is performed where,

$$\underline{\underline{F}}_s = M_s \int (\underline{v}-\underline{v}_s)(\underline{v}-\underline{v}_s)\ f_s\ (\underline{x},\underline{v},t)\ d^3v + \underline{\underline{\lambda}} \int f_s\ (\underline{x},\underline{v},t) \ln f_s\ (\underline{x},\underline{v},t)\ d^3v$$

$$= \underline{\underline{P}}_s + \underline{\underline{\lambda}} S_s \qquad (3.5)$$

Here $\underline{x}$, and t are fixed. If $\underline{\underline{F}}_s = \int \underline{\underline{G}}_s\ d^3v$, then the variation, $\partial \underline{\underline{F}}_s$ may be carried inside the integrals to become the variational problem $\delta \underline{\underline{G}}_s = 0$. Euler's equations are

$$\left(\frac{d}{dv_i}\ \frac{\partial}{\partial f_{|i}} - \frac{\partial}{\partial f}\right) \underline{\underline{G}} = 0 \qquad (3.6)$$

where

$$f_{|i} \equiv \partial f / \partial v_i\ , \quad i = x, y, z\ .$$

Then equations (3.6) yield the tensor

$$-M_s (\underline{v}-\underline{v}_s)(\underline{v}-\underline{v}_s) - \underline{\underline{\lambda}} (1 + \ln f_s) = 0 \qquad (3.7)$$

for each element of this tensor it follows that

$$f_s(\underline{x},\underline{v},t) \propto \exp - \frac{M_s(v-v_s)^2_{ii}}{\lambda_{ii}} \qquad (3.8)$$

at some fixed point $(\underline{x},t)$

Hence under the constraint (3.4), the pressure $\underline{\underline{P}}_s$ is an extremum when the distribution presents Maxwellian cross-sections in each orthogonal direction. It is not necessary that the thermal spread in each direction be the same. The tensor $\underline{\underline{P}}_s$ has been arranged so that only the diagonal elements are non-zero. The variation has been performed with respect to velocity-space functions only. The λ_{ii} may be found in the usual way, for a given problem, by normalization requirements on f_s. In collisional assemblies it is well known that a fluid which is adiabatically heated, (so that distributions remain Maxwellian and entropy is constant) is in a state of minimum internal energy. This is given by

$$(P_s/N_s)^{\gamma_s} = \text{Constant} \quad , \text{ or } \frac{T_s}{T_o} = \left[\frac{N_s}{N_o}\right]^{\gamma_s - 1} \qquad (3.9)$$

This merely corresponds to the solution (3.8) of the variational problem; the consequence of importance to the thesis is that if pressure is defined according to equation (3.1), and the species (ions) move in laminar, collisionless orbits, then distortion of a distribution from Maxwellian represents an <u>increase</u> in the non-flow energy of the species. The extremum (3.8) is in fact a minimum. The object of this thesis is to estimate the possible distortion heating in shock waves.

Fluid theories, which consider the evolution of systems which have been averaged over velocity space, are not aware of detailed

changes in the particle distributions. The heating mechanism examined above then requires the kinetic theory definition (3.1), rather than an averaged or thermodynamics definition of pressure.

The above analysis strictly determines that pressure is increased when distributions depart from Maxwellian. Experimental observation of shock waves yields instead the temperature of a species, which is proportional to the square of the thermal spread. In the laminar problem of this thesis, temperature is correspondingly given by equation (3.3). The variation above is applied at some fixed point $(\underline{x},t)$. The temperature depends on the space and time co-ordinates only, by (3.3). Thus it is possible that spatial behaviour allows density $N_s\ (\underline{x},t)$ to compensate for changes in pressure. However, if it is known that N_s cannot have spatial dependence, then temperature is proportional to pressure so they display the same behaviour.

The initial conditions on the unshocked plasma prescribe, given Maxwellians, the conditions far downstream. Then N_2, V_2, $T_2 = T_e + T_i$ are known. If the shocked plasma immediately behind the transition has averaged properties N_2, V_2, then these persist. The ion distribution may be distorted in velocity space. It is now possible to simply test for a super-adiabatic temperature by comparison of observed levels with the equations for adiabatic heating (3.9).. However, with N_2, V_2 fixed, for a component of (3.3) and using (3.9),

$$T_2 = P_2/N_2 > P_{ad}/N_2 \propto T_{ad} \quad , \text{ so that}$$

temperature is expected to be non-adiabatic.

An interesting two-stage process of ion heating is then proposed. Distortion of the ion distribution by ion dynamics in the Laminar fields is the first stage, extracting upstream kinetic energy consistent with the proper slowing of the ions. The non-Maxwellian ion distribution, if it is stable, then enters the second stage, downstream, where collisions rearrange the distribution of ions as Maxwellian, with possible increase in entropy.

However, the previous section has shown that fast ion beams may emerge downstream (Fig. 2.3 (c)), so that the distribution is unstable. In this case the second stage sees a rapid collisionless diffusion in velocity space of the unstable form, into a stable one, under the influence of unstable plasma waves. These are a source of entropy for the ions. Once stability is reached, collisions will establish a Maxwellian.

The second stage operates only on the velocity space of the downstream plasma; the conservation relations require that ions and electrons leave the shock with equal drifts, V_2. The beam velocity of the ions including the fast beam must be V_2. There is then no change in N_2, V_2, as even the unstable distribution drifts downstream.

The distortion heating idea above, reverses the attitude of current theoretical research into ion heating. Rather than search for an ion instability of sufficient growth rate, and turbulence energy level, to explain observations, it is now necessary that no

such instability occurs; for in this case only, can laminar ion orbits be expected. A further interesting fact will be demonstrated below, when it is shown that so much energy can be fed into the downstream by laminar distortion heating, that an ion instability must be invoked to suppress the mechanism - indeed a complete reversal of attitude!

That this is a sensible attack depends on whether the ion distribution may be expected to distort in crossing the shock. There are some obvious examples that are encouraging.

The previous section has shown that the ion behaviour in the shock transition is dominated by the electric potential. Thus at low Mach number, the ions satisfy the energy balance $\frac{1}{2}MV_1^2 = \frac{1}{2}MV_2^2 + e\phi$, and they are slowed by the electric potential with magnetic field effects ignorable. If the observed oscilloscope profile is substituted approximately with a step function in ϕ and B, then the ions are totally (in the transition) unaffected by the magnetic field. The velocity of an ion may then be switched across the shock according to

$$V_x \rightarrow \sqrt{V_x^2 - 2e\phi/M} \qquad (3.10)$$

But in the collisionless plasma, the distribution function f_i, is constant on orbits, so that equation (3.10) represents a distortion of the V_x- axis underneath the distribution. This has the effect of large stretching of the axis at $V_x^2 \gtrsim 2e\phi/M$, with smaller and smaller elongation as V_x increases. This skews the Maxwellian as is shown in Fig. 3.1 .

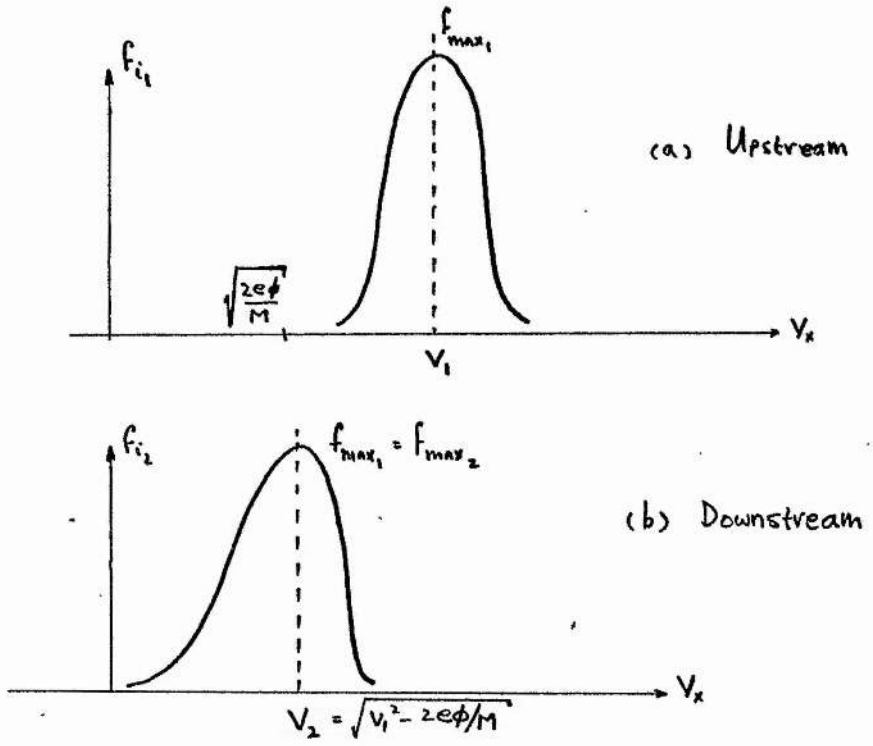

FIG 3.1

Then according to the above theory, f_{i2} must be heated in excess of adiabatic.

There is an interesting experiment due to Schumacher [24]. He obtained directly a profile for the ion distribution, by a Doppler broadening technique, which is shown in Fig. 3.2. The measurements were made downstream of a strong shock. Since the initial magnetic field was zero, this was not a magnetosonic shock wave, but the magnetic field profile was very similar to those of Culham, for example. Unfortunately no measure of the electric potential was taken, so that the demonstration is not perfect. Yet the similarity with Fig. 3.1 (b) is noticeable. In the direction parallel

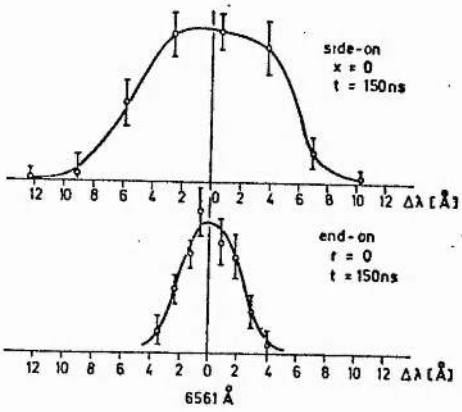

FIG.4. Comparison of Doppler broadening of D_α in end-on and side-on observation.

FIG 3.2

to B, the thermal spread corresponded to simple adiabatic compression. The profile shows near perfect Maxwellian form. This is to be expected too in the one-dimensional analysis of Fig. 3.1, since there is only a potential jump to v_x, and thus a broadening in this direction alone.

When the shock is stronger, and the thermal spread of the ions increases, it may occur that some ions do not surmount ϕ, and are reflected. They eventually penetrate the potential, and emerge as a tail of fast ions [20,21]. Again in the zero thickness approximation, the distribution may appear as in Fig. 3.3

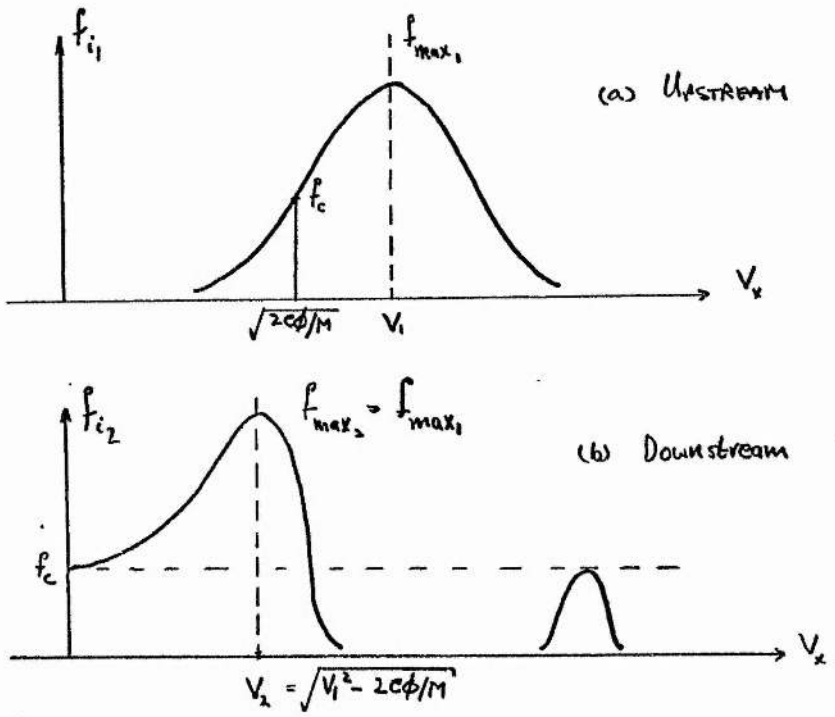

FIG. 3.3

A cut is effected at $V_x = \sqrt{2e\phi/M}$, where ions are slowed to rest. The main beam of transmitted ions shows skewing typical of the transformation (3.10). The fast tail should itself show a vertical face (there is no velocity space diffusion in the time independent model) and since f_i is constant on orbits, must maintain its height (the dotted lines).

The reflected ions are an obvious, extreme, source of distortion heating. This is encouraging as ion heating occurs experimentally at M>M*. Fig. 3.1 suggests that non-adiabatic heating should occur even at low M<M*. This is not compatible with observation. These examples are strongly directional and may operate in reduced degrees of freedom (m_i=2). This is in agreement with the work of Kornherr, [8] and of Schumacher.

It is noted, here, that if a distribution like that of Fig. 3.3 were to emerge from the rear of the shock, its thermalization could result in the heating of some electrons. It has been indicated that N_2 and V_2 will remain unchanged, as will total temperature $T_2 = T_{e2} + T_{i2}$ (by the conservation relations) as T_{i2} evolves downstream. If T_i were known, in Fig. 3.3, then the ratio T_e/T_i can evolve downstream. The two-ion-beam instability very efficiently heats the ions only (non-linear study due to Popadopoulos et al. [17]) when $T_e \sim T_i$. When $T_e >> T_i$, a simultaneous ion-acoustic instability is observed which heats significant electrons. In the former, better than 80% of ordered ion energy goes to random ion energy, in the latter it dropped to about 70%.

There is thus an experimental warning. Measurement of ion temperature must take into account the possible three-temperature state behind the shock, the degree of freedom (to properly calculate adiabatic levels), and should be made as soon as possible after the shock has passed.

In the next section, a Model is constructed to test this theory. A Maxwellian ion distribution is passed (numerically) through shock-like profiles, consistent with conservation relations. The distortion heating of the resulting downstream distribution is comparable with experiment.

4. On the Numerical Model

This chapter supplies the primary building block of the thesis, where now the emphasis drifts from a general ion heating mechanism as in Chapter 3, to a complete self-consistent steady-state study of a collisionless shock. The shock must display not only ion heating in regions consistent with experiment; outstanding theoretical problems in shock physics include determination of the electric potential jump, not given by the conservation relations, and an understanding of Kornherr's deduction that $m_i = 2$. Knowledge of the downstream ion distribution function gives valuable information of ion instabilities. While the primary inspiration for a laminar (as seen by the ions) time-independent shock is supplied by the ideas of chapter 3, many results of much wider application will occur.

The equations of motion of each ion are followed through the shock. Since the shock propagates perpendicular to the magnetic field, no motion in the direction of $\underline{B}(\underline{x})$ is found and the ions move only in the two perpendicular degrees of freedom. The numerical problem is then going to be of the "simulation" type, the solution of which is the ion distribution function, rather than a "continuum" type where the Vlasov equation might be solved directly. However, instead of calculating the self-consistent time development of the electro-magnetic fields and particles to a steady-state as is usual

in simulations (an example [7] is quoted above), the shock is regarded as ready-formed and constant in time.

To do this, approximations to the observed electro-magnetic profiles are chosen. If it is then assumed that these are the real, self-consistently evolved profiles, (for $\phi(x)$, $B(x)$), then the plasma equations reduce to Vlasov's equation for a collisionless plasma.

$$\underline{V} \cdot \frac{\partial f_i}{\partial \underline{x}} + \frac{e_i}{M_i} \left(\underline{E}(x) + \frac{1}{C} \underline{V} \wedge \underline{B}(x)\right) \cdot \frac{\partial f_i}{\partial \underline{V}} = 0 \qquad (4.1)$$

No time dependence occurs, and since $\underline{E}(x)$, $\underline{B}(x)$ are "known", Maxwell's equations need not be solved. This represents a considerable reduction in complexity of the problem!

Now it is emphasised that Laminar shock profiles $\phi(x)$, $B(x)$ are chosen. By Jeans' Theorem, equation (4.1) and its initial conditions

$$f_i \ (\underline{v}, \ x = -\infty) \qquad (4.2)$$

are equivalent exactly to knowing the equation of motion of each constituent ion. In the given fields, these are now

$$\frac{d\underline{v}}{dt} = \frac{e_i}{M_i} \left(\underline{E}\ (x) + \frac{1}{C}\ \underline{v} \wedge \underline{B}(x)\right), \qquad (4.3)$$

with appropriate initial values $\underline{v}(x = -\infty)$. (This represents the conversion from a "continuum" type problem, (4.1), to a "simulation" approach, (4.3)).

It is further possible to ignore the electrons in the collisionless plasma; charged species interact through the fields. But the

chosen profiles "are" the self-consistent fields, and electron effects are thus included automatically (as long as laminar ion behaviour is a good approximation).

It is noted again that specification of the shock according to initial plasma and Mach number, allows, through the conservation relations, downstream determination of N_2, V_2, B_2, but <u>not</u> the potential ϕ_2.

In the shock, thickness is chosen comparable with experiment. As a first approximation, a simple linear jump for an observed L_s is assumed. Then the potential profile remains undetermined.

As above, the shock frame is chosen so that the ions (and electrons) drift from $x = -\infty$, perpendicular to the magnetic field, the flow is maintained by the $\underline{E} \wedge \underline{B}$ drift, $cE_y B_z^{-1} \hat{x}$, where $\underline{B}_1 = B_1 \hat{z}$ and $E_y = \frac{1}{c} V_1 B_1$.

The geometry is indicated in Fig. 4.1, in the regions upstream, in the shock, and downstream.

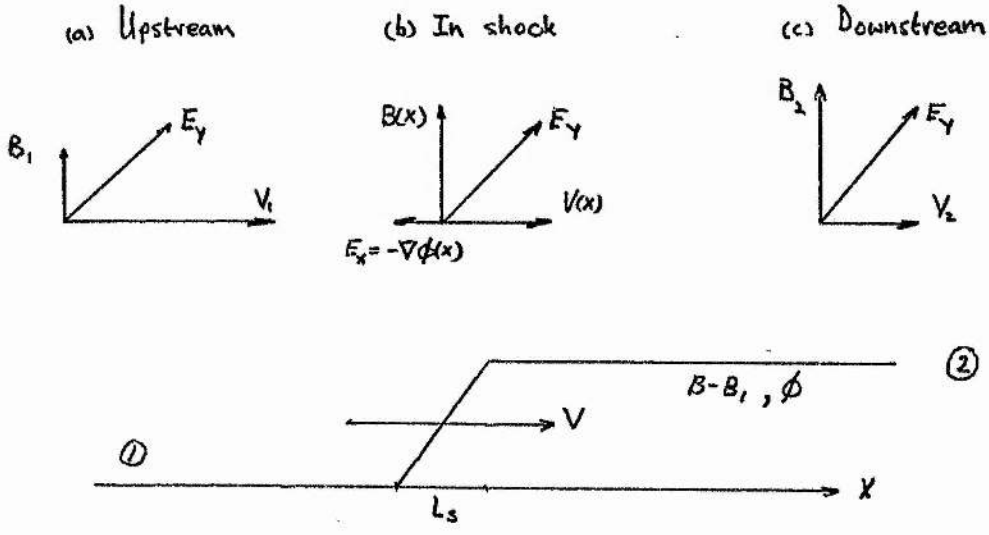

FIG 4.1

It is in this fashion that profiles are chosen for the shock. No force parallel to $\underline{B} = B\,\hat{\underline{z}}$, occurs so the ions are only x, and y, dependent. Computing time rises as the power of the dimension so this is a valuable time-saving device. Potential ϕ_2 is undetermined.

The equations of motion are a map, taking the upstream distribution function from velocity space $\underline{\mathcal{V}}_1$, to downstream velocity space $\underline{\mathcal{V}}_2$. Then $f_i : \underline{\mathcal{V}}_1 \rightarrow \underline{\mathcal{V}}_2$ is the solution sought. From f_i, by taking moments, the density n_2, ion flux, $(n_2 v_2)$, and temperature T_2, may be calculated. Not any level in n_2, v_2 is allowed, as these must be consistent with conservation relations across the shock. From the Rankine-Hugoniot relations of section 1, since laminar profiles (Fig. 4.1) are adopted, the calculated levels must agree with

$$\frac{N_1}{N_2} = \frac{V_2}{V_1} = \frac{B_1}{B_2} = \frac{1}{8}\left[\frac{5}{2M_A^2} + 1 + \frac{5\beta}{2M_A^2} + \sqrt{\left(\frac{5\beta}{2M_A^2} + 1 + \frac{5}{2M_A^2}\right)^2 + \frac{8}{M_A^2}}\right] \qquad (4.4)$$

$$B_{2x} = V_{2y} = 0 \,. \qquad (4.5)$$

It is then required that

$$n_2 = N_2 \,, \; v_2 = V_2 \,. \qquad (4.6)$$

Here the requirement of charge neutrality forces $N_e = N_i = N$, while flux conservation then gives $V_e = V_i = V$.

It is seen that B_2 is given by equation (4.4), by specification of the initial plasma and Mach number.

The vital information not supplied is the value of the electric potential jump. The fields cannot, apparently, be constructed.

However, equation (4.4) requires that

$$V_1 B_1 = V_2 B_2 \qquad (4.7)$$

which, ensures that the ions are slowed as much as the electrons; thus charge neutrality downstream is effected, compatible with the profile Fig. 4.1. No currents are allowed in the equilibria at $\pm \infty$. Now the Culham shocks show that the ions are slowed by the electric potential. At least when $M<M^*$, when no ion heating occurs, it is clear that

$$\tfrac{1}{2}MV_1^2 \sim \tfrac{1}{2}MV_2^2 + e\phi, \quad R_\phi \sim 1. \qquad (4.8)$$

The equation may be regarded as supplying only an initial estimate of ϕ, in conjunction with (4.4).

But if the ions are slowed by ϕ, then the profile $\phi(x)$ must be chosen so that (4.7) is satisfied. It is expected that v_2 will depend quite heavily on ϕ.

Thus finally, a procedure emerges for the determination of a self-consistent system, with ϕ now known: an initial estimate of ϕ is made (perhaps using (4.8)), for a given shock problem, and added to the proper information of (4.4). The ions are integrated through the shock and n_2, $(n_2 v_2)$ calculated;

the question:

$$v_1 B_1 = \frac{(n_2 v_2)}{n_2} \times B_2 \quad ?$$

is asked. If $v_2 = (n_2 v_2)/n_2$ is too small, ϕ is reduced, if too big then ϕ is increased. By a trial and error procedure, it is then possible to interpolate for the correct

value of ϕ.

It is noted that the ion flux across the shock is fixed according to $N_1V_1 = N_2V_2$, and satisfied whatever the value of ϕ, self-consistent, or not. If calculations show that this is not the case, then flux is lost due to numerical error, or due to ignorance of an unincluded ion dynamic.

For some choice of ϕ the, in general, incorrect downstream conditions occur as the following moment integrations

$$\begin{aligned} n_2 &= \int d^2v \quad f_2\ (\underline{v}) \\ (n_2v_2) &= \int d^2v \quad v_x \quad f_2\ \ (\underline{v}) \\ (n_2T_2) &= \int d^2v \quad (\underline{v} - \underline{V}_2).(\underline{v} - \underline{V}_2) \quad f_2\ (\underline{v}) \end{aligned} \qquad . \qquad (4.9)$$

They are performed in two dimensions perpendicular to $\underline{B}$. No change in upstream values occurs in the direction of $\underline{B} = B\ \hat{\underline{z}}$. In the following, small letters are reserved for the numerical integration, while capitals apply to the required conservation levels.

The problem now arises as to how to devise a numerical technique for effecting accurate integrals (4.9).

The conventional approach to simulation type numerical "experiments" consists of the evaluationof the initial distribution of particles, forward in time in self-consistent fields, until a shock is formed. The numerical particles necessarily simulate the real particles, moving forwards into the shock. Downstream, a scatter of particles in $\underline{V}_2$ will occur, even when the initial distribution has been regularly discretized. The integrations (4.9) must then be performed over this scatter. Numerically, this would normally involve an intermediate step; a surface would be fitted to the data and the integrations performed on this

surface. This adds to the cost of the simulation, while such fitting techniques involve a smoothing of the data which reduces the accuracy of the integrations. Estimates of downstream parameters are usually made visually from phase-space scatters. These simulations are usually irreversible, being designed to investigate anomalous transport effects of the turbulent plasma. The system then gains entropy.

The reversible nature of the model proposed here, allows a different approach.

A regular grid is established on $\underline{\mathcal{V}}_2$ downstream. Values of ϕ and B are chosen for convenient upstream initial conditions, which includes the specification of T_e/T_i; this requires use of the conservation relations. The equations of motion of each ion are now integrated backwards through the shock, from a point in the regular grid downstream to give a scatter of points in the upstream. The value of f_i (which is constant on the orbit), is not known until the ion reaches the upstream. Here the functional form of the initial ion distribution is known, and so a value of f_i may be assigned to each point in the scatter.

With f_i constant on the ion orbit, this value is then reassigned to the regular grid downstream. Thus an unusually accurate quantitative measure of the bulk ion properties is obtained. The integrations of equations (4.9) may be performed using the accurate $O(h^4)$ Simpson's Rule which has the restriction that an odd number of step lengths be taken in the directions V_x, V_y. This is not inconvenient.

The integrations cannot be computed over the whole of $\underline{\mathcal{V}}_2$. Thus some cut-off when f_i is very small, is chosen, outside of which no

significant contribution to the integrals will occur. This may be checked by the conservation of flux, $N_1V_1 = N_2V_2$. It is not initially known whether a point in $\underline{v}_2$ will integrate back to a region of significant f_i. This is a draw-back to the method, for considerable time can be spent adding nothing to the bulk properties downstream in a search for large f_i.

The attack of the model is to choose the initial conditions, with an initial guess for ϕ. A small sample M^2 of ions may be integrated forward through the shock to give a scatter in $\underline{v}_2$. But then the position of peak values of f_i downstream is known. Of course the drift V_2 is known, so that this is a suitable centre for the grid. However, ions gyrating off the shock front give a bump-in-tail type distribution in $\underline{v}_2$. The forward integration gives the centre of the tail which may be remote from the main beam. (But less accurately, for the maximum height of the tail depends on the position of the division of the upstream distribution into transmitted and reflected ions; this cut is not well known).

Once the high points of the main and reflected beams are known, the grid is regularly constructed point by point outwards, in the directions to $\pm V_x$, $\pm V_y$. This is done separately for each beam. Simultaneously, the contribution of that particular ion to the moment integrals is calculated, so that no storage of information of any single grid point is required.

If the reflected ion contribution is labelled sub-R, and that of the transmitted ions, sub-M (the Main beam), then downstream parameters are calculated finally as

$$n_2 = n_R + n_M$$

$$(n_2 v_2) = (n_R v_R) + (n_M v_M) \qquad (4.10)$$

$$(n_2 T_2) = (n_R T_R) + (n_M T_M)$$

The outward progression along each direction is halted when the contribution to these quantities is no longer of interest. The stop must also be consistent with Simpson's Rule which requires an odd number of grid points.

The equations of motion are, in the shock,

$$M \frac{dV_x'}{dt} = eE_x' - \frac{e}{c} V_y' B'(x)$$

$$M \frac{dV_y'}{dt} = eE_y' + \frac{e}{c} V_x' B'(x) \qquad (4.11)$$

The following non-dimensionalization is chosen to facilitate comparison of the numerical results with experiment. It follows naturally from the Rankine-Hugoniot relations (4.4) to define

$$n = \frac{n'}{N_1} \quad , \quad \underline{V} = \frac{V'}{V_1} \quad , \quad B = B'/B_1 \qquad (4.12)$$

The natural time of the ion motion is the inverse of the ion Larmor frequency. It is important that shock thickness be very much less than the Larmor radius, so that the ions are unable to follow their drift orbits. This is equivalent to $\Omega_i << 1/t_s$, where t_s is the time for an ion to traverse the shock. Larmor gyration is the source of ion non-flow energy in the Laminar model. Then let

$$t = t' \Omega_i \quad , \quad \underline{x} = \underline{x}' / \frac{v_1}{\Omega_i} \qquad (4.13)$$

The upstream electric field $E_y = \frac{1}{c} V_1 B_1$, is by Maxwell's equations a constant everywhere, and used to normalize the electric field.

$$\underline{E} = \underline{E}' \; / \; \left(\frac{\underline{V}_1 \underline{B}_1}{c}\right) \tag{4.14}$$

Then equations (4.11) reduce to

$$\begin{aligned} \frac{dV_x}{dt} &= E_x + V_y \, B(x) \\ \frac{dV_y}{dt} &= 1 - V_x \, B(x) \end{aligned} \tag{4.15}$$

These equations carry the ions forward through the shock, and they may be used to plot a rough scatter in $\underline{\mathcal{U}}_2$ to establish the region of downstream integration there.

The ions are integrated back through the shock by reversing the (now) initial velocities in $\underline{\mathcal{U}}_2$, with t = 0 there. The sign of $\underline{B}$ is changed to ensure a proper drift of the plasma towards $x = -\infty$. Then equations (4.15) give, in the shock and for backward flow,

$$\begin{aligned} \frac{dV_x}{dt} &= -E_x - V_y \, B(x) \\ \frac{dV_y}{dt} &= 1 + V_x \, B(x). \end{aligned} \tag{4.16}$$

In the linear profiles, $E_x = -\nabla\phi(x) = \text{constant}$.

Upstream of the shock, the relevant equations are, for backward flow,

$$\begin{aligned} \frac{dV_x}{dt} &= - V_y \\ \frac{dV_y}{dt} &= 1 + V_x \quad , \end{aligned} \tag{4.17}$$

since $E_x = 0$, $B_1 = 1$.

Downstream of the shock, for backward flow they are,

$$\frac{dV_x}{dt} = -V_y B_2$$

$$\frac{dV_y}{dt} = 1 + V_x B_2, \qquad (4.18)$$

with B_2 given by the Rankine-Hugoniot relations for an initial choice of parameters, β, M (equation (4.4)).

In the regions of equations (4.17) and (4.18), simple analytic solutions are possible. These are, for a given ion,

$$V_x = V_\perp \cos (B_{1,2} t + \alpha) - V_{1,2}$$
$$V_y = V_\perp \sin (B_{1,2} t + \alpha), \qquad (4.19)$$

where

$$V_\perp^2 = (V_{xo} - V_{1,2})^2 + V_{yo}^2 \quad , \quad \alpha = \frac{1}{B_{1,2}} \operatorname{Sin}^{-1} (V_{yo}/V_\perp)$$

Three basic orbit types can occur, and these are illustrated in Fig. 4.2.

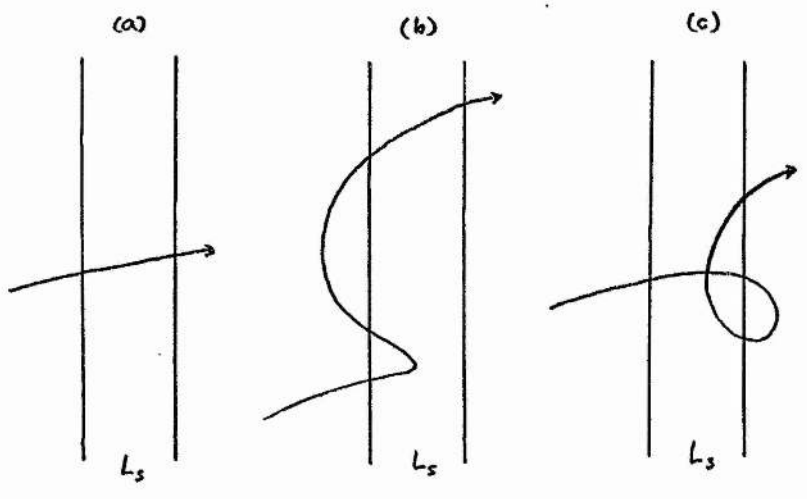

FIG 4.2

There is no simple analytic solution for the ions in the strong shock gradients. The equations are solved for each ion by a standard IBM Scientific Subroutine. This is a Runge-Kutta algorithm requiring equations (4.16), initial conditions $\underline{x}$ (t = 0), $\underline{x}$ (t = 0), a set of error bounds on the output and a time increment. The algorithm self-adjusts the time step by repeated halving or doubling, to meet the error bounds.

When an ion is reflected from the shock as in Fig. 4.2 (b), the Runge-Kutta routine is switched off and the analytic equations (4.19) used to calculate the ion gyration end point on return to the shock. The time spent by the ion in reflection may be very much longer than the time spent in the shock; it is always the case that $L_s << r_i = v_{th}/\Omega_i$, where r_i is on the scale of the upstream orbit. Thus the analytic step represents a considerable saving in computer time. Since the downstream state is given by the Rankine-Hugoniot relations, the orbit of type (c) may be followed there. Then it is possible to keep (numerical) flux high. An interesting point occurs in integrating from the downstream back through the shock, to the upstream. For orbits of type (c), there are two points of downstream exit from the shock, where the velocity is positive. These are marked (I) and (II) in Fig. 4.3

Then it is clear that the starting point of the orbit, in the reverse integration, is at I. Thus all points in the downstream grid of type II must be ignored, and the model must check for them. Only ions on final exit from the shock are included. Thus $v_x > 0$ always. A necessary condition for gyration from II to III, is that $V_\perp = \sqrt{(V_x^2 - V_2^2) + V_y^2} > V_2$. This is not sufficient as the phase of the ion may carry even such $V_\perp > V_2$ ions safely downstream; thus if $V_y < 0$ and $|V_y| >> |V_x|$, the ion is more likely to be returned to the shock, than if $V_y > 0$. Thus regions of $\underline{v}_2 : V_x > 0$ must be excluded from the initial grid. The above example is illustrated schematically in Fig. 4.4.

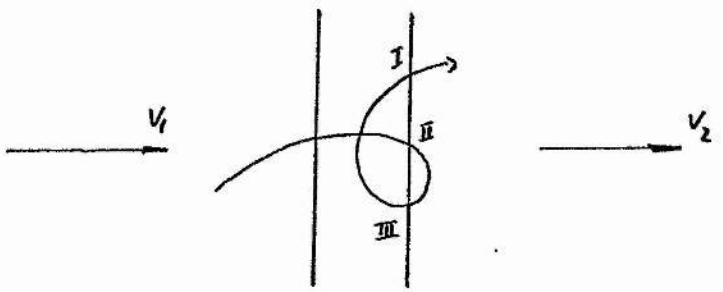

FIG 4.3

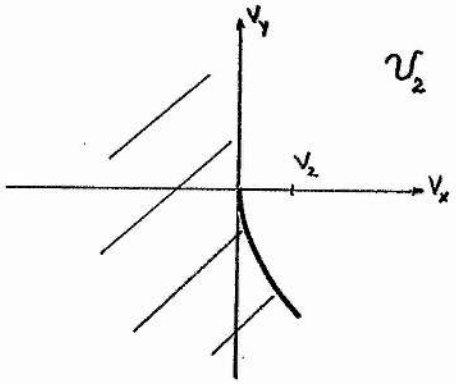

FIG 4.4

Their effect is never significant, f_i being very small in the neighbourhood of the boundary. Such regions are of course occupied, but have no relevance to the far downstream integrations over f_i. They occasionally occur in the Computations, and f_i is put equal to zero. The ion flux always remains high.

The dependence of the model on shock thickness must be tested. A sensitive response in temperature say, to a small variation in what is a crude approximation to real profiles, will jeopardize the usefulness of the model. It is useful, then, to construct an $L_s = 0$ model. It is clear from the Culham experiment, ($M<M^*$) where $R_\phi \sim 1$, that magnetic field dynamics are not important in the shock transition; an $L_s = 0$ approximation is then a sensible venture. In this case, the ions are quickly switched through the shock, or reflected and then switched through the shock. The solution is then trivial computationally (the same "backward" procedure must be used), using insignificant computer time.

When $L_s = 0$, an alternative approach may be used which avoids the trial-and-error procedure described above. There the model yields a number of function surfaces for variables of interest, over the space of independent parameters (M,β), for some T_e/T_i. The ordered grid of model runs (M,β) is convenient for comparison with experiment, where M and β are non-dimensional ratios.

When $L_s = 0$, the ions are slowed only by the potential jump, while the magnetic field in the shock is redundant. Then the new independent parameters (v_i,ϕ) and T_e/T_i (where v_i is the ion thermal velocity) allow the ions to be switched through the shock. Then

$v_2 = V_2$ (automatically) is calculated. But then $B_2 = 1/V_2$ is known so that M and β may be calculated from a suitably re-written form of the conservation relations. No trial-and-error procedure is necessary, but the method generates a non-regular scatter of results over M,β-space. Further, it is inadequate altogether if significant orbits of Fig. 4.2 (c) occur, since B_2 can be calculated only after all the orbits have been followed.

The model generates its own check on accuracy, since the physics requires flux be conserved, $N_1V_1 = N_2V_2$. This quantity shows that first, all orbit types have been included, and second, whether a sufficient number of ions is used to afford an accurate Simpson's integration. The step-size in $\underset{\sim}{\mathcal{V}}_2$ may be chosen different in the V_x and V_y directions. Further, different meshes may be used over the main beam, and the usually well-resolved reflected ion beam. The number of ions taken through the shock varies in the region 200-400, requiring computer time (on an IBM 360/44, with 88K Machine) of order 30-90 minutes. When $L_s \neq 0$, the model is clearly expensive, and made more so by the trial-and-error procedure, and the necessity of occasional searches of $\underset{\sim}{\mathcal{V}}_2$ by forward integration of ions. These times may then be doubled (at least) for a realistic estimate of computer time per self-consistent shock solution. When $L_s = 0$, computer time drops to less than 5 minutes per solution. The numerical ion orbit is checked for accuracy, by occasionally integrating forward and backward through the shock, requiring that it return to its point of departure.

The accuracy of interpolation between two or more guesses to a solution, will depend on the nature of the locus of such solutions. A linear interpolation is desirable due to large computing times. In most cases, this locus is found to be monotonic through the Rankine-Hugoniot levels, and approximately linear. Then even a coarse set of guesses will yield quite accurate results.

At large values of the ion thermal spread, computer time is high. Flux loss is held low at a few percent. But under these conditions curves may be checked fluent with an occasional very accurate integration, and with the easily obtained $L_s \neq 0$ case.

Typical experimental errors at the Culham and Garching Laboratories are in the region of $\pm$ 15%. The accuracy of the model is always better than 10% (measured by flux loss). The viability of the heating mechanisms of the model may then be sensibly compared with experiment.

The model for a perpendicular, collisionless, plane, shock wave has been suggested. In the collisionless, time-independent system, ions follow unperturbed orbits so that the ion distribution is constant on an orbit. In pre-chosen shock-like profiles, the downstream ion distribution is found by integrating ion orbits back through the shock wave to the upstream where the initial Maxwellian is known (in functional form). Relocation of this value at the downstream allows integration for moments of f_i to be made over a regular grid in velocity space. Ion velocity so calculated must be compatible with the jump condition $V_1B_1 = V_2B_2$. By adjustment of the undetermined electric potential (not given by the conservation relations), this

condition is met. A complete self-consistent solution then evolves, with ϕ determined.

The model is highly idealized, allowing principally no time dependence of the ion distributions. It is expected that when M>M*, they are two-ion-beam unstable. The dominance of distortion heating can only be estimated.

An important data output used below, is a computer-drawn display of a three-dimensional perspective of f_i over $\underline{v}_2$. The heavily distorted shapes so derived, indicate the presence of non-adiabatic heating as in §3. The integrals would show this result quantitatively, but the topology of f_i is strongly suggestive of instability studies; thus ion-ion instability is shown, the $T_\perp \neq T_\parallel$ instabilities of Harris [25] appear, while strong $T_x \neq T_y \neq T_z$ studies are suggested; every ion, in a distorted distribution, rotates in Larmor circles about the plasma drift thus causing the whole distribution to rotate - the effect of such rotation will be considered. The graphic display further offers information on the physics of the distortion, and so of the ion dynamics.

The model is non-physical. Thus the linear profiles used below cannot occur for they contain points of uncertain derivative, not allowed by Maxwell's equations (away from sources, etc.). It is not yet demonstrated from the Vlasov-Maxwell equations, that stationary shock waves exist at all [26]; turbulent electron heating has been observed in all collisionless shock waves. There is a further aspect in which the model is, pedantically speaking, non-physical. It has as its nature that it cannot explain the presence of the modelled components.

This is not the situation in numerical solutions of the full equations. The assumptions of a simulation routine are very simple, and physical, at least when a sufficiently powerful computer is available. The best simulation uses the plasma equations to approximate away terms that are inaccessible. No artificial form for significant variables is proposed, as in a model. The power of the model idea lies in reducing the complexity of the problem.

The resemblance to reality of the numerical simulations is often startling. The time sequence of shock profiles of Biskamp and Welter [20], seems perfect rerun of an experiment. Here lies a further problem of the simulation. The shock has been stressed as a multi-component event of great complexity. The best simulation will be a numerical rerun of an experiment; it will show all the detail of the real shock.

Simulation shock waves are becoming increasingly complex. Understanding the shock wave resides in isolating the independent events of the complex. Optimally, these events are presented as analytic solutions of the relevant differential equations. They must of course be tested against experiment, and here arithmetic begins. As the mathematical knowledge retreats from analytic solutions, back towards mere presentation of the differential equations and boundary conditions, the arithmetical link broadens into numerical techniques. It is symptomatic that the more difficult the differential equation is to solve, the wider is the numerical band between theory and experiment. Thus it is interesting to regard the model above, in its simple form, as being closer to the solution of the Vlasov equation in laminar fields, than a simulation might be to the full Vlasov-Maxwell equations. It is

interesting, too, that the more simple the model the more it departs from reality. Thus the simplification is potentially closer to its disproof. Failure of the model destroys the assumptions of the model once and for all.

[There is an interesting short story due to Borges [27]. He tells of an ancient map - making guild which, ever dissatisfied with its maps of the World made then larger and larger until an accurate reproduction of the World was created. This short, short story ends as soon as it has begun by relating the grim fact that traces of this now obsolete map may still be found in remote regions of the Sahara.]

In the following sections, the model is compared with experimental results, and then extended by parameter studies. The former yields information on the structure of a particular shock, the latter on the relative influence of shock parameters.

§5 On the Culham and Garching Experiments

The model is explicitly designed to test the nature of ion heating. This only occurs in M>M* shocks, so that other examples might be ignored. However, from the above sections, it has been pointed out that an undetermined shock parameter is the electric potential. Thus the M<M* model will give a comparison (when no ion heating occurs), with M<M* experiments where potential has been measured. Such a shock is the Culham example, where $M_A \sim 2.5 < M^*$, $\beta = 0.04$. Further, their M>M* shock will give comparison of potential and ion heating. The Garching shocks were designed to test the $T_e \lesssim T_i$ dependence of shock structure; as a spin-off of this program, ion thermal behaviour is amplified. Thus it may be hoped that the definite (direct) ion heating measurement at Garching can be repeated. Thus their M>M* shock is studied. They give no measure of electric potential.

(a) The Culham Shocks. The two experiments may be usefully numbered C1 (at $M = 2.4 < M^*, \beta = 0.04$) and C2 (at $M = 3.5 > M^*$; $\beta = 0.1$). Since no ion heating has yet been measured when M<M*, the model, C1, must show ignorable heating, in particular, few reflection ions should be observed, while small departure from Maxwellian of the ion distribution should occur. At M>M*, C2 should show these effects very strongly. Figures 5.1 and 5.3 show the computer-drawn topography of the ion distributions of C1 and C2 respectively.

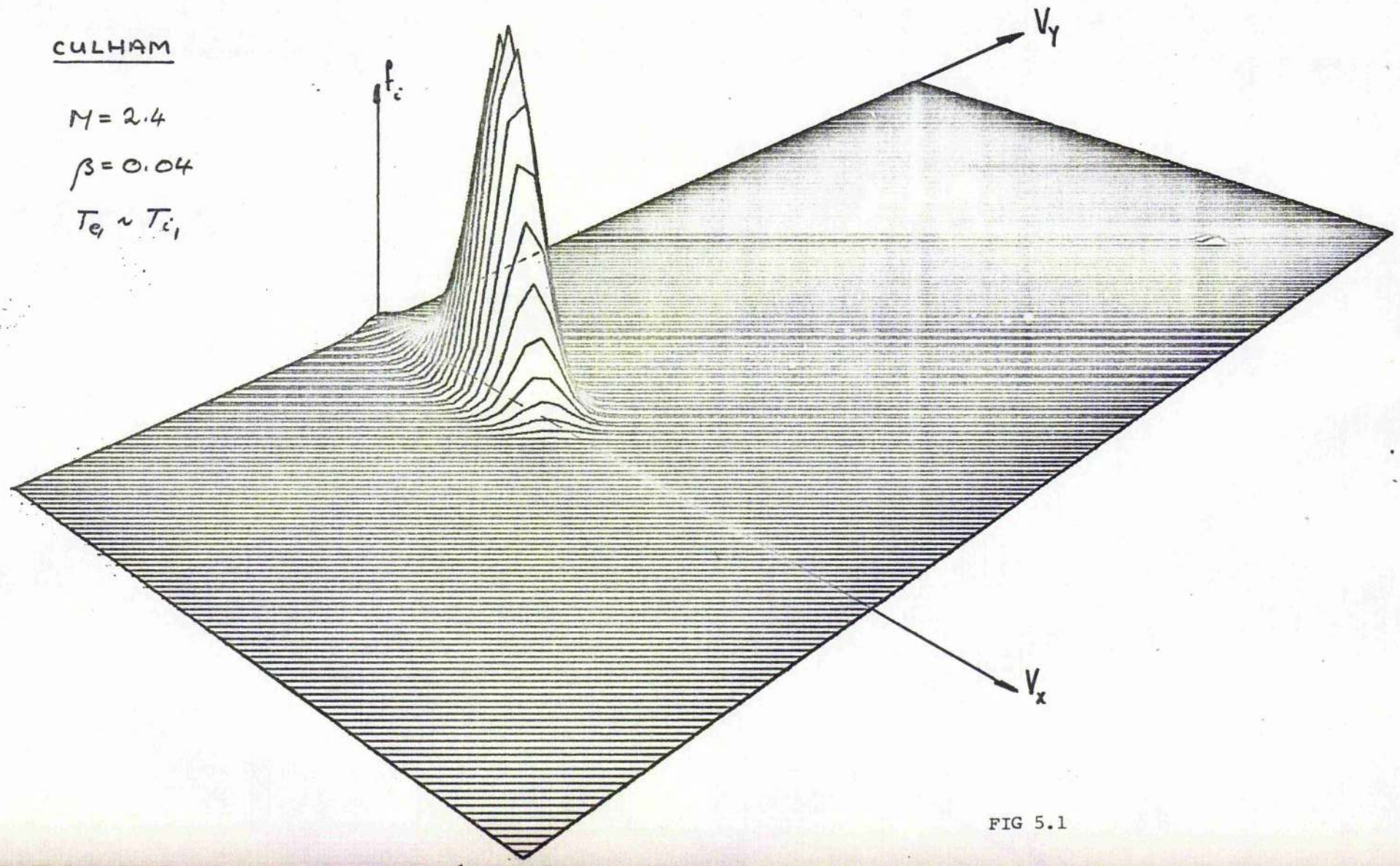

FIG 5.1

It is surprising then, that Fig. 5.1 shows strong distortion. There is elongation in the direction V_x, of the shock propagation. The elongation at small V_x is typical of the transformation of the axes under the distribution, $V_x \rightarrow \sqrt{V_x^2 - 2\phi}$ (in non-dimensional form) as discussed in §3. There is evidence of a small vertical cut at $V_x = 0$, with traces of reflecting ions occurring far into the first quadrant.

The behaviour is dominated, apparently, by the electric potential, with minimal ion reflection, in keeping with experimental observation when $M<M^*$. The value $M\sim2.4$ is quite close to the critical Mach number, $M^*\sim2.6$ (as given by Kornherr [8]) indicating that a quite sharp emergence of reflecting ions occurs at $M>M^*$. It is noted that the displays Fig. 5.1, 5.3, are generated under the convenient approximation $L_s=0$. A comparison of such presentations, with an $L_s\neq0$ case, is given below; no significant changes occur. The quantitative calculations are performed, of course, with $L_s\neq0$. Fig. 5.1 has no V_y- dependence then, and so pure Maxwellian cross-sections occur, unchanged from the upstream. The V_x-sections show significant stretching at low-V_x, with only small visual change from Maxwellian at higher values.

Quantification of the distortion heating held in such a distribution gives, for $M<M^*$,

$$T_{i2} / T_{i1} \sim 4.4 \text{ , while } T_{i2} / T_{iad} \sim 1.8 \qquad (5.1)$$

Thus even the low-Mach number shock finds ion heating. This result is reconciled with experiment for the following reason. The total downstream temperature may be calculated from the Rankine-Hugoniot relations,

and since laminar fields are assumed downstream (N_2, V_2, B_2, ϕ held constant) then by conservation of energy, T_2 is constant so that a comparison of the non-Maxwellian model with the R-H relations is permitted. Then the results (5.1) above show that ion heating is only $\sim$3.3% of the R-H level. The errors in measurement of electron temperature at Culham are $\pm$ 15%, so that detection of this small energy is impossible. The information (5.1) is then of no use in the verification of the model. The potential jump is found to be $\phi \simeq 0.4$, and this may be compared with experiment. Fig. 5.2 is a reproduction of the observed profiles of electric potential and magnetic field, taken from the first (1965) paper of Paul et al.[1]. The shock transition is marked, while the potential scale (volts) is duplicated by a non-dimensionalized (with respect to e/MV_1^2) statvolt scale. The very smooth rapid transition is noted in Fig. 5.2 (a), where $M<M^*$. In Fig. 5.2 (b), the foot structure is found, indicating reflecting ions at $M>M^*$. The rise $\phi \sim 0.4$, of the model, is then roughly comparable with example (a). As measured by the ratio of electric potential to the loss of beam kinetic energy of cold ions, $R_\phi = 2\phi/(1-V_2^2)$ in non-dimensional form, $R_\phi \simeq 0.96$; experimentally, $R_\phi \sim 1$ is claimed, and a favourable comparison may be made. An estimate from

over/

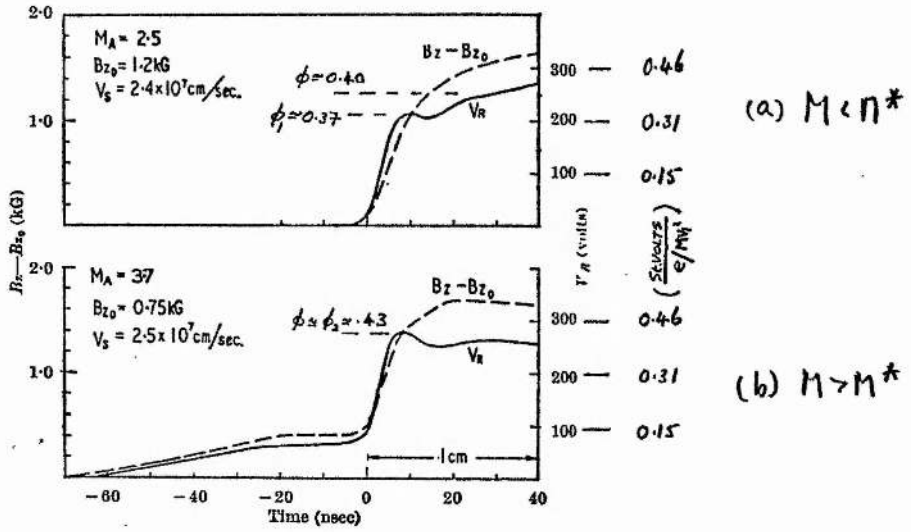

FIG 5.2

Fig. 5.2 (a), of the potential, gives $\Delta\phi \sim 0.37$, which is thus over-estimated by the model by some 8%.

Comparison may be made with C2 on two points - the ion temperature and electric potential. Here, the upstream β is increased from β = 0.04, to β= 0.1. Examination of the schematic distributions of Fig. 3.3 (a), (b), suggests that the number of reflected ions can be dependent on both the thermal spread of the distribution, and on the self-consistent value of the electric potential. The Culham experiments were varied by changing the initial magnetic field, but keeping the initial upstream plasma temperature fixed. Thus $T_{c1} \sim .0033$, $T_{c2} \sim .0036$ (in units of velocity V_1, and expressed as $2v_i^2$, where v_i is the ion thermal velocity). Comparison of the main beam of Fig.5.3, with Fig. 5.1, shows no visually perceptibly broadening. Since

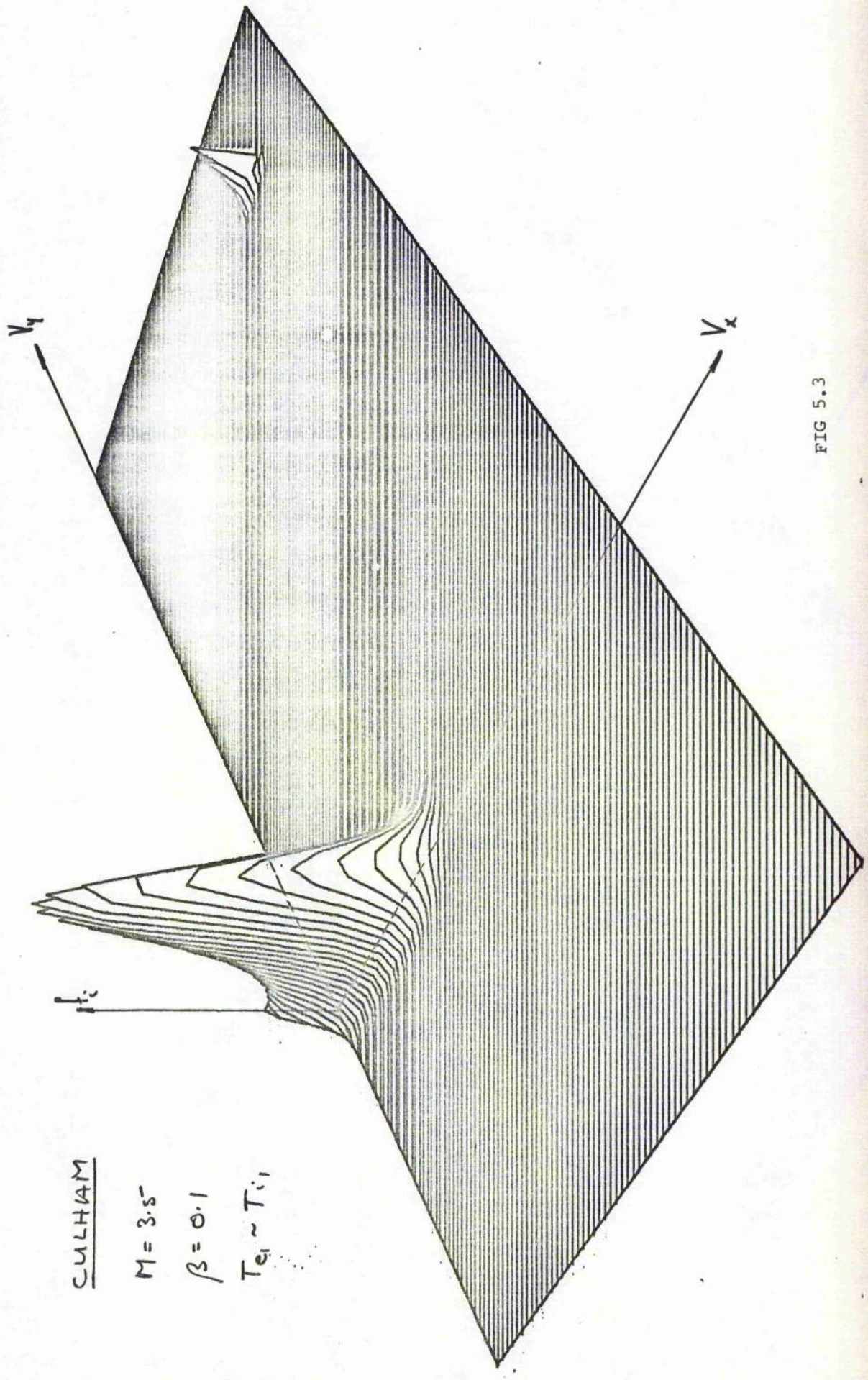

FIG 5.3

$\beta = Nk(T_e + T_i)/(B^2/8\pi)$, β is increased by a reduction of initial magnetic field. Since the ion thermal spread does not increase, the important changes when M>M*, are due to the electric potential.

The model finds $\phi_2 \underline{\sim} 0.43$. The ratio $R_\phi \underline{\sim} 0.96$, is again high, in spite of ion heating, but the Culham team noted that in their shock $R_\phi \sim 1$, M>M*. The model then has favourable agreement through R_ϕ, while the experimental value for ϕ gives, as estimated crudely from Fig. 5.2(b), almost precise agreement. It remains to examine the nature of the temperature jump.

In the case of the M>M* shock, these are, from the model,

$$\frac{T_{i2}}{T_{i1}} \underline{\sim} 17.4 \ , \ \frac{T_{i2}}{T_{iad}} \underline{\sim} 5.6 \qquad (5.2)$$

Then the model predicts strong non-adiabatic heating of the ions. The non-flow energy in the downstream is held in two degrees of freedom perpendicular to the magnetic field, and is held predominantly in the emergence downstream of a high-velocity tail of reflected ions. In spite of recrossing the shock potential, they retain enormous energy. With the total heating of (5.2) in mind, the breakdown into main beam, and that of reflected ions gives,

$$\frac{T_{i2}}{T_{i1}} \underline{\sim} 17.4 \ , \ \frac{T_{i2}}{T_{i1 \text{ main beam}}} \underline{\sim} 5.5 \ , \ \frac{T_{i2}}{T_{iad \text{ main beam}}} \sim 1.8 \qquad (5.3)$$

Where the adiabatic heating of the main beam is estimated using the total initial temperature. Only some 30% of the total energy resides here. The last result of (5.3) shows that the main beam is not heated significantly, as compared with the M<M* shock. The ratio of energies in the main

and reflected beams is

$$(T_{i2})_{Tail} \; / \; (T_{i2})_{Main\ beam} \;\; \underline{\sim} \;\; 2.1$$

Comparison with experiment is rather vague, due to the nature of the experimental results. These are shown in Fig. 5.4.

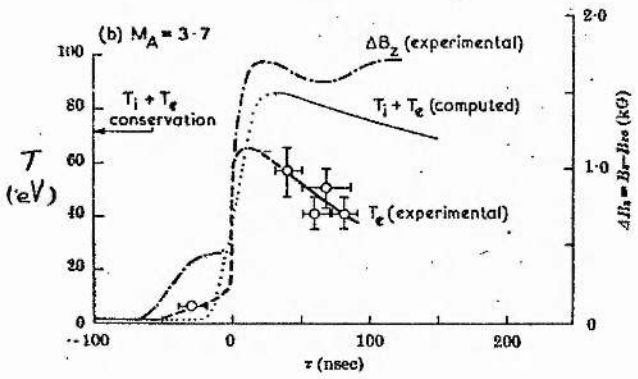

FIG 5.4

The measured conservation level is $T_e + T_i = 72$ eV. The peak electron temperature, in L_s, is calculated by extrapolating the measured results back so that the temperature profile corresponds with that of the magnetic field. When the error in this method, is superimposed on the $\pm$ 15% error loss, quite a large lee-way for the determination of ion temperature results. Peak electron heating in L_s is given by Paul et al. at $T_{e2} \sim 66$ eV. This represents an ion jump $T_{i2} \sim 6$eV, or a ratio $T_{i2}/T_{i1} \sim 5$. No direct ion temperature was taken. Further, no initial ion temperature was made. This can have quite strong effect on the final ion heating. It was calculated that the initial plasma exists long enough for thermal equilibrium $T_e \sim T_i$ to occur. These estimates were re-inforced by an MHD model [15] of the shock. This suggested a higher conservation level of 84 eV, allowing up to about 28% ion heating [4].

The smallest estimate, with $T_{i2}/T_{i1} \sim 5$, observed by Paul, is a temperature as calculated in three degrees of freedom behind the shock. The model finds $T_{i2}/T_{i1} \sim 17.4$, but in two degrees of freedom. If this energy is now dispersed in three dimensions, then the model predicts $T_{i2}/T_{i1} \simeq 6.6$. This may be compared with the experimental estimate, but allows for no electron heating in the thermalization of the distribution of Fig. 5.3. Fig. 5.4. shows, indeed, a reduction in electron temperature behind the shock which must be due to collisions, as thermal equilibrium is reached. The electrons emerge about 11 times hotter than the ions (in the model $T_{e2}/T_{i2} \sim 10$), and have considerable energy to share. These conditions are also ripe for electron heating (via unstable ion-acoustic modes) in the two-ion beam instability of Popadopoulos et al. [19].

The comparison then yields excellent agreement of electric potentials. The model, when the ion energy is dispersed in three degrees of freedom, gives $T_{i2}/T_{i1} \simeq 6.6$, while the experiment gives a minimum $T_{i2}/T_{i1} \sim 5$. (When electrons are considered, the model gives $T_{e2}/T_{i2} \simeq 10$, while experiment gives $T_{e2}/T_{i2} \sim 11$; conservation is at 72 eV). Thus, with some uncertainty which yet lies principally in the small ion heating with respect to the electrons (8.3%), the correct order of magnitude for ion heating may be claimed. There is then support for the laminar ion-heating mechanism, and that the ions have, experimentally, two degrees of freedom. Most of the heating is held in the fast tail. The matching of the observed foot of Fig. 5.2 (b), with the unimpeded orbit of a reflecting ion [14], is forceful suggestion

that some ion heating must be occurring as used in the model.

The ion heating was very tentatively suggested by the Culham team. The ion energy balance, if there is heating, does not apparently support the observed $R_\phi \sim 1$. This effect is reconsidered below, where a careful examination of theoretical predictions for ϕ is given, and represents new information on shock dynamics: that the reduction of ϕ in the balance

$$\tfrac{1}{2}MV_1^2 = \tfrac{1}{2}MV_2^2 + e\phi + [\text{heating}],$$

need not be met by the ion heating. (This may be roughly understood as an effective increase in upstream kinetic energy in the form of the accelerated reflected ions.)

The following data occurs, in the breakdown into the main and reflected beams:

$$\begin{aligned} V_2 &= 0{,}328 \quad & V_{2M} &= 0.319 \quad & V_{2T} &= 1.19 \\ V_{2y} &= 0.0 \quad & V_{2yM} &= 0.02 \quad & V_{2yT} &= 1.81 \qquad (5.4) \\ (n_2V_2) &= 1.01 \quad & (n_2V_2)_M &= 0.97 \quad & (n_2V_2)_T &= 0.04 \end{aligned}$$

Thus only about 4% of flux is lost to the reflecting ions. They have high beam velocities downstream. There is a clear resolution into main and reflected ions, and only one significant reflection off the shock front takes place. There is no confirmation for the results (5.4). A measurement of the density of a fast beam, which is supposed due to reflections, downstream of the Earth's Bow Shock has been made.[21] It is found to be about 10% of that of the main beam. But the conditions are not comparable with the Culham shocks, as the initial plasma is of much higher β. Some support can be found from a knowledge of the ion densities in the "foot".

The nature of the foot has been examined by Phillips and Robson[14].

They give an estimation for the jump in magnetic field there, in terms of the fraction of reflected ions. This is

$$b = \frac{B_{foot} - B_1}{B_1} = fG \cdot \frac{M_A^2}{M_A^2 - 1} \quad , \; G \sim 6 \quad , \qquad (5.6)$$

in an approximation of small b, f. Only the crudest estimate has been obtained from the model, for the density of the gyrating ions. The reflected ion beam has a flux downstream of ∿3.6%. Its mean velocity is ∿1.2, and after switching it back through the shock, should enter the shock with velocity, upstream, of ∿1.3. Then the density of only those ions entering the shock, is $f_E \underset{\sim}{\sim} .028$. To this should be added the density of ions leaving the shock by reflection. Regarded as accelerating from zero, back down the shock, and as having the same flux as when they enter the downstream, then $f_R \underset{\sim}{\sim} .038$. At the shock front the total density is estimated. From the observed height of the Culham foot, (5.6) gives an independent estimate for f. These are from model and (5.6) respectively.

$$f \underset{\sim}{\sim} 0.07 \qquad f \underset{\sim}{\sim} 0.08 \qquad (5.7)$$

There is thus reasonable agreement. But the densities upstream will have a difficult x- dependence in general, and no profound support for the model results. No explicit study of the dynamics of the foot has been attempted here. The growth of the magnetic field, its sensitivity to f, and to upstream perturbations remain a largely open research area.

The illustrations Fig. 5.2, show the smooth profiles in B and ϕ. These have been substituted by linear profiles which ignore the foot

structure. A quick estimate of the stability of the model solutions may be made by approximating $L_s = 0$. Then it is found that no significant change in any variable occurs. This is studied extensively below, but one interesting change emerges. From the results of (5.4), the downstream ions have no drift to the y-direction after leaving the shock. At the experimental value of L_s, the flux in that direction of the reflected ions is balanced by an opposite drift of the main beam. In the shock, these ions will see an averaged Lorentz force $-\frac{1}{C}\overline{V_x B}\,\hat{y}$. When $L_s = 0$, no such force occurs, and so there is no balance of ion flux. Conservation relations require that $V_{2y} = 0$. This results in considerations of shock thickness, below.

The effect of curving the profiles so that they merge smoothly with the upstream and downstream, merely alters the effective shock thickness. With respect to all variables, no significant change occurs. As long as ion currents in the shock are small (it is noted that the reflected ions have strong V_y in the shock, but small density), their effect on field gradients is small. From Ampere's Law in the Culham shock, $dB/dx = -J_y \sim 50$, while for the tail $J_{yT} \sim .05$, being 1000 times smaller. The linear profiles are then adequate.

The effect of the foot has small consequence to the ion dynamics. Being on the scale of the ion Larmor radius, they will see only a slow change in electric and magnetic fields. Since the effects of distortion heating of the transmitted ions, even in the resistive shock, are small (at least at the Culham parameters), there is no need to examine the laminar dynamics of the ions in the foot.

Thus some optimism for an agreement of the model with observations is felt. The mechanism of distortion heating is proposed and exhibited by the model, and displays temperatures that are of the order of those observed. The self-consistent electric potential generated by the model is comparable with experiment.

(b) The Garching Shocks. While only about 3.3% of total heating resides in the ion component of the Culham shock waves, the Garching experiments of Kornherr [18], and Kielhacker et al. [7], for example, have $T_i > T_e$ everywhere. The prediction of [8], is that under the conditions $\beta \sim 2.6$, $M \sim 4.9 > M^*$, $T_{i2}/T_{il} \sim 7.5$. Such heating is easily measured by the experimenter and the model may be sensibly tested. Again shock profiles were found to be smooth and stationary, so that laminar profiles could be considered. Shock thickness is $L_s \sim\sim 0.5\ C/\omega_{pi}$.

A second experiment with $M \sim 1.7 < M^*$, and $\beta \sim 0.4$ showed no ion heating. There is no apparent change of the two profiles. Thus as in the Culham example, the ions are unlikely to see turbulence at $M > M^*$ — this shock shows a "foot" in profiles [6], thus confirming the presence of reflecting ions.

These shocks seem ideal candidates for the model, as no explicit study of ion heating has been performed at other laboratories. Accordingly, at the parameters

$$M \sim 4.9,\ \beta \sim 2.6,\ T_e/T_i \sim 0.16,\ L_s = 0.5\ C/\omega_{pi},$$

and in the observed laminar fields, a run was attempted.

In the model, the "independent" variable in finding a solution

is the unknown electric potential. This must be varied until the ions reach a proper downstream drift, $v_2 = V_2$, consistent with the equilibrium there.

A plot of v_2 with ϕ is shown in Fig. 5.5

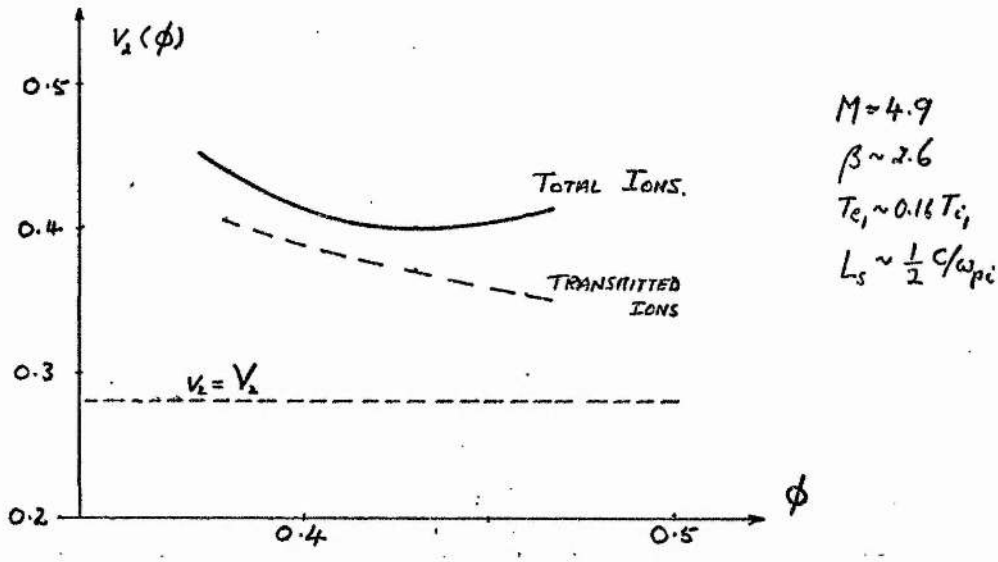

FIG 5.5

The hard line is the locus of the (not self-consistent) solutions for the total ion component. The dashed line represents the drift of the main transmitted beam. These make clear the effect of the fast reflected ion flux downstream. The electric potential is never sufficient to slow them consistent with the conservation relations, their velocity rising steeply as ϕ increases. The main beam cannot be easily slowed. Self-consistent solutions occur when the hard curve intersects the horizontal line $v_2 = V_2$.

Thus it is apparant that there is a limited solution subspace of the M, β-plane, available to the model. The space of solutions should be delineated, while the apparently suitable Garching experiments with

laminar steady-state fields, and measured ion dynamics, should be examined, if only to give a physical feel for the reasons for the model's collapse.

It is noted now, that in the region of the minimum of v_2, the model predicts $T_{i2}/T_{iad} \sim 9$, while Kornherr experimentally deduces $T_{i2}/T_{iad} \sim 7 \pm 1\frac{1}{2}$. Again most of the ion heating is due to the reflected ions. But it is further indicated that the density of the reflected beam, and its velocity, are increasing and thus growth rates of the ion-ion streaming instability increase. It is suggested then that the trapping of a few slow ions in the transition (the very ions that will be reflected) by a low level of ion-seen turbulence, might reduce the ability of the fast beam to overshoot the potential jump. Such ions will emerge in the main beam. Some heating can be sacrificed.

In the following sections, the physically relevant shocks will be examined first. Explanations of shock behaviour due to ion dynamics are examined in detail. In this, the advice of Sagdeev is followed, to investigate the simple, laminar, case first. Only in later sections will the appearance of turbulence in the model be discussed.

6 On the Ion Distribution Function

Some importance may be attached to the three-dimensional displays of the downstream ion distributions. Without them, the mechanics of the distortion is obscure. A number of these have been generated, and will appear in later sections. In this section, the shape is considered for a particular example.

The displays are drawn over a regular grid in $\underline{v}_2$. Construction of the surface is not automatic with the running of a model shock. The grid size is limited to 121^2 ions, which is seldom compatible with the requirements for accurate integration over f_{i2}; in general, the smooth main beam can be described over a coarse grid size, while the small sharp tail (Fig. 5.3) requires a finer. It is apparent from Fig. 5.3, that the tail as drawn would not give accurate definition of f_{i2}. Thus each display requires special construction.

The figures 5.1, 5.3 above are drawn in an approximation of zero L_s. In Figs. 6.1, 6.3, two runs at M=2.4, β=0.1, with shock thickness $L_s = 1/6\ V_1/\Omega_i \sim 16\ C/\omega_{pe}$ and L_s=0, respectively. Figure 6.1 is supplemented by a scatter of orbit end-points in $\underline{v}_2$, created by a forward integration of ions (dispersed on an initial regular grid over the ion Maxwellian). This holds further useful information on the ion dynamics. Shape is given to the scatter by truncating f_i at some suitably chosen contour of constant f_i in the distribution topography, so as to show the elongation of the main beam, and the position of the tail. The scatter is shown in Fig. 6.2.

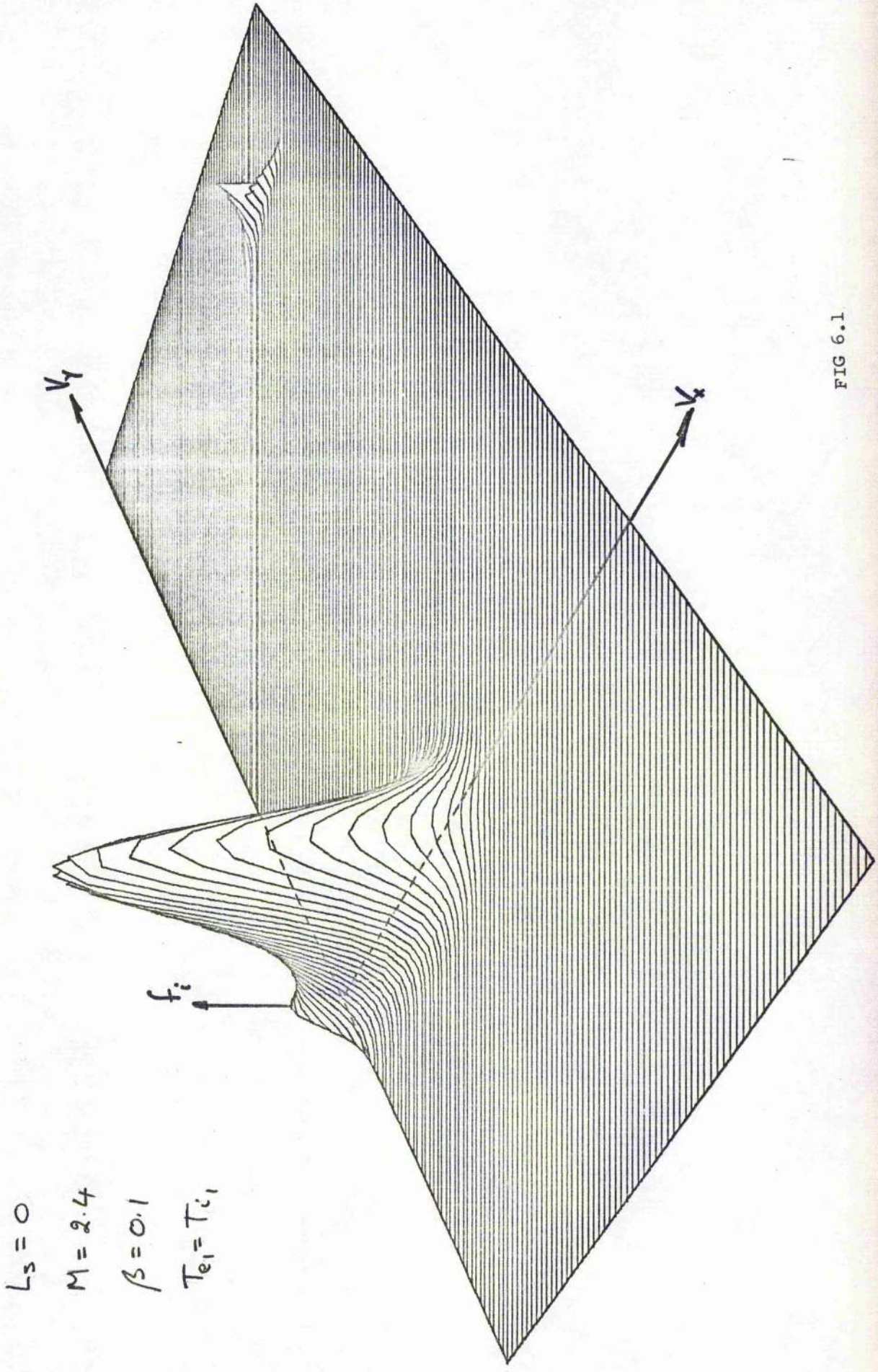

FIG 6.1

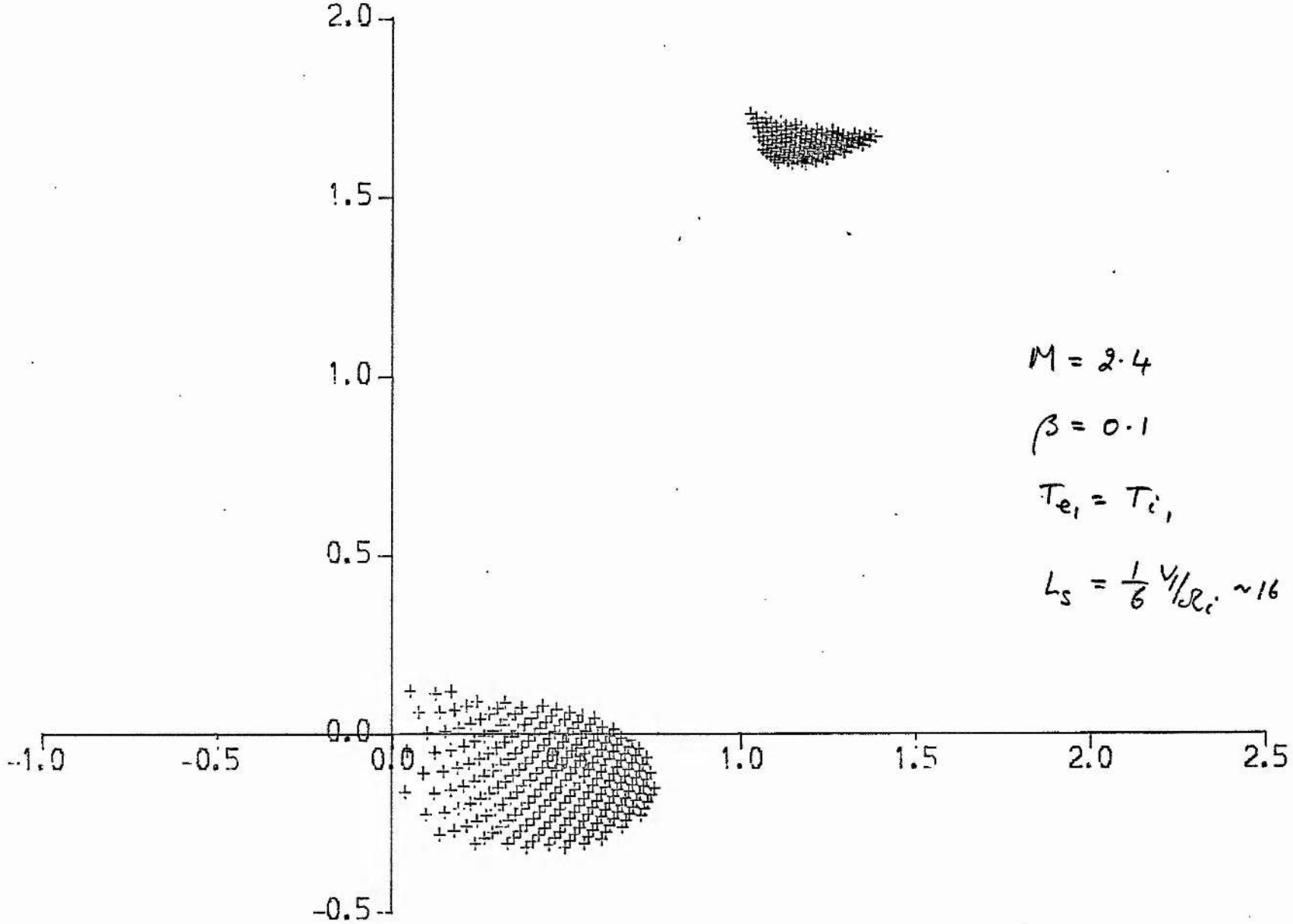
2.0
1.5
1.0
0.5
0.0
-0.5
-1.0
-0.5
0.0
1.0
1.5
2.0
2.5
M = 2·4
β = 0·1
$T_{e_1} = T_{i_1}$
$L_s = \frac{1}{6} V_{\parallel} / \Omega_i \sim 16\, c/\omega_{pe}$

FIG 6.2

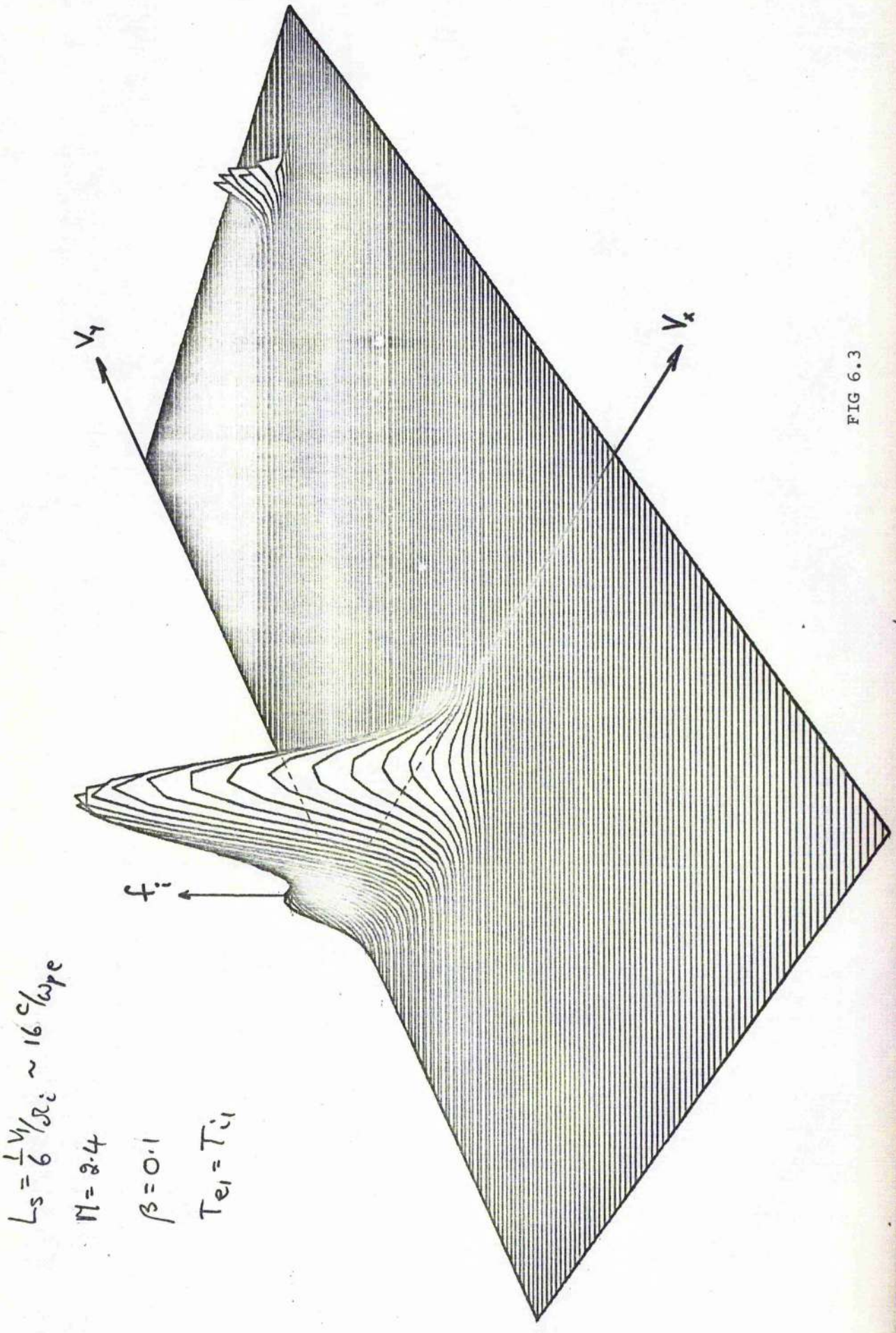
$L_s = \frac{1}{6} V_1/\Omega_i \sim 16\, c/\omega_{pe}$
$M = 2.4$
$\beta = 0.1$
$T_{e1} = T_{i1}$
f_i
V_y
V_x

FIG 6.3

Many points arise. The very clear separation into reflected and transmitted ion beams is again clear. The former beam has a considerable drift, $+V_y$, while the total drift relative to the main beam is of order $2V_1$. The initial upstream ion distribution is extremely localized at these small values of β_i ($= \frac{1}{2}\beta$), which in the non-dimensionalized model is essentially a measure of thermal spread. Thus the reflected ion beam, sliced by the potential from a narrow f_{il}, may be expected to be itself localized. In the time-frozen model, no diffusion in velocity space will occur, both to create a monotonic type distribution (stable) and to remove the vertical faces in the main beam and tail (non-resonant velocity space diffusion). Then again, the topology of the surface f_{i2} is maintained, with the vertical face well defined. The localized low-β tail is effectively turned by the potential at a single point close to the rear of the shock. As ion thermal spread increases, so significant ions are reflected from all points in the shock, helping to broaden the tail. The resolution of the tail is reduced further, at high β_i, as illustrated in Fig. 6.4.

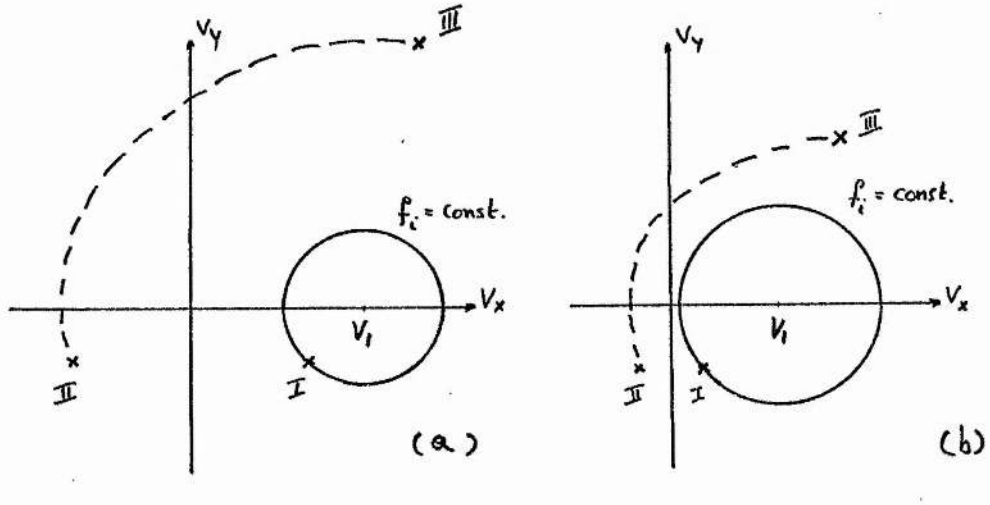

FIG 6.4

If the ion at point I(a) is bounced off the electric potential (say L_s=0), it reappears in velocity space at the point II(a), It then gyrates gaining energy to III(a), remote from the initial circular contour. In example (b), the same contour in a much hotter ion distribution, will result in the ion at I(b), re-emerging in velocity space at II(b), a small increase in ion energy. It then gyrates to III(b), where it re-enters the shock front. If $L_s \lesssim 0$, then no distortion of the distribution in the V_y-direction occurs, and the tail of example (b) is then less remote from the main beam, after crossing the shock, than example (a). This is illustrated below. Typical of the hot Garching ion beams, is a bridging of the two beams.

The figures show that only one significant reflection off the shock front is necessary at low β. This may be seen by the fact that there is no vertical cut at V_x=0 in the tail.

It is apparent from Fig. 6.1 that slopes of f_i up to the face of the tail are very steep. There are problems here in the numerical integration of the tail. The first lies in the precise location of the vertical face. The tail is located by a course forward scatter as in Fig. 6.2, but most of the contribution from the tail comes from the region very close to the vertical face. It is thus often necessary to run a fine-scale search along a line V_x=constant, through the tail, to find a point such that f_{max} (in the tail) $\sim f(V_x=0)$. Just one such point in the tail is sufficient to allow the outward progression of the model, point by point, from that point, and yet maintain high flux. The face in the tail is rotated so that it is no longer parallel to

that of the main beam. Each ion in the tail is locked into its Larmor orbit in the reflection procedure, and then has a shock transition time to gyrate about B, taking the distribution with it. The angle of the face to the V_x-axis is always small. Thus while the high-point of the tail is accurately calculated, the numerical progression along a Cartesian grid will see the peak values of f, along the cut, disappear into the discrete grid. However, the tail is quite localized in V_y = constant cross-sections, so that location of f_{max} (in the tail) gives sufficient accuracy.

The Simpson rule is of course very accurate. The requirement of an odd number of grid points, and the cuts in the beams make the numerical procedure slightly more involved. Fig. 6.5 indicates schematically how the Rule fits its parabolas to the very steep tail, as even or odd points are chosen.

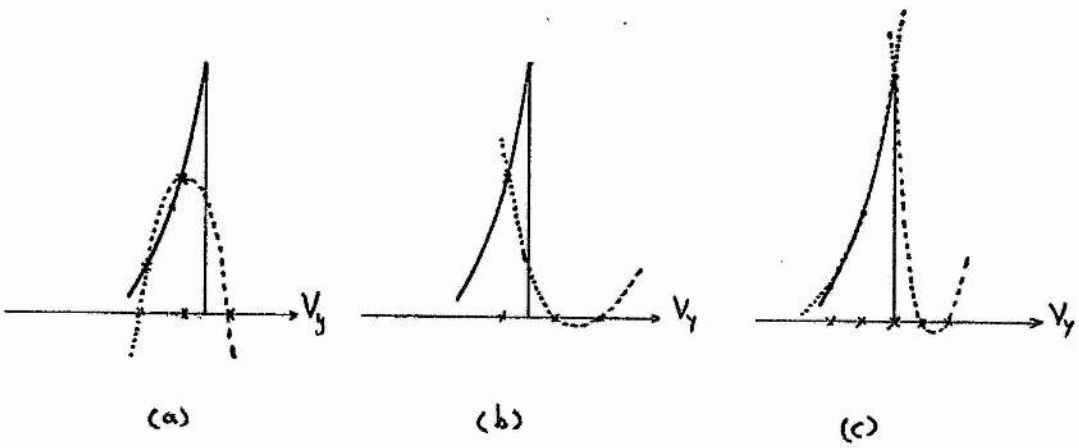

FIG 6.5

Examples (a) and (b) will show very different heights in comparison with $f(V_x=0)$, at the cut in the main beam. Large amounts of reflected ion flux may be lost, or when the beam is small, large thermal energy contributions (In Fig. 6.1, this represents some 80% of total heating downstream). Example (c) represents the way the model is designed to use the (current) three grid points, Accurate contribution to the left of the face occurs; the region to the right clearly deminds a fine grid size. If the parabolas were shifted one point either way, a strong over-estimate of flux would occur. In the main beam, this problem is overcome by starting the integration at the face, $V_x=0$. This is not convenient in the tail where the face is not well-defined.

The transmitted ions show a number of properties as well. First the expected elongation of the distribution along the direction of shock propagation is found, and is apparently the same in both $L_s=0$, $L_s=1/6 \times V_1/\Omega_i$ shock waves. In the latter case (Fig. 6.1) the whole beam has been rotated through some angle, again in the sense of ion gyration about B_z. The degree of rotation is dependent on transition time, and of course on a complicated variation with $B_z(x)$ in the shock. From Fig. 6.1, or Fig. 6.2, this rotation when $L_s \neq 0$, is not very strong. When the magnetic field dynamics in the shock is ignored, by setting $L_s=0$, no such rotation can occur. From a comparison of Figs. 6.1, 6.3, this would appear to be the only change. It is not surprising then that the Culham examples were accurately duplicated by $L_s=0$ approximations. In following sections, such $L_s=0$ displays are suitable for their purpose. In each case the rotation of the main beam must be understood.

Now in the physics of the model, which, again, is regarded as a good approximation to the physics of the real shock, the beams show strong non-Maxwellian form. As in the Culham example (plotted at $L_s=0$), the distortion of the main beam is typical of the transformation of the axes under the distribution

$$v_x \to \sqrt{v_x^2 - 2\phi} \quad : \quad f = \text{constant} \quad . \tag{6.1}$$

This is apparently little affected when $L_s \neq 0$, and the magnetic field dynamics are included.

The stretching near $V_x = 0$ is extreme. This is important. For while there is a flux of fast ions, with velocity much greater than that required by the conservation relations, downstream, it is necessary that the main beam be "over-slowed" to compensate. In the absence of reflected ions, the energy balance equation for the ions at $\pm\infty$ will be the usual form

$$\tfrac{1}{2}MV_1^2 = \tfrac{1}{2}MV_2^2 + e\phi + [\text{heating}] \tag{6.2}$$

Now the skewing to small V_x is vital in this case, for $R_\phi < 1 \Rightarrow V_x(f_{max}(1)) \to V_x(f_{max}(2)) > V_2$. Then if the distribution remains symmetric on crossing the shock (when $L_s = 0$), simultaneous slowing and heating of the plasma cannot be effected, consistent with the conservation relations. This is illustrated in Fig. 6.6 (a). Fig. 6.6 (b) shows that skewing of the ions towards low V_x can of course make $v_2 = V_2$.

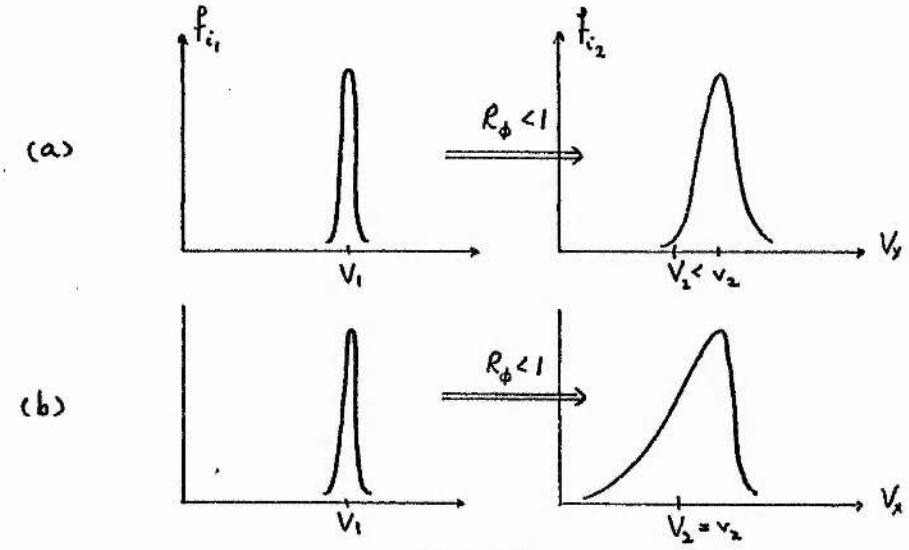

FIG 6.6

It might be argued that (6.2) does not apply when reflected ions occur, and that this is the only time (M>M*) when ion heating has been observed. However, the inclusion of the fast reflected ions is such that they sometimes cannot be slowed, as in Fig. 6.5 (a), whatever the value of R_ϕ (the Garching example) so that all mechanisms capable of over-slowing the ions are tested to an extreme. In the Culham example, with reflected ions, $R_\phi<1$, ion heating does occur, and so the main beam must be skewed only, to compensate for the fast tail. (Since $R_\phi<1$, $V_x(f_{max}(1)) \rightarrow V_x(f_{max}(2)) > V_2$, under the transformation (6.1)).

The scatter-gram of Fig. 6.2, indicates this skewing by a low density of ion endpoints in the region $V_x \gtrsim 0$. A transformation which preserved Maxwellian form, could not slow this shock properly. (The low "density" at $V_x \gtrsim 0$ has no physical meaning - density (proper) is measured by the height of f_i in this region and may be very high - except to say something of orbit types in the shock).

Information of the ion dynamics is easily drawn from the scattergram. The main beam shows a regular pattern of upward sloping ion endpoint loci. At small $V_x \gtrsim 0$, they are widely spaced, and as V_x increases they come closer together. Inclusion of magnetic field dynamics induces the sloping loci. It is obvious that these have rotated due to the transition time Larmor gyration of the whole distribution. But when compared with the rotation angle of the elongated distribution as a whole, they appear to have undergone a further convolution. In Fig. 6.7, the points II and III in $\mathcal{V}_1$, are on a contour of equal f_1. They transform to II', III' in $\mathcal{V}_2$. The point I is the position of f_{max}. It orbits to I' in $\mathcal{V}_2$.

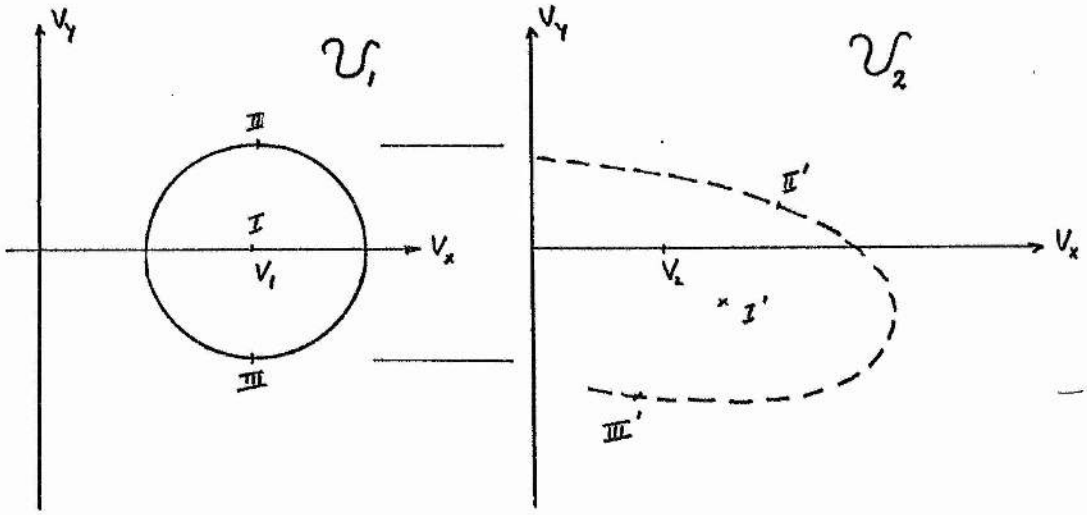

FIG 6.7

Ion number I at $f_{max}(1)$ is slowed by ϕ (such that $R_\phi<1$) to a point I' such that $V_x>V_2$. The magnetic field now allows the inclusion of a Lorentz force averaged across the shock, $\frac{e}{c}\overline{\underline{V}\wedge\underline{B}}$. Since $V_y(I)=0$ (at the shock front, at least), there is an averaged force $-\frac{e}{c}\overline{V_x B}$, in the direction of negative V_y. This accounts for the displacement to I' in $\underline{\mathcal{V}}_2$. If there is a final exit velocity $V_y \neq 0$, then there is a further adjustment to the V_x co-ordinate. Thus same averaged Lorentz force $\frac{e}{c}\overline{V_y B}$ will help the potential to slow the ion. The orbit is clearly complicated, even in this simple model.

The over-rotation of the locus through II', I',III', with respect to the rotation angle of the whole beam, is then brought about by the different V_y components of the ions II, III, in V_1. Ion II always has a positive V_y velocity. It thus experiences an averaged Lorentz force $+\frac{e}{c}\overline{V_y B}$, helping it through the shock. Ion III conversely, always sees a negative averaged force $-\frac{e}{c}\overline{V_y B}$, thus helping to slow it across the shock. Thus III' appears in $\underline{\mathcal{V}}_2$ with $V_{xIII}' < V_{xI}'$ while ion II' appears with $V_{xII}' > V_{xI}'$. The orbits followed by II and III are not in general symmetrical in L_s, so that differing displacements to V_y may result.

All ions will show this behaviour to lesser or greater extent. It is clear that the faster the ion enters the shock, the greater the mean Lorentz force $-\frac{e}{c}\overline{V_x B}$, to $-V_y$. There is minimal compensation for this displacement by some ions spending a longer time in the shock.

Thus the whole distribution sees a displacement to $-V_y$, in the main beam. In the region $M<M^*$, ion reflections do not occur. The drift V_{y2} must be halted by interaction with the electron current. When $M>M^*$,

reflecting ion currents with large drifts to $+V_y$, may balance this drift as has been seen in the Culham shock wave. This is of interest below.

The distortion of Maxwellians in V_y-cross sections is small. There is the electric field E_y-constant, covering the whole space. For an ion projected to $\pm V_y$, there is a change in velocity according to $V_{y_1} \rightarrow \sqrt{V_{y1}^2 \pm 2E_y Y}$, where y is the displacement on the ion. This is always found to be small. Opposing each motion is cyclotron gyration.

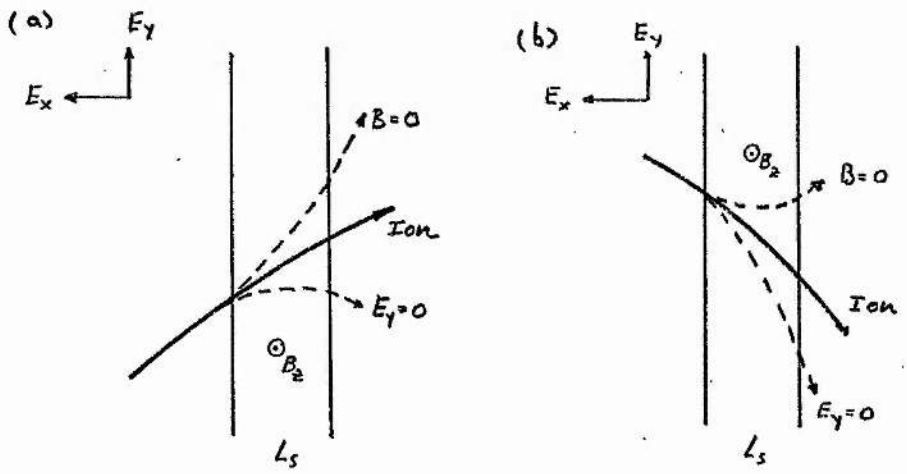

FIG 6.8

Fig. 6.8 illustrates schematically the actual ion motion (hard curve) and the motion if either field is turned off. The scatter of Fig. 6.2 shows very small variation in "density" with change in V_y, suggesting that the forces of Fig. 6.8 balance each other. Surpressing all magnetic field dynamics, by putting L_s=0, to force Maxwellian V_y-cross sections downstream, finds no significant reduction in distortion heating. The main effect of putting L_s=0, is, at some parameters, to

increase the number of reflecting ions.

The shape of the distribution is then fairly easy to understand within the framework of the model. Direct comparison of these mechanisms with experiment cannot be expected. Only the general shape of the electrostatic distortion (6.1) is shown in the one measured ion distribution known, due to Schumacher [24] (Fig. 3.2). The effects of rotation of the main beam will be small since $r_i >> L_s$, while for the same reason, the ion dynamics when $L_s=0$, mentioned above, will be ignorable. Their important consequences lie in ion heating. This is dominated by the reflected tail.

As indicated above, the simulations of Biskamp and Welter [20], and the Bow Shock measurements of Montgomery [21], show that some collisionless shocks will find a fast downstream beam. There is then some support for the model. Due to the dominance of the electric potential in the transition dynamics, it is important that this should agree with experiment. This causes the partition into reflected and transmitted ions. Then some attention should be given to the non-trivial reflected ion orbits.

The physical interpretation of the reflected ion heating may be taken from Fig. 6.9. Here the orbit of the mean reflected ion is plotted. The simple orbit of a transmitted ion is shown. The Larmor radii for upstream and downstream conditions are respectively $r_{i1} \sim 0.6$, $r_{i2} \sim 0.5$. Thus ion temperature has not quite matched the magnetic field jump across the shock, so that $r_i = v_i/\Omega_i$ (v_i = ion thermal velocity) has decreased slightly. The cyclotron frequency has been increased about 2½ times,

FIG. 6.9

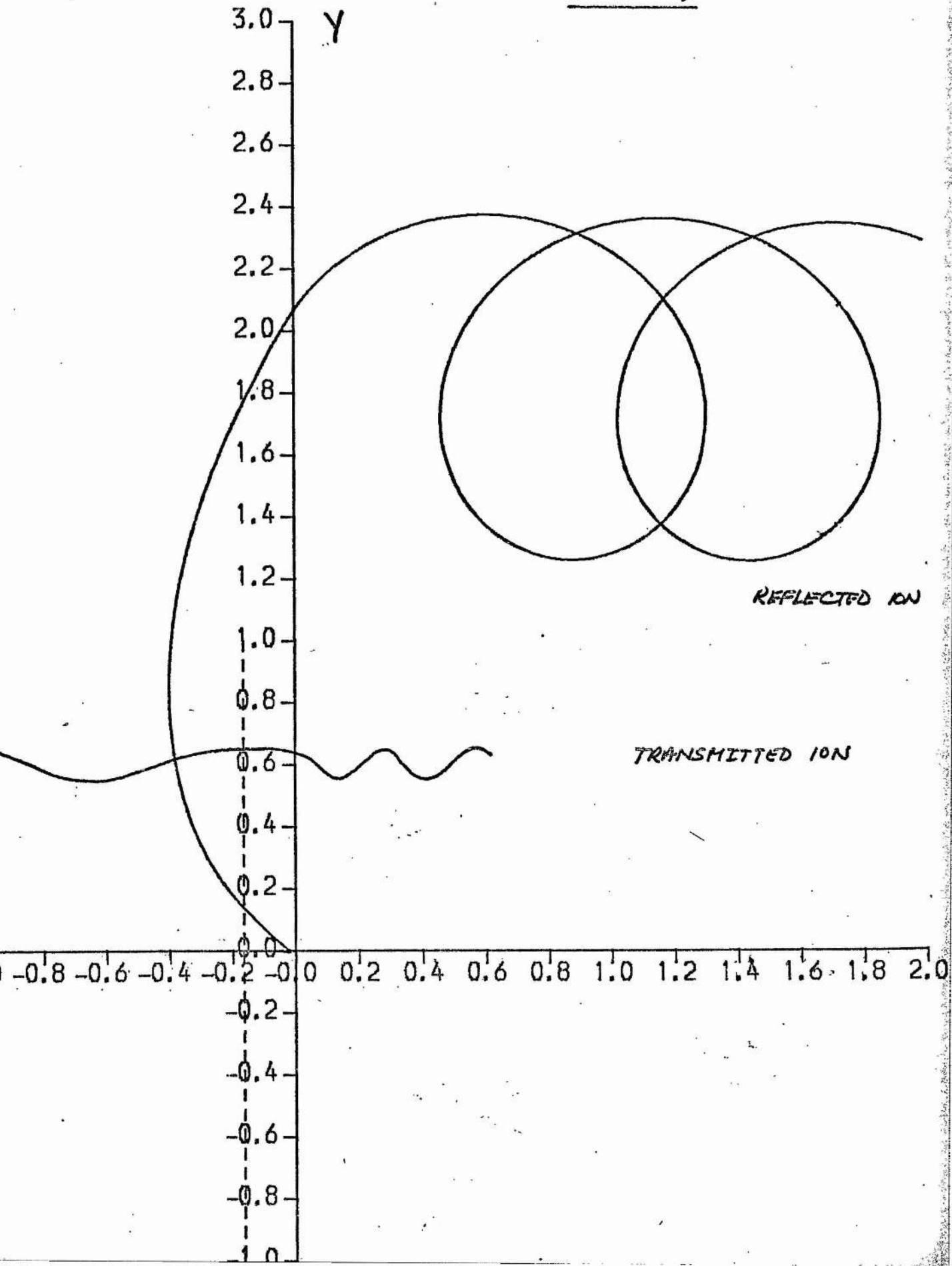
Y
3.0
2.8
2.6
2.4
2.2
2.0
1.8
1.6
1.4
1.2
1.0
0.8
0.6
0.4
0.2
0.0
-0.2
-0.4
-0.6
-0.8
-1.0
-0.8 -0.6 -0.4 -0.2 -0.0 0.2 0.4 0.6 0.8 1.0 1.2 1.4 1.6 1.8 2.0
REFLECTED ION
TRANSMITTED ION

consistent with the jump in B.

Since ion temperature is measured as non-flow motion (with respect to the conservation velocity, V_2, downstream), the transmitted ion temperature is small compared with the large Larmor gyration of the reflected ion, or its very large beam drift, $V_T \sim 1$. The transmitted ions have $V_M \sim V_2 \simeq 0.4$. Their Larmor radius is about 10 times smaller than that of the reflected ion. In this shock about 89% of non-adiabatic heating lies in the reflected ions. The rest lies in the distortion of the main beam. (This heating may be understood similarly as the creation via non-adiabatic orbits of larger Larmor orbits for some ions).

The spatial scaling of the beam, at its upstream turning point, is

$$x \sim -\ 0.4\ V_1/\Omega_i \sim -\ c/\omega_{pi}\ ,\ y \sim 2\ \ V_1/\Omega_i \sim\ 5\ c/\omega_{pi} \qquad (6.3)$$

These numbers will depend quite substantially on the initial phase of the ion orbit. Drawings similar to Fig. 6.9 have been derived by Auer et al. [18], in connection with a particle simulation on the Earth's Bow Shock. This paper suggests for the first time the importance of reflected ion beams in explaining an observed fast structure (Montgomery [21]), downstream of the Bow Shock. The paper is interesting for they deduce that the ion-ion instabilities cannot explain the observed thermalization of ions. Further they propose that ion reflections supply an initial coarse dispersion of ions in velocity space. It is in the program of this thesis to test this latter statement - a study not made by Auer et al. - and to extend their work.

There is one further orbit type found to occur. This is shown in Fig. 6.10, and is characterized by a temporary emergence into the downstream, of an ion.

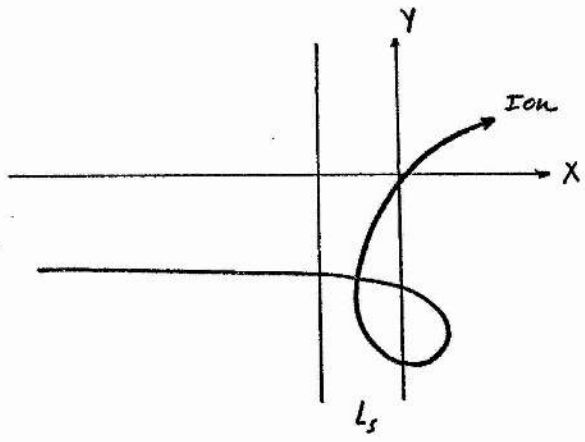

Fig 6.10

Calculation of this orbit clearly requires knowledge of the downstream state. They are infrequent and only at very high β_i, do they carry significant f_i. It may be noted that since Ω_i is large downstream, they spend a short time there, being rapidly returned to the shock. The accelerating electric field E_y will have a short time to operate, and be less dominant than upstream, in creating a high-energy orbit.

7 Further Considerations of Self-Consistency

It has been shown above that the model can give estimates of shock heating that bear comparison with the Culham experiments. Further, the self-consistent solution found matches other observed values quite well. At this point it is convenient to regard the model as a useful tool applicable in the study of collisionless shock waves, at least in some region of M,β- space, and that the mechanisms of the model occur to lesser or greater extent in all shocks. The model is of interest primarily in its physical relevance, that is, in the solutions that do occur. In the next sections variation of parameters will be made with M and β, only where sensible solutions can be found. It then remains to investigate the solution domain. Further, dependence of heating on other variables such as T_e/T_i, L_s, must be investigated. Thus a generalization of the model beyond the knowledge of a particular experiment is made. While T_e/T_i is independent, the role of L_s is not yet clear, and in this section is discussed.

From section §4, it was shown that downstream bulk velocity $V_{y2} = 0$. This is predicted by the R-H relations when $B_x = 0$, and is further built into the model as an assumption, in integration of orbits in the downstream (Eqns 4.17). Thus "two" definitions of non-flow energy of the ions can be made. These are

$$n_2 T_2^{(a)} = \int d^2v \, (v_x^2 + v_y^2 - V_{x2}^2) \, f_2 \qquad (7.1)$$

$$n_2 T_2^{(b)} = \int d^2v \, (v_x^2 + v_y^2 - V_{x2}^2 - V_{y2}^2) f_2 \, .$$

The second will give the proper non-flow energy. If the model is working well it must be identical with the first, which is thus held as a check on the self-consistency of the model. It is noted again, that at the observed values of parameters on the Culham shocks, no significant difference (less than 1%) is found between $T^{(a)}$ and $T^{(b)}$. A very small net drift, $V_y \sim -0.01$ is found, but V_y^2 is then negligible in the accuracy of the model. Some importance may be placed on the check, for the reflecting ions carry large kinetic energies into the downstream.

The study begins as a variation at fixed β=0.1, $T_{e1} = T_{i1}$, with magnetosonic Mach number. The aim is to elucidate heating dependence on M. The study must eventually be extended by additional curves at various β. The β = 0.1 study will show not only heating, but as a spin-off, some information occurs to suggest that a self-consistent shock length emerges from the model. The relation between shock thickness and ion dynamics has not been proposed quantitatively (and to present knowledge qualitatively) before.

In Fig. 7.1, the non-adiabatic heating of the ions according to the definitions (7.1) are shown. Total heating is given by the hard curve, while the contribution to the heating due to the transmitted ions is given by the dashed curves.

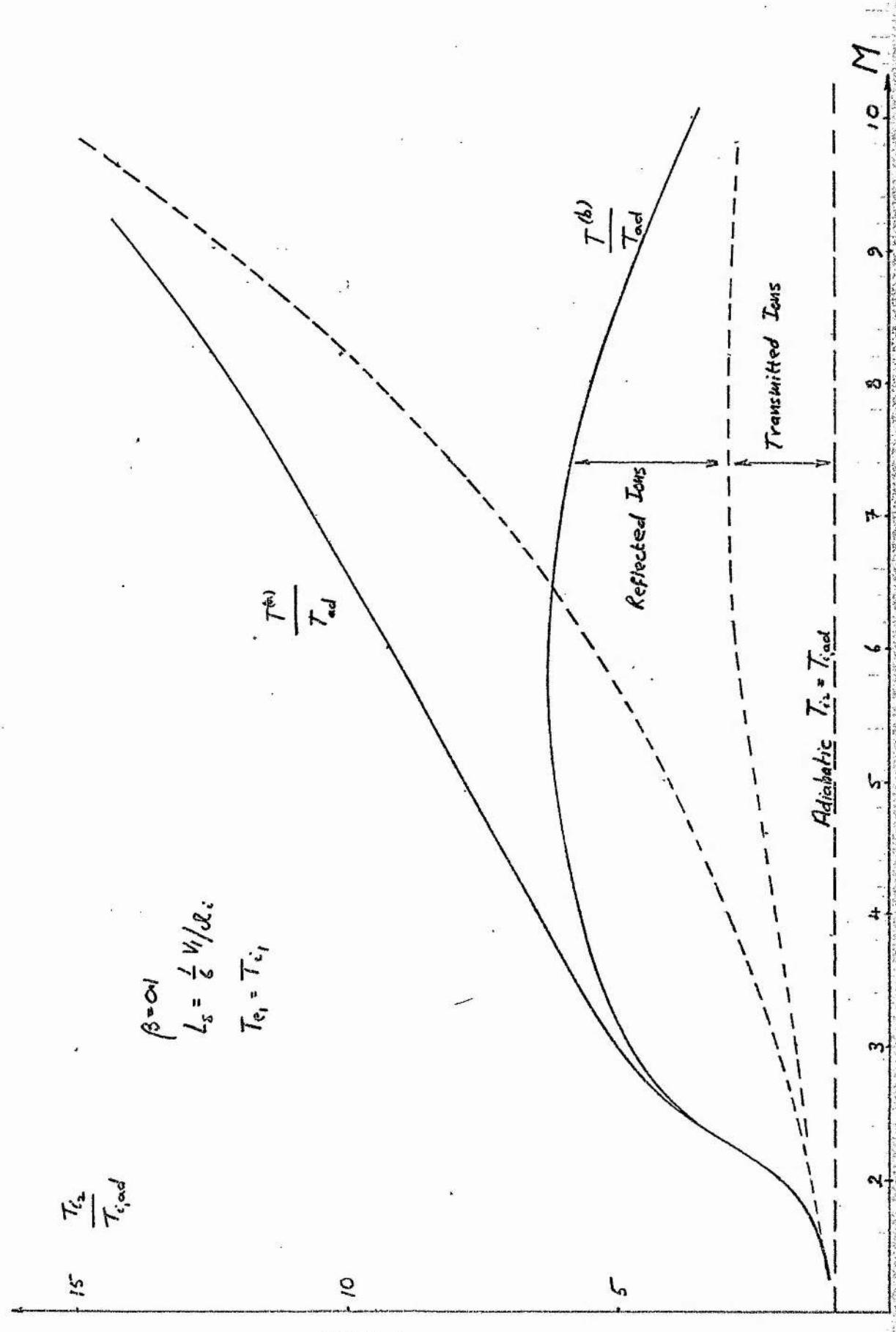
$\frac{T_{i2}}{T_{i,ad}}$
15
10
5
$\beta = 0.1$
$L_s = \frac{1}{6} V_1 / \alpha_i$
$T_{e1} = T_{i1}$
$\frac{T^{(a)}}{T_{ad}}$
$\frac{T^{(b)}}{T_{ad}}$
Reflected Ions
Transmitted Ions
Adiabatic $T_{i2} = T_{i,ad}$
2
3
4
5
6
7
8
9
10
M

FIG 7.1

There is noticeable, large, divergence in non-adiabatic heating at large $M \gtrsim 2.5$. Thus at M=8, $T^{(b)} \sim 0.4\ T^{(a)}$. The shock thickness has been fixed at $L_s = 1/6\ V_1/\Omega_i$. Then since $V_1/\Omega_i = M_A\ C/\omega_{pi}$, with $1/6\ V_1/\Omega_i$ fixed and M_A increasing, the $C/\omega_{pi,e}$ scales are decreasing with M. Or, at M = 10, for example $L_s = 1/6\ V_1/\Omega_i \sim 1.7\ C/\omega_{pi}$. Experimental observation of steady state shocks puts $L_s \lesssim C/\omega_{pi}$ in the low-β region of β=0.1, even for high Mach number. It seems clear that the choice of shock thickness is not arbitary in developing a self-consistent solution; it is not sufficient to choose ϕ, the electric potential, consistent with the condition $V_1B_1 = V_2B_2$ of the Rankine-Hugoniot relations. L_s must be adjusted so that $V_{y2} \simeq 0$. As $M_{ms} \to \infty$, then $V_2/V_1 \to \frac{1}{4}$ from above. (This limit comes from the R-H relations-increasing Mach number at constant β implies increasing upstream energy in Kinetic form, so with β= constant, less effect from temperature ($\to$0) and magnetic field ($\to$0) is expected). With $L_s = 1/6\ V_1/\Omega_i$ fixed, the velocity jump becomes a maximum, so that transit time for the ions increases. The propulsive force in the y-direction is an averaged Lorentz force $\frac{e}{c}\overline{V_x B}$. In the non-dimensionalized form here, the quantity $V_1B_1=V_2B_2 = 1$ at $\pm\infty$, for all shocks and so the mean Lorentz force may be regarded as approximately constant from shock to shock. Thus ions will be expected to show an increased displacement to -y with increasing M, when L_s is fixed at $1/6\ V_1/\Omega_i$, due to longer transition times.

To investigate the behaviour of the model in its y-dependence, additional moments of the distribution are calculated according to

$$(n_2 v_{2y}) = \int v_y f_2 \, d^2v = (n_2 v_{2y})_m + (n_2 v_{2y})_T$$

with $$v_{2y} = \frac{1}{n_2} \int v_y f_2 \, d_2 v \qquad (7.2)$$

In Fig. 7.2 is shown the variation of the scales lO C/Ω_{pe}, C/Ω_{pi} over the plane of M, β-space, when the shock thickness is held at $1/6\ V_1/\Omega_i$ in the whole plane.

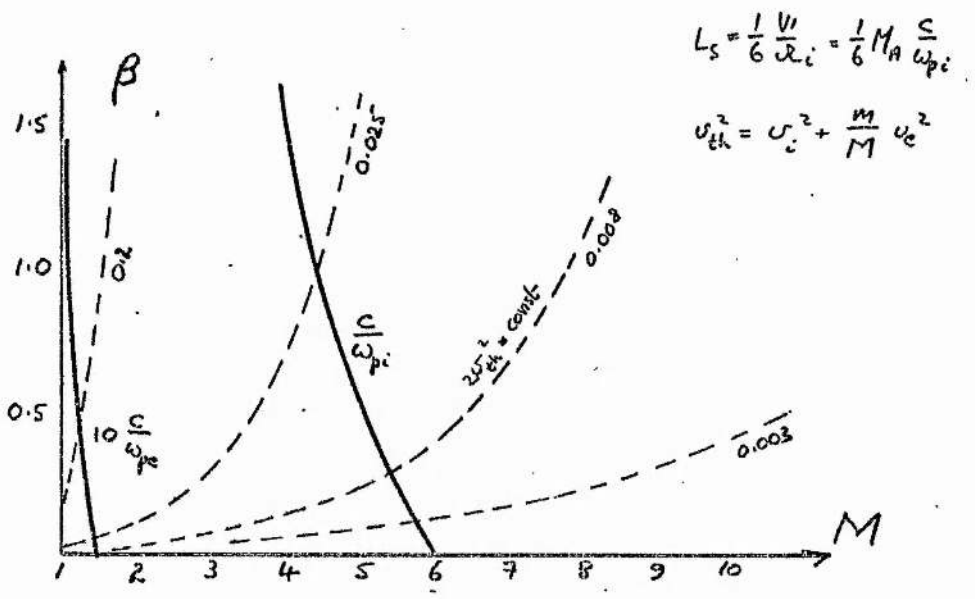

FIG 7.2

In Fig. 7.3 is shown a plot of v_{y2} with M. The hard lines give the drift of the total plasma (which is approximately that of the main beam of transmitted ions), while the dashed line indicates the drift of reflected ions. These values are measured as the shock emerges down-stream.

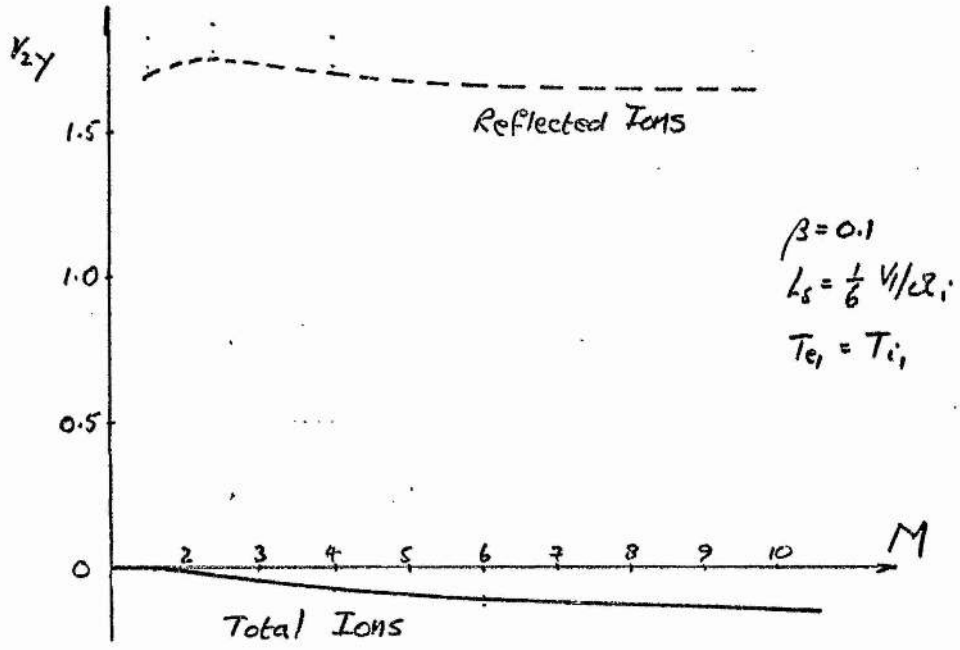

FIG 7.3

No reflected ions are found at M = 1.5, so that no velocity is ascribed to them. The total motion to V_y is thus negative, while $|v_{y2}|$ increases with m. These are very slow changes in v_y, so that the energy content of the drift remains low always. However, this may be reconciled with the drastic changes of Fig. 7.1 by consideration of the total down-stream energy of the ions as a function of M. This is plotted in Fig. 7.4 .

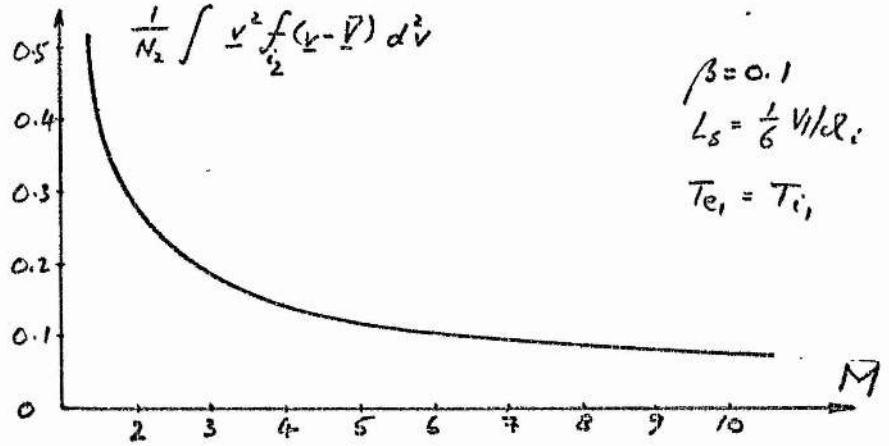

FIG 7.4

It is apparent that total ion energy (calculated here in the perpendicular direction) falls off rapidly with increasing M, while the (small) kinetic energy, $\frac{1}{2}MV_2^2$, is increasing, and thus more and more significant, accounting for the temperature divergence. The reason for the decay in total energy is clear from Fig. 7.2. Over M, β-space, the dotted lines are isotherms for the total plasma. If $T_{el} = T_{il}$ always, they hold too for the ions. By fixing β and varying M, the thermal spread of the ions is decreased thus leading to relatively smaller energies downstream. In the units of this work, $2v_{th}^2 = \beta/M_A^2 \to 0$ as $M \to \infty$, while downstream kinetic energy levels off in the x-component as $V_2/V_1 \to \frac{1}{4}$. Under these conditions the model is expected to be sensitive to V_y directed energies. The ratio $T^{(a)}/T_{ad}$ may of course increase, even as T_2 (total plasma) gets smaller (see Fig. 7.1), but it merely measures a distortion in shape of the downstream distribution. This may yield a considerable ratio even in a vanishing ion temperature state. It may be noted that as $M \to \infty$, the R-H relations give $2v_{th}^2 \sim (\frac{3}{4}V_1)^2$.

A considerable amount of energy is then injected into the V_y motion by the model. In Fig. 7.5, explicit calculation of this energy as a ratio $R_E = \frac{1}{2}M_i v_{y2}^2 \,/\, \frac{1}{2}M_i V_{x2}^2$ is made.

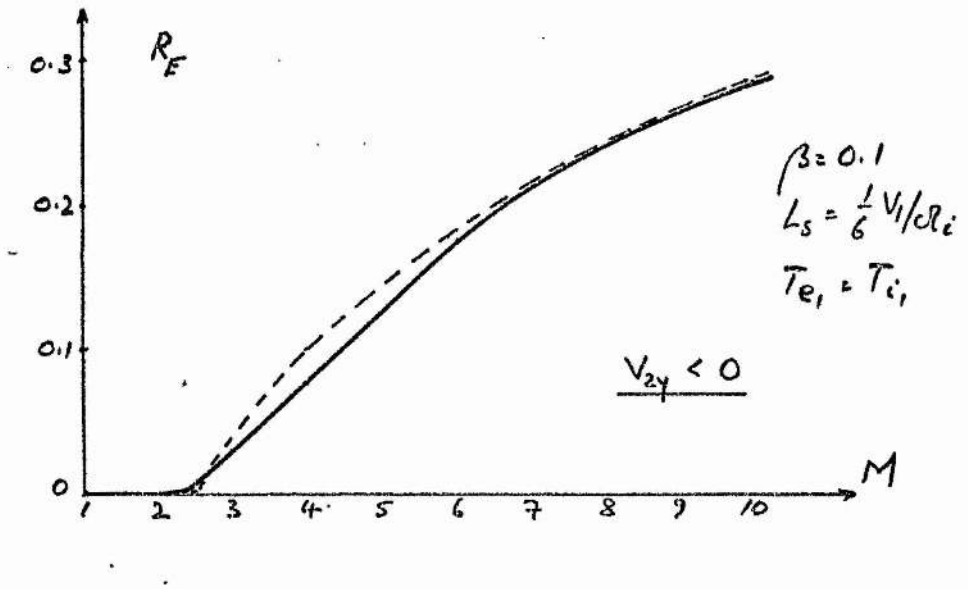

FIG 7.5

The dashed line is again for the transmitted ions only, and shows that they dominate the y-displacements in the shock. The total plasma (the mean) V_y drift is then twisted off the dotted line by the reflecting ions, which put in their appearance at $M \gtrsim 1.5$. It is curious that the energy of the mean plasma downstream should be less than that of one of its pairs. But the graph does not display total energies. It is then a possible solution to the self-consistent problem that while V_{y2} must be zero, components of the ion distribution may have significant directed energies in plane of the shock.

There is a sudden jump in energy in the region $M \gtrsim 2$. The critical Mach number for the overturning of the ion beam (failure of two-fluid model) is calculated by Kornherr at $M^* \sim 2.5$.

The Kinetic energy rises to ∿0.3 the energy to V_x, downstream. In the two definition $T^{(a)}$, $T^{(b)}$, it is seen from Fig. 7.1 that the heating of the reflected ions is not much affected by the definition, while most of the change is held in the transmitted ions. This is consistent with Fig. 7.5.

The behaviour indicated above, suggests that the shock thickness must be reduced (in units of V_1/Ω_1) as M increases. A simple extension may be made by considering the case L_s=0, while a realistic study may be made at observed shock thicknesses, at high Mach number of order C/ω_{pi}. For the case β=0.1, Fig. 7.2 indicates that at M=6, $L_s \sim C/\omega_{pi}$. The model shows this to be too thick, as significant displacement of the main beam occurs. It is thus decided to investigate heating at a constant 10 C/ω_{pe}. This is consistent with low Mach number shocks, as indicated before; the increase in Mach number across the critical level has been claimed to show an increase in thickness - this is ignored.

The L_s=0 model is at high Mach number an effectively opposite extreme of approximation to the case L_s=1/6 V_1/Ω_i. It is seen in the above paragraphs that at L_s=1/6 V_1/Ω_i, displacement to -y occurs, carried by the gyrating ions of the main beam. Fig. 7.5 shows that the reflected ions <u>oppose</u> the tendency to -y. When L_s=0, the displacement of the main beam can occur, so that drifts are dominated by the reflecting ions. The graphic displays of the previous section show the ions to have strong velocities in the +y- direction. Thus a net drift to +y is expected. In the example of the Culham shock wave, runs were made at L_s= 10 C/ω_{pe}, as observed, and L_s=0. The first very interestingly gave no drift to V_y, the second gave a drift to +y corresponding to a proportion of energy, at M∿3.5, ignorably small.

In Fig. 7.6 the dependence of ion drifts on L_s is shown. In example (a), at M<M*, where no reflecting ions occur, the L_s=0 model gives no V_y drift, while L_s = 0 will give a drift $-V_y$ under a mean Lorentz force $\frac{e}{c}\overline{V_x B}$.

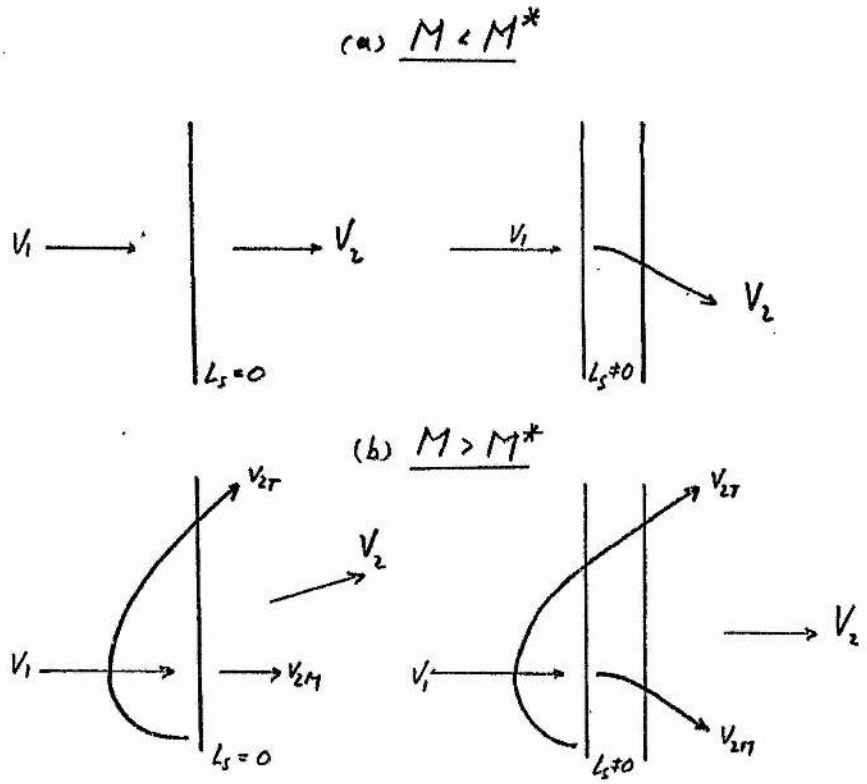

FIG 7.6

Since this flux to $-V_y$ at M<M* can only be met by an electron mass flux to $+V_y$, the model must allow some drift of the ion beam to $-V_y$. Some interaction between interdrifting ions and electrons must occur, in the real model. The ion beam drifts so as to increase gradients in the shock as given by Maxwell's Equations, $dB/dx = -(n_i v_i - n_e v_e)_y$. In the fixed gradients of the model, this implies a drop in the electron current (which is probably beyond detection at order 1% of the total drift as given by the gradient). In the physical shock, it is possible that

the gradients may steepen towards the rear of the shock to compensate for a now increased current flow. This is considered below.

In the case M>M*, the reflecting ions exit downstream with large velocities to $+V_y$. In spite of having low densities, their velocity is so high that they have greater flux than the main beam. At $L_s=0$ then, net downstream drift to $+V_y$ occurs as in example (b). When L_s is increased, this component may be reduced through zero, into a negative drift. The, dependence of V_{y2} on L_s is complicated, for while the main beam will acquire a drift to $-V_y$, it is not yet clear that the reflected ion beam will not compensate with increased flux to $+V_y$! Further, the problem must in a sense remain always unsolved (within the model), for the degree of drift to $-V_y$ that may be allowed (as is necessary in the M<M* case) is not determined.

Thus it is concluded that no entirely self-consistent model results

However, the principal aim of the thesis is ion heating and its consequences. It is valid to search for the model solutions, if the effects of different L_s on dependent parameters is not drastically unstable, giving wildly changing answers.

The possibility occurs then, that $L_s=0$ shocks may be a useful approximation to the real shock, if non-adiabatic heating and electric potential, are comparable with experiment and with observed L_s, model shocks. At the Culham conditions the measured heatings are the same to $\sim$1%

Some importance is attached to the $L_s=0$ curve at $\beta=0.1$, then. But it must be held in mind that $v_{y2}\neq 0$ at $L_s = 1/6\ V_1/\Omega_i$, $L_s=0$, with $v_{y2}<0$ in the first case, and $v_{2y}>0$ in the second.

Comparison of these curves is given in Fig. 7.7, as a plot of non-adiabatic heating with M.

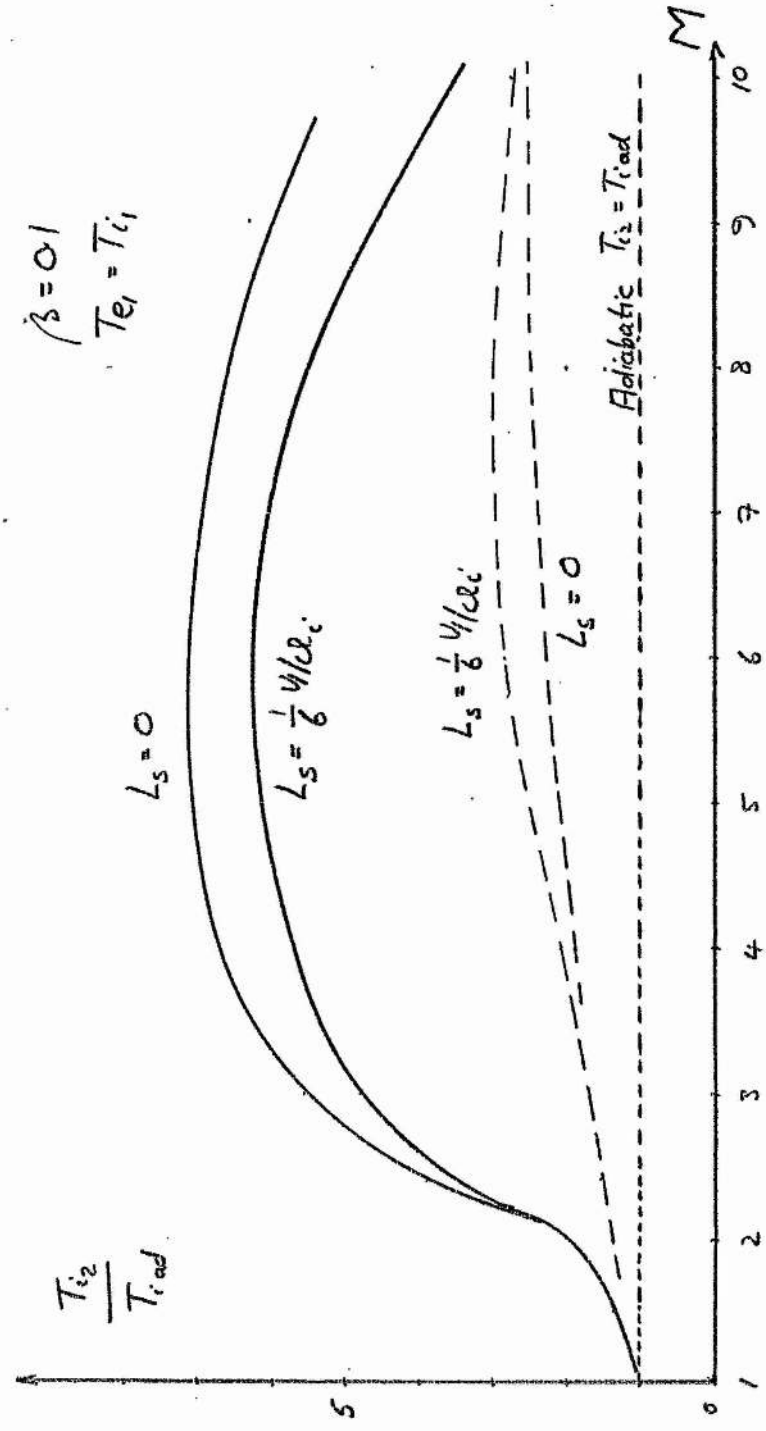

FIG 7.7

The hard curves indicate total heating. The definition $T^{(b)}$ is chosen since it calculates the thermal content of the L_s=1/6 case. They agree up to the point M~2. No reflecting ions are found here. There is then a sudden emergence of reflecting ions as represented by the difference between the hard curves, and dashed curves of the transmitted ion levels. This occurs for both cases, with the zero L_s shock showing slightly more efficient reflection abilities. If this is the case, then higher electric potentials may be expected in the L_s=0 shock, for a self-consistent solution according to $V_1B_1 = V_2B_2$. More striking comparison may be made by subtracting away the transmitted and adiabatic components to give Fig. 7.8.

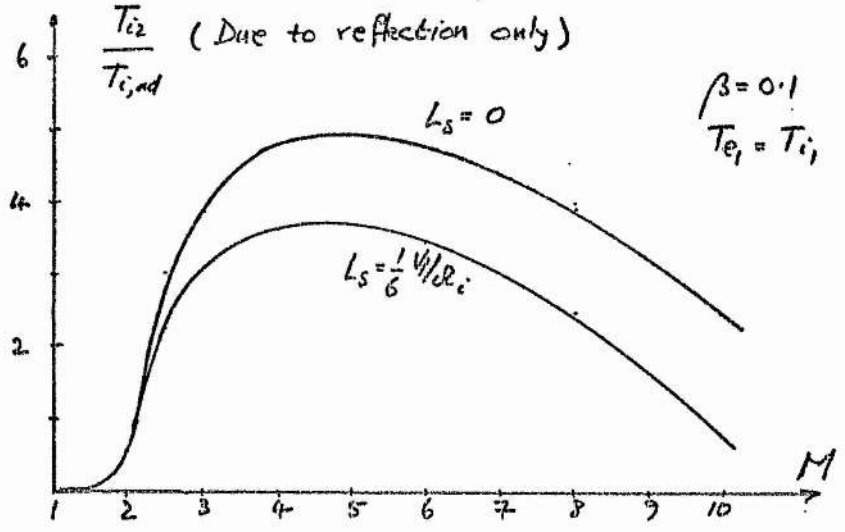

FIG 7.8

The dependence of electric potential, ϕ, on M, is given in Fig. 7.9.

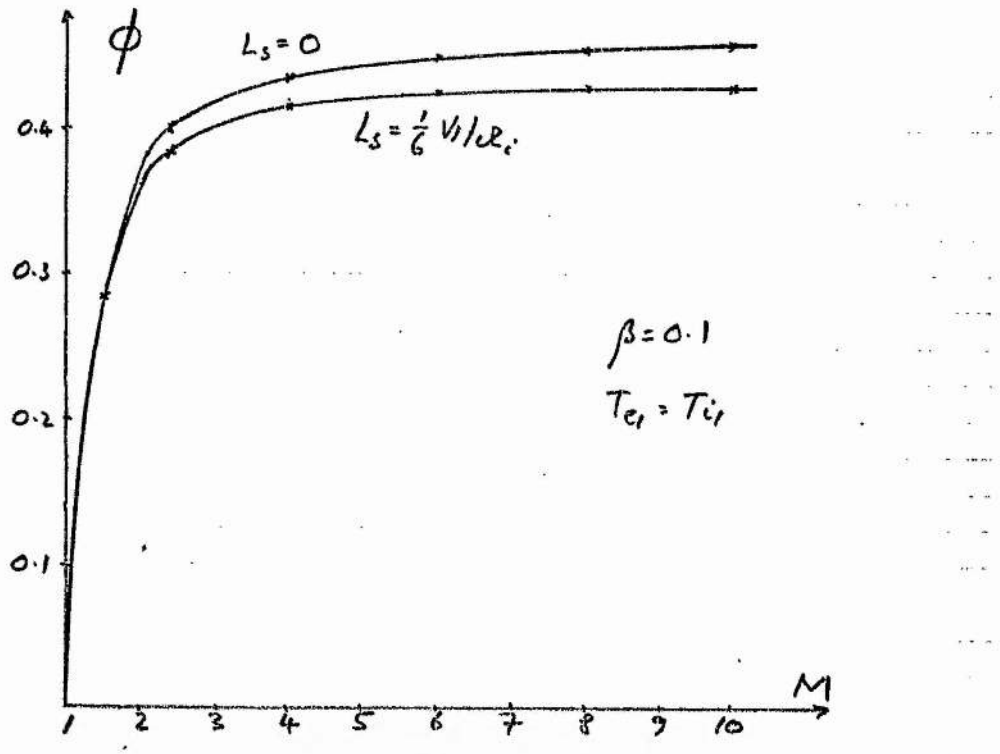

FIG 7.9

The important solution for ϕ will be expanded on below. Such self-consistent solutions for ϕ are rare, and very complicated. Both curves are self-consistent with slowing the ion beam. Not yet investigated is how ϕ (and of course T_i/T_{ad}, etc.) varies with the solution proper with zero drift velocity to $\pm V_y$. To this extent, the differences in ϕ explain the efficient ion heating of Fig. 7.8. Since $L_s = 1/6\ V_1/\Omega_i$ is valid at low Mach numbers, the proper value of ϕ lies close to the lower curve; at high M, since $1/6\ V_1/\Omega_i$ = constant $\Rightarrow C/\omega_{pi} \to 0$ with increasing M, the $L_s = 0$ curve is a better approximation. It may be mentioned here, that in an energy balance for ions across the shock according to

$$\tfrac{1}{2}MV_1^2 = \tfrac{1}{2}MV_2^2 + e\phi + [\text{heating}] ,$$

since V_2 is fixed by the Rankine-Hugoniot relations increased ion heating (L_s=0) should be accompanied by a decreased value of potential. This is not the case due to the presence of two mechanisms:- one is the fact that magnetic fields structure when $L_s \neq 0$ may help the ions through the shock ($V_{y2}<0 \Rightarrow$ a helping Lorentz force $-\frac{e}{c}\overline{V_y B}$, to the potential) thus leading to small ϕ; the other is that the fast reflecting ions may gain so much energy by reflection that the potential must work exceptionally hard to slow them properly, thus leading to a large value of ϕ. In general the ratio $R_\phi = 2\phi / (1-V_2^2) = 1$ taken from the above relation, does not prevent ion heating! The curves that result in Fig. 7.8 show both these effects, as will be shown below.

Thus far, there is qualitative agreement between the two models, on ion heating. Quantitatively, the $L_s = 0$ shock gives about 15% greater heating over the greater part of the axes shown. This estimate is in line with experimental errors, and so the curves may be of obvious use for comparison with real shock phenomena.

However it is possible to be slightly more pedantic, and ask for the variation of heating with Mach number, this time at a shock thickness fixed at $10\ c/\omega_{pe}$ over the whole range of M. This is given in Fig. 7.10, and corresponds closely to observed shock thicknesses.

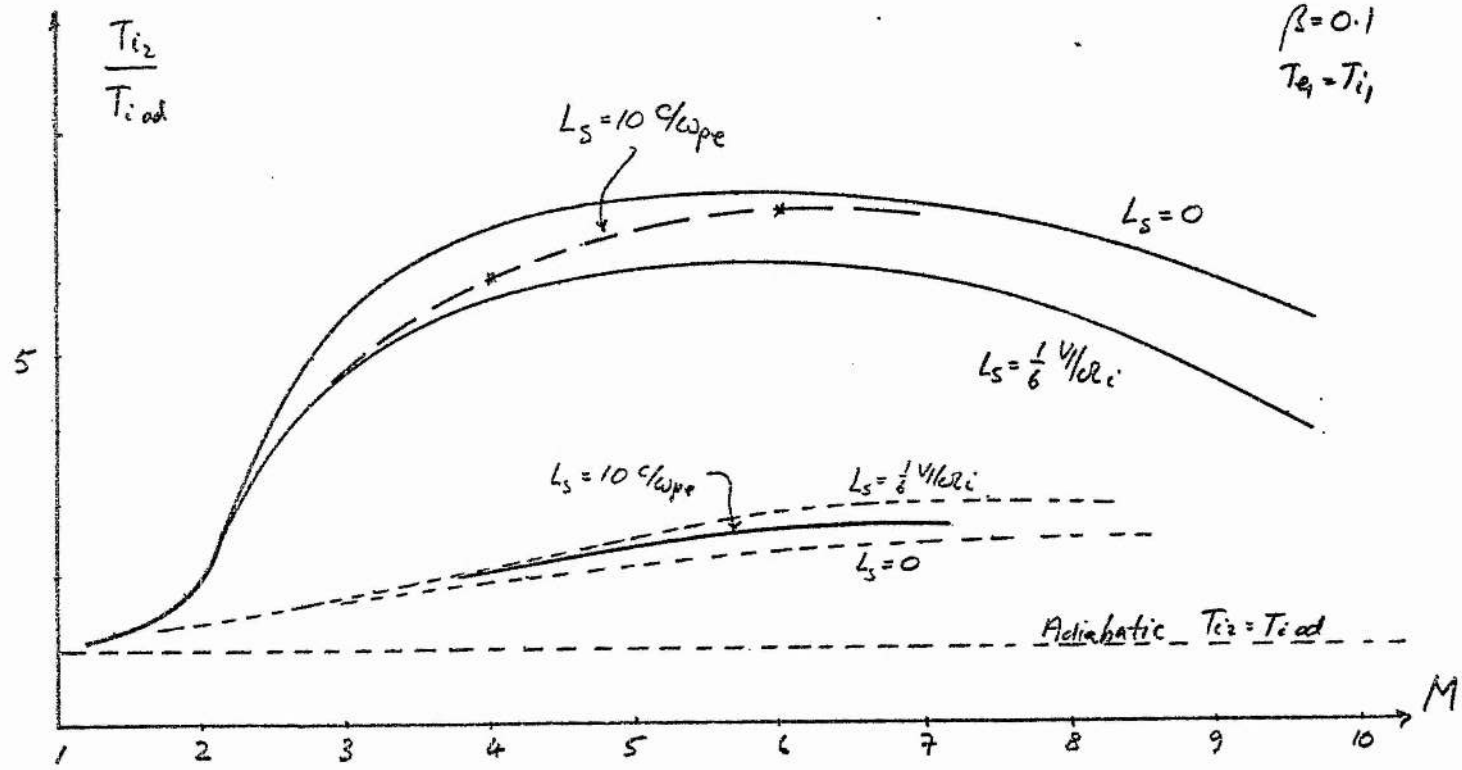
$\frac{T_{i_2}}{T_{i\,ad}}$
$\beta = 0.1$
$T_e = T_{i_1}$
$L_s = 10\ c/\omega_{pe}$
$L_s = 0$
$L_s = \frac{1}{6}\ V_1/\omega_{ci}$
5
$L_s = 10\ c/\omega_{pe}$
$L_s = \frac{1}{6}\ V_1/\omega_{ci}$
$L_s = 0$
Adiabatic $T_{i_2} = T_{i\,ad}$
M
1
2
3
4
5
6
7
8
9
10

FIG 7·10

As expected, since at low Mach number $L_s = 1/6\ V_1/\Omega_i \sim 10\ C/\omega_{pe}$, while at high M, $L_s = 1/6\ V_1/\Omega_i \Rightarrow C/\omega_{pe} \to 0$ as $M \to \infty$, or $L_s = 10\ C/\omega_{pe} \to 0$, the curve crosses over from the lower curve to the higher. The increase in temperature is carried by the transmitted ions, as $L_s = 10\ C/\omega_{pi} \to 0$ which is not consistent with the $L_s = 0$ case. Thus the transmitted ions retain a dependence on shock thickness which suggests that the $L_s = 0$ approximation will not always be useful. The drifts to V_y are such that $T^{(a)} = T^{(b)}$ when $L_s = 10\ C/\omega_{pe}$, thus justifying this choice of L_s.

The ratio R_E above, was quite sensitive to a sudden emergence of V_y-flux, in spite of reflecting ion opposition at higher M. In Fig. 7.11 for the lower Mach numbers, comparison is made with the $10\ C/\omega_{pe}$ shocks. The departure is quite startling.

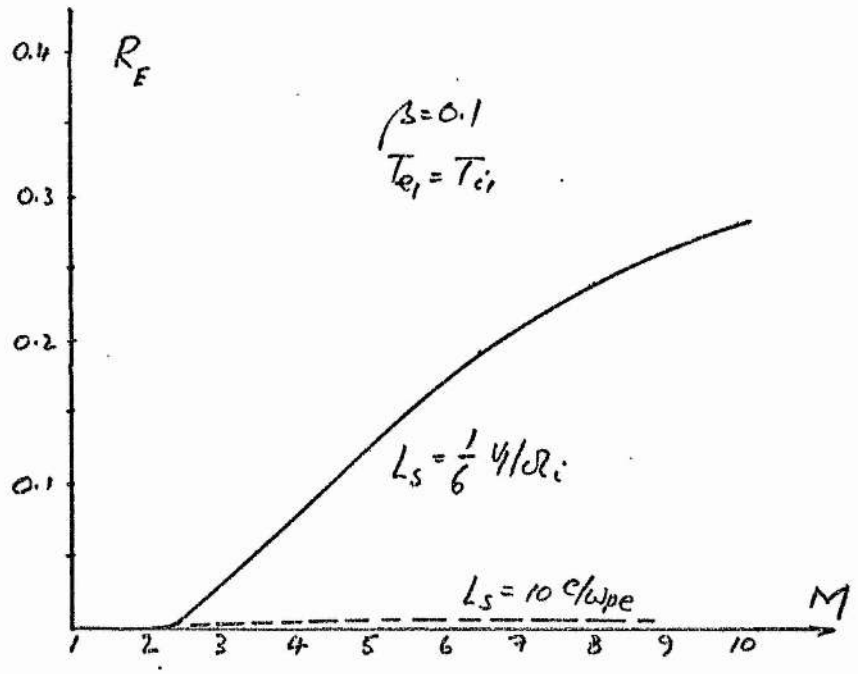

FIG 7.11

It is of note that although the reduction of L_s from C/ω_{pi} to $10\ C/\omega_{pe}$ at M = 6, has reduced the kinetic energy ratio according to Fig.7.5 from $\sim$18% to $\lesssim$1%, there remains a very slowly increasing drift to $-V_y$. This suggests that L_s should not be increased with M, but should rather be reduced if anything. This is important, and is discussed below. It is commonly held that L_s increases across a critical Mach number. The β-dependence of the model is of interest then. Experiments are sometimes run for different shocks by fixing initial temperature, but varying magnetic field. This leads often to an increase in β across M*, the critical Mach number.

Equivalent to Fig. 7.1, it is possible to generate T/T_{ad} curves on various values of β. The levels β=0.005, and β=0.3 are chosen, and shown in Fig. 7.12, for the cases $T^{(a)}$, $T^{(b)}$ again.

At the high-β value of β=0.3, the temperatures agree up to a value M$\sim$5. In line with above arguments, the shock thickness becomes too broad after this point, and allows excessive drift to $-V_y$ in the downstream, carried by the transmitted ions. At low values of Mach number the small $L_s \sim 10\ C/\omega_{pe}$ at M=1.5 does not show dangerous drift, but has the expected drift to $-V_y$ in a region where a very small number of reflected ions are occuring, insufficient to compensate for the main beam.

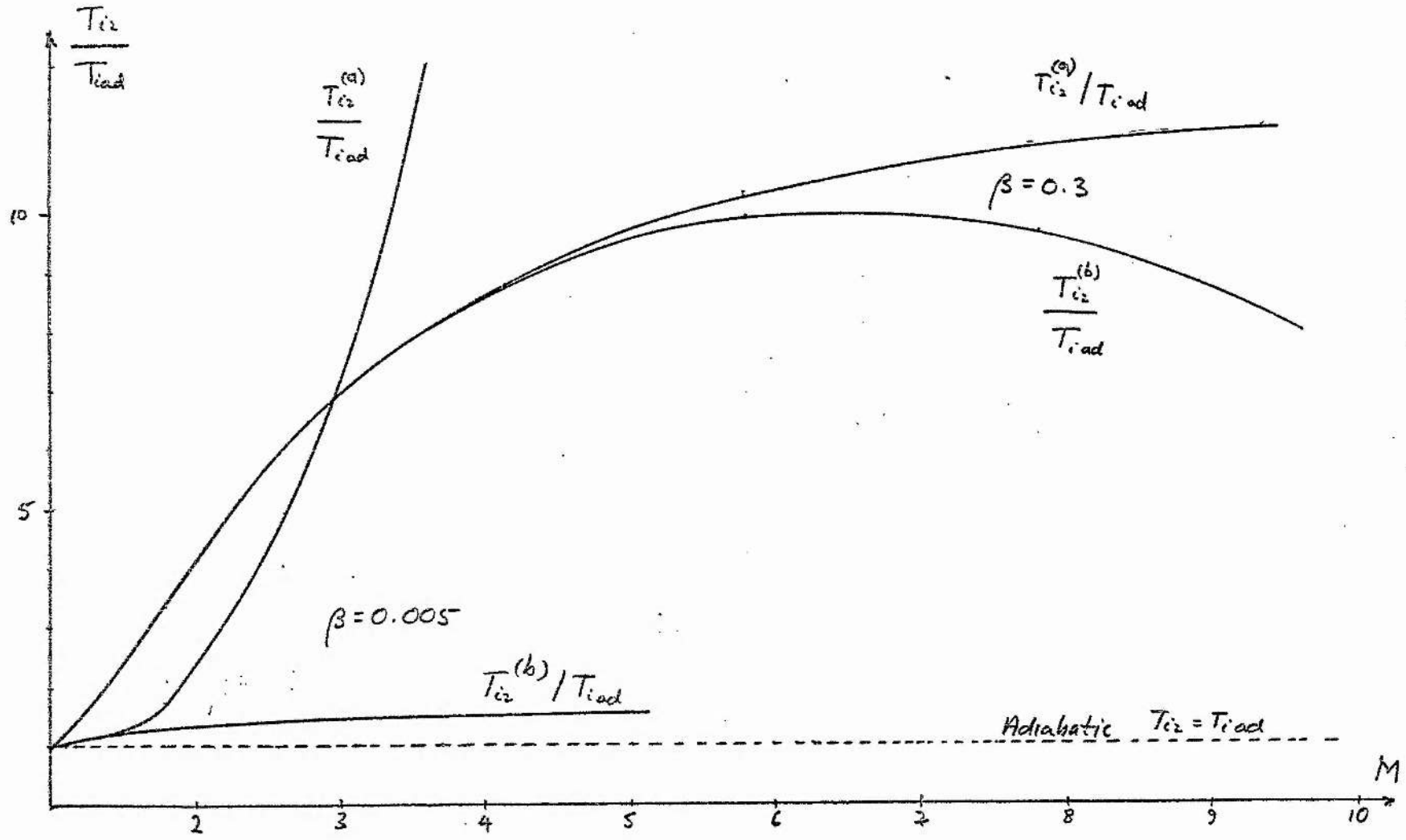
T_{i2}/T_{iad}
$T_{i2}^{(a)}/T_{iad}$
$T_{i2}^{(a)}/T_{iad}$
$\beta = 0.3$
$T_{i2}^{(b)}/T_{iad}$
$\beta = 0.005$
$T_{i2}^{(b)}/T_{iad}$
Adiabatic $T_{i2} = T_{iad}$
10
5
M
2
3
4
5
6
7
8
9
10

FIG 7.12

At low β = 0.005, the definitions agree only up to M$\sim$1.5. There are no reflecting ions at all at this low temperature, for all M.

If the separation point is labelled $\hat{M}$ say, there is seen to be a progression of increasing $\hat{M}$ with increasing β. It was noted above that at β=0.1 , $\hat{M} \sim M^*$, the critical Mach number. This is fortuitous, since while β increases, M* decreases [28], but from Figs. 7.1, 7.2, $\hat{M}$ increases. The events are not independent however. It is noted that the fewer the reflected ions (non at all at β=0.005,M=5, say), the more drastic the separation of measured and test temperatures. It is commonly held that M>M* implies the overturning of the ion beam by reflections (a wave-breaking phenomena clearly not acceptable at β=0.005, M*=2.8 [28]) and so there is some relation between the M* and $\hat{M}$.

The reason for increasing $\hat{M}$ lies of course in the ability of the reflecting ions to reduce the main beam tendency to $-V_y$. The flux of such ions must then be increasing with β, at a given M. It is shown below that the variation in ϕ with β is small, while the thermal spread of ions increases. Both these effects increase the flux of reflecting ions.

The following table gives a comparison of parameters at the separation points, for these three values of β.

	(i)	(ii)	(iii)
	$\beta = 0.005$	$\beta = 0.1$	$\beta = 0.3$
$T_{el} = T_{il}$	$\hat{M}$ ~ 1.5	$\hat{M}$ ~ 2.5	$\hat{M}$ ~ 5
	M^* ~ 2.8	M^* ~ 2.5	M^* ~ 2.2
L_s is fixed at $1/6\ V_1/\Omega_i$, that is:	$L \sim 10.5\ C/\omega_{pe}$	$L \sim 18\ C/\omega_{pe}$	$L \sim .95\ C/\omega_{pi}$
	$\phi \sim 0.2$	$\phi \sim 0.39$	$\phi \sim 0.42$
	$(n_2 v_{2y}) \sim -.02$	$(n_2 v_{2y}) \sim .07$	$(n_2 v_{2y}) \sim .35$
	$(n_2 v_{2y})_{tail} \sim -$	$(n_2 v_{2y})_{tail} \sim +.05$	$(n_2 v_{2y})_{tail} \sim +.2$
	$(n_2 v_{2x})_{tail} \sim -$	$(n_2 v_{2x})_{tail} \sim .02$	$(n_2 v_{2x})_{tail} \sim .15$

The last two lines show the rapid large increase is reflected ion flux and how they are distributed to V_x and V_y. Further, the large increase in ϕ is noted. A comparison of R_E for all three ratios is interesting, as it helps to establish the large thermal content added into the downstream shock by just a small increase in β. If this is so, then kinetic energies to $\pm V_y$ will be expected to have smaller significance in the definitions of ion heating. At high β it is hoped then that solutions are increasingly independent of the choice of L_s. In Fig. 7.13 the ratio R_E is given for three values of β=0.005, 0.1, 0.3. It is noted then that in spite of there being large drifts to V_y (at β=0.3) for $M<\hat{M}$, the temperatures $T^{(a)}$, $T^{(b)}$ agree for $M<\hat{M}$.

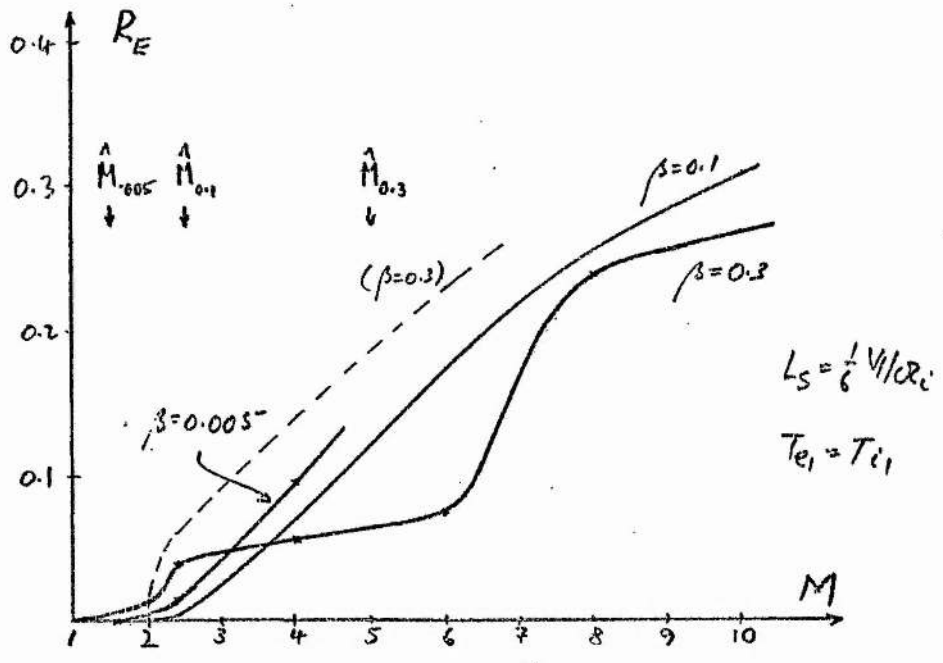

FIG 7.13

The dashed lines refer as usual to the transmitted ion; the large separation between the kinetic energy to V_y of the mean plasma, with that of the transmitted ion at $\beta = 0.3$ is noticeable. Also the curves appear to undergo quite rapid changes at $\hat{M}$. At high β the dotted curve is smooth showing the rather sudden effects of a reflected ion decrease. (This is explained below for $M>\hat{M}$.)

The importance of the point $\hat{M}$ lies, in each case, in giving a region in which the effects of the V_y drift in downstream solutions may be ignored. Thus up to $\hat{M}$ comparison with experiment is valid. When $M>\hat{M}$, then shock thickness becomes too large (at constant β, and fixed L_s, $L_s \propto V_1/\Omega_i$)

Further study of shock parameters should then depend on the sensitivity of temperature, electric potential, ion reflections, with changing L_s as an independent variable. It is hoped that suitably stable solutions are found, so that a completely self-consistent run can be avoided. Since choice of ϕ requires two runs, and then choice of L_s requires at least two finite -L_s runs, the average computer time per point in M, β-space will rise four times (at best) to order four hours.

For a short while, then, this section will be concerned with plots over L_s. All the time it is hoped that parameters will not depend dangerously on L_s, so that some physical information, of relevance to shock experiments may be deduced not only on these parameters, but also as regards shock thickness.

In Fig. 7.14, a plot of the downstream non-adiabatic heating ratio is given against L_s. The upper curve is heating due to the total ion component, the lower is due to transmitted ions only. The dashed lines represent $T^{(a)}/T_{ad}$, the solid line $T^{(b)}/T_{ad}$. The indication of the previous results are that even with $V_y \neq 0$, the definition $T^{(b)}$ continues to give good measure of temperature, comparable with the $L_s=0$ case, and the case L_s such that v_y is small. The figure is plotted at M=6, β=0.3, $T_{el} = T_{il}$. These values are quite close to $\hat{M}$ and are chosen at high β so that reflected ion fluxes are quite large. The length scales are duplicated in units V_1/Ω_i and $C/\omega_{pe,i}$.

At the standard length $L_s = 1/6\ V_1/\Omega_i$, very strong heating is found, so that non-adiabatic levels are about 90% of total ion heating. This represents an ion thermal energy jump of about 36, while, spreading this energy into 3 dimensions for comparison with the Rankine-Hugoniot relations,

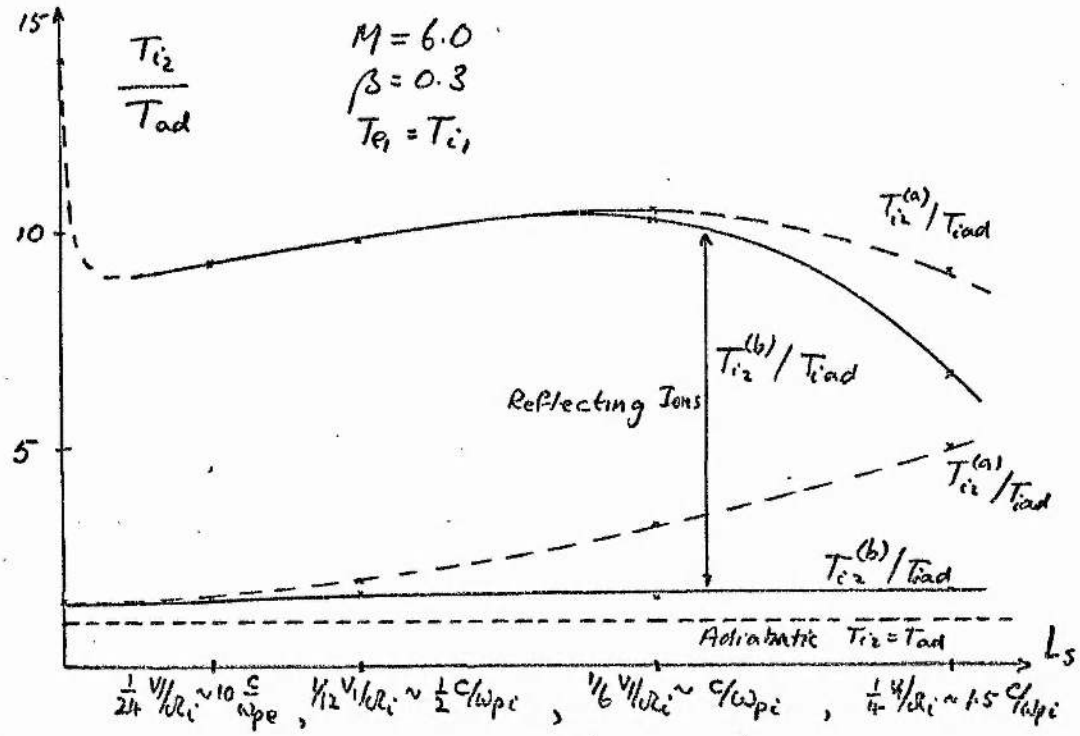

FIG 7.14

the electron jump is about 3 times the ion jump. Thus the ion heating is considerable when compared with the total. Most of this energy is held in the reflected ions, and temperature dependence with L_s is expected to be sensitive to such ions only; the transmitted ions are dominated by the transformation across the electric potential as discussed above. It is seen then that the variation of heating with L_s is quite constant, at least on the range $L_s \lesssim 1/6\ V_1/\Omega_i \sim c/\omega_{pi}$. For the transmitted ions, it is constant for all L_s shown, reinforcing the idea that the potential dominates ion shock heating. The reflecting ions show a variation of about 10% which is, again inside experimental errors, for $L_s \lesssim 1/6\ V_1/\Omega_i$. Shock thickness greater than c/ω_{pi} are unusual, while if $L_s = 10\ c/\omega_{pe}$ is chosen, heating drops by

about 10%.

It is clear too, that the drifts to $\pm V_y$ are unimportant for $L_s \gtrsim 1/6\ V_1/\Omega_i$, as was shown in Fig. 7.12, as indicated by the divergence of $T^{(a)}$, $T^{(b)}$. The transmitted ions show the most change. The appearance of the divergence clearly has an L_s -dependence. By reducing shock thickness at any point in the plasma, (M>M*) the real and fast temperatures can be made to agree. There is (at least at these parameters) an encouraging lack of temperature dependence.

The dotted curve at L_s=0 is a hypothetical link-up with the easily generated L_s=0 solution. There is sudden very rapid increase in ion heating. This may be attributed to improved efficiency in generating reflected ions, but this conclusion must be tempered. It has been indicated above, that no solutions can be found for shocks of the order of the Garching parameters ($M\sim4.9$, $\beta\sim2.6$, $T_e/T_i\sim.16$). The effect of zero L_s is to reduce the domain of solutions to a region $\beta \lesssim 0.3$. It will be discussed below, but solutions generated with increasing β lie on a surface over M which folds back on itself. There is thus a point at which $\partial/\partial M,\ \partial/\partial\beta \to \infty$. It occurs that this solution surface is beginning to fold in the region of the shock of Fig. 7.14. The effect is then not of great importance, but emphasises that the L_s=0 solutions must be treated with caution.

At large $L_s \sim \frac{1}{4}\ V_1/\Omega_i \sim 1.5\ C/\omega_{pi}$ there is pronounced decline in reflected ion heating. This must sensibly be tied to one of a small number of possible causes. Most likely is a drop in reflected ion fluxes. As $L_s \to \infty$, the point of reflection must stay far to the back of the shock, to effect a division into reflected and transmitted ions.

However, it will occur that such a large bulk drift of the incoming ions to $-V_y$ results that the ion gyration significantly helps to slow the plasma fluxes. Alternately, L_s could be so large that even "reflecting" ions need not leave the shock but gyrate in L_s. In the steady state model the fluxes ($n_2 v_{2x}$) are shown in Fig. 7.15.

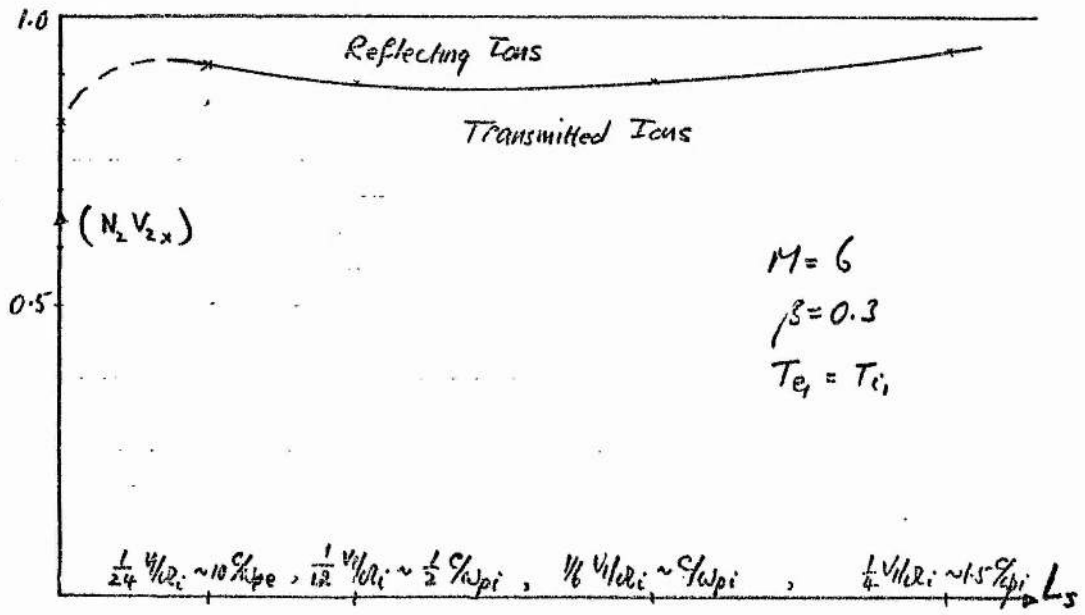

FIG 7.15

There is variation at very low L_s where the limits of the solution space are approached, and at large L_s. The middle region stays quite constant at about 11% reflection. These are small numbers, so that even a small change relative to total flux can be quite extreme - thus as indicated above, 11% reflection can carry most of the energy. Then a loss of flux to reflection of order 5% is a 31% drop in energy. The effect can be large. Errors may amplify in there small numbers, so that a better

guide will be in plots of the electric potential which are accurate to two significant figures. These are given in Fig. 7.16, against L_s.

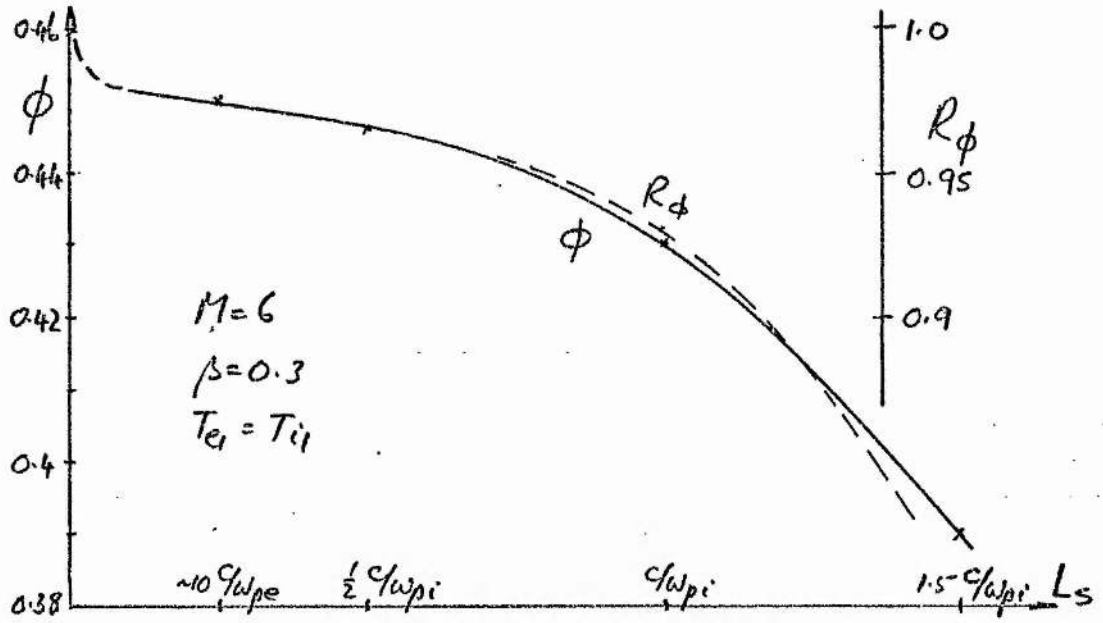

FIG 7.16

A 15% drop in ϕ has occurred This explains the low distortion heating of the main beam downstream, as given in Fig. 7.14, dominated as it is by the electric potential. The dashed "temperature" indicates the rising drift of these ions to $-V_y$, while the difference between total and transmitted levels falls (for both sets of curves).

Again there is rough constancy in ϕ with variation in $L_s \lesssim 1/6\ V_1/\Omega_i$. It is very interesting that at $L_s=0$, $R_\phi=1$. In conservation of energy across the shock, where considerable ion heating has occurred, this value should be expected smaller. However, the potential is working hard to slow the plasma, thanks to the reflected ion beam. Variation with L_s then merely underlines the growing effect of ion magnetic field dynamics,

notably ion gyration, in the shock. Low values of R_ϕ are discussed below in connection with other variations for ϕ and in the light of published estimates of ϕ.

The variation with L_s at other points in M,β-space, are given in Fig. 7.17; T/T_{ad} is plotted.

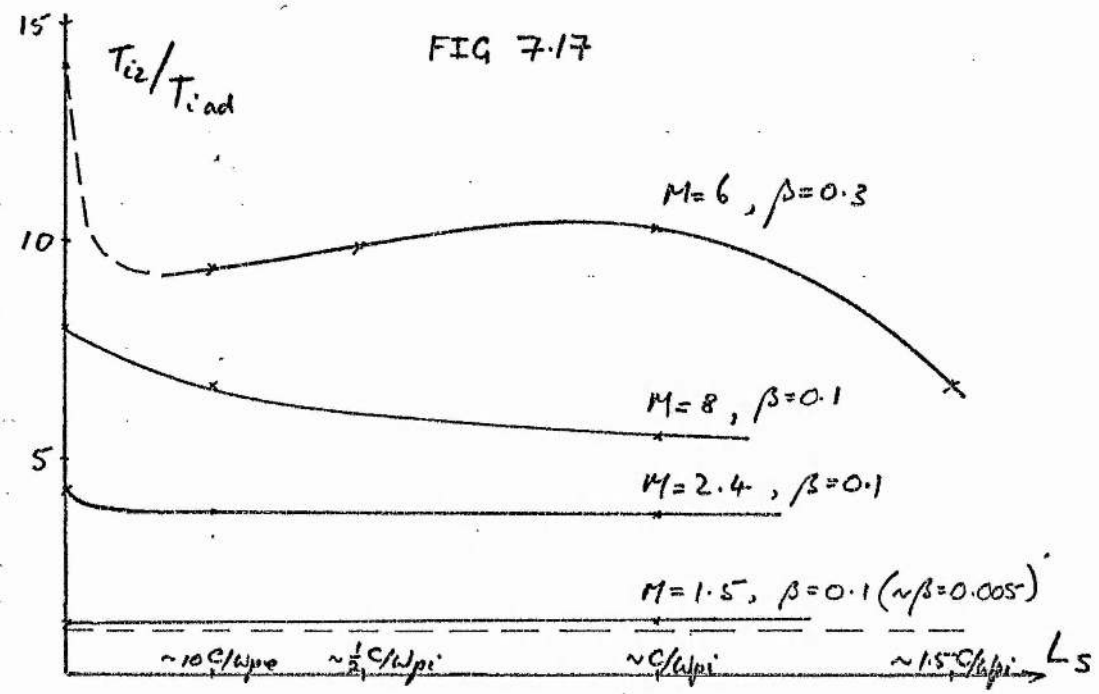

At lower β=0.1, and smaller Mach numbers, the heating remains quite constant. There is some variation in the region of L_s=0 always, but again this is not likely to affect the $L_s \neq 0$ model. At low β, the agreement there is found to be better than at β=0.3. Again, for $\beta \lesssim 0.1$, the L_s=0 curves appear to be a reasonable approximation. The results have not been extended to $L_s > 1/6\ V_1/\Omega_i$.

It will be held, from now on, that choice of L_s is not critically dependent for measuring T. It is shown above that even while large drifts to V_y occur ($T^{(a)} \neq T^{(b)}$), the measured temperature $T^{(b)}$ is of order the "adjusted-L_s" temperature. From Figures 7.7 and 7.8, $T^{(b)}$ at low M for $L_s = \frac{1}{6}\frac{V_1}{\Omega_i}$ and high M for $L_s=0$, gives good approximation to an adjusted $-L_s$ shock. It can be settled then to use the definition $T^{(b)}$ which is less than, or order, the temperature at 10 C/ω_{pe}, as an estimate of shock heating useful for comparison with experiment.

However, one may sensibly ask if there is some indication of a proper shock thickness, for a given M, β. Strictly, R-H requires $V_{2y}=0$. At $M<M^*$ this cannot be met by the model, implying some transient interaction of the ions with their fields, or with the electrons. At $M>M^*$, $V_{2y}=0$, but there is no reason to suppose that the transient interaction ceases. At very small β, the model gives no V_y -balance for all Mach numbers. (Of course, charge neutrality requires, as for the V_x-component, $V_{ye}=V_{yi}=V_{y2}$). It is felt then that while the model cannot strictly reach a self-consistent L_s, parameters do not depend significantly on the choice of L_s. Attention is thus concentrated on the heating (and other) properties. Further information on L_s occurs below, and a discussion of the rather tentative evidence for a determination of L_s is postponed.

§8 On the Variation of Ion Heating with Mach number

It slowly emerges then, that important characteristics of the model are held in these points:

(i) that large adiabatic heating of the ions can take place in a laminar, reversible, co-operative process;

(ii) that this general "distortion heating" occurs through two different orbit types, one wholly within the shock transition, the other leaving the shock in a violent bound off the electric potential - these effects may be considered as of separate importance;

(iii) that the model predictions may be compared with experiment (Culham) at least in some region of the M,β-space;

(iv) that the laminar ion model fails (Garching), and the effects of ion instability must be considered.

It is recalled that up to the present, explanation of ion heating as turbulent resistive heating due to ion instabilities in the transition, has been frustrated by the long growth times to saturation of the unstable waves, as compared to transit-times. The model proposes that the initial coarse broadening of the ion distribution is due to laminar orbits, with a slow turbulent second stage that effects stabalization and thermalization. The model measures the temperature of unstable ion distributions for $M>M^*$, and non-thermal distributions for $M<M^*$.

It is now proposed to generalize the model results in a parameter study with the magnetosonic Mach number, M. Experiments, as they occur, may then be easily compared with the curves obtained. Information on the physics of the shock becomes apparent by contrasting solutions.

In Fig. 8.1, is presented the important set of curves of heating, at constant β, as a function of M. As above, the heating is measured as the ratio of the non-drift energy, to the adiabatic heating. The first is calculated as

$$T_{i2} = \frac{1}{n_s} \int d^2v \; (\underline{v} - \underline{V}_2)^2 f_{i2} = T_x + T_y \quad , \qquad (8.1)$$

as calculated in two degrees of freedom perpendicular to B_z. Thermalization, downstream, will distribute this energy in three dimensional velocity space. A measure of a temperature appropriate to comparison with the conservation relations (the Rankine-Hugoniot prediction is suitable), is then

$$T_{i2}^{RH} = (T_x + T_y + T_z) \; / \; 3,$$

where $T_z = T_{i1}$, since no motion at all occurs along B_z. Again the adiabatic heating for comparison with (8.1) is

$$T_{ad} = \left(\frac{n_2}{n_1}\right)^{\gamma_i - 1} \cdot T_1 \; ,$$

where $\gamma_i = (m_i + 2)/m_i$ is the adiabatic index, and of course $m_i = 2$. Then T_{i2}/T_{ad} is the measure of downstream energy, not associated with drifts, that is used in Fig. 8.1.

All calculations are made with $L_s=\frac{1}{6} V_1/\Omega_i$, fixed. From the previous section, there is then some likely error for $M>\hat{M}$. It was found there that this is always less than, or of order, the experimental error, but that at high Mach, number, the $L_s=0$ approximation will be more accurate. Fig. 8.2 is then presented. Equivalent to Fig. 8.1, L_s is now zero, and may be used when $M>\hat{M}$. It is noted that in the latter, the progression with β halts at $\beta=0.1$; at $L_s=\frac{1}{6} V_1/\Omega_i$, it halts at $\beta=0.3$.

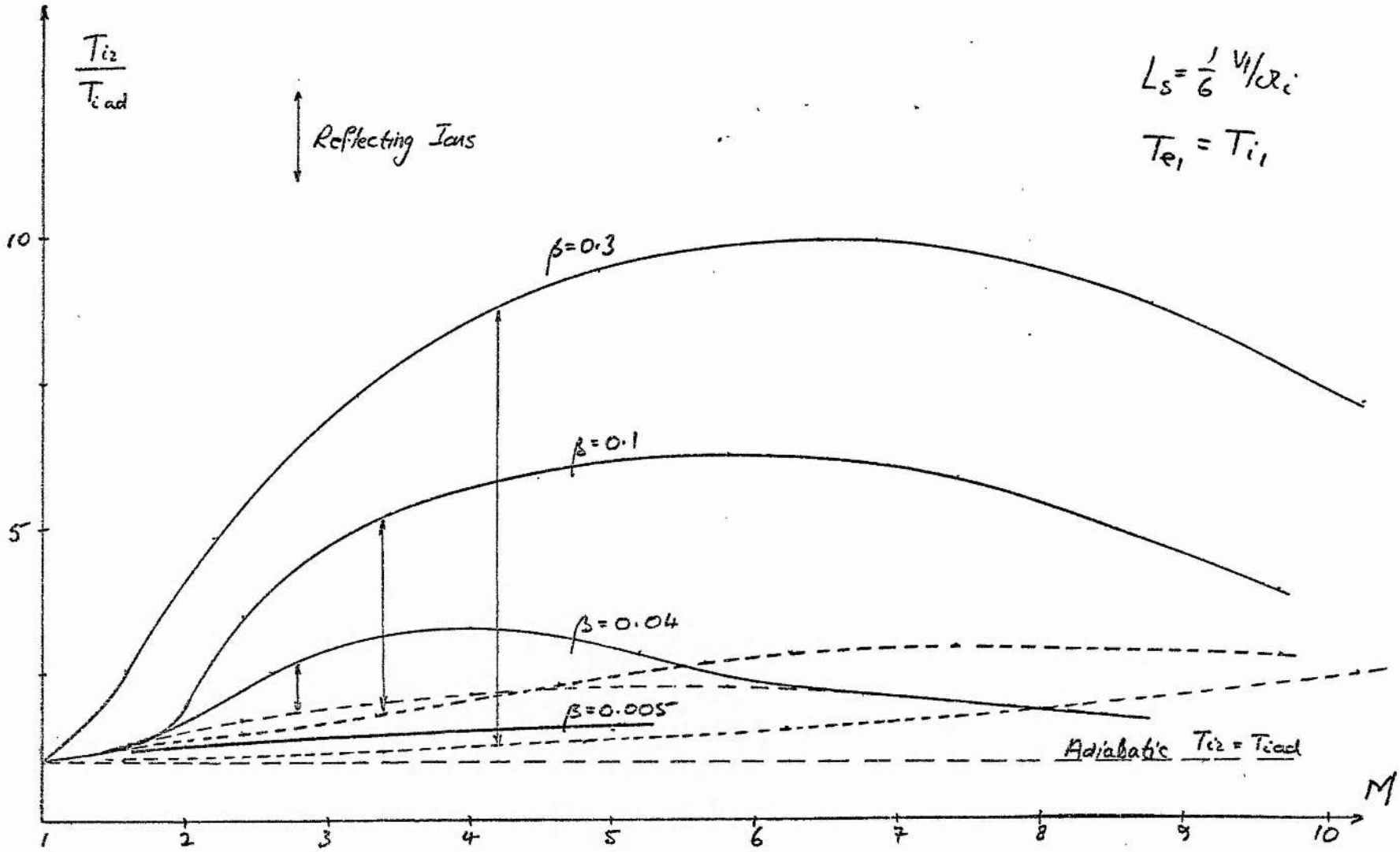
$\frac{T_{i2}}{T_{i\,ad}}$
Reflecting Ions
$L_s = \frac{1}{6} V_1/\alpha_i$
$T_{e1} = T_{i1}$
10
5
β=0.3
β=0.1
β=0.04
β=0.005
Adiabatic $T_{i2} = T_{i\,ad}$
M
1
2
3
4
5
6
7
8
9
10

FIG 8.1

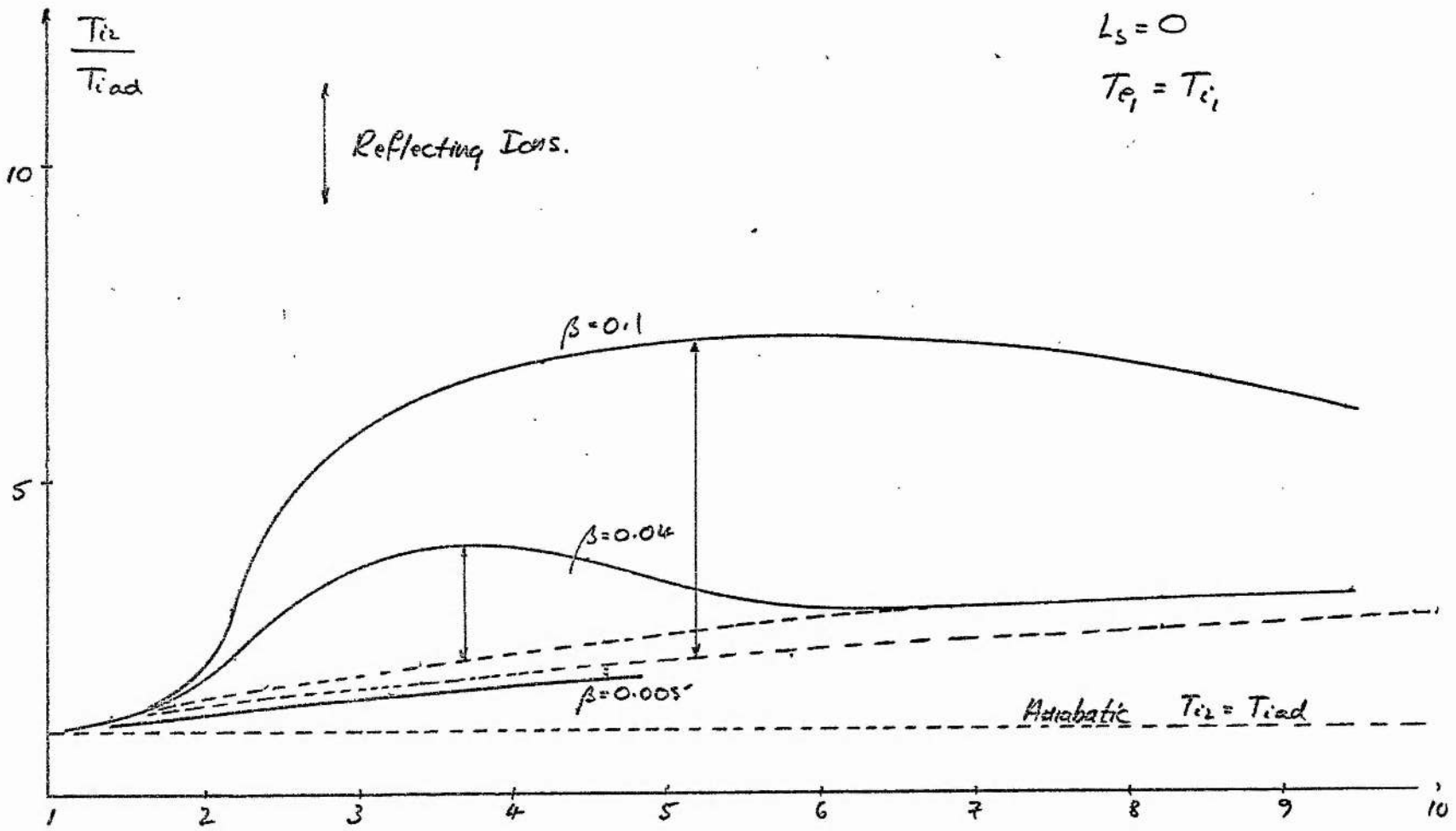
$\frac{T_{i2}}{T_{iad}}$
$L_s = 0$
$T_{e_1} = T_{i_1}$
Reflecting Ions.
10
5
$\beta = 0.1$
$\beta = 0.04$
$\beta = 0.005$
Adiabatic $T_{i2} = T_{iad}$
1
2
3
4
5
6
7
8
9
10

FIG 8.2

Fig. 8.1 is an important conclusion of the thesis, and is rich in information on the low-β behaviour of a shock.

At $M \leq 1$, when no shock develops, no heating is found above adiabatic level. For each value of β there then occurs a smooth increase in T_{i2}/T_{ad} with M. Various behaviours occur at each β; the case $\beta=0.1$ may be usefully analysed first. This may then be compared with §7, in the study of L_s-dependence. Now the general shape of the curve should be explained.

From Kornherr's work [8], the critical Mach number is $M^* \sim 2.5$. It is seen that a quite sudden emergence of reflecting ions occurs at $M \sim 2$. Up to this point T/T_{ad} rises to about 1.5. This energy gain is $\lesssim 5\%$ of total heating as given by comparison with the R-H level, and cannot be measured. It is recalled that the $M<M^*$ Culham example, at $\beta=0.04$, gave an energy gain of about 3%. The heating is due to simple distortion of the transmitted ions (in this case the total ion component). On the region $M<M^*$, the model so far gives no information that is not accessible to a two-fluid theory (with anamalous resistivity). But $M \geq M^*$ represents the breakdown of these theories, where profile solutions are generally found to go three-valued. This is interpreted as wave-breaking, or the overturning of the ion beam. The complicated problem of dealing with the reflecting ions, even as a cold fluid, has prevented studies on $M>M^*$. What is interesting in Figs. 8.1, 8.2, is then an unusual graph of temperature dependence, on this region.

The hard curves represent the total ion component, the fine, dotted lines the non-adiabatic heating of ions transmitted directly through the shock.

Then at M$\sim$2, the suddenly significant reflected ion heating is apparent. The vertical line is a measure of this heating - a maximum occurs at M$\sim$5, and is about 70% of non-adiabatic heating. The Culham experiment falls at M$\sim$3.55, where approximately the same proportion holds. The rapid appearance of reflections (which has yet to be explained) at M$\sim$M*, is in line with the general success of fluid shock theories at M$<$M*.

As M increases, both components increase until a point is reached at M$\gtrsim$6, where total heating begins to decline. It is apparent that at M$\sim$10, the reflecting ions play only a small part in the total ion heating. This behaviour is interesting, and easy to understand from Fig. 7.2 above, where isotherms are plotted in M,β-space. Thus at β=0.1, the temperature falls with increasing Mach number. Thus the thermal spread of the ion distribution diminishes and the number of reflected ions must decrease. But it appears from Fig. 3.3, that this number depends not only on the temperature, but on the value of the electric potential as well.

Now as M increases, so $V_2/V_1 \to \frac{1}{4}$, which is a maximum jump obtained from the conservation relations. The ratio is found by putting $B \to 0$, $v_{th} \to 0$. In the non-dimensionalized form, as $M \to \infty$ at some fixed β, then the upstream kinetic energy of the plasma dominates. But since $B \to 0$, then the ions must be stopped by the electric potential. As Figs. 8.1 ,

8.2 show, ion heating becomes small in the tail. It will be shown below that this ion heating becomes a small part of total heating. It then seems likely that reflections will cease as $M \to \infty$, and that ion heating falls. Than the ratio $R_\phi = 2\phi/(1-V_2^2) \sim 1$ must be true. Then ϕ should be increasing with M. At intermediate M, in regions where both magnetic field and distortion heating occur, ϕ may have a complicated form.

The behaviour with ϕ is given in Fig. 8.3, as predicted by the model. The value

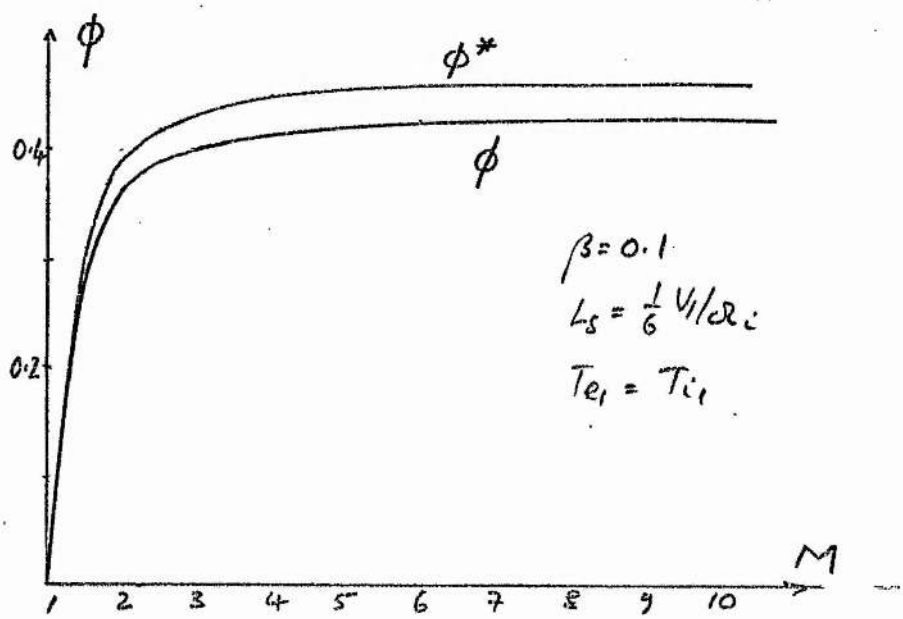

FIG 8.3

of ϕ such that $R_\phi = 1$, (i.e. the potential sufficient to slow a cold ion beam) is labelled ϕ^*. It is plotted as the dotted line, and may be calculated for any M, β, since V_2 is predicted.

It is clear that when $\beta = 0.1$, the ions are not slowed only by the electric potential, but also by the conversion of upstream kinetic energy into downstream thermal energy, this is accomplished

by non-adiabatic ion orbits in the laminar fields.

However, it suffices that ϕ is monotonic increasing, indicating that the fall in reflected ion heating is due to falling initial temperatures only. It is further noted from Figs. 8.1, 8.2, above, that as $L_s \to 0$ (or as $M \to \infty$), the efficiency of ion reflections goes up. Thus choice of L_s is not in favour, as $M \to \infty$, of the reduction of ion fluxes. The variation of fluxes for each component, with M, is then displayed in Fig. 8.4.

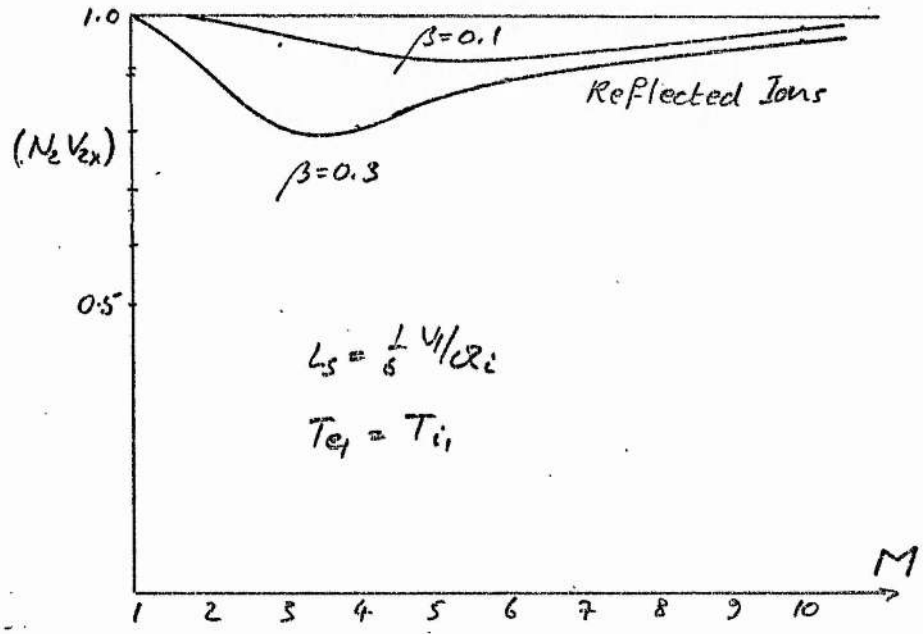

FIG 8.4

It is then apparent that heating at large M is coincides with the loss of reflected ions.

There are less obvious reasons for decreasing reflected ion heating. Thus the energy downstream depends on their reflection orbits. The larger these orbits, the larger is the energy put into

Larmor gyration downstream, that is, the temperature. A measure of the effect of the reflection orbits is given by their drift co-ordinates downstream.

In Fig. 8.5 is shown the behaviour of $v_2=V_2$, with M. The curves are velocities for the total, and reflected ion beams. Since the prescription $V_1B_1=V_2B_2$ is followed, the former curve is known from the Rankine-Hugoniot relations, and so is not new. It is seen that at $M\sim10$, $V_2\sim V_{min}(M=\infty) = \frac{1}{4}$, which represents the disappearance of all magnetic field dynamics. This limit is reached quite rapidly, so that M does not have to be abnormally large for the approximation $V_2\sim V_{min}$ to apply. The total drift is approximately equal to the drift of the transmitted ions alone. There is very small variation with $\beta=0.1$, 0.3,

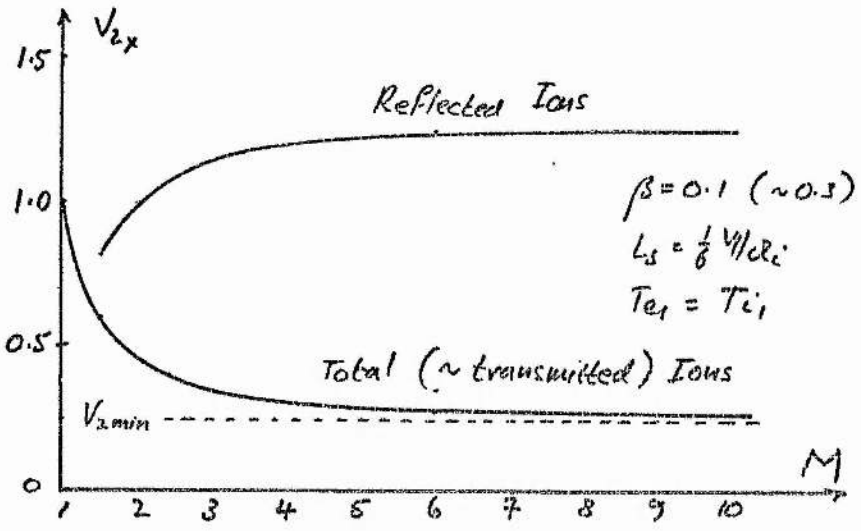

FIG 8.5

and the curves may further be taken valid, at all M, with regard to

shock thickness.

The drift of reflected ions downstream is increasing, but very slow change occurs at high M as the effects of dominating electric potential, and disappearing magnetic field are felt. As all upstream energy goes into the plasma kinetic energy, so ions are reflected off the potential with greater velocity. This is carried to the downstream. Since this energy is then measured as temperature the tendency is to increase ion thermal energy when M is large. It is interesting that the exit velocity to V_y of the reflected ions falls with M_1 as may be seen from Fig. 8.6, the companion to Fig. 8.4. The decrease is very slow and it is expected that loss of energy, gained by the reflection orbit, does not account for decreased ion heating at high M. The decrease in V_y is expected as the higher exit velocities to $-V_x$, as M increases, will alter the phase of the "mean reflected ion", and cause it to be turned more rapidly upstream.

Thus it is noted that the quantity $\frac{1}{2}M(V_x^2 + V_y^2)_{tail}$, is increasing. This does not mean that the tail is increasing its energy, as the number of reflected ions is falling. Thus finally, the loss of reflected ion heating is due to the low initial ion temperatures alone, as $M \to \infty$.

In Fig. 8.7 the flux in the y-direction is plotted, and may be compared with Fig. 8.4. Since $(n\, v_y)_{tail}$ falls with M, and density falls with M, V_y must fall. This is shown in Fig. 8.6.

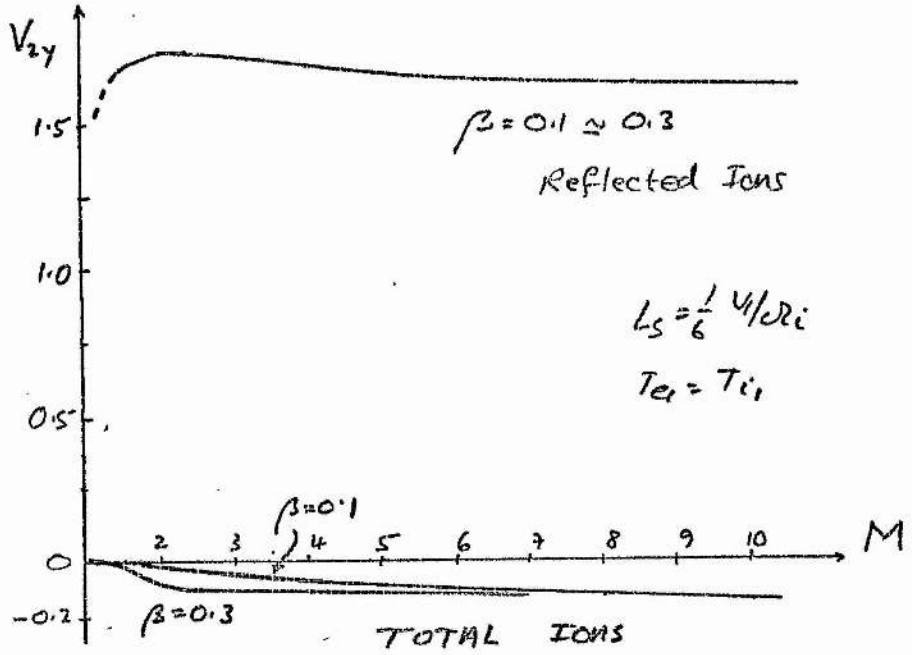
V_{2y}
1·5
1·0
0·5
0
-0·2
$\beta = 0.1 \simeq 0.3$
Reflected Ions
$L_s = \frac{1}{6} y_1/\rho_i$
$T_{e_1} = T_{i_1}$
$\beta = 0.1$
2 3 4 5 6 7 8 9 10
M
$\beta = 0.3$
TOTAL IONS

FIG 8.6

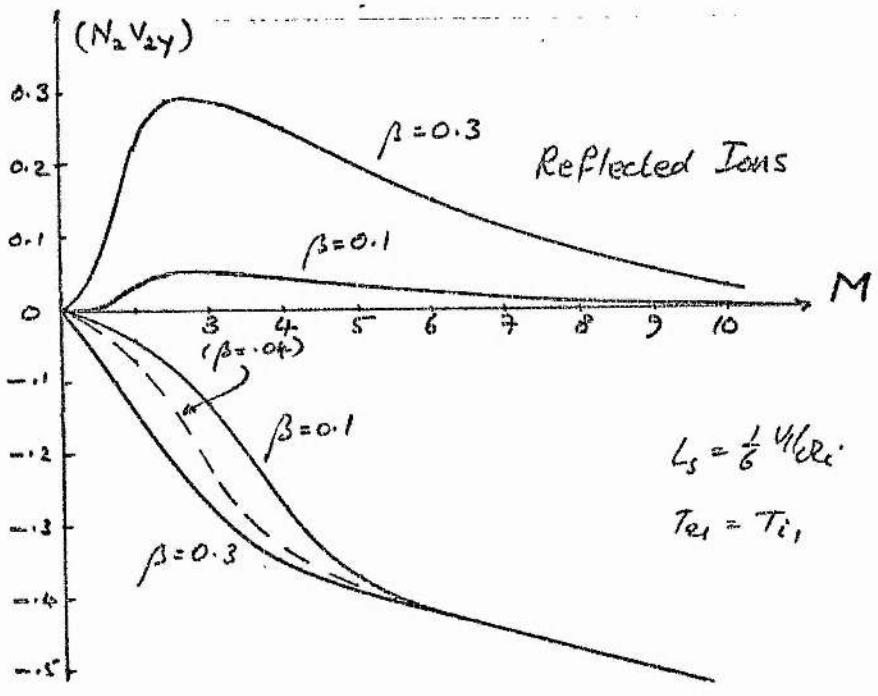
$(N_2 V_{2y})$
0·3
0·2
0·1
0
-·1
-·2
-·3
-·4
-·5
$\beta = 0.3$
Reflected Ions
$\beta = 0.1$
3 4 5 6 7 8 9 10
M
$(\beta = .04)$
$\beta = 0.1$
$\beta = 0.3$
$L_s = \frac{1}{6} y_1/\rho_i$
$T_{e_1} = T_{i_1}$

FIG 8.7

In spite of these drifts in the y-direction of the total ion component, the previous section has shown that they may be ignored. Thus it does not occur that when V_y is suppressed by a convenient value of L_s, that the drift kinetic energy reappears as temperature. In the non-self-consistent model, energy need not be conserved. What saves the model is the small dependence of ion temperature on L_s. It is otherwise not unimportant that these drifts occur in the model, for they help understand its physics, as occurs in section §7.

Figs. 8.4, 8.7, both show strong dependence on β, while the pure velocity curves do not. There is noticeable flux at β=0.3, even for M<M*, while at β=0.1, flux stays low. The total ion component gains a large net flux, roughly the same for both values of ϕ, in the y-direction as explained above.

At low M, β=0.1, where the initial temperature is a more significant proportion of upstream energy, the small ion heating observed in Figs. 8.1, 8.2, is due to the low values of fields in these weak shocks. The small values of ϕ in Fig. 8.3 are then responsible for small distortion heating of the main beam, while few reflections occur.

The behaviour at β=0.3 is an amplification of that at β=0.1. The question of behaviour at β>0.3 is then tantalizing. These cases are discussed below, as they suggest a new regime of shock types. The extrapolation to M>10 is easy to infer. The reflecting component eventually vanishes altogether, while some simple distortion heating takes place. The proportion of downstream ion energy (relative to the

total) has not yet been considered, but distortion heating of progressively colder ions must vanish. Indeed for $M\to\infty$, the model predicts undetectable ion heating. This must be compared with experiment.

At $\beta=0.04$ (the value of the low-β Culham experiment), small reflection is occuring. At any fixed value of M, Fig. 7.2 shows that falling β implies falling thermal ion spread (for some fixed T_e/T_i). The heating due to reflections vanishes at $M\gtrsim 6$, while the total ion component then falls. These results support the extrapolation to M>10, of the previous paragraph. The fluxes in the x-direction are small, and Fig. 8.4 finds them squeezed out of significance. The fluxes to V_y are more interesting. The large flow remains as M gets larger (Fig. 8.7). At $M\sim 3$, the fluxes are ordered oddly; thus $(nv)(\beta = 0.1) < (nv)\ (\beta = 0.04) < (nv)\ (\beta = 0.3)$ The explanation lies in the growing fluxes to $\pm y$ of both ion components as β increases. When no tail occurs, $(nv)\ (\beta = 0.04) \sim (nv)(\beta = 0.005)$, to -y, and is unchanged. As β increases to 0.1, so the main beam acquires small drift as the tail suddenly emerges. The displacement of the main beam is then increased as β rises to 0.3.

At $\beta=0.005$, a few plots to growing M show no emerging reflected ion flux at all.

Fig. 8.1 is a ratio of two more directly interpretable quantities. Thus the downstream thermal energy of the ions is $T_{i2} = T_x + T_y$ as above, while part of this heating is given by the adiabatic (no increase in energy) compression $T_{iad} = T_{i1}\ (n_2/n_1)^{\gamma_i - 1}$. Here $\gamma_i=2$ as required by the laminar field dynamics, and as qualitatively suggested by the experiments of Kornherr and Schumacher. Each of these

components having direct physical meaning should give new information. The adiabatic levels are not an unknown of the shock problem, and may be calculated from the Rankine-Hugoniot relations, and the initial ratio T_e/T_i. Useful further, for comparison purposes, is the ratio T_{i2}/T_{i1}.

Downstream temperature is shown in Fig. 8.8. Together with totals, given by the hard curves, are shown the usual transmitted ion contributions (dotted curves) and the adiabatic level (dashed curves). Non-adiabatic heating is now the difference between the hard and dashed curves.

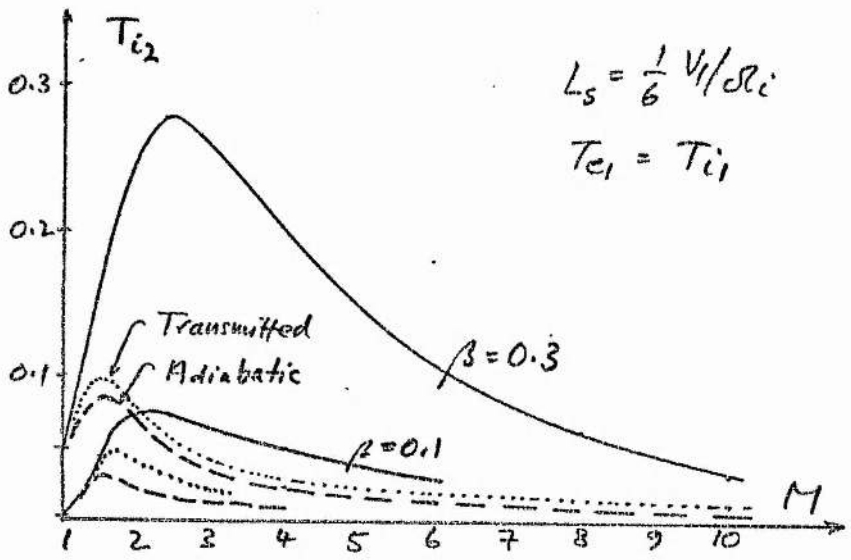

FIG 8.8

Such heating is clearly falling more rapidly than the adiabatic. The familiar asymptotic behaviour at large M is shown by the latter. The argument following Fig. 8.1, is easily applied to the explanation of these curves. Adiabatic (and other) levels are seen to rise from

M=1, in a region where density is increasing faster than initial temperature is falling, with M at fixed β. The enormous increase in ion energy in going from β=0.1 to β=0.3 is demonstrated. This matches the rapid rise in ϕ (of Fig. 8.3), while initial ion temperatures rise. Then as ϕ goes asymptotic to ϕ^* (approximately), low ion temperature causes a fall in T_{i2}.

The temperature jump in going from the up- to the downstream is shown in Fig. 8.9

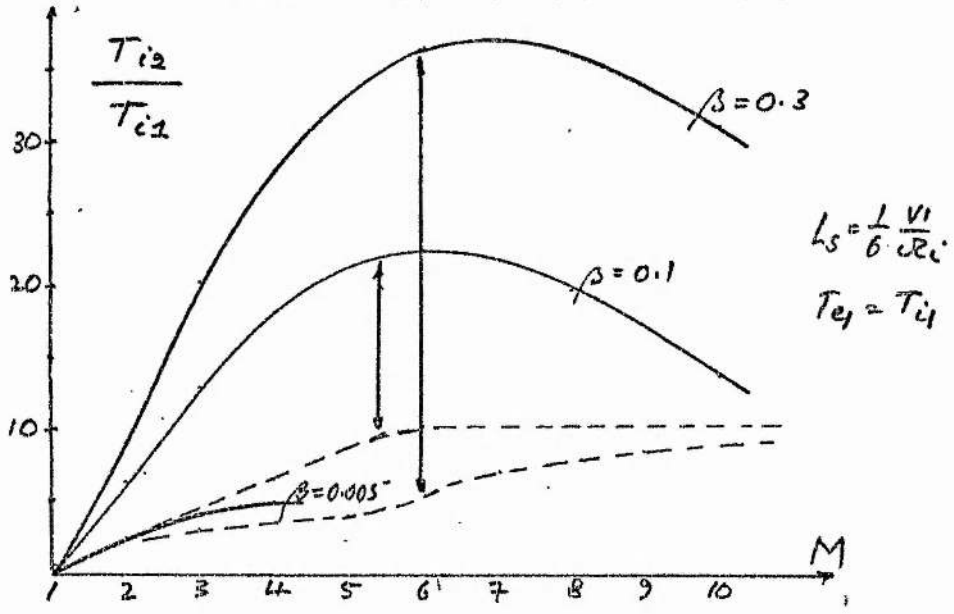

FIG 8.9

The Culham shock is at M$\sim$3.5, β=0.1. In the perpendicular direction, the ions have been heated about 16 times. The low β=0.005 shocks, show the ions heated about 5 times (most of this is adiabatic). The transmitted components are quite interesting. While total and transmitted energies increase when β increases, the energy jump of the transmitted has decreased. The measure of transmitted ion heating

is made downstream by integration over this beam only, and is quite accurate. In the upstream it is necessary to decide whether the temperature of the ions, to be transmitted, is equal to that of the whole initial ions, or to that of the initial ions with the reflected (to be) ions removed. Here the initial ion temperature is used so that an underestimate of transmitted ion heating might occur. The "cut" made by the electric potential in f_1, into the two ion types is not simple (Fig11.13, below), making estimates of separate beam densities obtainable only by numerical integration of the upstream f_1, once the cut has been determined. However, as long as the ions are not too hot, with a few reflections occuring, the error is small This error will increase with β.

The adiabatic heating is calculated using the measured density n_{2M}. Then due to increasing loss of density to reflections, with increasing β, the temperature jump of the main beam may get smaller. This can be illustrated, too, in the easily and accurately generated L_s=0 case (Fig. 8.2).

The variation of heating with β is quite slow, as may be seen from Fig. 8.10.

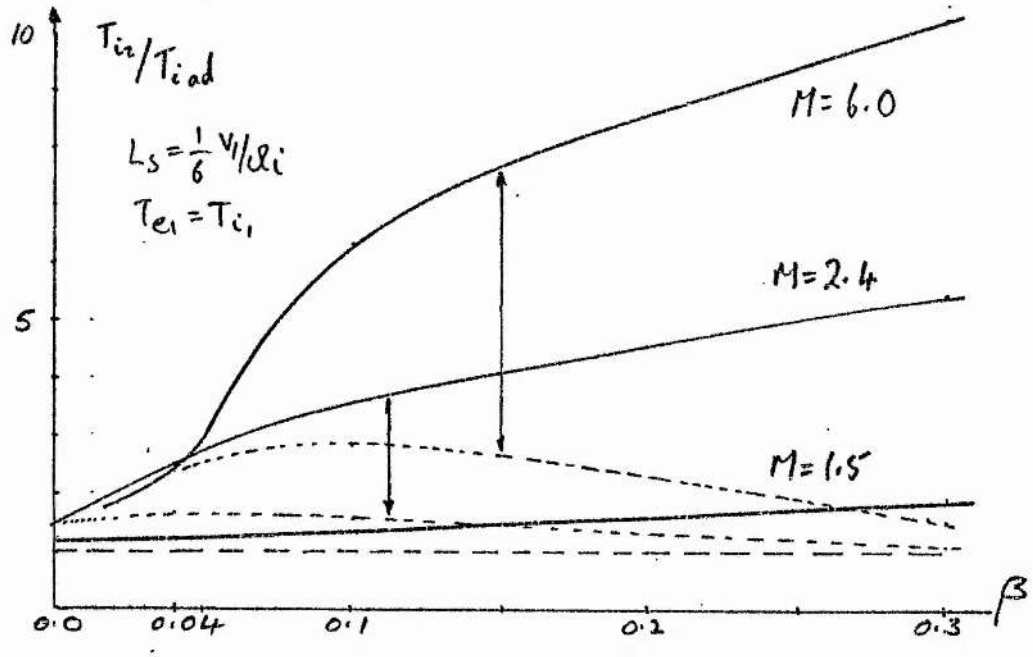

FIG 8.10

Taking sections of the heating surface T/T_{ad} (over M,β-space), at constant M, gives variation with β at M=1.5, 2.4, 6.0. At small $\beta \gtrsim 0$, a behaviour similar to that at small M occurs. Thermal spread is so low that no reflections occur and only small heating is expected. At β=0.005, the $L_s=0$ and $L_s=1/6\ V_1/\ell_i$ cases are more or less the same, and even at large Mach number, low-β heating is small. It has been noted above that at $\beta \lesssim 0.04$, reflecting ions occur when M>M*. Thus at M=1.5, the curve remains slowly increasing while there is quite rapid increase for higher M=2.4>M* and M=6.0>M*. As β increases now, or as thermal spread increases, so there is significant continuation of the trend. But now the trend may continue as β goes

greater than 0.3, so long as the model holds. So, Fig. 8.10 shows increased non-adiabatic heating with β. The behaviour of the M=1.5 curve, contrasted with that of the transmitted ions at higher M, again shows the decreasing effect of the main beam as its density diminishes at the expense of reflections.

The variation of initial temperature with β may easily be seen from Fig. 7.3. The other important factor in ion heating is the electric potential. This is shown in Fig. 8.11.

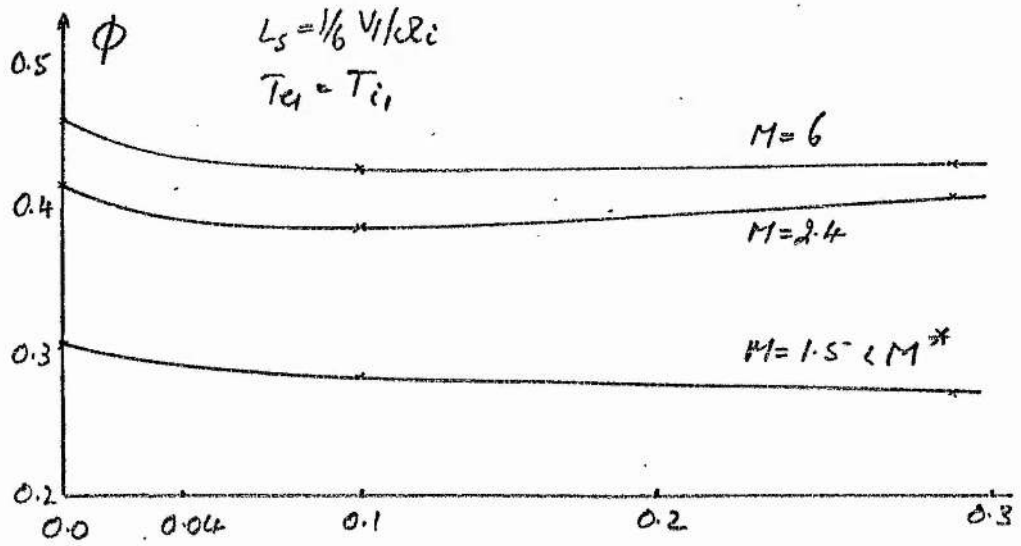

FIG 8.11

At low β there is a fall in ϕ. When M>M*, ϕ then remains roughly constant with β. For M<M*, the curve falls all the way to β=0.3. There is again only slow dependence on ϕ, so that ion thermal spread must be invoked to explain reflection contributions to Fig. 8.10. The lower curve is of interest. No reflecting ions occur at β=0.005, and

the model is clearly finding it easier to slow the ions as β increases. This is of course due to distortion heating of the ion Maxwellian even at $M \leq M^*$. (The value ϕ^*, required to slow the cold ion beam increases very slowly with β). Now at higher Mach number, much greater ion heating is observed as shown in Fig. 8.10, so that similar and exaggerated behaviour of ϕ at high $M > M^*$ is expected. This is patently not the case. Growing reflections are forcing an increase in ϕ to effect their proper slowing consistent with V_2, downstream. It has been seen above that the model will sometimes fail to adequately slow the ions (Garching parameters), whatever the value of ϕ. This increasing potential at high β heralds the collapse of the laminar model in an extrapolation to higher β.

It is expected that as ϕ increases, to try and slow the fast ions, so the flux of ions should increase. These are shown in Fig. 8.12.

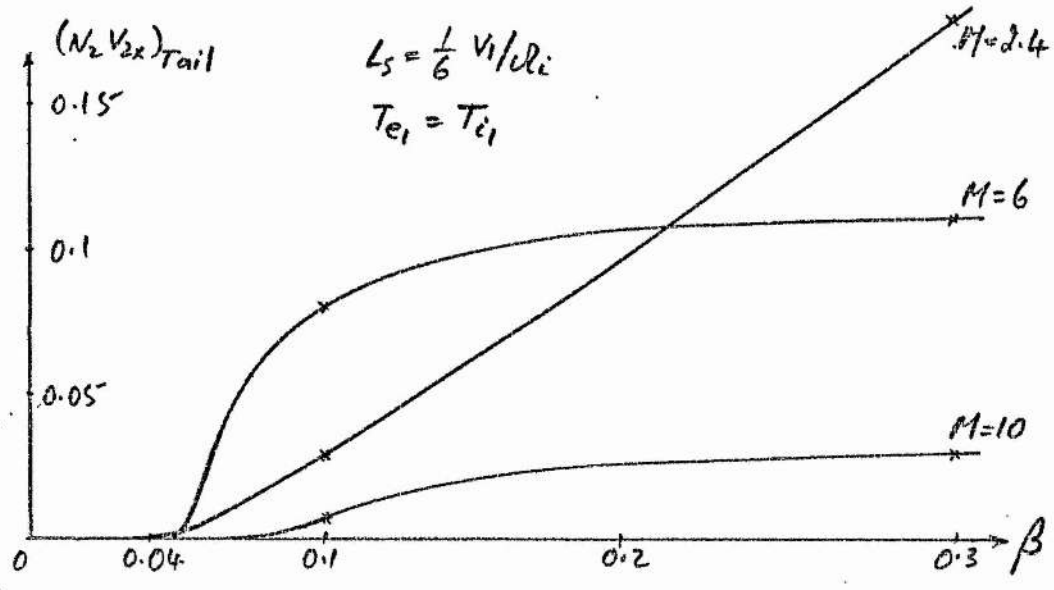

FIG 8.12

The curves are at first sight slightly odd, for $(nv)_{M=2.4}$ > $(nv)_{M=6}$ at $\beta=0.3$, where ϕ is increasing. This curve should be inspected simultaneously with Fig. 8.4 for flux variation with M- there this fact is explained. Here the variation at constant M is considered. Then the intriguing event is the large slope of these curves at M=2.4, $\beta=0.3$, where reflections are a maximum. The increase in ϕ should be most noticeable in this region, and indeed, the M=2.4 potential shows traces of a more rapid climb, than does the M=6 curve. At M=10, low flux is apparent, and previous paragraphs have suggested that in an extrapolation to high M, reflected ions disappear entirely. It would then be expected that at M=10, ϕ has the same behaviour as the M=1.5 case. Indeed it is found that ϕ decreases monotonically on this range of β.

Then the evidence above, as concerns the ion heating may be summarized as follows:

(i) First, in variation with M, there is a low $M<M^*$ region (for all β) where few reflections occur, with some heating due to distortion of f_1 by the potential-but the shock is weak and the effects likely to be small; when $M \gtrsim M^*$, significant reflections rapidly appear with a strong contribution to downstream ion energy - in this domain a balance is struck between reflections off the electric potential and the ability of that same potential to properly slow the ions; when $M>>M^*$, the ions become so cool (at fixed β), that no significant ion behaviour can be expected, heating stays low, and the electric

potential approaches a level where $R_\phi \sim 1$.

Strong visual support for these points is given by a rapid progression of displays of the downstream ion distribution f_2, over its two-dimensional velocity space. Then at $\beta=0.1$ and in an order M=1.5, 2.4, 4, 6, 10, Figs 8.12, 13, 14, 15, 16, are presented.

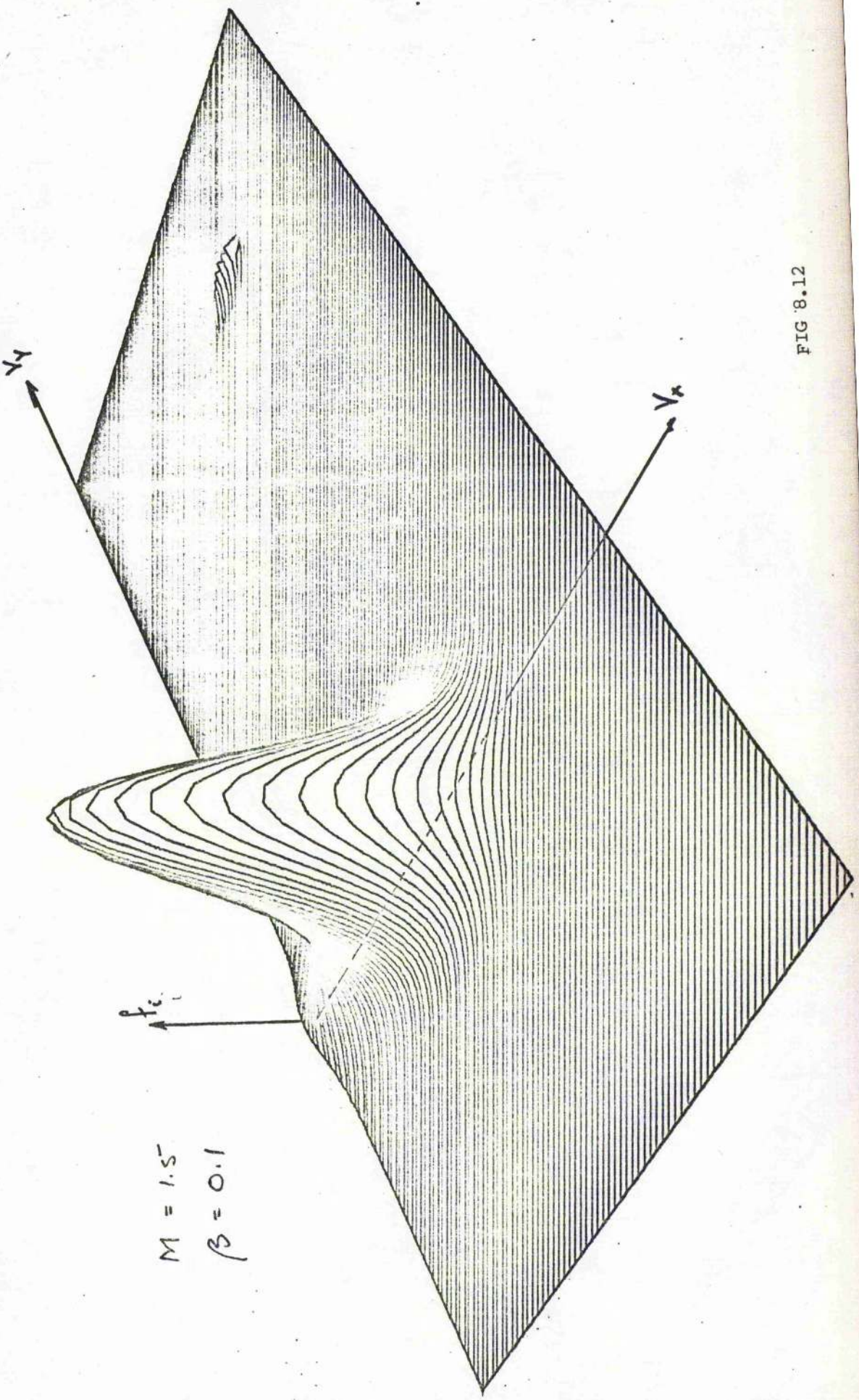

FIG 8.12

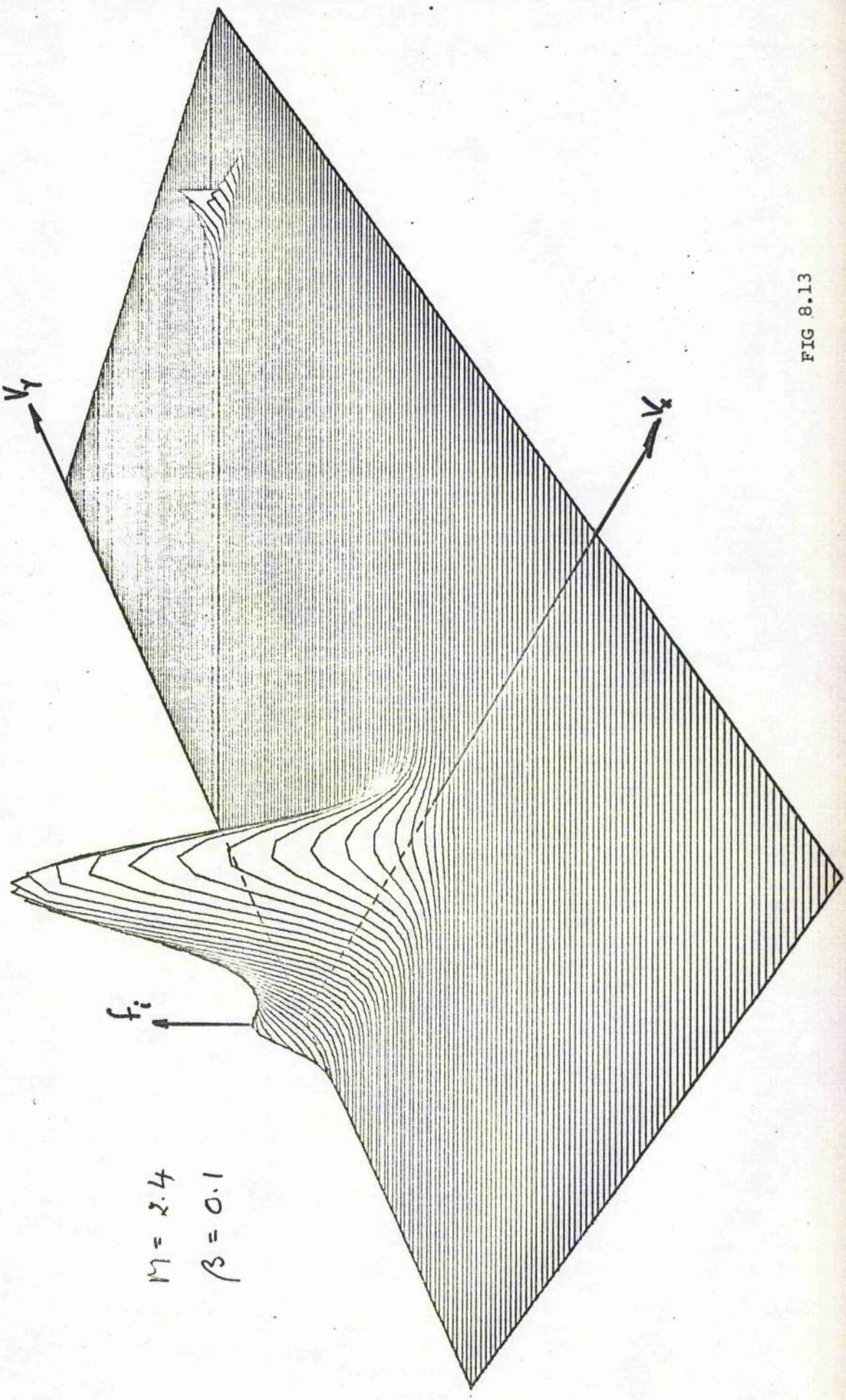

FIG 8.13

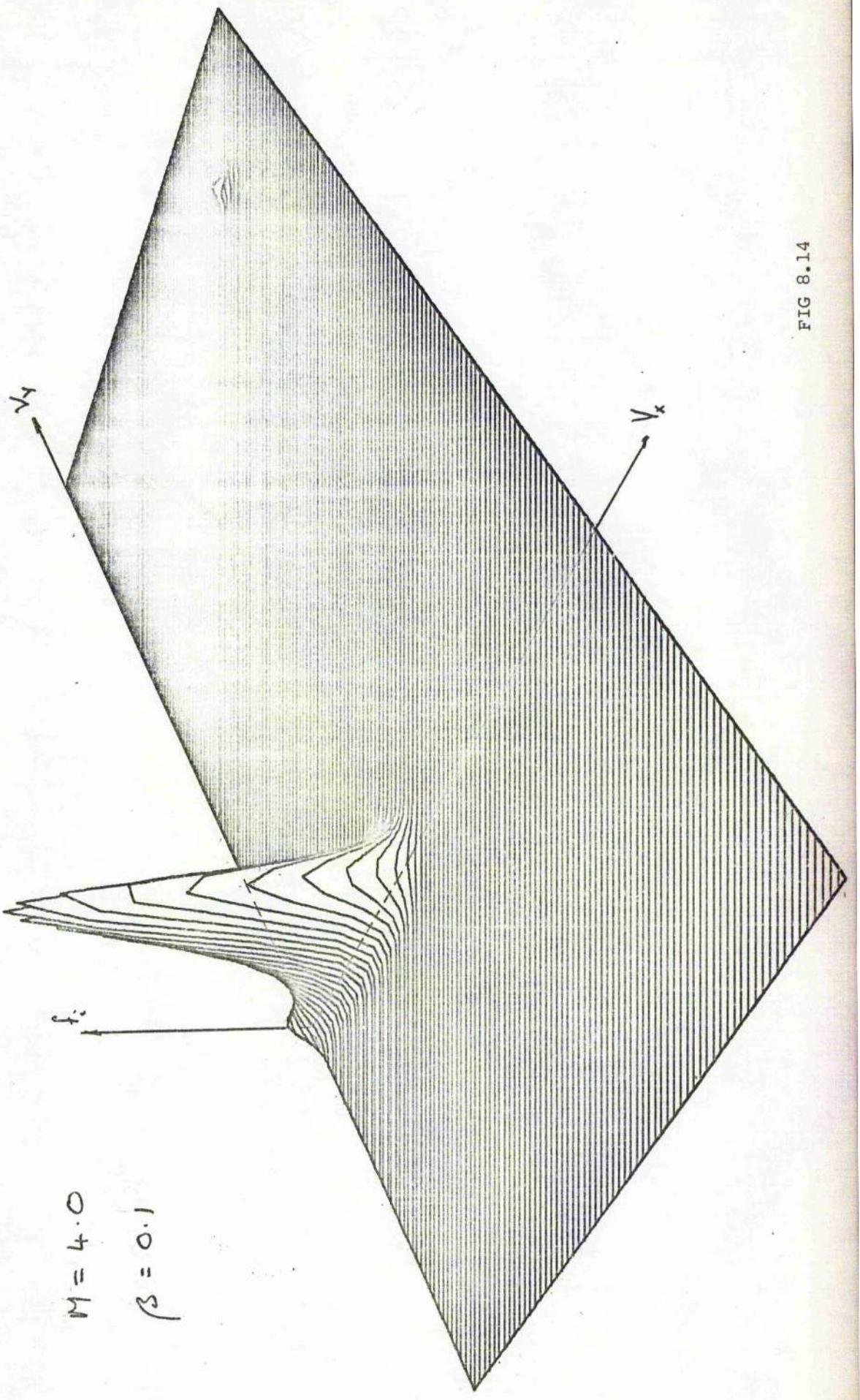

FIG 8.14

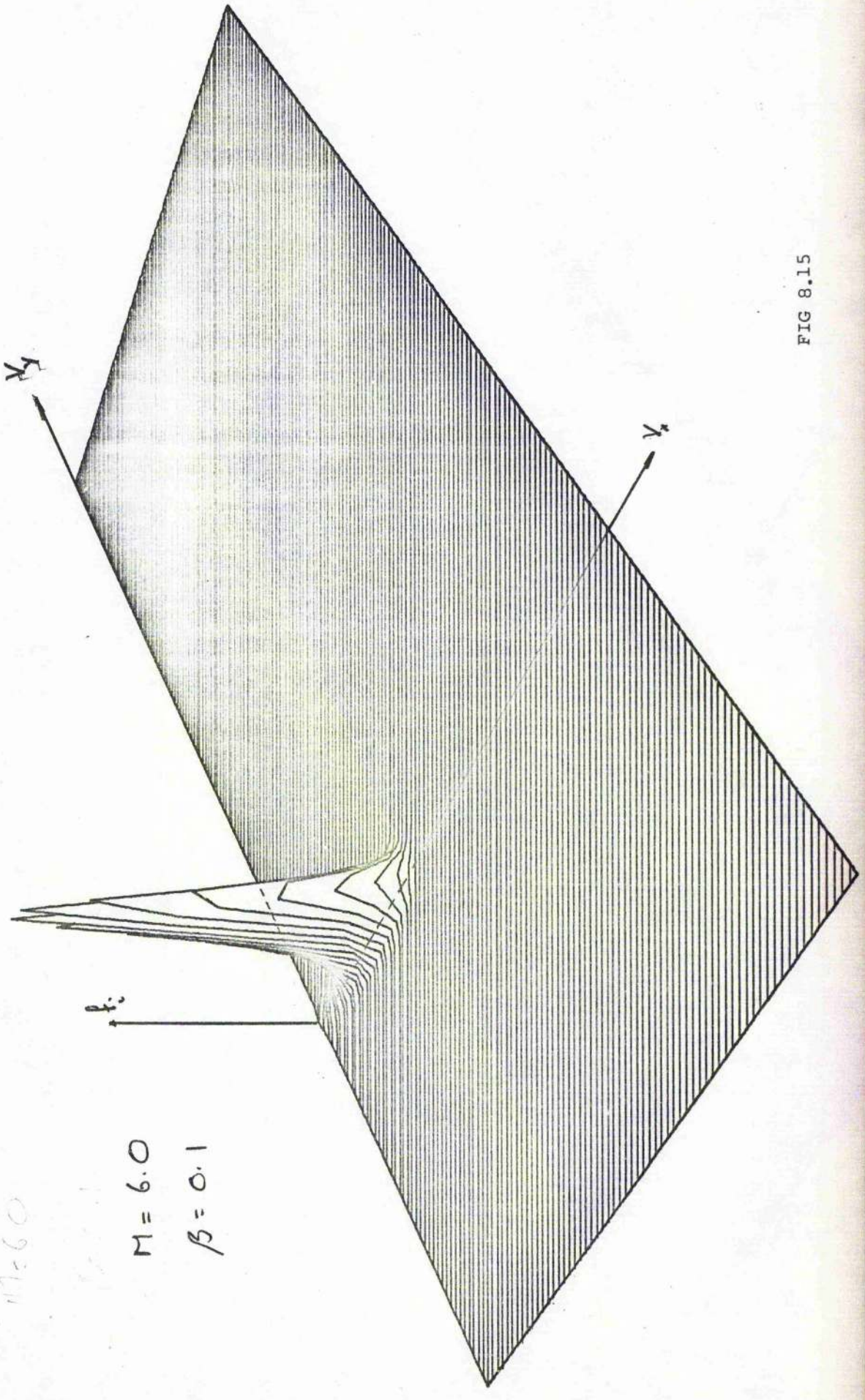

FIG 8.15

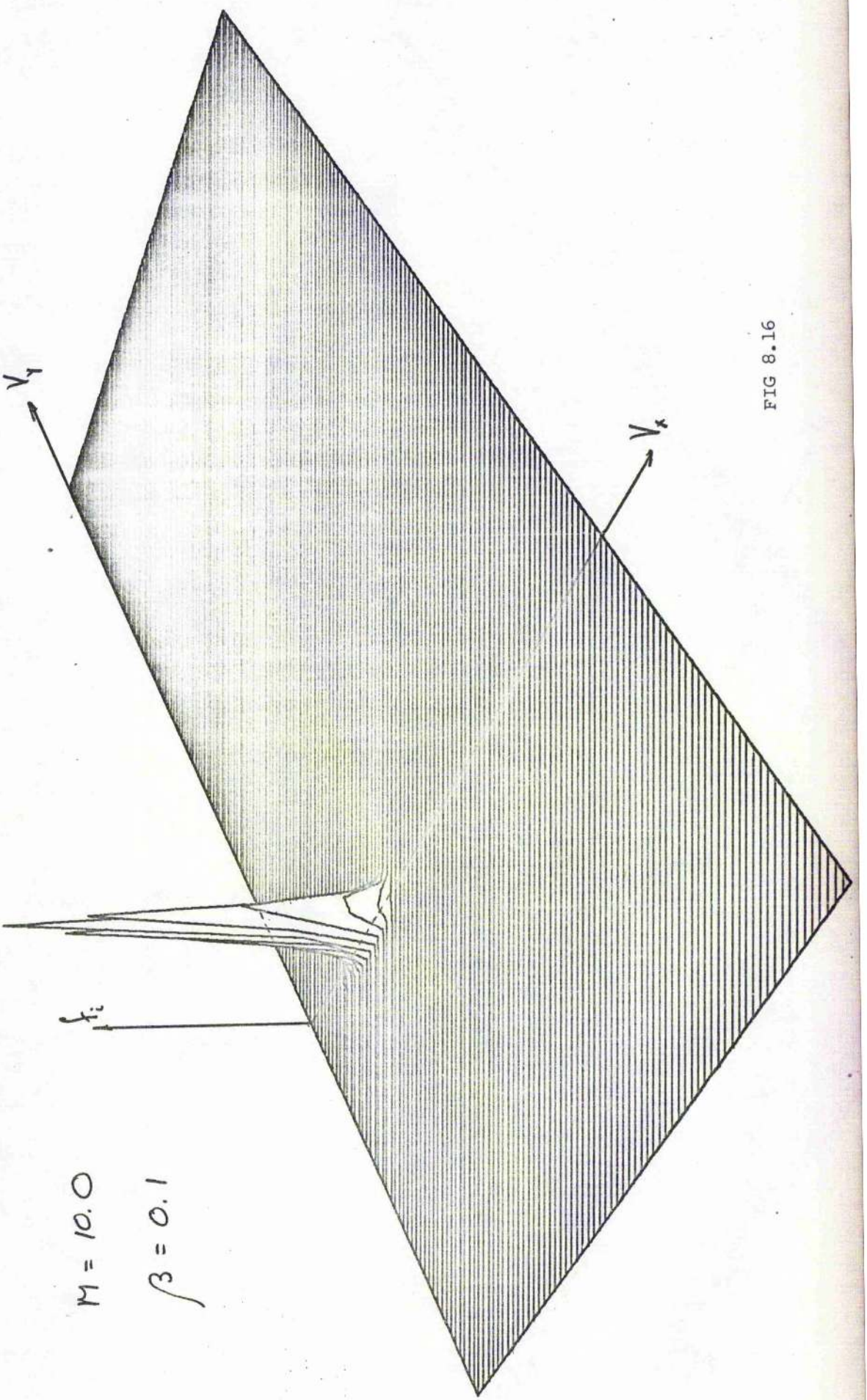

FIG 8.16

A useful feel for the explanations above results. The distribution holds all the information on the shock, except for the self-consistent electric potential.

At low M=1.5, just a trace of reflections are occuring, with none detected by the model at finer grid sizes. The wide thermal spread is noted. In the progression to M=2.4, the main body of ions is noticeably slimmer and more elongated. It may be expected, then, that this suffers stronger heating. Clearly some flux has been lost to a fast beam of reflected ions. The numerical integrations show that never-the-less, this main body is heated above that at M=1.5. The reflections manifest themselves by the vertical face at V_x=0 - the truncation of the upstream Maxwellian by the potential - and by their reappearance with large $+V_x$, $+V_y$ - coordinates in $\mathcal{V}_2$. The height of the (roughly drawn to this grid size) fast beam, at the face, is approximately that of the V_x=0 face. At this point, about 64% of ion non-adiabatic heating resides in this small beam. As M is increased now to 4 (Fig. 8.14), the fast beam is disappearing. The main beam shows further cooling, by its reduction in width. The face at V_x=0 shows that the display is losing some of the reflecting ions, but it has been significantly reduced from the M=2.4 example. (Fig. 8.13) At M=6, the face at V_x=0 has almost vanished. The integrations show that once again the (now total) main body has increased its temperature above adiabatic, as compared with M=4.0. At M=10 (Fig. 8.16), no vestiges of reflections are found. The ions are highly localized in $\mathcal{V}_2$.

It must be remembered that these plots are made under the approximation $L_s=0$, and so the rotation of each distribution about the magnetic field in the shock, or the Lorentz displacements of the beams, are ignored.

The height of each distribution is automatically scaled by the computer to fit the page. Thus it is necessary to observe the scaling of f_i. This is given usefully by f_{max} which increases strongly as the ions get colder; they rise from $f_{max}\sim 16$ at M=1.5, to $f_{max}\sim 630$ at M=10. This is very pleasing visual information, and yet is easily underestimated. For it is these surfaces, and not the integrals over them, that are the solutions to the shock problem, together with ϕ.

Attention may be drawn to the large elongation at low V_x of the main beams. The effect is strong and it is noted again thay they supply a necessary bias of this beam to a drift $v_2<V_2$, for $R_\phi<1$ and reflecting ions occur with drift $v_2>V_2$.

(ii) Second, in variation with β, there is a low-β region, which is denoted $\beta<\tilde{\beta}$, (in parallel with (i)) where no reflections occur, but may be situated at M>M* - the conditions M>M*, $\beta<\tilde{\tilde{\beta}}$ then show that breakdown of the two-fluid theories is here not due to the overturning of the ion beams as is commonly assumed; when $\beta\gtrsim\tilde{\tilde{\beta}}$, a region of ion reflections results where (when M>M*) as in (i), a balance is found between ion reflections off ϕ, and consistent slowing of the ions; the question of $\beta>>\tilde{\beta}$ must yet be considered, but the indications are that ϕ is inadequate (Garching parameters) and the laminar model fails.

Then as in (i), visual support is given to these ideas by Figs. 8.17, 18, 19 where at M=2.4, β=0.005, 0.1, 0.3, respectively.

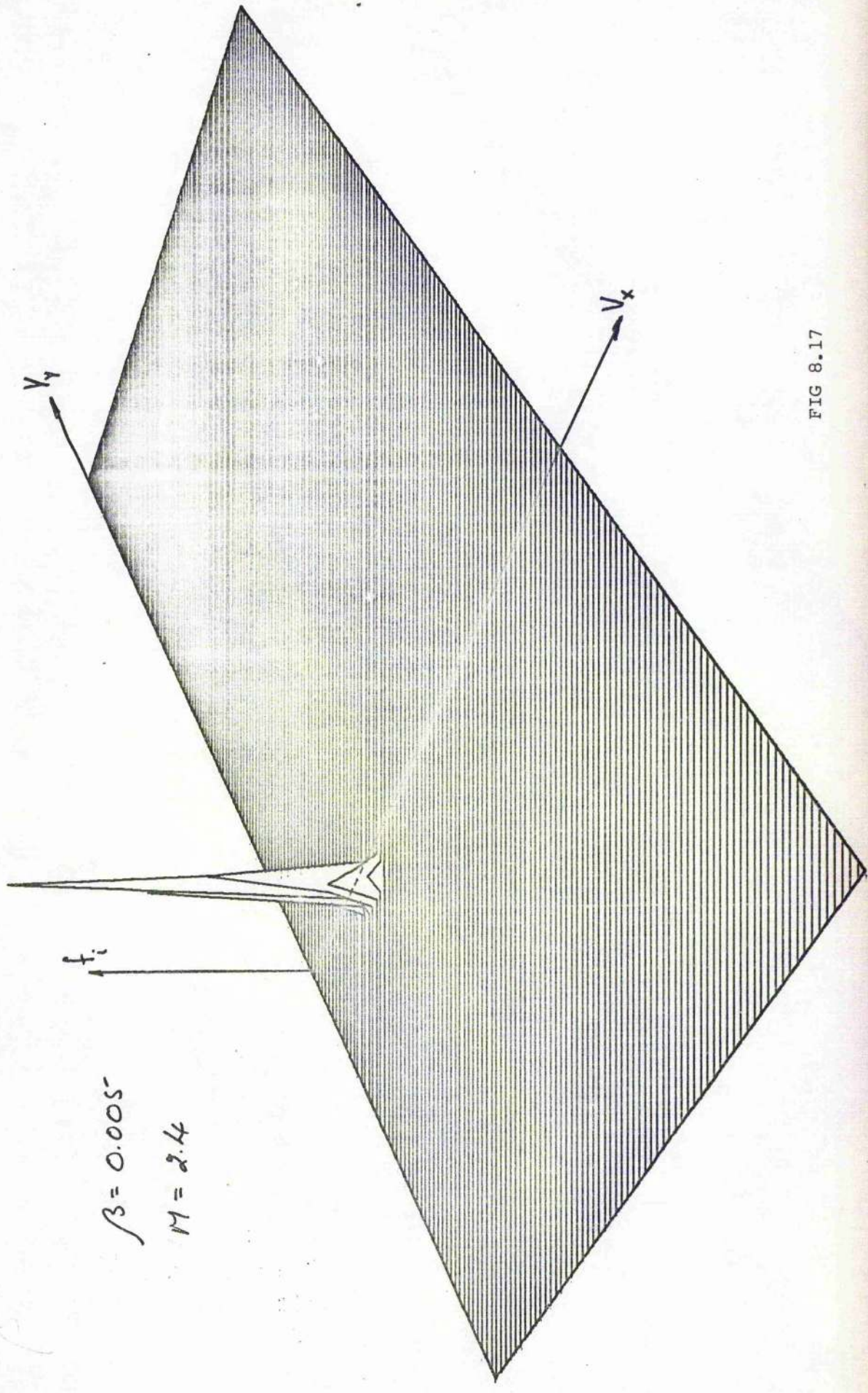

FIG 8.17

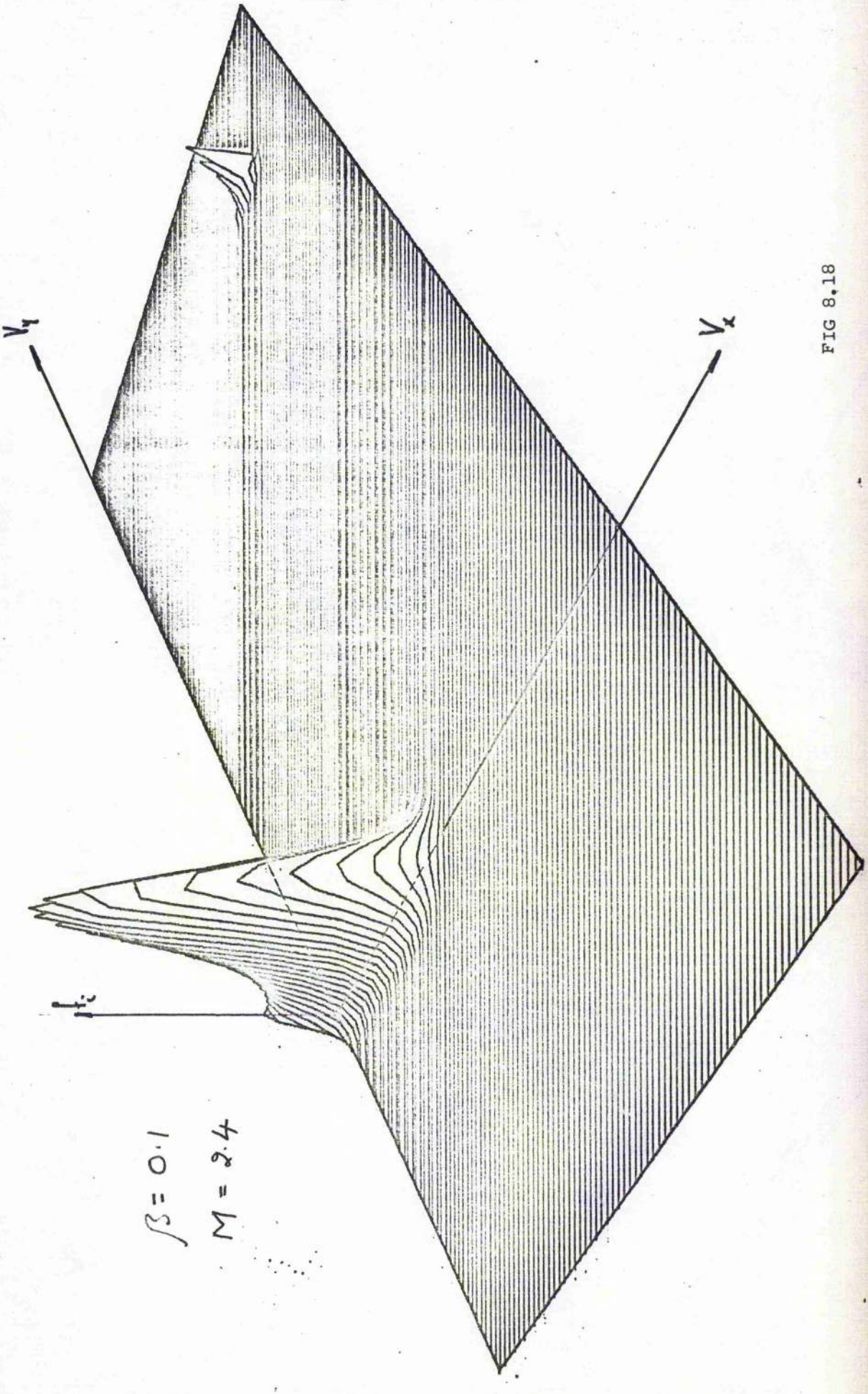

FIG 8.18

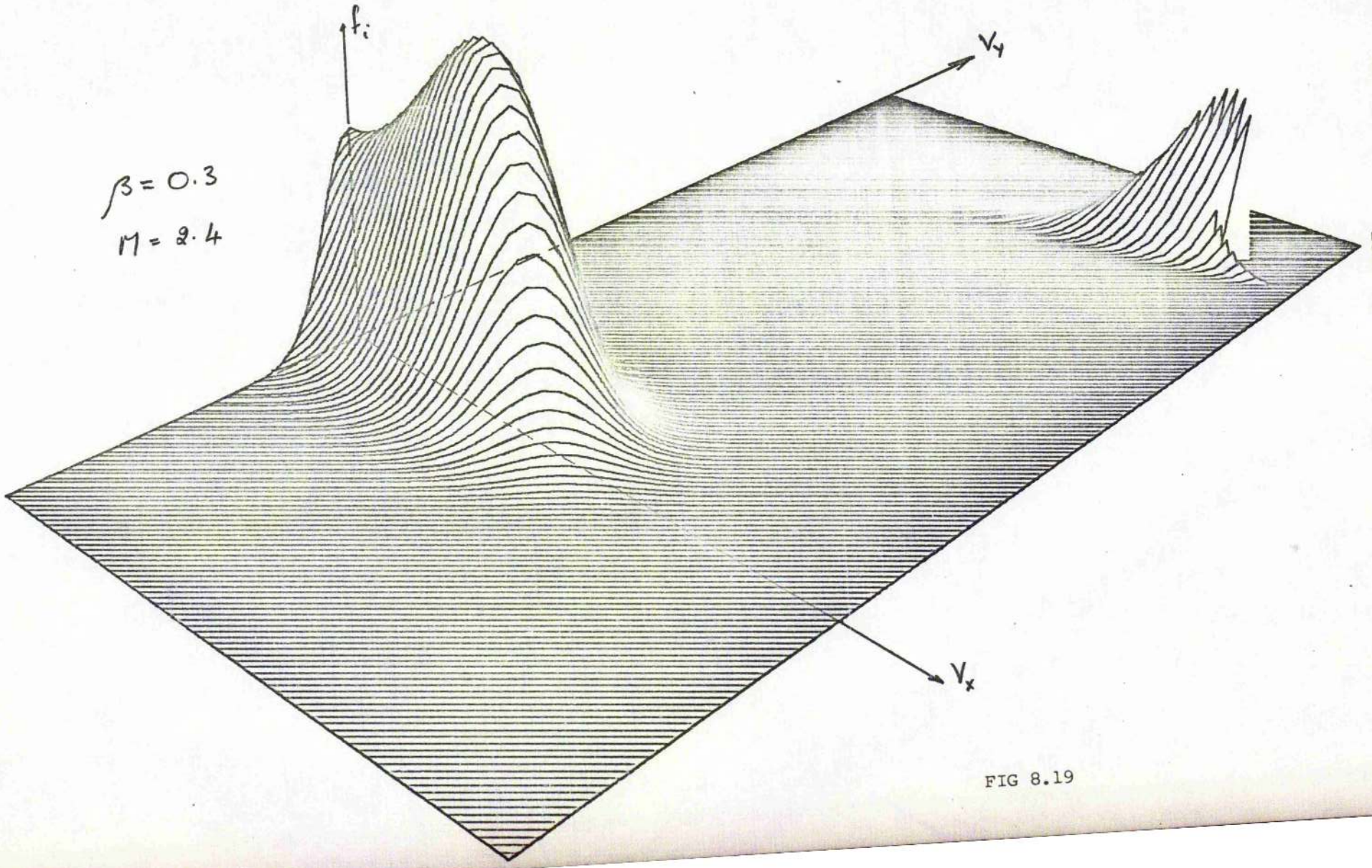

FIG 8.19

The remoteness of the low-β example from the v_x=0 axis is extreme. No skewing is found, while neither this display nor the numerical integrations can detect reflected ions. This is then the behaviour for all M. The collapse of the fluid theories is due to their ignorance of the velocity space distortions, in the laminar fields, and not to the appearance of three-valued flows, wave breaking, and the appearance of turbulence. This heating is small at all M, and a change in the nature of electron heating is not expected. At higher values of $\beta > \tilde{\beta}$, some reflections are seen (Fig. 8.18). This display is a reproduction of Fig. 8.13. At β=0.3, a very marked reflected ion tail is found. Again, extrapolation of these trends must be considered. The following paragraphs will suggest a solution to the problem.

The Rankine-Hugoniot relations allow the total temperature, $T_2=T_{e2} + T_{i2}$, to be calculated. In the laminar fields, this level applies even to the distributions of the model. Then

$$5T_2^{RH} = 5T_1 + (1-V_2^2) + \frac{2}{M_A 2}\left(1-\frac{1}{V_2}\right) \quad . \qquad (8.1)$$

It is now assumed that the ions gain or lose no thermal energy after they have left the shock, but merely rearrange this energy equally in 3 degrees of freedom. Then T_{i2} is this temperature, calculated as

$$T_{i2} = (T_x + T_y + T_z) \; / \; 3 \qquad (8.2)$$

In Fig. 8.20, plots of T_2^{RH}, and T_{i2} are given. The upper curves are the Rankine-Hugoniot levels. It is striking that at $M \lesssim 2.5$, the ion energy is of the order of the total allowed thermal

content downstream! On $1.4 \lesssim M \lesssim 2.4$, a self-consistent solution is not obtained, for energy is not conserved. Since this abnormal energy is held in the reflected ions (the transmitted level is shown by the dotted curve), and the flux of these ions will increase with β, it seems that at $\beta > 0.3$, the model collapses (at low, but increasing with β, values of M).

FIG. 8.20

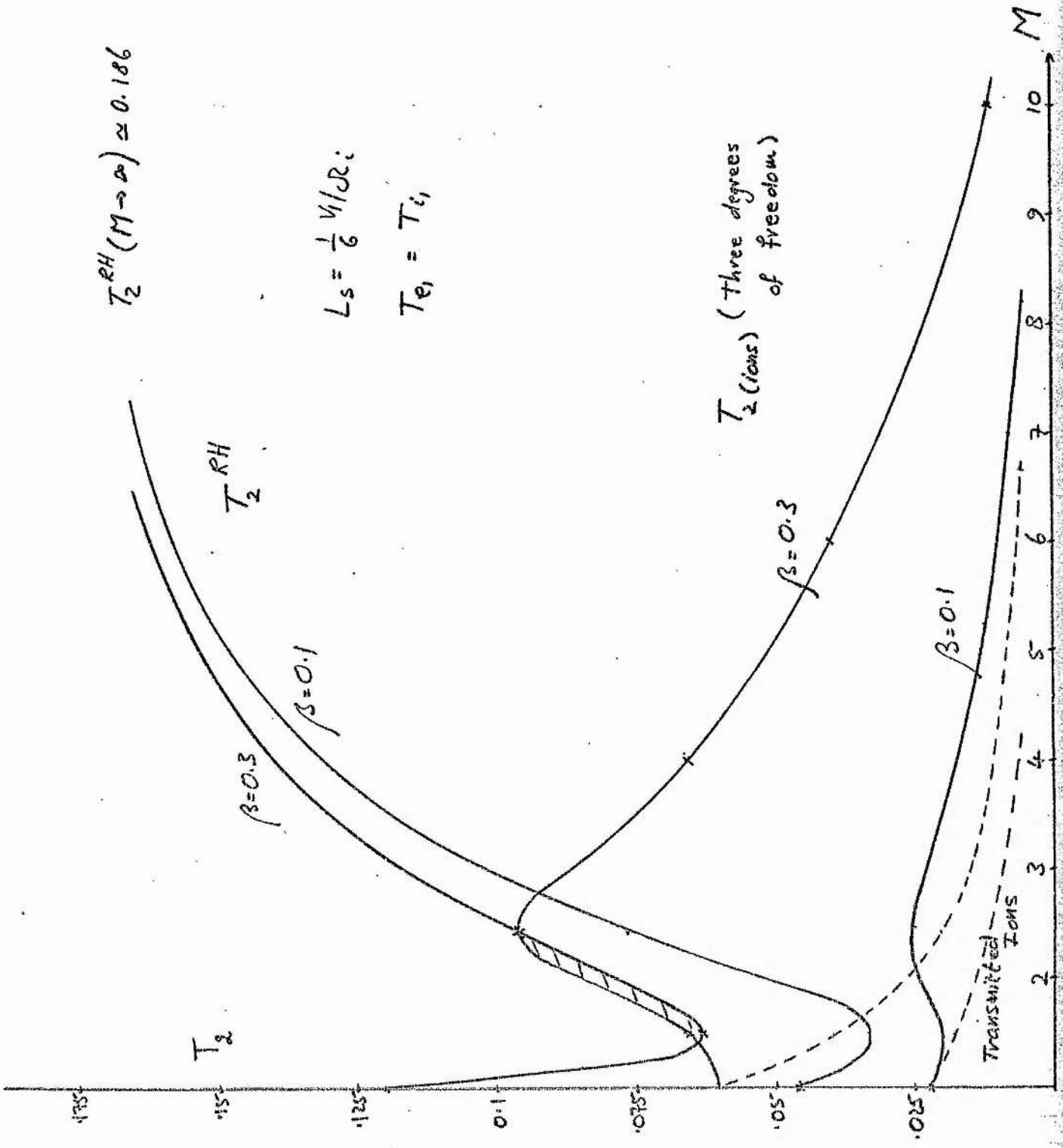
$T_2^{RH}(M\to\infty) \simeq 0.186$
$L_s = \frac{1}{6} V_1/\Omega_i$
$T_{e_1} = T_{i_1}$
T_2^{RH}
$T_{2\,(ions)}$ (Three degrees of freedom)
T_2
$\beta=0.3$
$\beta=0.1$
$\beta=0.3$
$\beta=0.1$
Transmitted Ions
M
.135
.15
.125
0.1
.075
.05
.025
2
3
4
5
6
7
8
9
10

It would seem that all the requirements of the conservation relations have been met. Thus flux is high always, $N_1V_1 = N_2V_2$. The ions have been properly slowed, $V_1B_1 = V_2B_2$. It is discussed in section 7, that the proper choice of L_s must be made, to conserve momentum in the y-direction. However, at low M, the $L_s=1/6\ V_1/\Omega_i$ choice is quite accurate ($M<\hat{M}$). Yet energy is not conserved.

It is now required that the jump in ion energy must be checked consistent with the conservation relations.

Then extrapolation to higher β, of Figs. 8.17-19, represents the breakdown of the model.

The results of the β=0.3 runs allow no electron heating at all, which is clearly unreasonable, and the $\beta\sim$0.3 limit is favourable to the model. At larger value of M, Fig. 8.20 shows a strong fall in the role of ion heating. This fall corresponds to the decreasing initial ion temperatures at fixed β, and increasing M. The graph is interesting as it requires large electron heating. At M=10, β=0.3, ion heating is about 6% of the total, and beyond experimental detection. Electron temperature ratios T_{e2}/T_{e1}, T_{e2}/T_{i2}, are shown in Fig. 8.21.

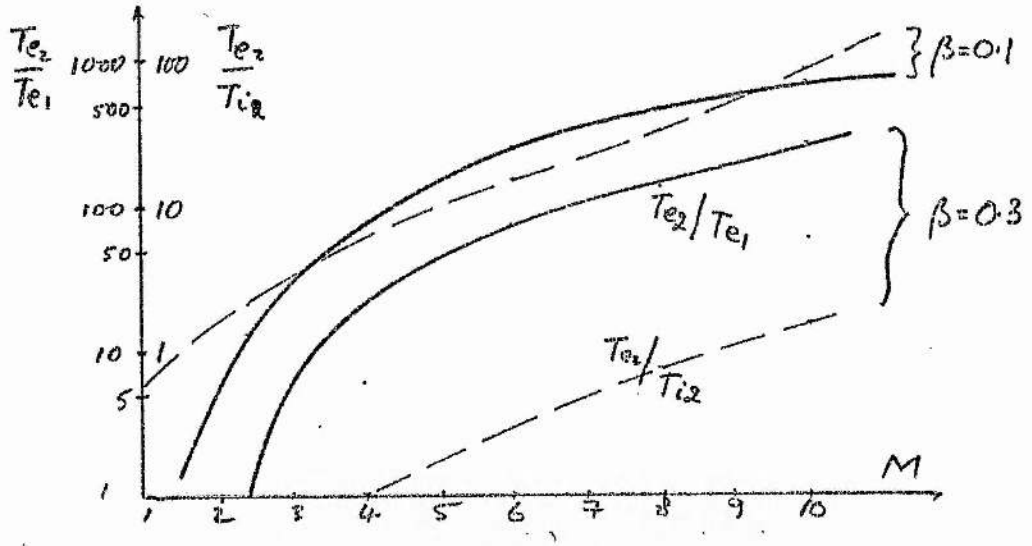

FIG 8.21

They are clearly decreasing with increasing β, but even at M=10, β=0.3, $T_e \sim 10 T_i$. The form of the R-H solution at high M_1 hides the mechanism of electron heating. The rapid fall at M<M* of T_2^{RH}, is due to the term $2(1-1/V_2)/M_A^2$ of equation 8.1. As M→∞, this tends to zero and T is determined by $(1-V_2^2)$. It is noted that this is just $2\phi^*$. Heating is found from the slowing of the ion beam. The electric potential dominates and ion heating is small with $R_\phi \sim 1$. There then appears to be a return to the case of low-M, simple, resistive shocks with anomalous electron heating. It has been assumed in this work, that some adequate form of electron heating always exists. The high M example is unclear but the following point emerges. That if $L_s = 1/6\ V_1/\Omega_i$ is fixed, then $dB/dx = -J_y^{(e)}$ is fixed. Increasing electron heating over ion heating at high M by a universal instability will be suppressed. On the other hand, a $C/\omega_{pe,i}$ dependence gives increasing dB/dx, and increasing currents in the shock face, since in units of V_1/Ω_i, $L_s \propto V_1/\Omega_i \to 0$ when $L_s = C/\omega_{pe,i}$, always, This is then further argument for a shock thickness in units of $C/\omega_{pe,i}$.

At high M, if the electrons are adequately heated without introducing ion-scale turbulence, and ion reflections have ceased, a second critical Mach number is suggested which marks the end of the overturning of the ion beam, If the model is satisfied, then ion distortion heating occurs. Otherwise, the laminar profiles are suspect. In either case, the two-fluid theory will not apply, consistent with M>M*.

9. On the Electric Potential

It has frequently been necessary to invoke data on the electric potential, in previous chapters. This quantity is itself an important unknown of the model. A solution in the case $\beta=0.1$ has been given above in Fig. 8.3. At face value it is extremely simple, and may be compared with the plot of $\phi^* = (1-V_2^2)/2$ for an explanation of its smooth shape. An ion heating mechanism has of course been proposed and so $\phi<\phi^*$ is not unexpected. But this curve hides a wealth of detail, so that as perhaps the second major concern of the model, these are now studied.

The final solutions for ϕ are shown in Fig. 9.1. At fixed $\beta=0.005$, 0.1, 0.3, ϕ is plotted over the variable M, at $L_s = 1/6\ V_1/\Omega_i$.

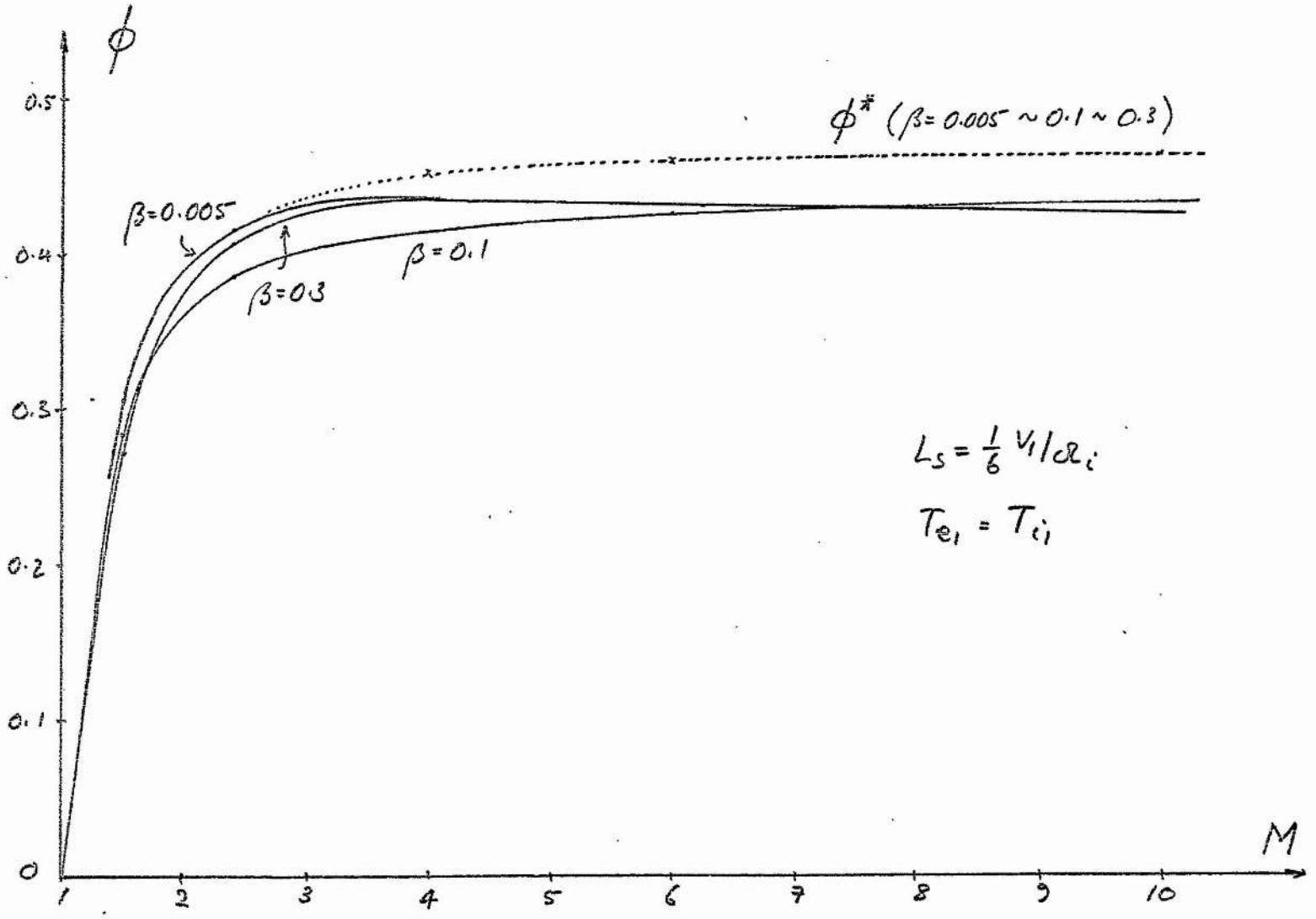
ϕ
ϕ^* ($\beta = 0.005 \sim 0.1 \sim 0.3$)
$\beta = 0.005$
$\beta = 0.1$
$\beta = 0.3$
$L_s = \frac{1}{6} V_i / \omega_{ci}$
$T_{e_1} = T_{i_1}$
M
0.5
0.4
0.3
0.2
0.1
0
1
2
3
4
5
6
7
8
9
10

FIG 9.1

The dotted curve indicates the (often used) potential to slow a cold ion beam. The energy jump of this beam is calculated for shocks at constant β=0.005, and varying M, and yields the potential $\phi^*_{0.005}$= $(1-V_2^2)/2$. Only this value of β is used, as the variation of ϕ^* with β is less than 1%. Because the properties of ϕ^* are clearly defined, it is a useful tool for comparison purposes. When $\phi \leq \phi^*$, it is recalled that $R_\phi = 2\phi/(1-V_2^2) \leq 1$. When R_ϕ=1, and it is insisted that the ions are cold, then the simple energy balance

$$\tfrac{1}{2}MV_1^2 = \tfrac{1}{2}MV_2^2 + e\phi, \qquad (9.1)$$

is satisfied. The ions are slowed only by the potential. Since every ion follows the same orbit in L_s, no distortion of the initial distribution occurs, and the cold ions are unheated. There are no ion reflections.

The shape of ϕ^* is the same for all β. At M=1, no magnetosonic shock exists and so ϕ^*=0. As M>1, so $V_2<V_1$ and ϕ^* must increase to slow the ions to V_2. There is a sharp rise at low Mach numbers, but then the asymptotic nature of V_2 (to $\frac{1}{4}V_1$) results as $M \to \infty$, in an asymptotic behaviour for ϕ^*. Then $\phi_{max} = 15/32 \underset{\sim}{\sim} .47$ in the non-dimensional units of this thesis.

The general conformity of the solutions of the model, with ϕ^*, is interesting and encouraging, for the model attempts an involved estimate of ϕ.

At β=0.005, the solution $\phi \underset{\sim}{\sim} \phi^*$ is found at low M<M*. There is

very little ion heating and no ion reflection, and this is as expected. At $M>M^*$, small ion heating occurs, and $\phi<\phi^*$.

At $\beta=0.1$ a further reduction in ϕ has occured. Again as expected, some upstream kinetic ion energy goes into downstream "temperature" to account for $\phi<\phi^*$.

The shape at $\beta=0.3$ is then very curious. At $M<M^*$, the potential has again been reduced below the levels of $\beta=0.1$; ion heating has increased, and so ϕ is reduced. But when $M\gtrsim M^*$, and downstream temperature continues to rise, the potential now increases! In this case the understanding of the energy balance is affronted. Then at $M>>M^*$, the potential again drops below that at $\beta=0.1$.

Explanation of the experimentally observed $R_\phi<1$ has been quoted as an important problem in shock physics [9], as it is closely related to the ion heating [11,12,14]. The observation is always simultaneous with $M>M^*$ and reflected ions, as shown by the foot in field profiles. The paper of Eselevich et. al. [11], gives low-β (≤ 0.05) measurements of R_ϕ. The model offers an ion heating mechanism so has an explanation for $R_\phi<1$. But it also predicts an increase in R_ϕ as β increases above $\beta\sim 0.1$.

In Fig. 9.2, plots of R_ϕ are given for the above explanation (Fig 9.1). Here $L_s = 1/6\ V_1/\Omega_i$, $T_{el} = T_{il}$. The effect is seen to be moderate, and always less than $\sim 15\%$.

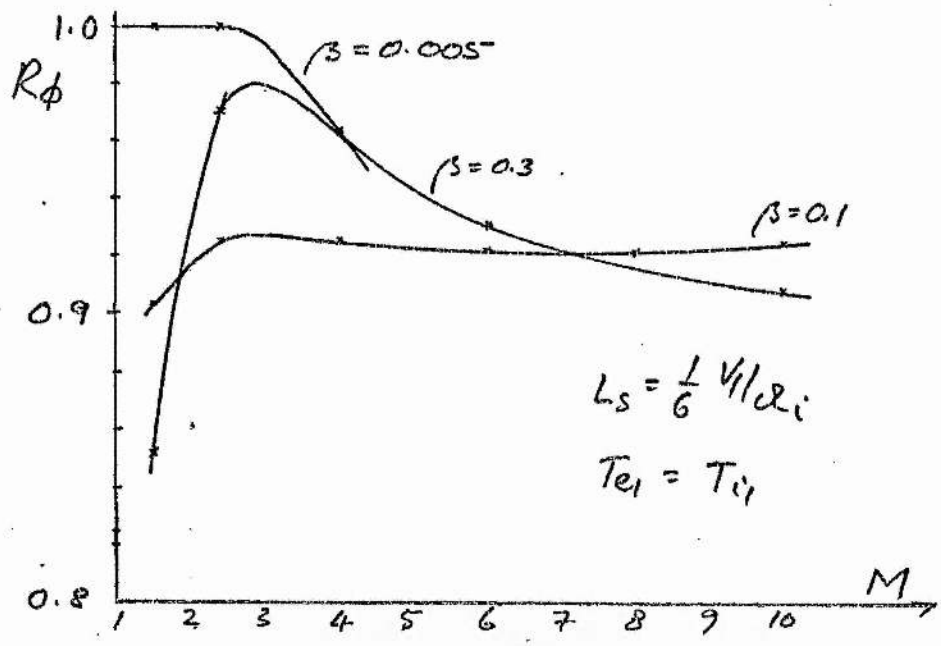

FIG 9.2

Only an ion thermal energy increase can result in decreased R_ϕ - at least when only electric potential dynamics are considered.

At β=0.005, $R_\phi \sim 1$ at M<M* so that no ion heating can have occurred. The numerical work shows that there is no distortion heating at low Mach numbers. Then at β=0.005, and M=1.5, 2.4, 4, respectively,

$$\frac{T_{i2}}{T_{iad}} = 1.1 \ , \ 1.4 \ , \ 1.5$$

while

$$R_\phi = 1.0 \ , \ 1.0 \ , \ 0.96.$$

The noticeable heating at M=2.4 has not affected $R_\phi \sim 1$, for the proportion of ion heating is small ($T_{e2}/T_{i2} \sim 135$). The simple energy balance (9.1) is well satisfied. At M=4 however, R_ϕ=.96 and $\phi<\phi^*$. Then the downstream terms of (9.1), at an initial kinetic energy $\frac{1}{2}MV_1^2$=0.5,

give (non-dimensionally)

$$\tfrac{1}{2}V_2^2 + \phi \underset{\sim}{\sim} 0.48 \qquad (9.2)$$

There is then a 4%"loss" of ion energy. It is expected that this energy should reappear downstream as temperature. Now in spite of an increase in non-adiabatic heating as given above, this energy is only $\sim$0.1% of the initial kinetic energy. This is very small and clearly cannot account for the reduction in ϕ. Some explanation over and above the heating hypothesis, which has been proposed in the literature, must be given.

In Fig. 9.3 are presented plots of R_ϕ against M; the condition $L_s=1/6\ V_1/\Omega_i$ of Fig. 9.2 is now changed to $L_s=0$. The hard curves are given at $\beta=0.005$, $\beta=0.1$. The dotted curves

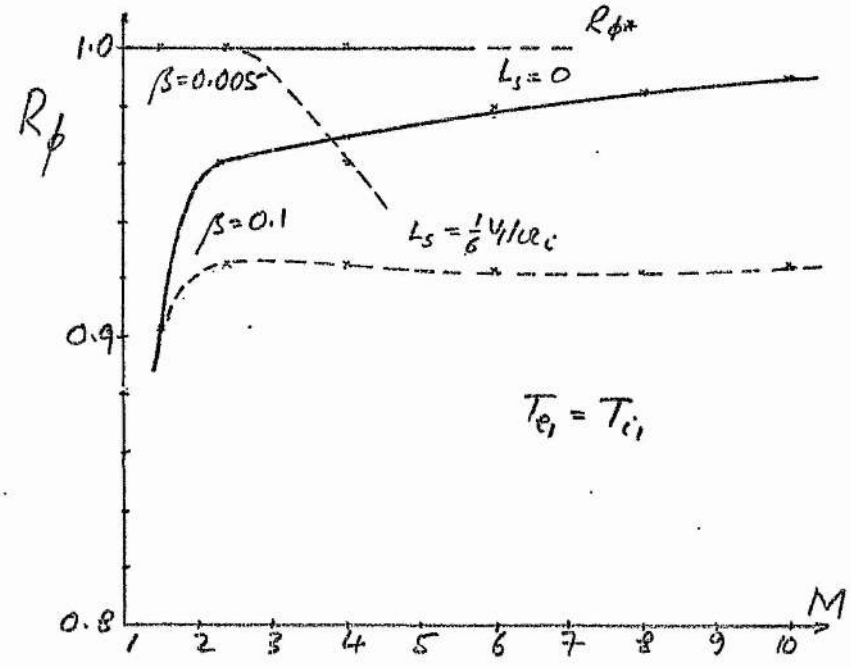

FIG 9.3

are the finite-L_s solutions, reproduced from Fig. 9.2. The graph re-introduces the problem of shock thickness. For $M<\hat{M}$ ($\hat{M}$ is that Mach number beyond which the downstream ions have no longer ignorable drifts in the y-direction) the two cases agree. For $M>\hat{M}$, the potential required to slow the ions so that $v_2=V_2$ is lower when $L_s\neq 0$. It is necessary to examine the effects of ion drift to v_y, on the slowing of the ions. At $\beta=0.005$ no reflections occur, and all ions have a shock transit time to go into their gyro-orbits. They acquire a drift to $-V_y$, and thus experience an averaged Lorentz force which in turn retards their motion across the shock. This force helps the electric potential to slow the ions. An energy balance is then given by the form

$$\tfrac{1}{2}MV_1^2 = \tfrac{1}{2}MV_2^2 + e\phi + \frac{e}{c}\,\overline{V_y B L_s} + [\text{heating}] \quad . \qquad (9.3)$$

It is sensible to suppose that if $L_s \sim r_i$ (the ion Larmor radius) then all their motion could be converted by gyration in the gradient in B, to flow to -y on exit from the shock. They would then be independent of electric potential dynamics. Fig. 9.4 illustrates the forces and typical orbits when $L_s \ll r_i$, $L_s \gtrsim r_i$.

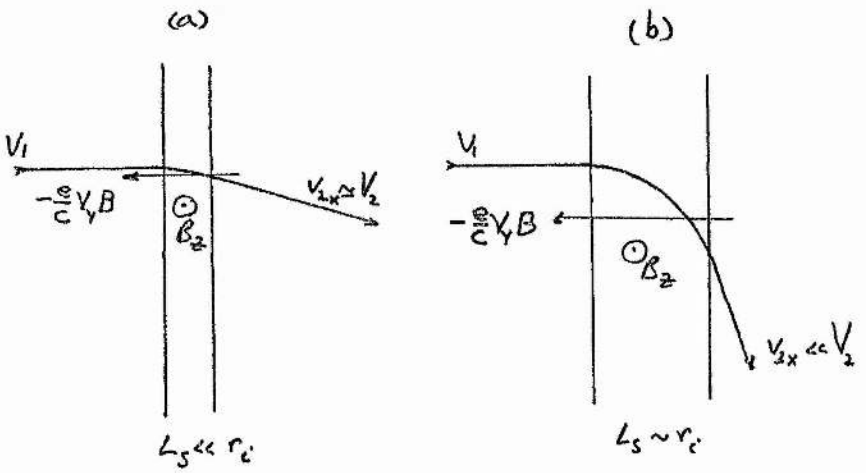

FIG 9.4

At β=0.005, even for M>M*, it now occurs that R_ϕ>1, with the small ion heating ($\lesssim$1%) not registering. It has been shown above that ion heating may be regarded as constant when L_s is varying, for $M<\hat{M}$, while for $M>\hat{M}$, remains comparable with experimental errors. As $M\to\infty$, it has been shown that the L_s=0 shock becomes a reasonable approximation. Thus the L_s=0 curve giving $R_\phi \sim 1$ is taken true, at β=0.005 - not least because R_ϕ<1 could never be experimentally verified.

In the examination of model dependence on L_s, data at a fixed L_s = 10 c/ω_{pe} was accumulated. At $M \lesssim 2.4$ ($\sim M$), and β=0.1, the measured values of ϕ agree with the $L_s = 1/6\ V_1/\Omega_i$ cases, while at $M \gtrsim 4$ they were found to agree with L_s=0 shocks. This is demonstrated in a plot of R_ϕ for L_s=0, 10 c/ω_{pe}, 1/6 V_1/Ω_i, with M, in Fig. 9.5

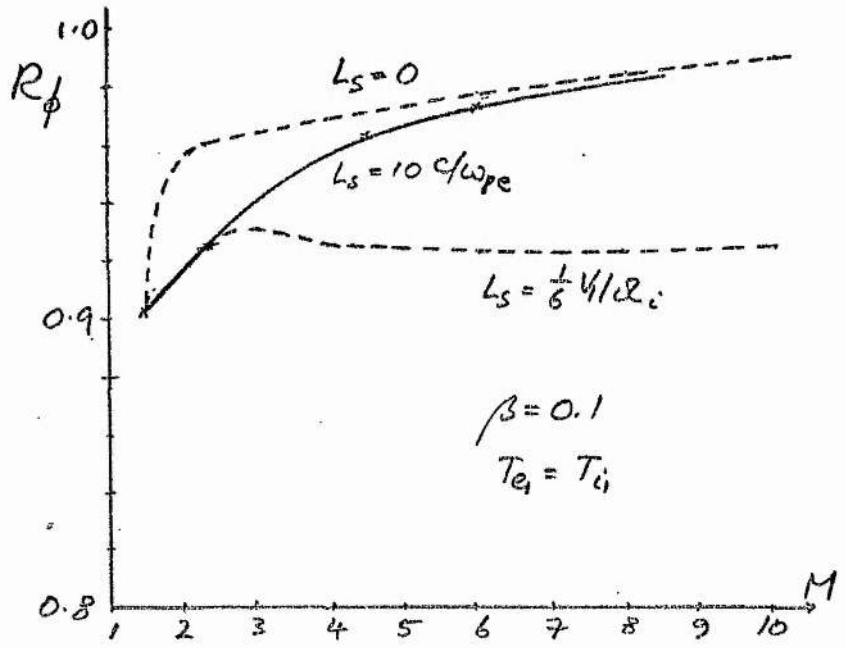

FIG 9.5

While choice of L_s at β=0.005 allowed large changes in R_ϕ, so that $R_\phi \sim 1$ resulted, this does not appear to be the case at β=0.1. Removal of drifts to -y does not return R_ϕ to order unity, so that shock thickness effects do not operate alone. It may now be asked if the difference is due to thermal energy increase.

At M=1.5, $R_\phi \sim 0.9$ when β=0.1; again, with initial kinetic energy of 0.5,

$$\tfrac{1}{2}V_2^2 + \phi \underset{\sim}{\sim} .478 \qquad (9.4)$$

An energy loss of $\sim$4.4% is found. This holds for all shock thicknesses and is now found to reside in the temperature increase. Thus there is measured distortion heating ($\sim$0.024) which is about 4.8% of initial ion kinetic energy.

As must be expected, then, at M=1.5, β=0.1, distortion heating of the ions can account for the reduction in R_ϕ. No reflecting ions were registered.

At M=1.5, β=0.3, a 2% flux of reflecting ions is found. They are effective in boosting ion temperature so that the model gives

$$\tfrac{1}{2}V_1^2 + \phi \underset{\sim}{\sim} 0.453. \qquad (9.5)$$

Then an energy loss of $\sim$9.4% must be accounted for. The jump in heating ($T-T_{ad}$) is $\sim$.042 at $\sim$8.4% which satisfactorily accounts for the low value of R_ϕ. [It must be recalled from Fig. 8.20 of the previous section that this shock is not self-consistent, as conservation energy levels are marginally exceeded].

At low Mach number, then, and at least for $\beta \lesssim 0.3$, simple distortion heating can account for the drop in ϕ, by an energy balance of the form

$$\tfrac{1}{2}MV_1^2 = \tfrac{1}{2}MV_2^2 + e\phi + [\text{heating}] \qquad (9.6)$$

. It was necessary to consider the effects of L_s on the model. But even in the case of the $M>\hat{M}$ shock at $\beta=0.005$, this equation must apply for the self-consistent solution requires no net drift in the y-direction, downstream, so that magnetic field dynamics need not be involved.

At high β, and $M>M^*$, it now becomes necessary to consider a new aspect in the explanation of R_ϕ-levels; thus adjustment of shock thickness and inclusion of ion heating cannot reduce the problem to that of type (9,6).

At $\beta=0.3$, $M=2.4$, as the most exaggerated example available (this shock is marginally self-consistent, while the $M=1.5$ shock is not), very strong ion heating has been measured (Fig. 8.20). This resides mostly in the reflected ion component, representing about 80% of non-adiabatic heating. This is carried by a flux of about 15% of the total. As before, the downstream terms of (9.1) give

$$\tfrac{1}{2}V_1^2 + \phi \simeq 0.488, \qquad (9.7)$$

or about 2.4% of upstream ion kinetic energy. The large ion heating is found to be about 46% of that energy - while this large heating should be apparent in Fig. 9.2 as a reduction in R_ϕ to $R_\phi \sim 0.4$, this is patently not the case, for $R_\phi \sim 0.93$!

A similar occurrence occurs at M=2.4 and the lower β=0.1. But a much smaller flux of about 3% reflecting ions is found, yielding about 78% of non-adiabatic heating. While an energy balance like (9.6) predicts $R_\phi \sim 0.85$, the model forces this higher to $R_\phi \sim .93$. The effect is decreasing as β gets smaller, and Fig 9.3 shows that it is amplified by reduction of shock thickness, for $R_\phi \to .96$ as $L_s \to 0$, an increase of some 3%. This is expected for lack of field dynamics leads to increased ϕ, as was shown in the discussion of shock thickness.

At higher $\beta (>\tilde{\beta})$ and M>M*, the new event is the emergence of the reflecting ions. The reflection process adds large energies into this component upstream of the shock, and an energy balance becomes quite difficult. It is clear that the effect of reflections is to effectively raise the apparent speed of the ions at the shock front, and thus to raise the left hand side of equation (9.6). Then each term (other than $\frac{1}{2}MV_2^2$) can be increased to match. Heating has been found to increase, with reflections. Now the occurrence of high R_ϕ implies that ϕ also increases. This is shown quite clearly by returning to Fig. 9.2, and a comparison of the curves β=0.1, 0.3. The expected behaviour is that since ion heating increases with β, so R_ϕ should show an orderly decrease with β - as in the progression β=0.005 to β=0.1. On the contrary, however, R_ϕ strongly increases in the presence of the reflecting ions. At M=10, β=0.3, this effect is lost and the situation returns to that of (9.6). In Fig. 9.1, ϕ is exaggeratedly reduced by gyration as in Fig. 9.4.

It is emerging then, that the potential works quite hard to slow the ion component. In the absence of reflections, equation (9.6) shows

that $\phi \leq \phi^*$ always, for if $\phi > \phi^*$, then cooling of the ions must take place which is not allowed by the conservation relations (for the total plasma) or by the variational principle of section §3, for each charge species separately. But it is not clear that this is the case when reflections occur. An increase in R_ϕ of ∿4.7% occurs on the small jump β=0.1 0.3, M=2.4. At this point the model breaks down, (Fig. 8.20) by excess ion heating. The loci of search points for the self-consistent solutions at Culham and Garching suggest that $R_\phi > 1$ can occur, but with undetermined heating levels (see Fig. 5.5). These loci are discussed below. But no analytic demonstration of an ordering $\phi \gtrsim \phi^*$ seems possible, for the interdependence of ion heating and ϕ is difficult to determine. The problem is complex, and left open.

Measurement of R_ϕ at $\beta \gtrsim 0.3$, M∿2.4, in an experiment, would be a very good test of the model. It has been held, up to the present, that equation (9.6) applies. In particular, in dependence with β, R_ϕ should be tested for the form shown in Fig. 9.6. This is contrary to equation (9.6)

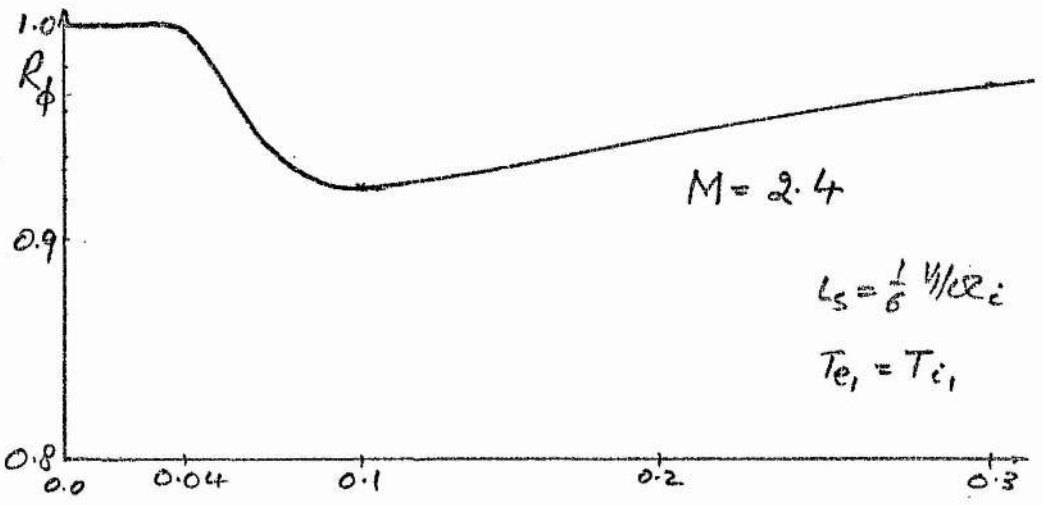

FIG 9.6

There is not much experimental evidence. The Culham M>M* experiment gives good agreement with R_ϕ as given by the model, $R_\phi \sim 1$. If R_ϕ is calculated from the heating levels of the model, assuming (9.6) to be true, then $R_\phi \sim .87$ would result. Thus Culham gives tentative support to the high-part of Fig. 9.6. Restriction to $R_\phi < 1$ at low-β has been observed in oblique shock waves,[28] and in the presence of oscillatory subshocks of some low-β perpendicular shocks.[11] These latter are not strictly comparable with the steady-state model, and their β-dependence is uncertain. But on a low-β ($0.005 \rightarrow 0.05$) region and $M_A > M^*$, R_ϕ varies between ~ 0.71, at $M_A > 2.4$, and $R_\phi \sim 0.5$ at $M_A \sim 5$. This latter result is far in excess of the model, even at lower β, but suggests qualitative agreement with Fig. 9.6. While the M>M* shock of the Culham papers shows from Fig. 5.2, a good agreement of ϕ with the model, their M<M* shock shows a potential slightly lower relative to the model. Now a condition for the appearance of the subshock is that $T_e >> T_i$ (they are ion-acoustic events[9] occurring when $M_A < 1$ while $M_S > 1$, where M_s is an ion-acoustic Mach number, V_1/C_s) so that their appearance at low-β is expected from Fig. 8.21 which shows strong reduction of T_{e2}/T_{i2} with increasing β.

The suggestion is then that at low-$\beta \lesssim 0.05$ corresponding to the experiments of Eselevich et al.[11] the electrostatic subshock appears. The strong oscillatory potential will reflect ions from the first potential maximum[14], while these oscillations average about some lower level behind the shock. It is this first potential maximum that must be compared with the model, in the low $\beta = .04$ results. Knowledge of the amplitude of the oscillations would enable a calculation from the model of R_ϕ downstream,

corresponding to the averaged oscilloscope traces of the Culham experiments.

At high β, since T_e/T_i drops, so the effects of the subshock will decrease until in shocks like that at Garching, $T_e/T_i<1$ always and they disappear. While at Garching, $T_{e2}/T_{i2}\sim 0.08$, the Culham shock at $M>M^*$ gives $T_{e2}/T_{i2}\sim 10$. The agreement of this latter example with the model, and the observed $R_\phi\sim 1$ there, combine to suggest that the subshock does not exist even at $\beta \gtrsim 0.1$.

These arguments can account for the high values of R_ϕ given by the model, as compared with Eselevich's results. The detection of $R_\phi\sim 1$ at high $\beta \gtrsim 0.3$, in a steady-state shock [averaged electric field] would be good confirmation of the effect of reflections to increase ϕ, as predicted by the model.

The behaviour of the self-consistent potential has been examined. Some idea of the difficulty of evaluating ϕ has been given by the discussion of reflected ion effects. Even without these, determination of ϕ by (9.6) requires measurement of ion heating, itself an unknown of the shock problem. Ideally, separate expressions for ϕ, and T_i, would be given in terms of the initial plasma, and Mach number. Papers by Woods[29] (1969) and Morse[30] (1973) give expressions for ϕ in terms of ion and electron heating, respectively. These are

$$\begin{aligned} \phi_w &= \tfrac{1}{2}\left(1 - \frac{1}{B_2}2\right) + \frac{5}{2}\left(T_{i1} - T_{i2}\right) \\ \phi_M &= \frac{1}{M_A}2 \quad (B_2 - 1) + \frac{5}{2}\left(T_{e2} - T_{e1}\right), \end{aligned} \tag{9.8}$$

in the non-dimensionalized quantities of this thesis. Fluid models were used, and temperatures are calculated in 3 degrees of freedom. The equations are defined for purely resistive shocks, which must automatically restrict them to $M<M^*$ - a comparison of ϕ as calculated using model heating with model solutions for ϕ would not be expected there. The similarity of these two independently derived equations suggests that they might be related, and indeed the one may be derived from the other via the Rankine-Hugoniot relations; thus $\phi_W = \phi_M$. In a rederivation of the Rankine-Hugoniot relations, and based on a method of Cairns [31], Sanderson [32] has obtained these equations assuming that all current in the shock is carried by electrons. This technique is reconsidered in the light of the model, below, for it makes no assumptions about ion heating other than that the ions must carry no current, $-J_y^i$. However all theories, as averages over the ion distribution function will lose information. In particular, it is not expected that they will register distortion heating.

The equation (9.8) may be tested against the model. Using the temperatur observed there, ϕ may be calculated from (9.8). In Fig. 9.7, this is labelled ϕ_C. The model's self-consistent prediction for ϕ is plotted for comparison, while also shown is a value of ϕ, calculated from equations (9.8), but using the temperature of the transmitted ions only. This is labelled ϕ_R. The high $\beta=0.3$ value is chosen, as it exaggerates the effects of ion reflections. It is recalled that these shocks are self-consistent for $M\geq 2.4$ and $M\lesssim 1.4$. Finally, the standard comparison $\phi=\phi^* = (1-V_2^2)/2$ is plotted. The temperature of the model is assumed to distribute in 3 degrees of freedom, downstream, for optimum comparison with (9.8). Then

$$T_{i2} = (T_X + T_Y + T_Z)/3, \quad T_z = T_{i1} \quad .$$

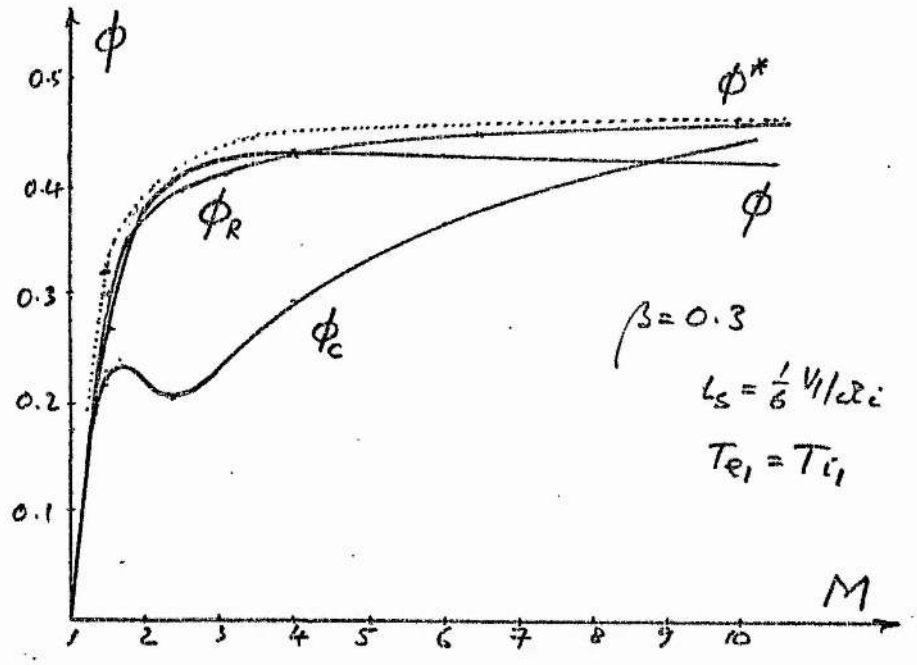

FIG 9.7

At M=1.5, where $M<M^*\sim 2$, some reflections occur, and ion heating is known to be quite large (Figs 8.1, 8.20). The steep slopes at low Mach number make comparison quite difficult, but the calculated values are in decreasing order,

$$\phi^* = 0.32 \ , \ \phi_R = 0.30 \ , \ \phi = 0.27 \ , \ \phi_C = 0.23 \qquad (9.10)$$

That $\phi^* > \phi$, has been explained above. It is seen ϕ_C underestimates by about 17% at M=1.5, showing that the laminar heating of the model is in excess of that allowed by (9.8). It is known that at $\beta=0.3$, M=1.5, the shock is not self-consistent due to excessive ion heating. However, as M increases, and the model becomes self-consistent, this divergence, $\phi > \phi_C$, increases to some 50% at M=2.4, which is clearly related to the reflected

ions. Then the pure resistive derivations (9.8) do not apply. In this region, deletion of the reflected ion temperature gives the approximation $\phi=\phi_R$, which is seen to have a natural comparison with ϕ^* and with ϕ and highlights the effects of reflections. At large M∿10, as reflections reduce, so ϕ_c increases to $\sim\phi$. But there is no qualitative agreement. As ion heating gets smaller, so $\phi_c \to \phi^*$ as expected from equation (9.8). But ϕ is now dropping in the combined effects of distortion heating ($R_\phi<1$), of reduced reflections and shock thickness effects.

At a more moderate, and from Fig. 8.20, a more sensible, value of $\beta=0.1$, similar curves are shown in Fig. 9.8.

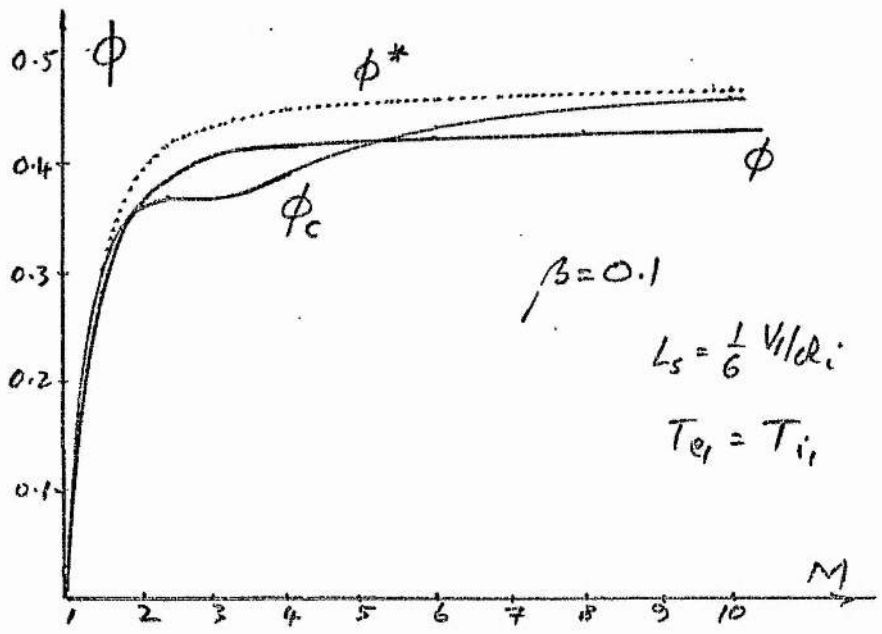

FIG 9.8

Now ϕ_c underestimates ϕ by at most only 5%, as against 50% at $\beta=0.3$. But the same general behaviour is shown. Reflected ions cause a drop in ϕ_c due to their non-resistive heating type. In the derivations of Cairns and Sanderson, the requirement that the electrons carry all the current $-J_y$ must be violated.

The model then strongly suggests that if laminar ion heating occurs, noticeably by ion reflections, then the equations (9.8) do not hold. Support for these equations is given by Woods[29], in a comparison with the Culham experiment at M>M*. But Fig. 9.8 shows that $\phi_c \sim \phi$ within experimental errors, so the test is not important. There is unfortunately little published information on the electric potential levels, and further comparisons of both the model and (9.8) cannot be made.

The argument for the derivation of (9.8) is best given as in reference [31], and may be made like this: Assume that the electrons carry the current neV_y^e, in the shock front. As the ion displaces down the shock front, the ion-acoustic instability (for example) occurs, and V_y^e falls in consequence (at the expense of the growing plasma waves). Integration of electron equations of motion in laminar fields, shows that they follow equipotentials and so do not gain energy from these orbits [1]. The effect of falling electron velocities V_y^e, in the shock turbulence, causes the electrons to depart from equipotentials and be accelerated across the shock into the downstream, by ϕ. Now there is the ubiquitous constant electric field $E_y = \frac{1}{c} V_1 B_1$, in the direction of this drift, so that the potential drop experienced by the electron in crossing the shock may be written as $\phi - \Delta y E_y = \phi - \frac{1}{c} V_1 B_1 \Delta y$; Δy is the displacement of an electron in the y-direction. But then this energy has been lost to turbulent heating of the electrons. Assuming that the electrons appear as Maxwellians downstream, the electron temperature increase is then proportional to $\frac{2}{3}$ of this quantity. Thus

$$T_e = \frac{2}{3}\alpha(\phi - \frac{1}{c} V_1 B_1 \Delta y) \qquad (9.11)$$

But the current is carried totally by the electrons, so that $dB/dx = 4\pi/c \cdot NeV_y^e = 4\pi/c \cdot NeV_x^e \cdot dy^e/dx$.

Since $N_1V_1 = N_2V_2$, $dB/dx = 4\pi/c \cdot N_1 e V_1 \, dy^e/dx$ which may be integrated to give

$$\Delta B = \frac{4\pi}{c} e N_1 V_1 \Delta y. \qquad (9.12)$$

Together with equation (9.11), this gives

$$T_e = \frac{2}{3}\alpha(\phi - \frac{B_1(B_2-B_1)}{4\pi N_1 e}) \qquad (9.13)$$

The constant of proportionality has been evaluated by Sanderson to be $1/\gamma_e$, where γ_e is the ratio of specific heats for the electrons, and $\gamma_e=5/3$. Equation (9.13) is then identical with (9.8).

Now the interesting new effect suggested by the model, is the possibility of significant ion drifts in the y-direction. These occur for the whole ion beam in the laminar fields at $M<M^*$, and at $M>M^*$ as fast currents in the shock of reflected ions. This latter fact has been noted by Auer et. al. [18], who predicted the observation of ion currents in front of the shock. Such motions have been experimentally measured directly, by Phillips and Robson[14]. No experimental detection of downstream currents J_y^i has been made. They are predicted by the model, while Biskamp and Welter[20], report evidence of fast ion beams downstream of a one-dimensional simulation shock. The Earth's Bow Shock[21], shows evidence of a fast beam, but its y-dependence has not been determined.

Considering only the positive current of reflecting ions, in the transition L_s, Maxwell's equations give the form

$$\frac{dB}{dx} = \frac{4\pi}{c} Ne \left(V_y^e - \frac{n_R}{N} V_y^i\right) , \qquad (9.14)$$

where now a reduced electron current must occur. Here n_R is the density of reflecting ions in the shock, while N is the density of the total electron or ion component. Now the electrons will be slowed by the turbulence, as in the analysis above, to give the new potential drop $\phi - \frac{1}{c} V_1 B_1 \Delta y^e$. The ions will help the electrons in the y-direction, thus counter-acting the effects of turbulence (this may be understood in terms of the driving mechanism of the turbulence - thus the driving energy of the (universal) instability lies in the relative drift $v_d = V_y^e - V_y^i$, and reduction of this quantity would decrease turbulence fluctuation levels). For a given dB/dx, V_y^e is now smaller and so Δy^e is expected smaller, when ion current occurs.

Again, the electrons see a potential drop $\phi - \frac{1}{c} V_1 B_1 \Delta y^e$. But from (9.14) this now gives the form

$$T_e \simeq \frac{2}{3} \alpha \left(\phi - \frac{B_1(B_2-B_1)}{4\pi Ne} - \frac{1}{c} V_1 B_1 f_R \Delta y^i\right), \qquad (9.15)$$

for the increase in electron energy. The last term is derived using

$$\frac{n_R}{N} V_y^i = f_R V_x^i \frac{dy^i}{dx} ,$$

as above, but integration of Ampere's Law has assumed that f_R can be regarded as constant, and that V_x^i for the reflecting ions is of order the upstream drift V_1. Fig. 8.5 shows that this last is not unreasonable, but f_R will have a complicated x-dependence in the transition. Compression of the beam across L_s could

increase its density by about 30%, at β=0.3 in a simple ϕ-dependent shock. The last term of (9.15) is then a crude approximation to the integral, but it is evaluated below at the trailing edge of the transition, and compared with the model. The determination of the ion current profile in the transition is non-trivial. There are ions both reflecting off ϕ, and re-entering after reflection, while the main beam of ions has been shown to acquire a flux in the negative y-direction to roughly match the positive flux of reflecting ions. At the rear of the shock, there is then no ion flux (nor electron flux) so that dB/dx = 0, properly. But in the shock, the main beam follows an orbit as shown in Fig. 9.9, and for much of the time will have no flux to -y, while the reflecting ions do. This suggests that f_R should be approximated at some point inside L_s, where ion flux is a maximum.

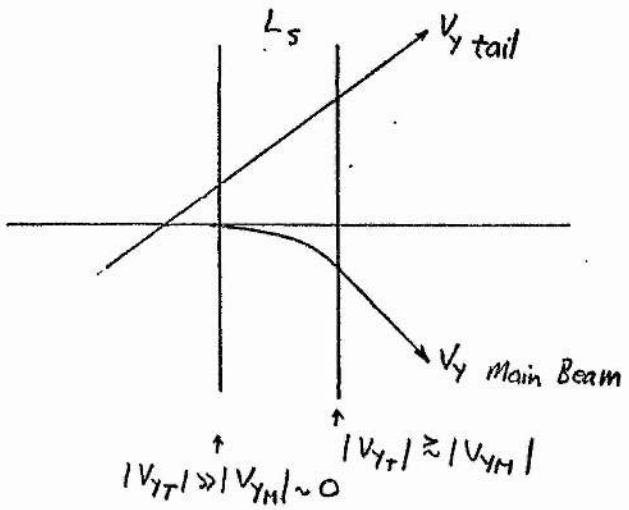

FIG 9.9

However, in the spirit of the derivation of (9.13), no reason for the acceleration of the electrons across the shock need be given, (i.e. explanation of the electron turbulence) while for the ions, some representative heating, $f_R \Delta y^i$, can be used to explain the results of Figs. 9.7, 9.8. By means of the Rankine-Hugoniot relations, equation (9.15) is rewritten in a form suitable for ion temperature measurements.

$$\phi_{NEW} = \phi_c + f_i \Delta y^i = \tfrac{1}{2}(1-V_2^2) - \frac{5}{2}(T_{i2} - T_{i1}) + f_i \Delta y^i \qquad (9.16)$$

Again $\gamma_i = \frac{5}{3}$ for heating in 3 degrees of freedom. It is immediately apparent that some ion displacement may increase ϕ above ϕ_c. The presence of reflecting ions at M>M*, corresponding with their displacement far down the shock face (albeit mostly outside the shock - an immaterial point for Δy^i is proportional to the energy gain due to E_y which is everywhere constant), gives ϕ_{NEW} the required behaviour, qualitatively, with M. This equation remains insensitive to simple distortion heating. The equation may, however, be regarded as explanation of the increasing values of R_ϕ, where strong heating occurs, as studied in the previous section. There seems to be no absolute way to determine the ordering of the magnitudes of the last two terms. Considering $f_R \Delta y^i$ as the source of reflection ion energy, the heating term should then be greater as it must include not only the tail energy, but also that of the main beam. Thus it appears that $\phi<\phi^*$, always. Some of this energy ($f_R \Delta y^i$) must go to overcoming the potential however, and so $\phi>\phi^*$ might result. This is mentioned again below, but observation of $\phi>\phi^*$ would be a possible verification of the model, so it is not an unimportant question.

Some estimates of ϕ_{NEW} can be made. Fig. 6.9 above shows that $\Delta y^i \sim 2\ V_1/\Omega_i \sim 2M_A\ C/\omega_{pi}$. On the other hand, at extreme $\beta=0.3$, the maximum observed value of f_R by the model is $f_R \sim 7\%$. The effect might in a simple approximation be taken dominantly dependent on f_R, for at $\beta=0.3$, the $L_s=0$ model can be used to show that $\Delta y^i \sim 2.3$ over the observed range of Mach numbers.

Then in Fig. 9.10, a comparison of ϕ with ϕ_c and $\phi_{NEW} = \phi_c + f_R\ \Delta y^i$ is given. The

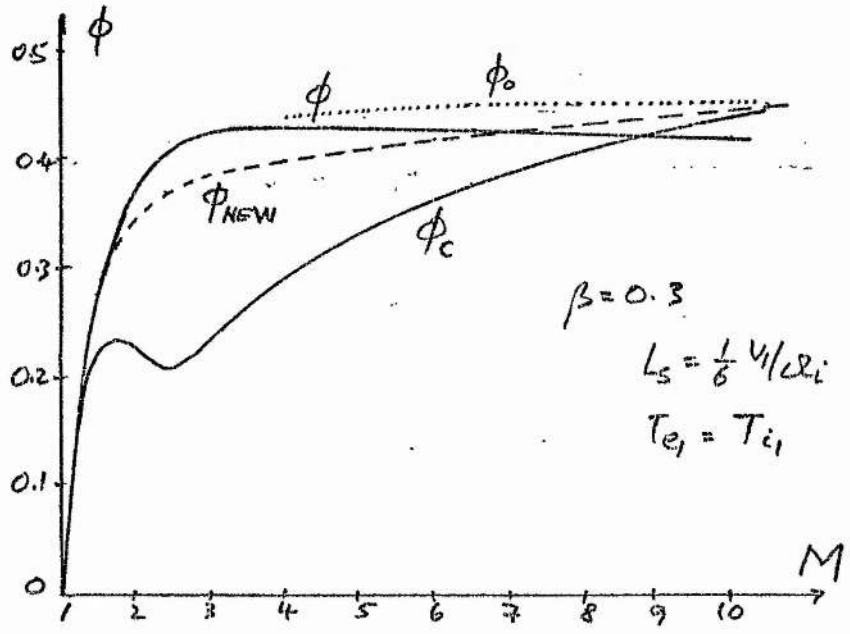

FIG 9.10

agreement has improved significantly, and is now within 10% of the model. The shape of the curve is now qualitatively compatable with ϕ, thanks to the f_R dependence chosen. The level $\Delta y^i \sim 2.3$ (chosen as the y-displacement from the point of entry into the shock upstream, to the point of final exit downstream) seems to be of the correct order of magnitude. But the

crude analysis to obtain (9.16) does not set great quantitative value on ϕ_{NEW} as in Fig. 9.10.

At high M, ϕ_{NEW} is seen to become an unfavourable estimate of electric potential as compared with the model. The indications are, from (9.16), that $f_R \Delta y^i$ must change sign. Then the ions must be displacing in the negative y-direction, and indeed, at the large shock thicknesses of high M=10, β=0.3, the transmitted ions now have a large flux about 16 times that of the reflected ions in this direction. Here $L_s \sim 2\ C/\omega_{pi}$ which is larger than observed levels. If the model is non the less used, then in the shock a small net flow to -y occurs and ϕ_{NEW} will decrease below ϕ. Alternatively, an L_s=0 run at β=0.3 shows that the model gives $\phi \sim \phi^* = 0.466$, while temperature increases slightly. In this case the correct ordering $\phi \sim \phi_{NEW} > \phi_c$ results with small error as all heating mechanisms decline. The high-M model has been shown in section §7 to have better behaviour at L_s=0. The dotted line labelled ϕ_o, of Fig. 9.10 indicates this latter model solution.

The properties of ϕ are of importance. The simple profiles of Fig. 9.1 hide a wealth of information on the properties of the laminar shock. Noticeable is the increase of ϕ with increased β in Fig. 9.6.

Experimental measurement of ϕ is a sensitive test of the model, for while ion heating shows a behaviour expected by the literature, the $R_\phi \sim 1$ at high β result is unusual.

Equation (9.16) gives a qualitative explanation for the measured, unexpected increase in R_ϕ. Rough agreement of this simple form, with the model is found.

In the next section, the breakdown of the model at high β is examined.

§10 On the Breakdown of the Model

In previous sections, it has been shown that the laminar model of a plane, perpendicular, collisionless, shock wave may break down in two ways. The first was the obvious one, as an initial requirement of the model - thus the self-consistent electric potential is found in some shocks to be incapable of a proper slowing of the ion beam according to the conservation relations. An example was shown in section §5, by a run at the Garching parameters. The second type of breakdown was unexpected - the collective heating of the ions, by reflections, is so efficient that such heating may exceed the total conservation level downstream. Both these threats must be simultaneously met for a self-consistent representation of a shock. It is noted that in section §6, it was shown that L_s must be carefully chosen to satisfy the conservation relations. However, it is now assumed that this choice has no effect on the breakdown of the model, for as long as $r_i << L_s << r_e$, the dynamics of this thesis are unchanged, and from section §6, L_s may be adjusted to give $V_{y2}=0$ as desired.

This chapter will investigate the domain of self-consistent model solutions. The non-dimensionalized study of this thesis has chosen the three ratios M, β, T_e/T_i, to define the initial plasma and shock strength. The first two are sufficient to define the total properties of the downstream plasma, via the conservation relations, while if $T_e/T_i = 1$, as in the work above, the solutions domain is then well defined as a subspace of M, β - space.

Clearly, (at fixed T_e/T_i) a trial-and-error search of the M, β-plane must be carried out, and such a search is conveniently performed in the $L_s=0$ approximation.

The model may be used in two ways, when $L_s=0$. The first isolates the boundary of the solutions subspace by seeking for a violation of the relation $V_1B_1=V_2B_2$. This is done by fixing M, and increasing β, as suggested by the exaggerated β-dependence of reflecting ion properties. At each point (M,β), the model is used in the conventional way to find ϕ such that $v_2=V_2$, where $v_2(\phi)$ is the numerical integration downstream at any trial-and-error choice of ϕ. If a shock solution is found, then for some ϕ, $v_2=V_2$, and the locus $v_2(\phi)$ has a form illustrated in Fig. 10.1 as example (a). The curve intersects $v_2=V_2$ at a point $\phi < \phi^*$ so that ion heating is immediately expected. (It is noted, too, that the locus is almost linear so that simple interpolation between two guesses on $v_2(\phi)$ will give a quite accurate estimate for ϕ at $v_2=V_2$).

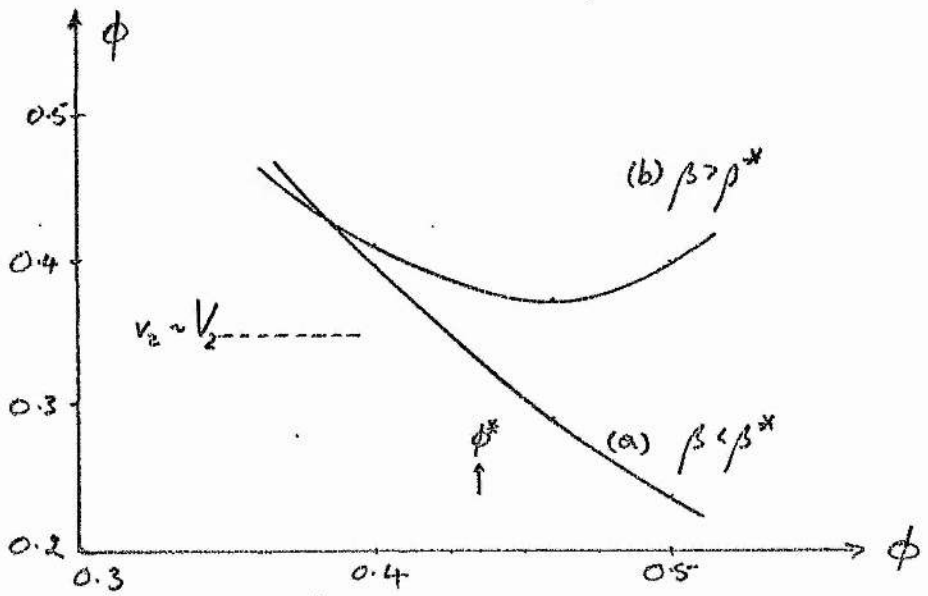

FIG 10.1

If no shock solution can be found, then $v_2(\phi)$ has a form as illustrated by example (b) of Fig. 10.1. Then $v_2 > V_2$, for all ϕ. This behaviour has been seen in the Garching example. At the value of β where $v_2(\phi)$ is tangential to $v_2=V_2$, marginal shock solutions are found. This value of β is labelled β^*.

By this technique, a point (M,β) at fixed temperature ratio T_e/T_i, is used to calculate N_2, B_2, V_2, $T_2=T_{e2}+T_{i2}$ by the conservation relations, while the complete use of the model specifies ϕ. A solution is then T_{i2}. This may be represented symbolically as

$$\{M,\beta \xrightarrow{(T_e/T_i)} V_2 \xrightarrow{(R\text{-}H)} \phi\} \Rightarrow T_{i2} \qquad (10.1)$$

Now $L_s=0$ so that no magnetic field dynamics occurs in the transition, and only the electric potential determines shock behaviour. A different form of the model, at $L_s=0$ may then be proposed. For specification of ϕ and initial temperature ratio T_i (and T_e/T_i) followed by integration of the ion orbits across the shock (by the usual "reversing" procedure), will give v_2. If this is assumed to be the conservation level, $V_2=v_2$, then B_2 may be calculated. (Since B_2 is unknown, no downstream gyration of an ion, with re-entry to the shock is allowed). But now M,β may be calculated. This procedure is merely the reverse mapping of the brackets in (10.1). It is denoted by

$$\{\phi,\ T_i \xrightarrow{(T_e/T_i),} V_2,B_2 \xrightarrow{(R\text{-}H)} M,\beta\} \Rightarrow T_{i2} \qquad (10.2)$$

Clearly at any point in M,β space, the two models must give the same solutions for T_{i2} (at least in a design where downstream dynamics may be ignored). This method avoids the trial-and-error procedure, but will yield a peculiar locus of points M,β, in the plane. By using this second technique, the same marginal

solutions curve, $\beta = \beta_o^*$, must be generated. Then T_i is fixed while ϕ is varied and solutions progress along isotherms in the plane, to terminate at β_o^*.

Further, both these techniques must give the same value of T_{i2}. Fig. 8.20 has shown an example of a shock which is properly slowed, but where $T_{i2} > T^{RH}$. This solution "catastrophe" then occurs for $\beta < \beta_o^*$ at these parameters. But it is indeed very difficult to determine exactly when ion energy conservation ceases. Electron heating is observed at the parameters of Fig. 8.20, in experiments. Thus even at high $\beta = 1.0$ in an experiment due to Hintz [10] ($M_A \sim 2.7$, $\beta \sim 1.0$) electron heating is found. So it is probable that the ion heating of even the fully self-consistent examples (at $\beta = 0.3$, $M = 2.4$) should be modulated to allow for some electron heating. But this latter is undetermined by the model. From equations (9.8) and using the model's measure of ϕ, it could be calculated. But ϕ is in this case so large (due to reflecting ions) that the electron heating <u>itself</u> is now in excess of the R-H level T_2^{RH}! Electron adiabatic heating could be deducted but it is always much less than total electron heating (experimentally) and not important. These ideas are strongly suggestive that the role of turbulence in the collisionless shock is merely to <u>reduce</u> ion reflections. Thus as regards the breakdown of the model, the delineation β_o^* according as $T_{i2} \geq T_2^{RH}$ will have little physical relevence. On the other hand, finding β_o^* such, that $v_2 \geq V_2$ for all M, β, is an extreme test of the laminar model. Then this latter criteria results in β_o^* as shown in Fig. 10.2. The search technique is time consuming, and the curve is kept accurate to a few percent of β^*. Since inclusion of turbulence must help slow the ions and so alter β^*, it is of essentially qualitative use physically.

Fig. 10.2 shows a not unexpected behaviour for β_o^*. From above, the destructive nature of ion reflections (to the model) is observed at $M \gtrsim M^*$. Then it is at just this point that β_o^* has a minimum, at $\beta_o^* \lesssim 0.23$. This is rather small, and leaves a forbidding amount of M,β- space inaccessible. However, a great volume of experiments have been performed at $\beta < \beta^*$.

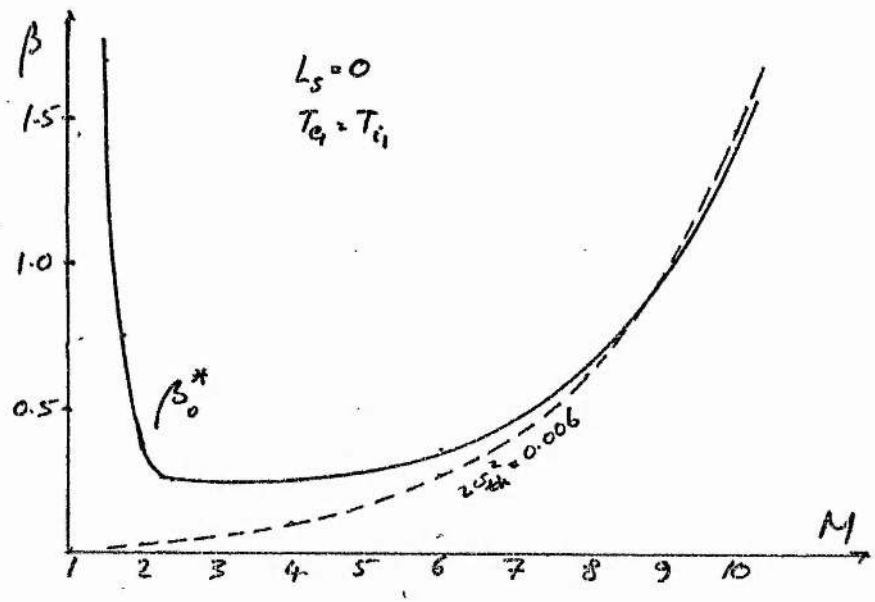

FIG 10.2

If higher values of M are chosen, then reflected ion flux (at constant β) drops, and so β^* may increase. It has been shown how reflected ions eventually completely disappear, for all β as M increases, so that a simple energy balance (9.6) may again operate. Then ϕ must at worst be responsible for the slowing of the cold ion beam, as $M \to \infty$. But in these conditions $V_2/V_1 \to \frac{1}{4}$, so that $\phi^* = (1-V_2^2)/2 \to 15/32$ and is itself asymptotic to a finite value. This is easily prescribed by the model, as was seen in the previous section, with $\phi \gtrsim \phi^*$ at large M. The fraction f_R of reflecting ions that may be properly slowed by ϕ must then limit, and since this otherwise depends on the

ion thermal spread, this must in its turn limit. An isotherm is shown in Fig. 10.2, and its small variation at high M, relative to β^* is noted. The ratio $f_R = n_R/N$, downstream, stabliizes at $f_R \sim 3\%$, while reflected ion flux limits at about 20%. The isotherm will always cross β^*. At T_{il} shown, the behaviour of reflected ion flux may be estimated as follows. When T_{il} is small, then the upstream ion distribution is as shown in Fig. 10.3.

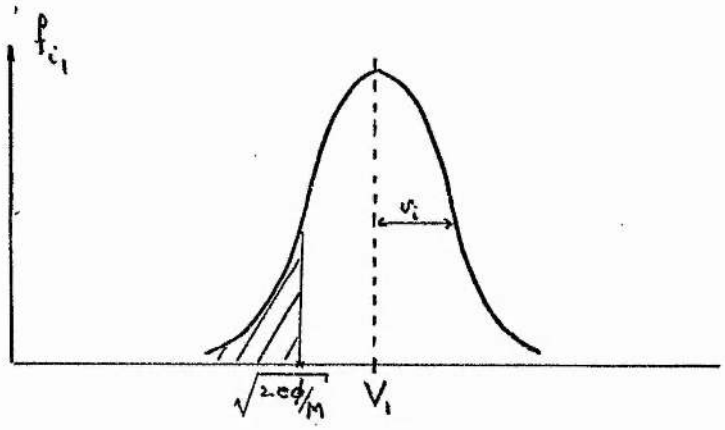

FIG 10.3

Since $v_i \ll V_1$, and since only ions such that $v_x > \sqrt{2e\phi/M}$ can surmount the potential, a one-dimensional estimate of fluxes of each ion component is given by

$$(nv)_M = \frac{1}{2\pi v_i^2} \int_{\sqrt{\frac{2\phi e}{M}}}^{\infty} v_x \exp - \frac{(v_x-1)^2}{2v_i^2} \, dv_x$$

$$(nv)_T = \frac{1}{2\pi v_i^2} \int_{-\infty}^{\sqrt{\frac{2\phi e}{M}}} v_x \exp - \frac{(v_x-1)^2}{2v_i^2} \, dv_x \qquad (10.3)$$

No dynamics is invoked outside of the transition, for fluxes must be conserved. Then if erf and erfc are the error and complementary error functions,

$$(nv)_M = \tfrac{1}{2} \quad \{ \operatorname{erfc}(x) + \sqrt{\frac{2v_i^2}{\pi}} \cdot \exp - x^2 \}$$

$$(nv)_T = \tfrac{1}{2} \quad \{ \operatorname{erf}(x) - \sqrt{\frac{2v_i^2}{\pi}} \cdot \exp - x^2 \} \quad , \qquad (10.4)$$

where

$$x = (\sqrt{2\phi} - 1) \Big/ \sqrt{2v_i^2} \quad .$$

Directly $(nv)_M + (nv)_T = 1$.

Since flux is conserved, these levels are applied to the downstream. Then Fig. 10.4 shows the strong exchange of transmitted and reflected ion fluxes at fixed T_i (along the isotherm of Fig. 10.2), and increasing electric potential.

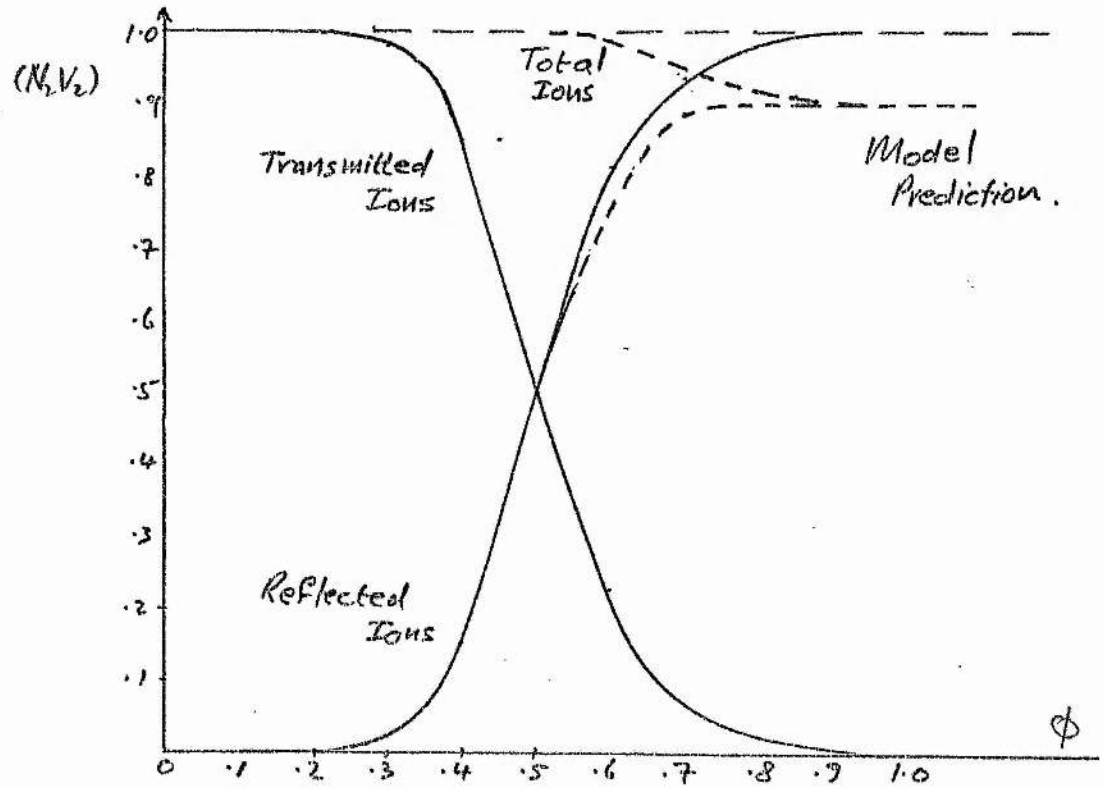

FIG 10.4

The dotted line represents a check of the L_s=0 model, against the computed flux (10.4). It is noted that at very high ϕ, far beyond the applicability of the model ($(nv)_T > (nv)_M$), some model flux is lost. This is due to a loss of ion information with the appearance of a second reflected ion beam; the large volumn of V_2 occupied by such a distribution makes it expensive to compute. This fact reconfirms that one ion bounce is sufficient physically, in the domains of interest here. (Flux has been maintained high in all work above). The curves then agree very well, and it is seen that at ϕ=0.5 > $\tilde{\phi}^* \underset{\sim}{\sim} 0.47$, reflected ion flux exceeds transmitted levels. Together with upstream acceleration, this point must signal that the model is no longer functioning. Thus at constant T_i, these curves apply first at $\beta < \beta_o^*$, with at $\beta > \beta_o^*$, the isotherm and β_o^* always intersecting. As ϕ increases, so V_2 decreases reaching a minimum at $\tilde{\phi} \sim 0.5$, while as T_{il} decreases, so V_2 decreases. If $V_2/V_1 \sim \frac{1}{4}$, then the mapping (10.2) will imply that $M \to \infty$. Clearly, the cooler the initial ions, the easier they are to slow, and the closer is V_2/V_1 to its limit. Then again $M \to \infty$. Thus as $\phi \overset{\sim}{\to} 0.5$ in Fig. 10.4, so shocks progress along an isotherm with $\beta \nearrow \beta_o^*$, in such a way that the distance along T_{il}=constant increases with decreasing T_{il}.

This situation does not apply at low values of Mach number, where the shocks are weak (field jumps are small) and possibly large ion temperatures must be considered together with the effects of the potential. Thus low ϕ (rather than low T_{il}) implies low reflections, but as β increases, or T_i increases so their numbers increase slowly, to cause a slow asymptotic

collapse of β_o^* to M=1 as $\beta \to \infty$. The significance of this is postponed until later in the section.

It is clear from Fig. 10.1 that ϕ for a self-consistent solution need not be less than ϕ^*, as has been commonly held in the literature. On $\beta = \beta_o^*$, the two are always in close agreement, and together with inclusion of some ion-seen turbulence, the state $\phi \lesssim \phi^*$ seems likely. Fig. 10.5 illustrates how tangential $v_2(\phi)$ may develop in a progression of increasing β.

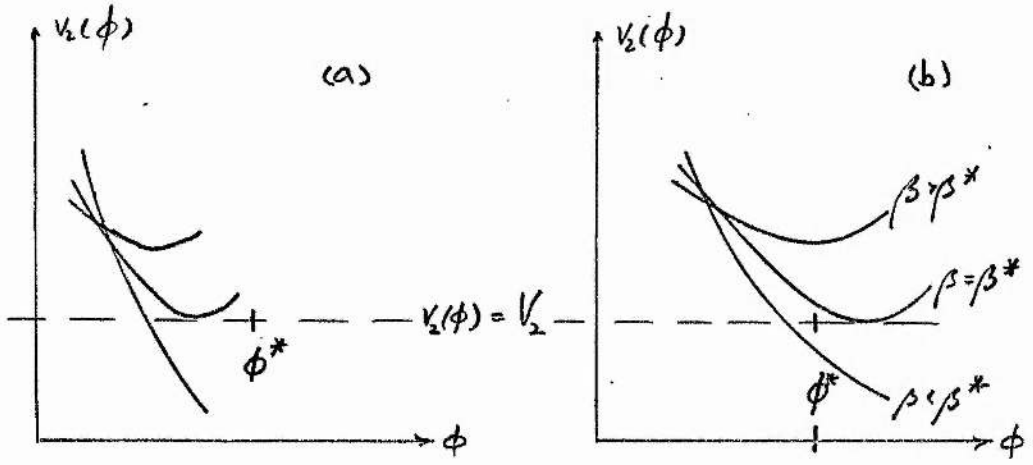

FIG 10.5

Example (a) shows $\phi < \phi^* = (1-V_2^2)/2$ on β_o^*; this is not observed except marginally at high M,β. Example (b) shows $\phi > \phi^*$ on β_o^*, and is the common event. Once again it is noted that observation of $R_\phi \gtrsim 1$, in the presence of strong ion heating, would be a confirmation of the laminar-ion model, and bear out the qualitative behaviour as in Fig. 10.5.

It is then suitable to examine the finite L_s case. This is more realistic for comparison with experiment, while the evidence suggests that the solution domain is extended (Fig. 8.20 shows $\beta^* \gtrsim 0.3$ at M=2, $L_s = \frac{1}{6} V_1/\Omega_i$, while, Fig. 10.2 shows $\beta_o^* \sim 0.2$ at M=2, $L_s=0$). Some extension of the qualitative understanding of the shock should result. The important difference now is that the model is restricted to the conventional method (10.1), for at finite $L_s \neq 0$, the magnetic field dynamics must be specified in the transition; this requires knowledge of B_2.

In Fig. 10.6, the locus of marginal shock solutions at $L_s = \frac{1}{6} V_1/\Omega_i$ is shown. This is labelled β^*, and is compared with β_o^*. The errors on β^* are shown. Then slightly improved ability to slow the ions is shown. As $M \to \infty$, so $L_s \to 0$ as constant units of C/ω_{pi}. Thus the upper curve will more realistically tend to the $L_s=0$ approximation as suggested by the dashed curve. The $L_s \neq 0$ curve was generated by using the $L_s=0$ case to make a guess at β^*. That this is successful is shown by the similarity of β^* and β_o^*, solutions.

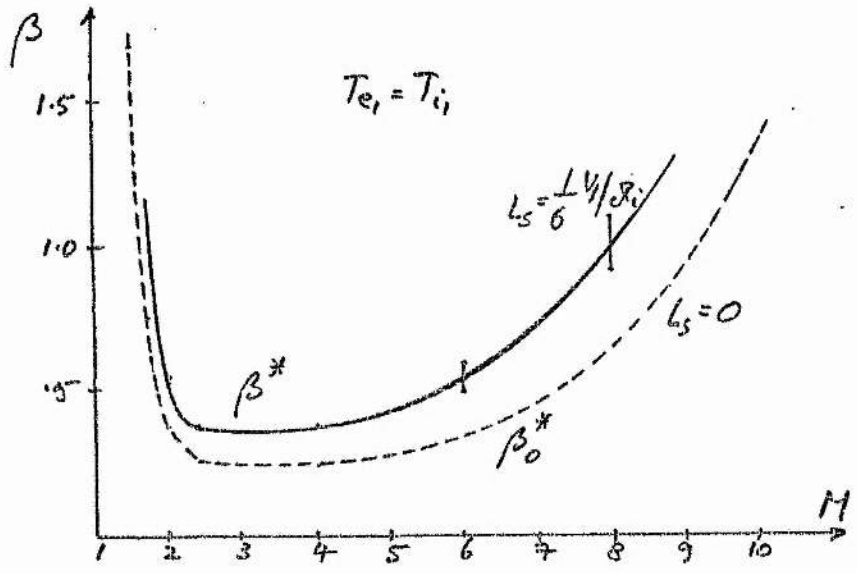

FIG 10.6

This dependence on shock thickness can be examined. Improved ability to slow the shock has been illustrated above, by the reduction of ϕ with increasing L_s. Here it can be demonstrated by the locus $v_2(\phi)$, as in Fig. 10.7.

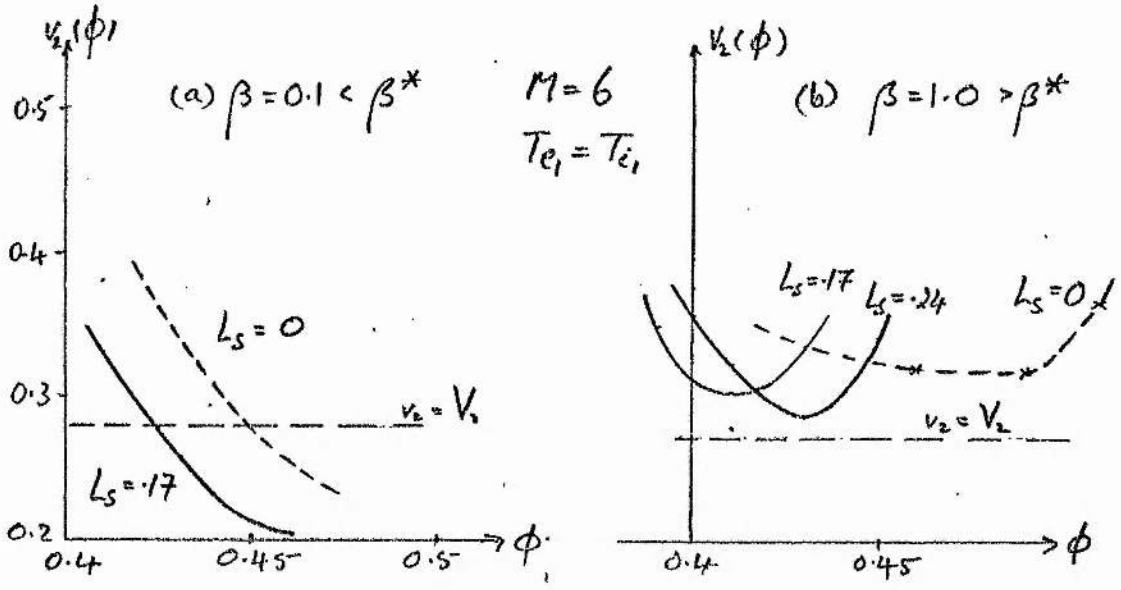

FIG 10.7

Example (a) shows loci in a region $\beta < \beta_o^*$, with ϕ increasing when $L_s = 0$ to slow the ions. At high $\beta = 1.0$, the $L_s = 0$ locus is both lowered (a more efficient slowing) and moved to smaller ϕ (improved slowing by smaller ϕ) when $L_s = .17\ V_1/\Omega_i$; while at $L_s = 0.23\ V_1/\Omega_i$, further slowing occurs, but ϕ must now increase to slow the ions. This last is unexpected, but the broad shock effectively reflects ions within its own width. The effect is a smearing of the two ion beams, with a new deposit of ions at low $v_x < V_2$. While ions are still reflecting requiring increased ϕ, new flux at $v_x < V_2$ helps to slow the ions. (This effect will not save the model at high β, for

it requires shock thicknesses well above the $\sim C/\omega_{pi}$ observed experimentally). This is shown in Figs. 10.8, 10.9, which give scattergrams in V_2 of the $L_s \neq 0$ examples of Fig. 10.7. They are made at $v_2(\phi)$=minimum, and neither is self-consistent, but they help to illustrate how ion dynamics will change with L_s. The loss of resolution of the reflected beam is noted.

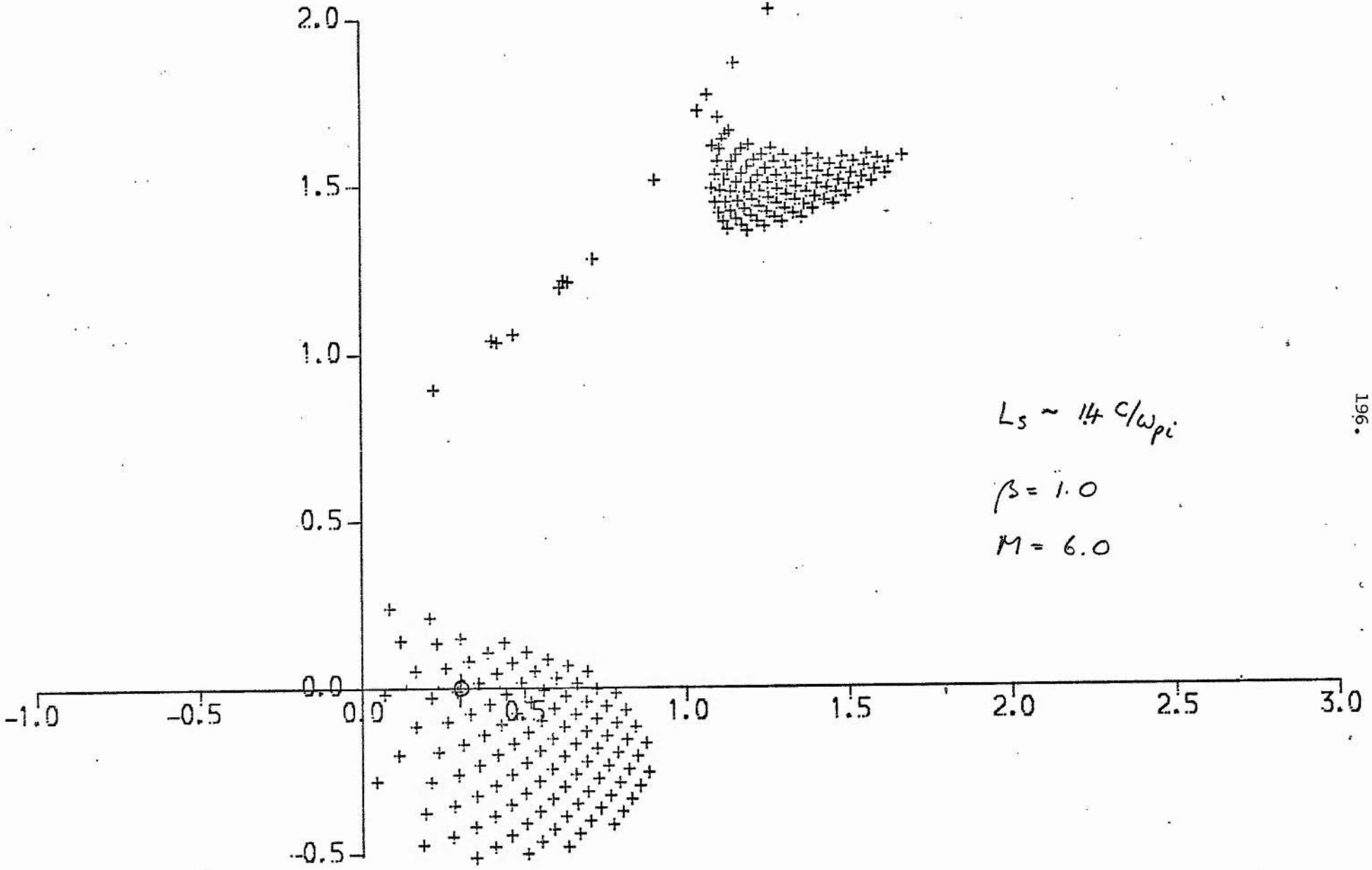
2.0
1.5
1.0
0.5
0.0
-0.5
-1.0
-0.5
0.0
0.5
1.0
1.5
2.0
2.5
3.0
$L_s \sim 14\ c/\omega_{pi}$
$\beta = 1.0$
$M = 6.0$

FIG. 10.8

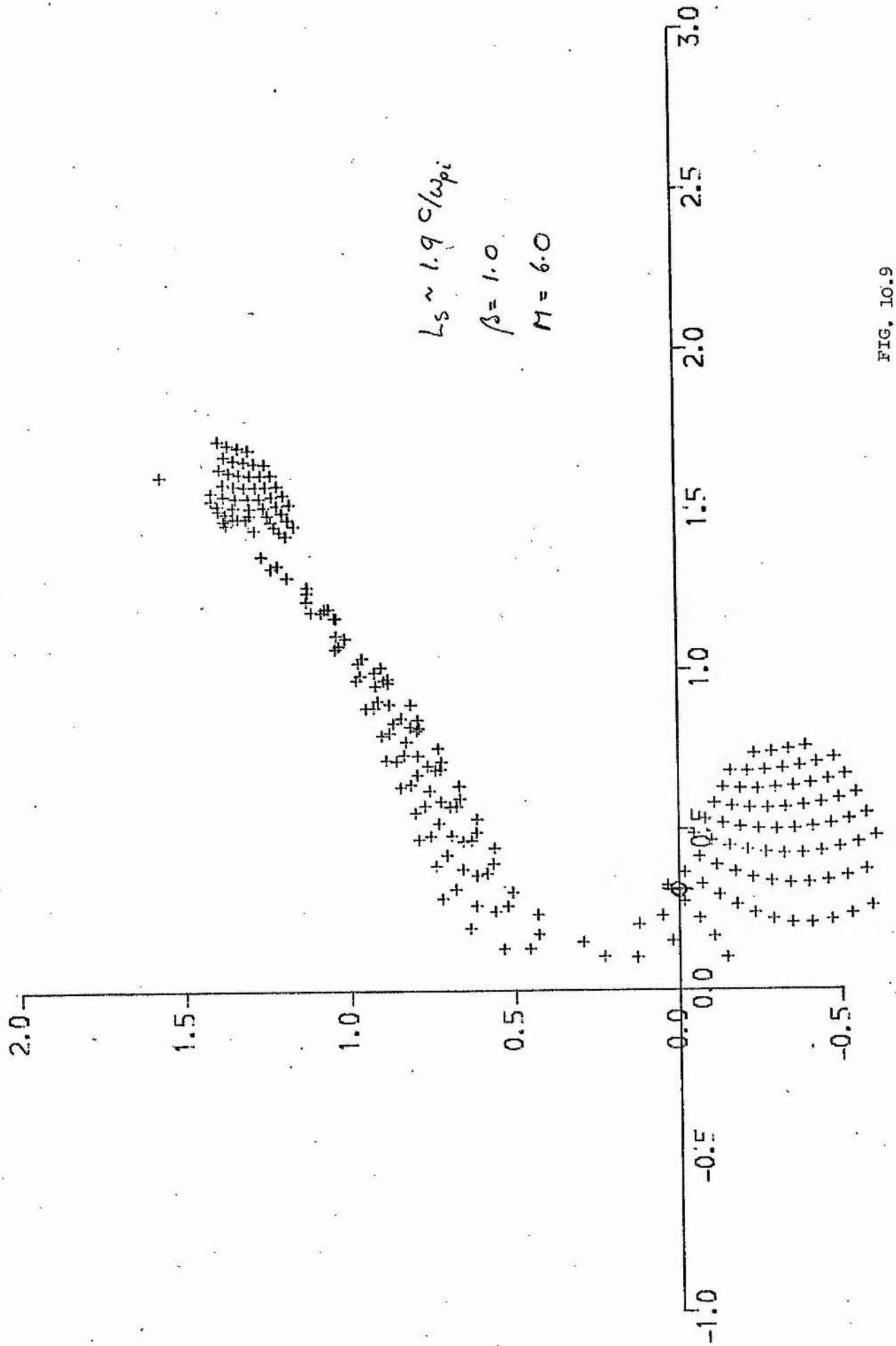
$L_s \sim 1.9\, c/\omega_{pi}$
$\beta = 1.0$
$M = 6.0$
3.0
2.5
2.0
1.5
1.0
0.5
0.0
-0.5
-1.0
2.0
1.5
1.0
0.5
0.0
-0.5

FIG. 10.9

It is at this point interesting to consider the dependence of shock parameters on the upstream temperature ratio T_{el}/T_{il}. A value $T_{el}/T_{il}=1$ is the common experimental situation where creation of a reproducible equilibrium usually requires sufficient time for thermalization to occur[1,12,33]. The Garching shock waves have $T_{el}/T_{il}<1$ while an example $T_e/T_i>1$ is not known. Reduction of ion temperature will lead to a region of increased applicability of the model in M,β-space.

Non-adiabatic heating, T_{i2}/T_{iad}, is plotted against T_{el}/T_{il} in Fig. 10.10. The plots are made at $M=6$, $\beta=0.3$, in a region where computer time is low, but significant reflections occur. Unfortunately, no solution is found at $T_e/T_i=0$, for $v_2>V_2$ for all ϕ. After this point, the curve decreases as expected as the ion thermal spread, and so the reflecting ion levels fall. The variation of ϕ is given in Fig. 10.11, and shows no significant variation so that falling T_{i2}/T_{iad} is due to ion temperature above.

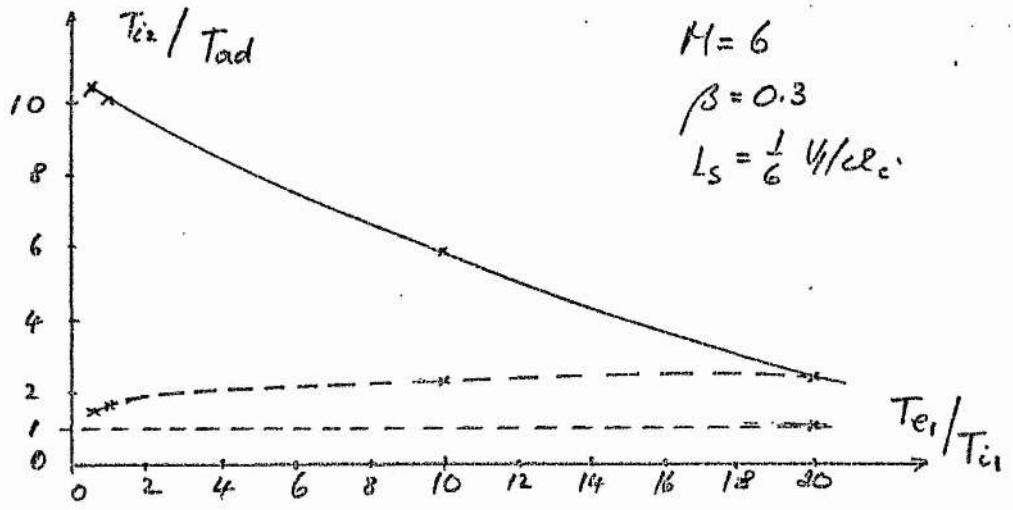

FIG 10.10

The constant level maintained by ϕ is a co-incidental balance between a tendency to increase as T_{i2} decreases, and a tendency to decrease as reflections decrease.

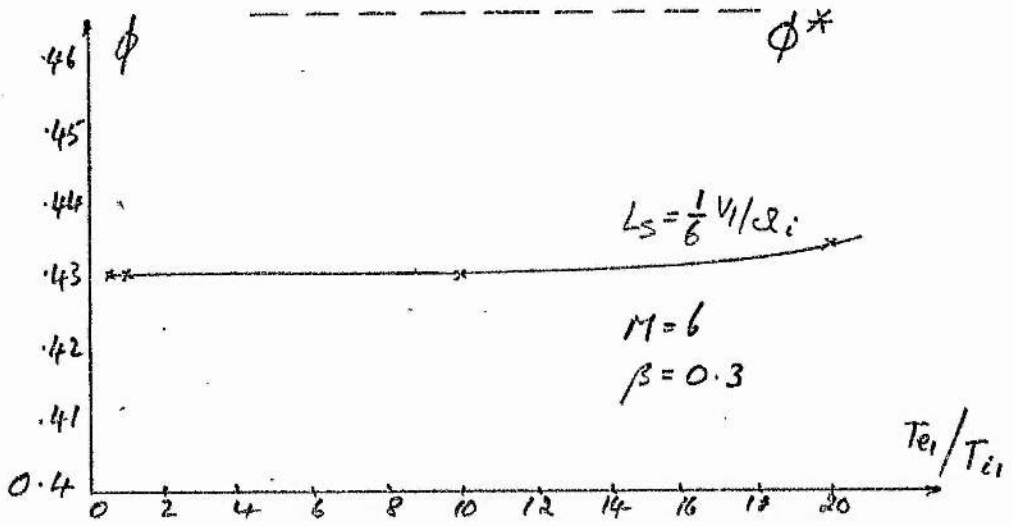

FIG 10.11

Further, $R_\phi < 1$, even in the absence of significant ion heating, implies that shock thickness is too large at $T_e/T_i \sim 20$. The potential then tends to ϕ^* when $L_s = 0$.

The rapid fall in reflecting ion fluxes is shown in Fig. 10.12.

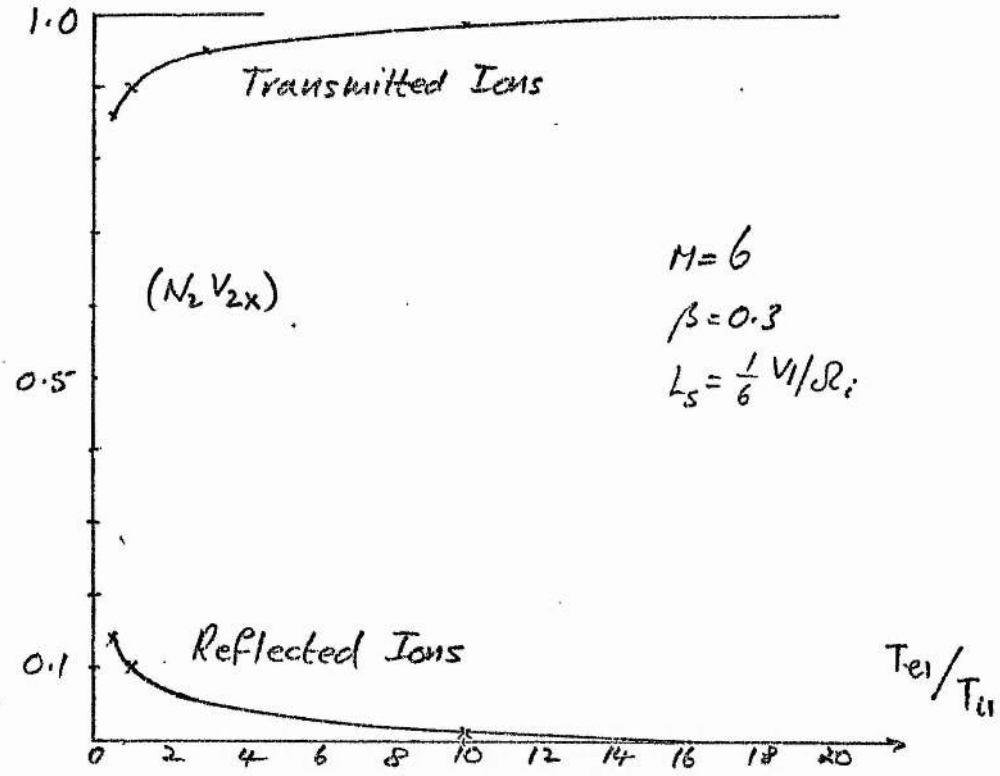

FIG 10.12 (a)

At T_{ei}/T_{il}=10, there is only 2% reflected ion flux. At T_{el}/T_{il}=0.5, the level is 15%. The rapid loss of significance of the ion component is best illustrated by a plot of T_{e2}/T_{i2} (downstream) with the upstream ratio. This is shown in Fig. 10.13.

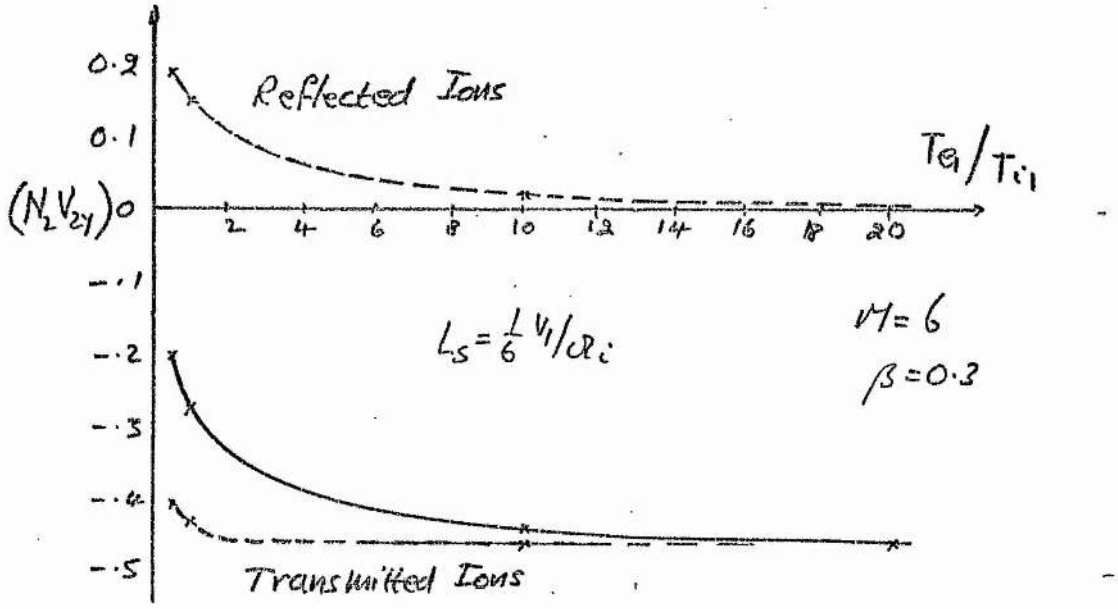

FIG 10.12 (b)

At $T_{el}/T_{il} \gtrsim 5$, the ion heating falls below common experimental errors and so is not detectable.

These few curves help to explain the change of β_o^* with T_{el}/T_{il}, as shown in Fig. 10.14.

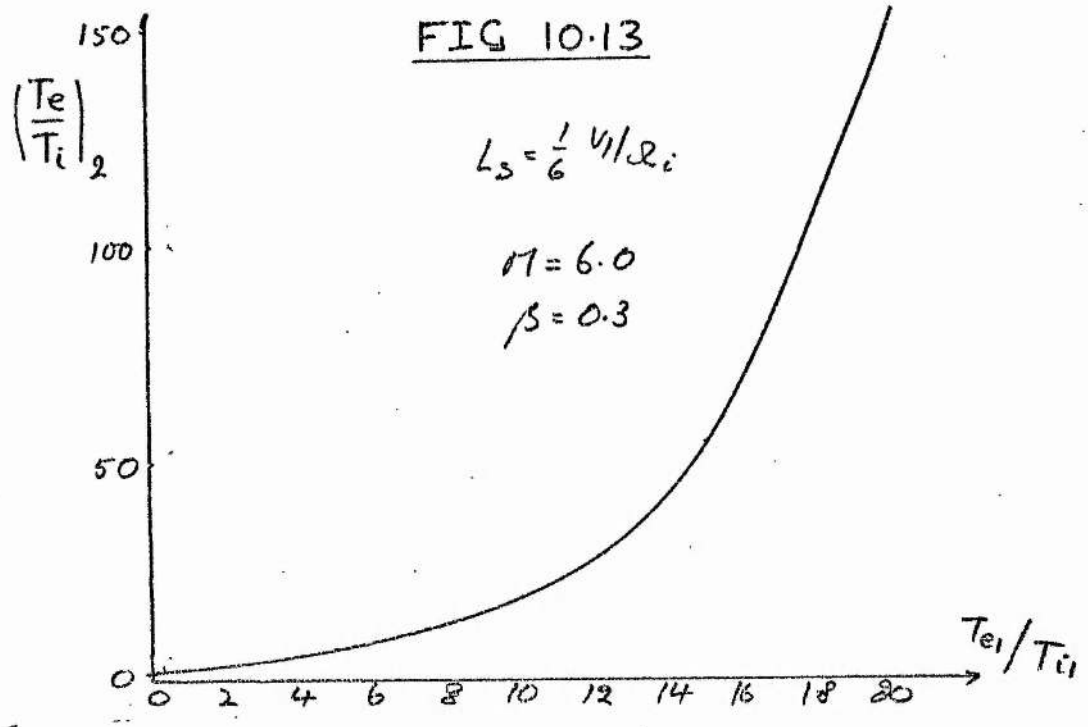

When $T_e=0$, and all initial thermal energy goes to the ions, an expected reduction of β_o^* occurs for the reflected ion flux increases (Fig. 10.12). The effect is not very pronounced so that $T_{el}/T_{il}>1$, as at Garching, does not lead to a significant reduction, or vanishing of model solutions. At $T_e=5T_i$ where very low reflections occur, an enormous region of M,β-space becomes available. This may graphically demonstrate how a reduction of reflections can extend the applicability of the model. Since $L_s=0$ for each of these β^*, inclusion of finite L_s will further improve the extent of the solution sub-space.

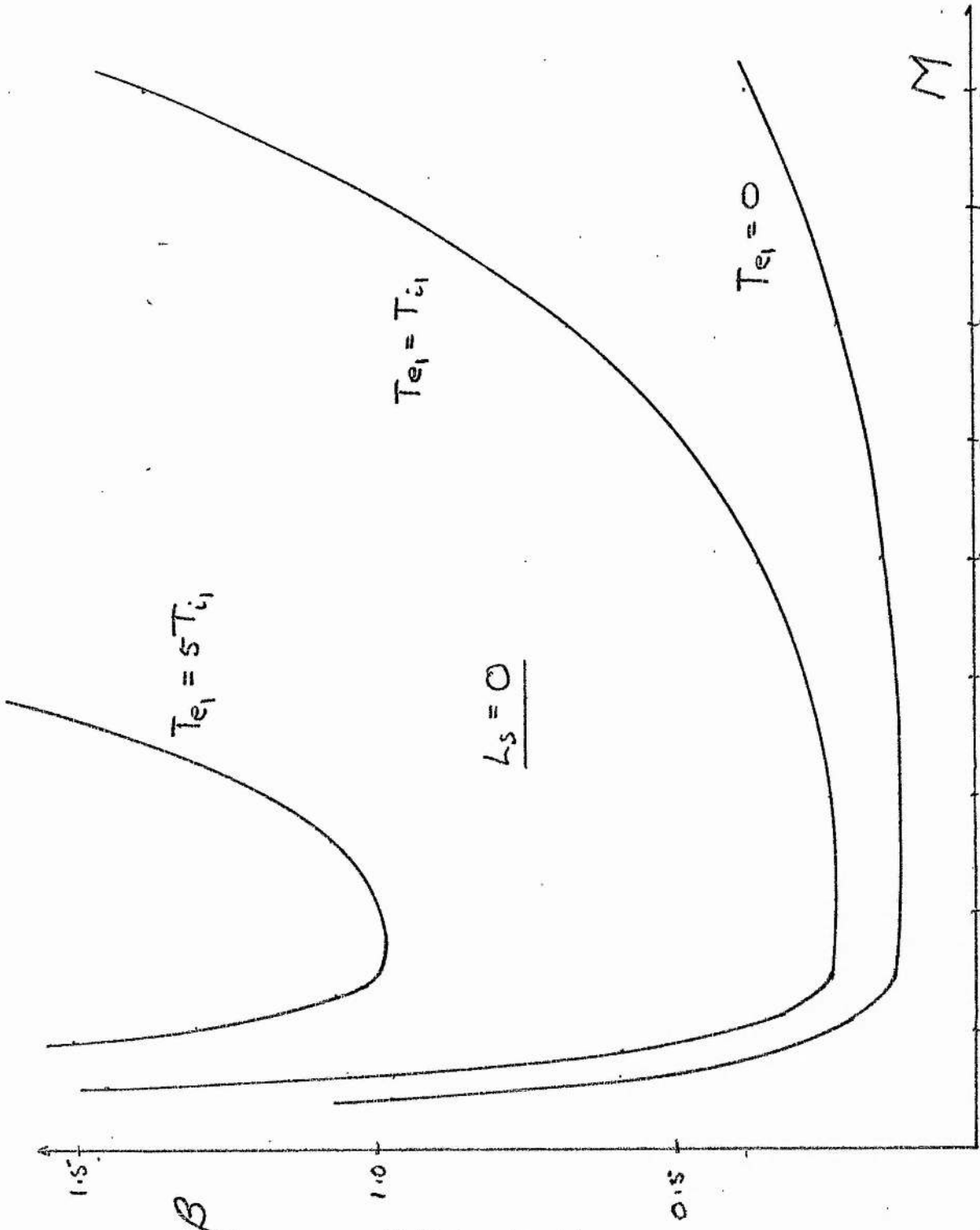

FIG 10.14

The considerations of this section, concerned as they are with the "mathematical" limits of the model, are not without physical relevance. This is held in the relation between the critical β^* of this thesis, with the critical Mach number, M^*, in common use in the literature. Early mention of a Mach number limit is given in the review of Sagdeev[22] in 1964, where the breakdown of a two-fluid representation of a shock is found in a theoretical study of solitons. The low amplitude, cold plasma, frictionless soliton breaks at $M_A^*=2$, while modification to this theory gives a now accepted $M_A^* \simeq 2.76$[9]. These estimates are independent of β_i, and involve no ion heating. A useful β-dependence for M^* has been given in[8], especially for the case of a magnetosonic shock. The energy equations for two fluid species of electrons and ions, yield an equation of the form

$$\frac{dV_x}{dx} \sim 1/\left(-M_i V_x + \frac{1}{V_x}\left(\gamma_i k T_i + \gamma_e k T_c\right)\right) = \frac{1}{-A+C} \qquad (10.15)$$

The ordering A>C for all x, is reversed with increasing M, so that at some M^*, dv_x/dx diverges. If A=C is a condition for the breaking point then it may be added to the Rankine-Hugoniot relations to fix a relation between M^*, and β. Fig. 10.15 shows $M^*(\beta)$, as calculated by Kornherr[8], and the β_o^* of the model. At $\beta=0$, $M^*=2.8$ in agreement with the soliton theory.

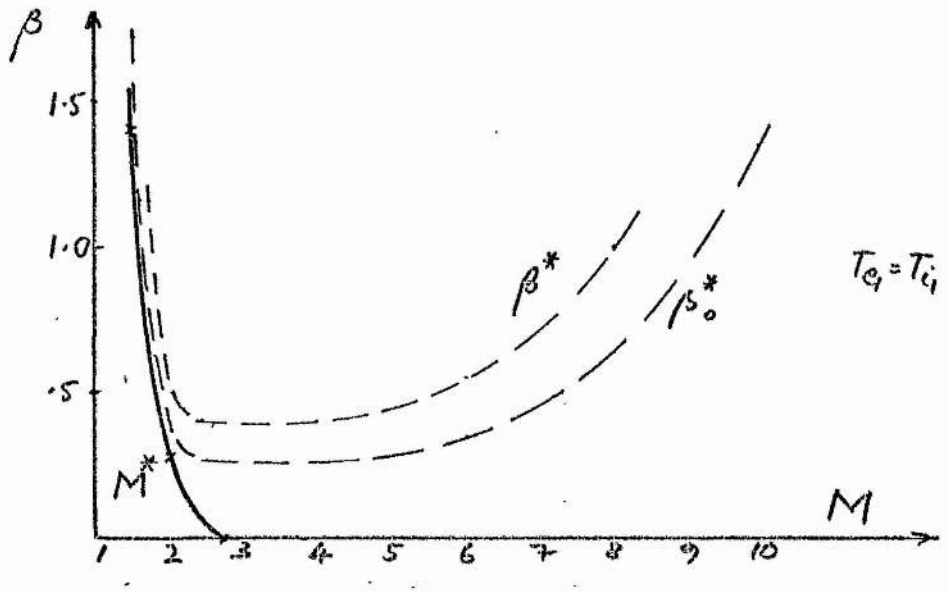

FIG 10.15

Then for $\beta \gtrsim 0.2$, the fluid model, and the laminar kinetic theory model shows excellent agreement. The significance of these critical paths is that they predict a change of state for the system. It is then a problem to determine how the system changes, for there may be many possibilities. Thus surface waves in water may pass through a number of critical points as illustrated in Fig. 10.16.[47]

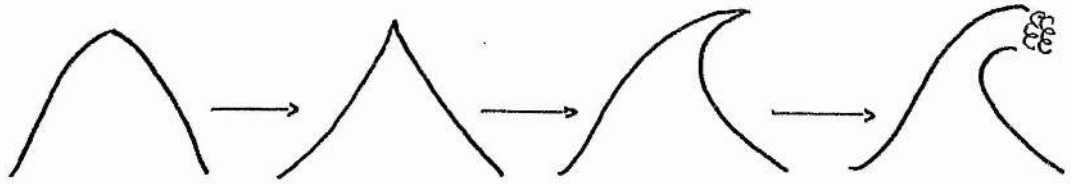

FIG 10.16

It is noted in particular that the state may alter from laminar to laminar, or, from laminar to turbulent. Theoretical description of the laminar locus is possible, while the turbulent state is in general very difficult to understand.

Similar questions may be asked of the geometrical properties of the plasma shock wave. The observations of reflecting ions[14] have led to the obvious conclusion that the change of shock state at M>M* appears as a three-valued flow (no unique two-fluid solutions). Further, the smooth profiles in the "foot", and the observation that foot length corresponds to the radius of an unimpeded ion orbit, combine to suggest continuing laminar form across M*. These very ideas have been exploited in this thesis. On the other hand, attempts at explanation of downstream ion temperature have assumed the presence of an ion turbulence.

Fig. 10.15 shows that for all M<M*, the fluid theories and the model allow laminar shock solutions for the ions. (All observed collisionless

shocks show turbulent electron heating; this may be modelled on M<M* by an anomalous resistivity in the "laminar" fluid equations). But at M>M*, the new information is that laminar shock solutions are possible for $\beta < \beta^*$, while turbulent ions must be considered otherwise. The turbulence must be confined to the transition, for a laminar foot is observed even at high β[7], while the model further suggests that turbulence must be such as to "absorb" reflecting ions in L_s. The turbulence region is always dominated by a fast reflecting ion tail, in the ion distribution function.

The laminar region M>M*, $\beta < \beta^*$ has two different ion distribution types. For $\beta \gtrsim 0.01$, a fast ion tail is present, sufficient to carry ion energy downstream as shown by the model. But at $\beta \lesssim 0.01$, no reflections occur (a region labelled $\beta < \tilde{\beta}$, above). Thus M* does not indicate the accepted change of state as the appearance of three-valued flows. Instead a velocity-space change occurs, as a significant distortion of the upstream Maxwellian. This idea is not accessible to the fluid theories. The experiments of Eselevich et. al.[11], which detect ion-acoustic subshocks at these low β with ion reflections, force a reconsideration of the idea of laminar ions at M>M*, $\beta << 1$. They also find that the subshock ceases at high Mach number, $M_A \sim 5$, with continued presence of a "foot". This appears to be at high $\beta \sim 0.05$ (no initial temperature is explicitly given) and may correspond to the model solutions ($\beta \gtrsim 0.04$, Fig. 8.1). It thus remains a possibility that at very high M, the shocks will remain laminar.

A schematic subdivision is shown in Fig. 10.17, of M,β-space. Here β is plotted on a log scale to amplify the low-β behaviour.

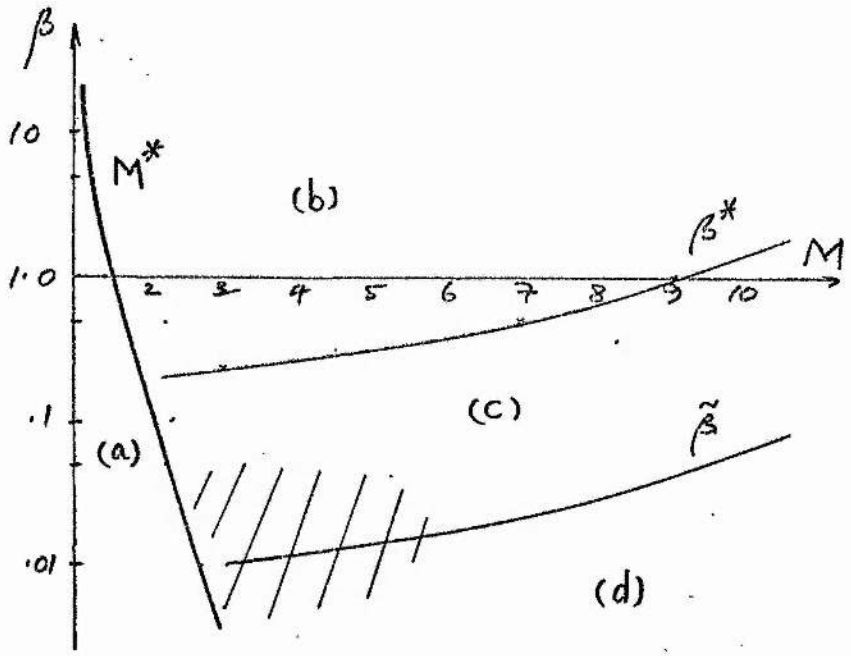

FIG 10.17.

A quite sophisticated extension of the idea of the critical Mach number arises, with many suggestions for ion distribution behaviour when the time component is released. The regions are summarized as

(a) Approximate region for application of the fluid equations. Anomalous resistivity is sufficient to explain shock heating, due to electrons only.

(b) Region characterized by significant non-laminar ions, in the shock transition. At $\beta \gtrsim \beta*$, downstream temperature as ion Larmor gyration might be expected. At $\beta >> \beta*$ instabilities may be sufficient to result in complete turbulent dissipation of the ion beam, in L_s; this seems unlikely for calculate ion instabilities appear inadequate for all observed shocks. Unimpeded upstream reflection always occurs, as the source of ion energy downstream.

(c) Region where no ion turbulence is required in L_s, but is expected downstream due to the fast ion tail. The presence of "super-heated" ions in (c) does suggest an early appearance of turbulence here. At very low β, some evidence of ion-acoustic subshocks (non-stationary) is experimentally found, contemporary with the appearance of reflections, and a time independent model might be inappropriate - their influence on the ions is unclear. They are detected in the shaded region, shared with

(d) A region where $\beta<\tilde{\beta}$, and M>M*, and laminar shocks can occur, but with a state change in velocity space. Ion energy is carried downstream not by a fast tail, but by a simple distortion of the main beam, which affects downstream instabilities.

It is noted that the low-M shocks at Culham and Garching lie in region (a), the high-M Garching shock in region (b), and the similar Culham example in (c). At least the existence of simple, distorted ion distributions, at M>M*, is suggested by Schumacher's example[24] (Fig. 3.2), albeit in the case of an initial $B_1=0$ shock; no ion reflection can occur for there is no turning magnetic field, so that downstream ion heating has been absorbed by the distortion. The different ion energies of Fig. 3.2 are unexplained in that paper. No measurement of electric potential has been made, while no mention of the time dependence of profiles is given. Hintz[10] displays a $B_1=0$ shock with smooth profiles in a domain $T_e>>T_i$, of negligible ion dynamics. Application of the theory of this thesis to such shocks would be of interest, amplifying as it does the simple distortion in the absence of reflecting ions.

§11 On Non-Laminar Ions and Ion Instabilities

The immediate problem is the nature of the $\beta > \beta^*$ shocks. The boundary β^* is of course in reality not a clear divide between laminar and non-laminar shocks. Thus the finding that $T_{i2} \sim T_2^{RH}$ when $\beta < \beta^*$, probably requires non-laminar ion dynamics to allow some electron heating. On the other hand, the apparently laminar ions of the $\beta > \beta^*$ Garching experiments suggest continued relevance of the model.

This is reminiscent of electron heating problems where collisional resistive heating remains important even while it is inadequate to explain collisionless shocks. A mixed behaviour results. The effects of ion collisions, as a non-laminar behaviour, are first considered. It has been mentioned in section §2 that the Garching shocks showed collisions. Yet the purely laminar model gives heating of the correct order of magnitude, though it is not self-consistent.

In the shocks of Kornherr[8], the low initial ionization (~50%) allowed further ionization and dissociation in the shock transition. A non-trivial source of plasma resulted, with $N_1 V_1 < N_2 V_2$. The shock wave remains a magnetosonic event with non-colliding neutrals (hydrogen) simply passing without effect through the shock. This creation of flux required a rederivation of the jump conditions.

It was found that the ratio of ions created, to the observed downstream density was $\varepsilon \sim 25\%$, in the $M \sim 4.9, \beta \sim 2.6$ shock. Among the conservation relations are

$$N_1 V_1 = N_2^{col} V_2^{Col} \cdot (1-\varepsilon) \qquad (11.1)$$

$$V_1 B_1 = V_2^{Col} B_2^{Col} \qquad (11.2)$$

For this $M>M^*$ shock, the usual R-H relations predict $s_B=B_2/B_1=3.6$. The observed ratio is $s_B \sim 2.9$ Now by (11.2) the plasma is slowed as usual to preserve overall charge neutrality, so that while s_B is smaller when $\varepsilon \neq 0$, the ratio V_2^{Col}/V_1 may be larger, with $V_2 < V_2^{Col}$. But then the ions need not be slowed as much when $\varepsilon \neq 0$; this is as expected when ionizing collisions increase N_2.

Now, if there is any laminar heating in this shock, it should be easier to achieve a self-consistent solution. The initial ions will remain approximately laminar if downstream flux is created by neutral-neutral collisions only, with no ion-neutral interaction. Let this be assumed. The initial ion Maxwellian can be passed through the shock and checked for self-consistency in the usual way. However the model conserves flux so that $n_2 v_2 = 1$, and so (11.1) is violated (where $v_2 = V_2^{Col}$, for self-consistency). The creation of new, even laminar, ions cannot be modelled, for f_i is undetermined on their orbits. Thus if ion collisions are ignorable and $v_2 = V_2^{Col}$ in a model run, it would be necessary to artificially adjust the downstream. The extended R-H relations allow determination of missing density and flux; thus if $\Delta N = N_2^{Col} - N_2$, from (11.1) these new ions must be placed at $V_\varepsilon = \varepsilon/\Delta N$. At Garching with $\varepsilon \sim 25\%$, $\Delta N \sim 0.7$, then $V_\varepsilon \sim 0.36 \sim V_2^{Col}$ and the new ions must be deposited with the downstream drift, consistent with the laminar ions slowing to V_2^{Col}. It can be shown that downstream temperature is increased by $\sim 22\%$, for $\varepsilon \sim 25\%$.

It has been assumed that the model can slow the (non-colliding) initial ions to the more favourable $V_2^{Col} > V_2$, when $\varepsilon \neq 0$, these ions remaining purely laminar. Now it has been seen in previous chapters that at the Garching parameters it is very difficult to slow the laminar ions. Thus when $\varepsilon = 0$, $v_2 = 0.4 >>$

V_2=0.28. But further it is noted then that v_2=0.4>V_2^{Col}≈0.34, as observed by Kornherr. Thus the laminar ions cannot be properly slowed and they in turn must be (as is likely) involved in collisions. (The observed shock thickness is $L_s \sim \frac{1}{2} C/\omega_{pi} \sim .07\ V_1/\Omega_i$, which is thin in units of V_1/Ω_i. Thus ion dynamics remain dominated by the electric potential, with reduced B_2/B_1 having no effect when $\varepsilon \neq 0$. An L_s=0 model will give a reasonable approximation).

In spite of these ions undergoing collisions, it was in Kornherr's shock that the ions were found to be heated in two degrees of freedom, in excess of adiabatic. Again a totally collisional behaviour is ruled out, and some laminar dynamics may be retained. The problem is then, at its simplest, to properly slow the ions by ion collisions by operating on the fast reflected ion beam which defines the region $\beta > \beta^*$. Working aroung the properties of the laminar model, it is the large reflection orbit (in two degrees of freedom) that is the dominant laminar heating mechanism (especially at high β), and this should be preserved.

It is noted that the ions on the point of reflection will be moving very slowly relative to the bulk fluid velocity $V \geq V_2$, and it is just these ions that will be the most susceptible to collisions. The equation of motion of an ion is

$$v_x \frac{dv_x}{dx} = -\frac{e}{M} \cdot \frac{d\phi}{dx} + \frac{e}{Mc} v_y B(x) - \nu (v_x - V) \qquad (11.3)$$

where ν is an ion collision frequency and $V \geq V_2$ is the local bulk velocity of the plasma. If $L_s \sim 0$, then the Lorentz term can be ignored, and integrating once gives

$$\tfrac{1}{2}(v_x^2 - v_1^2) + \frac{e}{M}\cdot\phi = -\nu\int(v_x - V)dx \qquad (11.4)$$

If $\nu=0$ the ion is slowed by ϕ, as usual. If $v_x \sim V$, or ν is small, for fast ions, then the right hand side is small. If $v_x \sim 0$, and ν is large (the model shows the slow ions spend about 30% longer in the shock than the "mean ion"), then this term is maximal so that

$$-\nu\int(v_x - V)\,dx \;\underline{\sim}\; \nu\int V dx \sim \nu\,\bar{V}L_s \quad ,$$

where $\bar{V}$ is a mean velocity across L_s. If $L_s=\bar{V}\tau$, where τ is the shock transit time, then

$$\tfrac{1}{2}(v_x^2 - v_1^2) + \frac{e}{M}\,\phi \sim \tau\,\nu\bar{V}^2 \qquad (11.6)$$

An effective potential

$$\phi - \frac{M}{e}\,\tau\,\nu\,\bar{V}^2 = \phi - \phi_\nu\,, \qquad (11.7)$$

results, but is seen only by the slow ions. In particular, for reflection $e\phi \sim \tfrac{1}{2}MV_1^2$ so that the factor $\tau\nu \lesssim \tfrac{1}{2}$ can effect significant reduction in ϕ for slow ions. Thus some of the ions reflected when $\nu=0$, may now pass, without laminar heating, into the downstream.

This, together with the appearance of these ions with low $v_x \ll V_2^{Col}$ in the main beam, will cause proper slowing of the ions, with the preservation of some reflection heating. It is noted from section §9 that a reduction in the fraction $f_R = {}^{n_R}/_N$ of reflected ions may in turn lower self-consistent ϕ according to $f_R\Delta y^i$. The displacement Δy^i will be unchanged.

The slow ions will have unimportant properties in the downstream. Their flux will be known if the flux of the otherwise laminar reflected and transmitted ions is known. It must be assumed that they are deposited in $\underline{\mathcal{V}}_2$ in such a way that proper slowing results. Slowing will result more as a loss of fast beam flux, than by deposit of slow ions at $v_x \gtrsim 0$, in $\underline{\mathcal{V}}_2$. The temperature of these slow ions will be low. If they are regarded as accelerated into the downstream by ϕ_ν, a heating estimate $\frac{2}{3} f^{Col}_{\ \nu} \tau \overline{V}^2$ results where f^{Col} is the fraction of transmitted ions. This is small and is ignored.

An estimate of the effect of this mechanism is made, using the $L_s=0$ model. Fig. 11.1 shows the initial ion distribution in one dimension, with $v_x = \sqrt{2\phi}$, and $v_x = \sqrt{2(\phi-\phi_\nu)}$, indicated (non-dimensionalized). Between these are the "slow ions", marginally transmitted in each case.

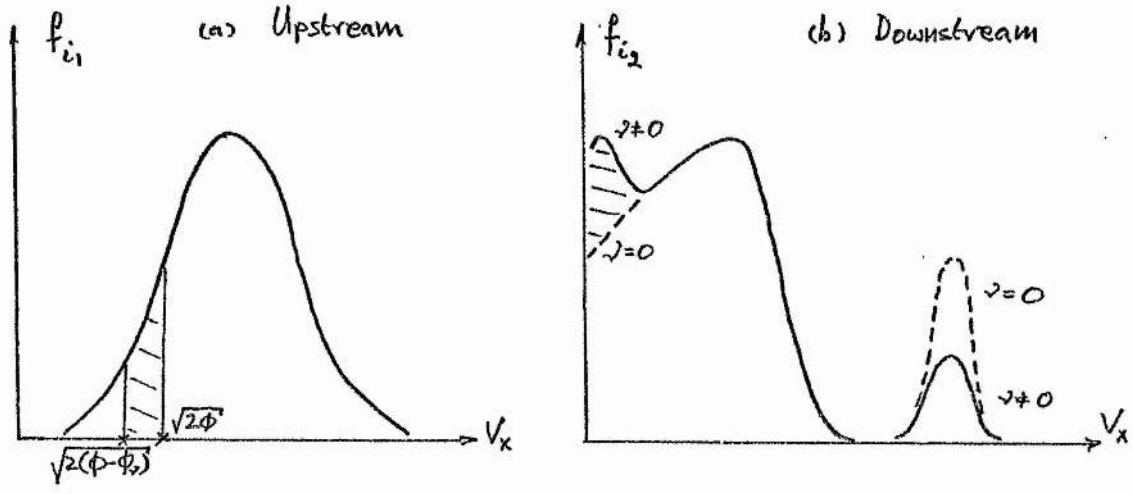

FIG 11.1

The slow ions are shown appearing at small V_x in the downstream. As ν increases so successive cuts will be taken from the steep vertical face of the fast tail. The remaining ions in the tail will be unaffected. When $L_s=0$, this can be modelled by simply reducing ϕ for the tail only, leaving the main beam heating (and slowing) unaltered. A run is made at the Garching parameters. The potential is arbitrarily chosen at $\phi=\phi(V_{2\ min})$ in Fig. 5.5. The reduction in total heating, and the fraction f_R of reflected ions is plotted in Fig. 11.2, with ν, and ϕ_ν. Here $\tau=L_s/V_1$ from the observed shock (this is less than a typical time in the shock of a slow ion) and $\overline{V}=(V_1+V_2)/2$

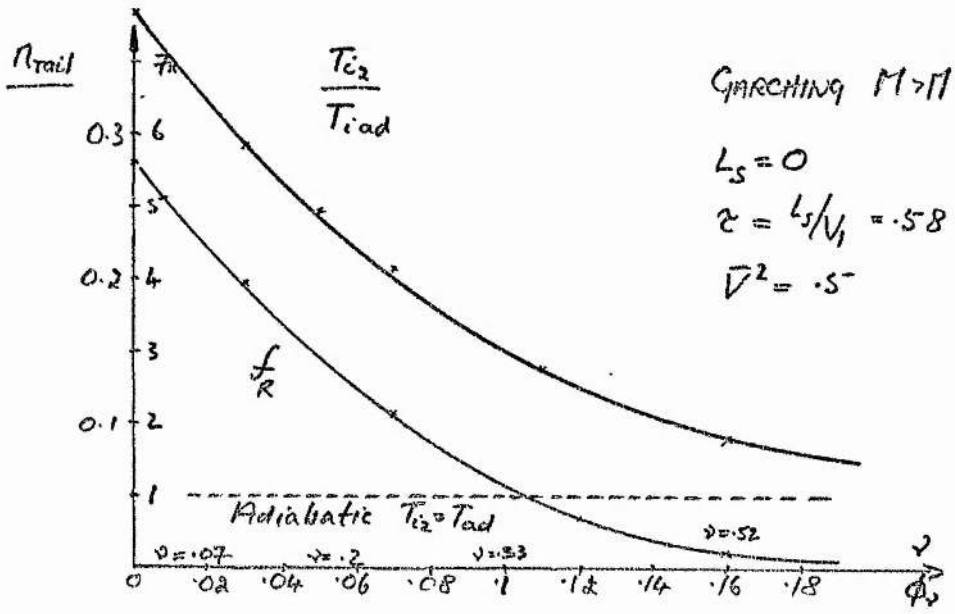

FIG 11.2

The rapid reduction in f_R is noted. The curve is quite sensitive to ν_1 so that the fast beam is easily reduced in importance. The non-laminar heating shows the same behaviour as

f_R, clearly being dependent on the density of reflected ions. This demonstrates the dominance of this heating process. Only laminar heating is shown.

At $\nu \sim 0.1$, $T_{i2}/T_{iad} \sim 6$, flux lost is about 9% and applied to the observed jumps of the Garching experiment, the slow ions must emerge with $n_v \sim 1.5$, $v_v \sim 0.06$; this last is a very low velocity, in line with Fig. 11.1(b), and so this collisional slowing mechanism will be doubly effective.

At Garching, the number of ions created in a shock transit time required an ionization rate of $\sim 1.7\Omega_i$ ions/sec. This is due to both ion-neutral and neutral-neutral collisions. The former will result in approximately one-third of the new ions (if the two species have the same temperature at ~50% initial ionization); so $\nu \sim 0.6\ \Omega_i$. This is a lower limit for ion collisions in the shock, and yet is much greater than the levels of Fig. 11.2 - at $\nu = .5$, $T_{i2}/T_{iad} \sim 2$, much reduced but still significant. Another estimate for collisionless ions gives $\nu < V_1/L_s$. For Kornherr's shock, $V_1/L_s \sim 1.5$ so that $\nu \sim 0.6$ is small. Estimated for ion-neutral collisions as $\nu = \langle n\sigma' v_{th} \rangle \sim v_i/L_{mfp} \sim v_i/L_s$ where σ' is the collision cross section[5], then $\nu \sim 1.7$ in front of the shock, which is close to the first estimate.

At $L_s = 0$ the tail is then quite vulnerable. There are some extenuating circumstances however. The heating observed by Kornherr will include ionization energies which is in addition to compressive ion heating so is non-adiabatic. If all this energy goes into the ions it was shown above that it can increase T_2 by about 20%. Thus the required laminar component is at $T_{i2}/T_{iad} \sim 6$, allowing larger collision frequencies for comparison ($\nu \sim 0.1$). The reason for the steep fall in these curves (Fig. 11.2) lies in the highly

localized tail of the L_s=0 model. This is shown in Fig. 11.3, in a surface of f_i over $\underline{v}_2$. Most of the ion density lies close to the vertical face. This should be compared with the scattergram of f_i over $\underline{v}_2$ of Fig. 11.4, made at observed shock thickness. There is a noticeably broadened tail, so that loss to collisions will be slower than predicted by Fig. 11.2.

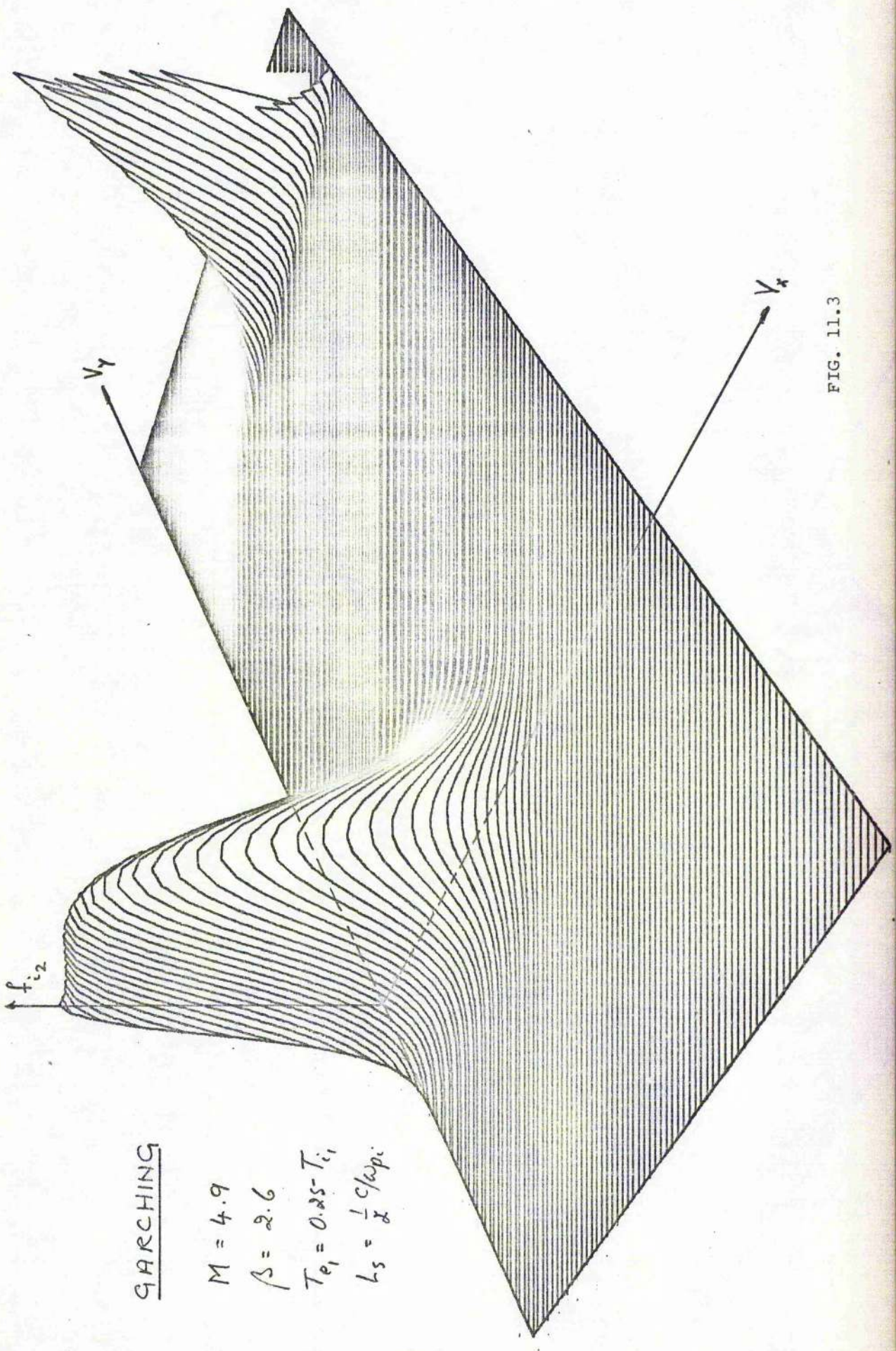

FIG. 11.3

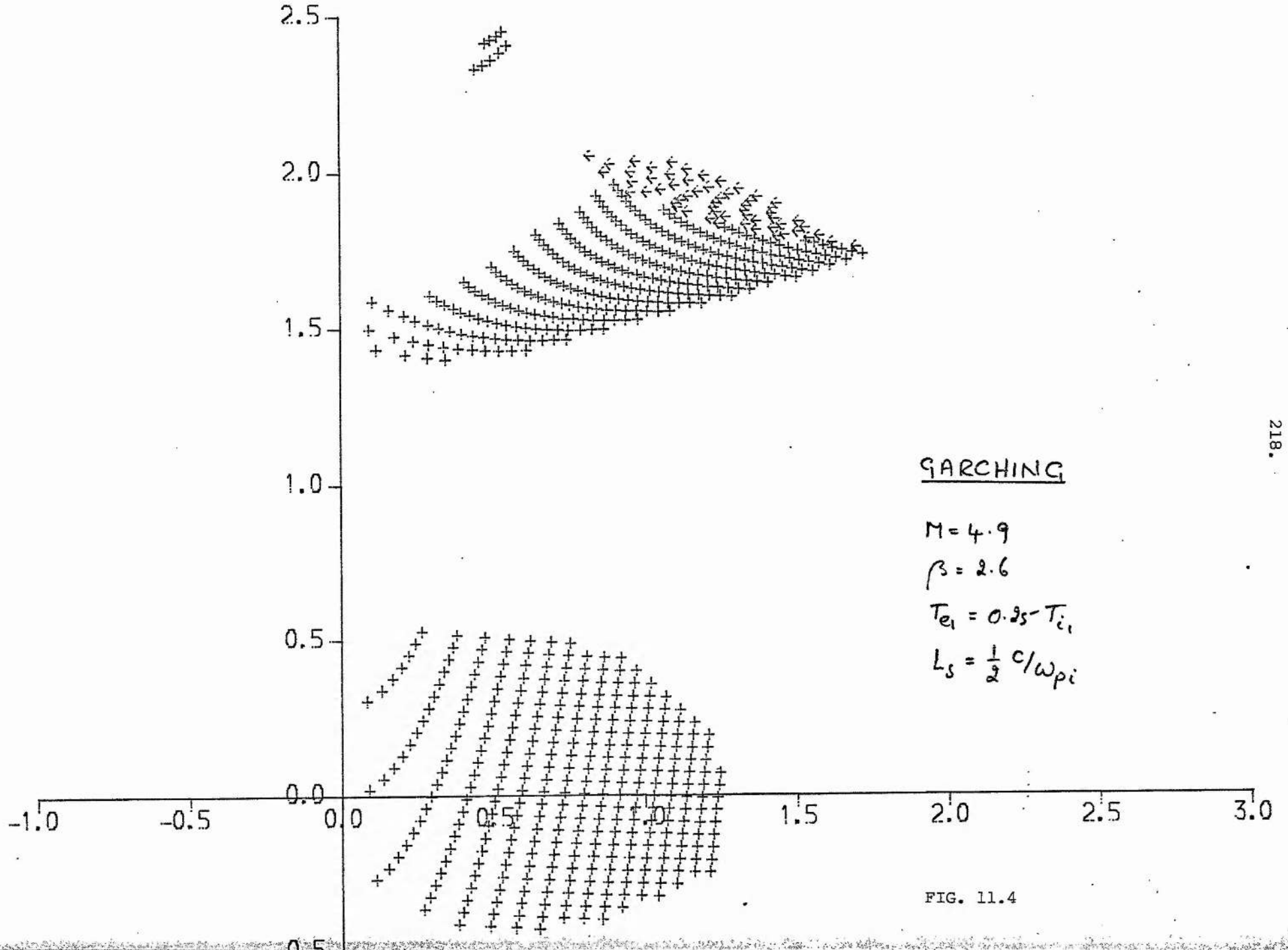
2.5
2.0
1.5
1.0
0.5
0.0
-1.0
-0.5
0.0
0.5
1.0
1.5
2.0
2.5
3.0
SARCHING
M = 4·9
β = 2.6
$T_{e_1} = 0.25 - T_{i_1}$
$L_s = \frac{1}{2} c/\omega_{pi}$

FIG. 11.4

Fig. 11.4 shows that a small second tail begins to emerge. This will be easily absorbed by collisions. Also the main beam no longer shows strong elongation so $T_{iM}/T_{iad} \sim 1$ for those ions. This is typical of high-β runs.

Thus the effect of binary collisions may play a compatible role with laminar ion heating in the shock, by helping to slow the over-fast ions of the $\beta > \beta^*$ region. Their effect will be considerable, especially at low $\beta \gtrsim \beta^*$ where the ions are cool enough to ensure a highly localized tail. The upstream laminar acceleration remains the heating process. There is also the possibility that collisions will occur in the "foot". The ion-neutral mean free path is about 2½ times the foot length. The ion displacement in the y-direction is easily of this order, but the high ionization (~80%) will require more collisions to slow the ions[1]. The ratio $R_\phi \sim 1$ observed, is in line with the laminar model. A study of the collisional dependence of the foot profiles would be of interest. Thus while small ion heating takes place by collisions in L_s, and very efficient slowing occurs, collisions in the foot allow some acceleration of the reflected ions giving increased heating downstream but less efficient slowing.

It is in fact very difficult to find an experimental shock wave that is not influenced by collisions. The Culham shock at $M > M^*$ is satisfactorily explained by the laminar model in important aspects, but is a $\beta < \beta^*$ example. The Garching high-β experiment due to Keilhacker et al.[7] is highly ionized (better than 80%) and might be expected to show low collisional effects. Direct measurement of ion heating is made when $M \sim 2.5 > M^*$, $\beta \sim 1 > \beta^*$, $T_i > T_e$ everywhere. Laser scattering at wavelengths less than the Debye radius shows $T_{i2}/T_{iad} \sim 1.7$. If

a parallel model run is made, this ratio is found to be ~4, without proper slowing of the ions, and so reduction of the fast tail is required. Now comparison of the measured electron and ion temperature of [7], with the Rankine-Hugoniot relations gave good agreement. Thus all ions were seen by the laser scattering ion temperature measurements, and thus all ion energy is held downstream as thermal fluctuations ($\lambda<\lambda_D$ = Debye radius). Thus there is no likelyhood of a downstream fast beam (which would not be seen by laser scattering), nor of turbulent fluctuations ($\lambda>\lambda_D$). Further, the intensity of ion density fluctuations was found to be Maxwellian so that an equilibrium had been established. Further, the electron temperature ($T_{e2}>T_{i2}$), was found to fall very rapidly after the main shock transition indicating collisional thermalization. The ions must see significant collisions even though the initial plasma is highly ionized. Then, as before, laminar heating can be efficiently reduced by absorption of slow ions. There is no sign of a tail downstream, but collisions seem capable of establishing a Maxwellian form.

This shock showed no foot in field profiles. The loss of precursor structure at high β has been noted by Hintz[10], but is observed in the Bow shock ($\beta>\beta*$). A study of the susceptibility of the foot to shock parameters would again give useful clues to ion behaviour. Thus β and collision dependence, and also reflection-number dependence, is required. This has not been done to present knowledge. The foot must have at least an ion reflection time to form, and Hintz suggests that the finite dimensions of his experiment might limit its growth.

If in Laboratory shocks, collisions so far appear to play an important part, it is apparently possible to imagine initial conditions of very low density and high temperature, such that $\nu=0$ for the ions. Thus at $\beta \lesssim \beta^*$, the $M=2.4$, $\beta=0.3$ shock of Fig. 8.20 shows excessive ion heating, $T_{i2} \sim T_2^{RH}$. It is then at least imaginable that binary collisions are absent and some other non-laminar ion process should be involved. Heating in this example, and for $\beta > \beta^*$, is as always due to the fast beam; the new alternative can only be wave instabilities inherent in the many-beam ion distributions of the region.

It is hoped to show that the dominant[9] ion two-stream instability need not help slow the ions.

Early linear studies have shown that in the absence of a magnetic field, instability occurs only for $T_e/T_i \gtrsim 3.5$[38]. Two equal ion beams were used, symmetric about the electron distribution. This limit is raised (instability requiring relatively hotter electrons) when unequal ion beams are used[39]. Two later papers by Auer et al.[18] and Papadopoulos et al.[19], will be quoted here. The first investigates the full electromagnetic linear dispersion relation, the second the quasilinear development of the electrostatic case for propagation perpendicular to $\underline{B}$. Both use simulations. The second shows that if $T_e/T_i \gtrsim 1$, $\underline{B} \neq 0$, the instability may now persist. Quasilinear theory agrees with simulation in the electrostatic domain. The first paper[18] shows that for hot ions the growth rates are reduced when the complete electromagnetic case is used. A simulation on the Bow Shock is performed.

Since $r_e \ll L_s \ll r_i$, and $\Omega_e \gg \tau^{-1} \gg \Omega_i$ in observed shocks, the wave regions

$$k^2 r_i^2 >> 1 >> k^2 r_e^2$$
$$\Omega_i^2 << |\omega|^2 << \Omega_e^2, \qquad (11.8)$$

are studied. It is possible to regard the ions as unmagnetized, while the electrons are tightly bound to the magnetic field.

Papadopoulos et al. consider the following simple electrostatic dispersion relation:

$$\frac{1}{(\omega - kVd)^2} + \frac{1}{(\omega + kVd)^2} = \frac{2(1+\omega_{pe}^2/\Omega_e^2)}{\omega_{pi}^2} = \frac{1}{\omega_o^2} \qquad (11.9)$$

for equal, cold ion beams, drift $\pm V_d$ perpendicular to $\underline{B}$ with $\underline{k}$ parallel to V_d. The electron temperature must satisfy $T_e << MV_d^2/1$.

Then these waves are unstable only for k such that $0 < k^2 V_a^2 < k_c^2 V_d^2 = 2\omega_o^2$ The maximum growth rate is

$$\gamma_m = \omega o/_2 \qquad (11.10)$$

$$\text{at} \qquad k_m^2 = \tfrac{3}{4}(\omega o^2/_{V_d}{}^2) \qquad (11.11)$$

To satisfy (11.8) it is necessary that $\omega_{pe}^2/\Omega_e^2 >> 8m/M$. From (11.10), if $\alpha^2 = 1 + \omega_{pe}^2/\Omega_e^2$, then

$$\frac{\gamma_m}{\Omega_i} = \tfrac{1}{2} \frac{M}{m} \frac{\alpha^2 - 1}{\alpha^2} \qquad (11.12)$$

and it is seen that for large α^2, $\gamma_m \lesssim 21\ \Omega_i \sim .5\ \omega_{pi}$, for hydrogen.

These may be compared with shock transit times, but of interest here is the slowing of the fast beams. This requires, at least, a quasilinear study for the velocity space diffusion of a beam. Papadopoulos gives the following information.

Moments of the quasilinear equation for $f_i(\underline{v},t)$ yield rate equations for

$$K_j(t) = \frac{M_j}{2}\int \underline{dv}\ (\underline{v} - \underline{V}_j(t))^2 f_j(\underline{v},t), \qquad (11.13)$$

a "temperature"

which is the energy of the j^{th} beam relative to its drift $V_j(t)$, for $V_j(t)$ itself, and for a reversible electron energy due to an averaged $\underline{E}\wedge\underline{B}$ drift, $K_{ye}(t)$. These quantities are coupled via the rising field fluctuations $\varepsilon_F(t) = \Sigma_k\ |E_k(t)|^2\ /\ 8\pi$. For each of the variables $\psi_{(j)} \equiv K_j(t)\ /\ \tfrac{1}{2}MV_d^2$, $(1 - V_j^2(t)\ /\ V_d^2)$, $K_{ye}(t)\ /\ \tfrac{1}{2}MV_d^2$, an equation of the form

$$\frac{d\psi(t)}{dt} \quad \propto \quad \alpha^2 \frac{d}{dt}\frac{\varepsilon_F(t)}{\tfrac{1}{2}nMV_d^2}$$

occurs. Growth rates are then closely dependent on α^2. Also for ε_F,

$$\frac{d}{dt}\ |E_k(t)\ |^2 = 2\ \gamma_k(t)\ |E_k(t)|^2, \qquad (11.14)$$

where $\gamma_k(t)$ is obtained from the linear dispersion relation (11.9) with $\omega = i\gamma_k$, and V_d replaced by $V_j(t)$. Again (11.9) is dependent on α^2.

Now these equations hold only as long as the ions retain their straight-line orbits. When field fluctuations rise to sufficient level, and ions become hot enough, ion trapping occurs and the quasi-linear approximation breaks down. Thus a numerical simulation is used to compare with the theory,

and extend the study into the non-linear regime.

Fig. 11.5 illustrates Papadopoulos' results for the slowing of a beam.

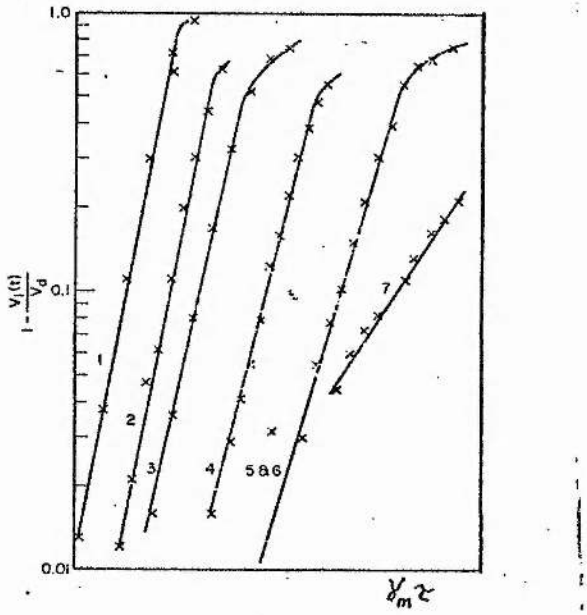

FIG 11.15

The approximately rectilinear regions are the quasilinear regime, and agreement between theory and simulation was excellent. In each case the instability saturates at $\gamma_m \tau \sim 7$, and it is roughly at this time that trapping occurs. It is now possible to look at two mechanisms that might enable solutions for pure collisionless, $\beta > \beta^*$ shocks.

The first is the interesting possibility of a collisionless "absorption" of slow ions by turbulent trapping, analogous to (11.6) above.

Up to $\gamma_m \tau \sim 7$, while the ions slow, directed energy is transferred to $K_j(t)$. Ion phase-space (v_x, X), shows in the simulations "unclosed vortices", with ions slowing and speeding in the rising turbulent fields,

but not trapping; this occurs when the simulations show significant ions moving at the phase velocity of the unstable waves as in Fig. 11.6(c). For unequal beams these occur at $v_p=\omega_R/k\sim 0$, where ω_R is the real part of $\omega=\omega_R + i\gamma$.

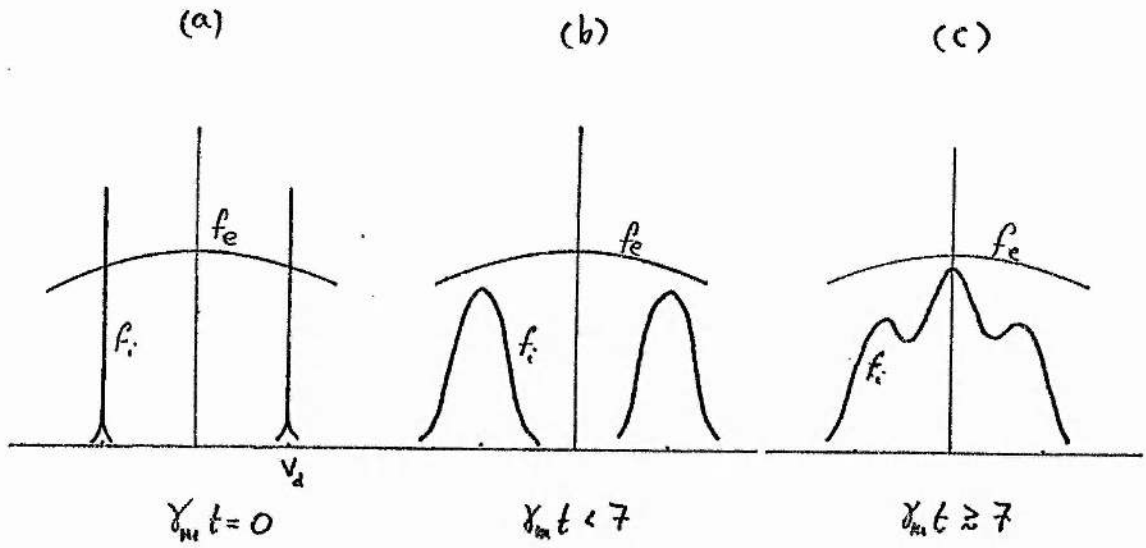

FIG 11.6

When the problem is applied to the shock, and again slowing in the x-direction is considered, the fast tail has low density relative to the transmitted ions (~10% typically) and unequal beams must be considered. In the shock frame, Fig. 11.7 illustrates schematically the distributions at some point in the shock with bulk velocity V. The region of unstable modes is indicated, with $v_p \lesssim V_d$

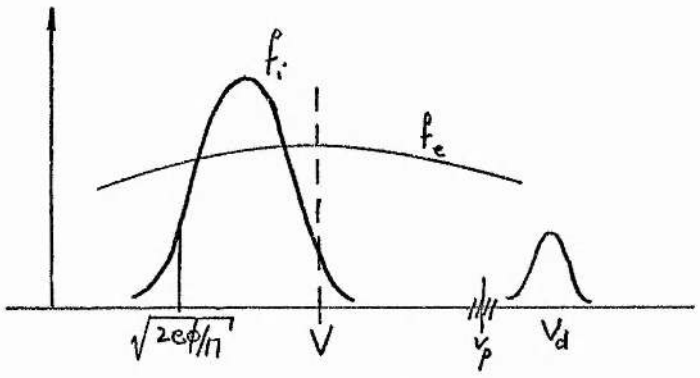

FIG 11.7

Then it is noted that the slow ions, velocity $\sim\sqrt{2e\phi/M}$, are remote from v_p, and will not be trapped.

A further important distribution type will occur in the foot in laminar profiles. Reflected ions leave the resistive potential rise with negative velocities $-v$, and return with high positive velocity $+v'$. The total initial Maxwellian of incoming ions is present, ready to impinge on the resistive profiles. A schematic for cool and hot ions is shown in Fig. 11.8.

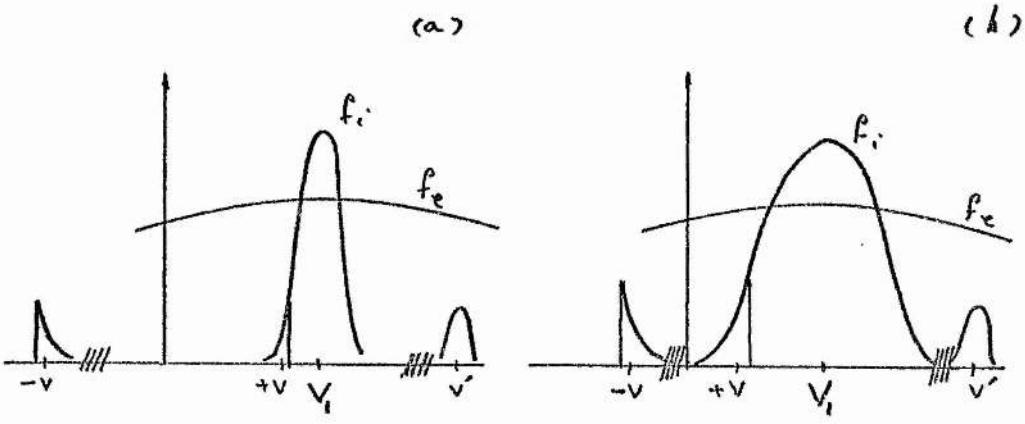

FIG 11.8

At low T_i, v_p is again remote from the slow ions, while it is noted that at very high thermal spread ($v_i \sim V_1$), v_p approaches $v \sim \sqrt{2e\phi/M}$. Again it is unlikely that the "slow ions" will see the turbulence and be trapped - even assuming that the instability can saturate in L_s.

The significance is that an undisturbed initial Maxwellian will reach the resistive potential, and that turbulence will not alter the number of reflected ions as compared with the laminar model.

Thus it is necessary to consider the other more obvious mechanism for slowing the fast beam - simply the quasilinear slowing, itself. The normal approach to the instability has been to attempt to compare the saturation times of the ion turbulence with the shock transit time. This has failed[9]. Now a more delicate question is proposed, that is, for the degree of slowing, only, of the fast beam. This may occur in the foot, perhaps ten times thicker than L_s, or in L_s.

A quite positive answer can be given to the second region, L_s. The large downstream ion energies found in the laminar model are due to the reflection orbit, so that on return to the shock front, they already have this energy. They may lose some energy in crossing L_s. Now even if the laminar model fast beam is slowed by turbulence <u>in L_s</u>, so that a self-consistent solution can take place, the energy of the beams passes very efficiently into ion heating $K_j(t)$. Some electron heating results. Now for the region $\beta > \beta^*$, it has been shown that $T_{i2} \gtrsim T_2^{RH}$, allowing no electron heating. The source of T_{i2} is the large Larmor gyration of the laminar tail. Turbulence in L_s will only change the nature of this "thermal" energy, and depending on the energy of the fluctuating fields, $T_{e2}+T_{i2} > T_2^{RH}$ will persist. Again Papadopoulos has derived an expression for the maximum turbulent field

energy.

$$\frac{\varepsilon_{Fmax}}{\frac{1}{2}nMV_d^2} \simeq \frac{0.23\lambda^4}{1 + \omega_{pe}^2/\Omega_e^2}, \qquad (11.15)$$

which agrees well with the computer simulations. Normalized with respect to the upstream, $\varepsilon_{FMax} \lesssim 23\%$ at $\alpha^2 \sim 1$. The simulations average at $\varepsilon_{FMax} \sim 6\%$ of total energy, for various $0.25 \leq \omega_e^2/\Omega_e^2 \leq 4$. The equation is notably independent of M/m. Experiments examined here have $\omega_e^2/\Omega_e^2 \sim 10^2$-$10^4$, in which case ε_{FMax} is drastically reduced.

If α^2 is as small as possible ($\geq 1 + 8m/M$), then (11.12) gives $\gamma_m \sim 1.5\ \Omega_i$. If $\alpha^2 \sim 10^4$ (Garching), then $\gamma_m \sim 21\ \Omega_i$. The shock transit times t_s $0.3/\Omega_i$ (at β=0.3, M=2.4 and calculated from the model), $t_s \sim 0.5/\Omega_i$ ($=L_s/V_1$, at Garching) and $t_s \sim 0.07/\Omega_i$ (at Culham, model calculated) are known. But in both the cases of high and low α^2, the field energy will be small (the first because the instability has no time to develop, for with time to saturation of $\tau_s \sim 7/\gamma_m$, the slopes of Fig. 11.5 estimate a beam slowing of less than 1%; the second because $\varepsilon_{FMax} \sim 10^{-4}\% \ll N_2T_{i2}$). The factor $\lambda \leq 1$ of (11.15) is to allow for some wave damping, and is to the high fourth power. Simulations showed good agreement with (11.15), but with λ determined from the change in γ_m from the theoretical level.

Thus the two-stream instability would seem to be inadequate in slowing the fast beams, in L_s, by violating the temperature jump conditions.

Thus the dynamics in the foot must be considered. It has been shown that no reduction in the number of the reflected ions is likely to occur, so slowing must be considered.

The foot is broader than the resistive transition ($\sim 10\ L_s$) so has more time to develop. The extremes $1.5\ \Omega_i \leq \gamma_m \leq 21\ \Omega_i$ (from 11.2), with saturation time $\gamma_m \tau_s \sim 7$, must now be compared with the time an ion spends in the foot. The model predicts this is $t_f \sim 0.5/\Omega_i$, comparable with the transit time of the bulk plasma (total orbit time for these ions is much longer, when time in L_s is considered). The estimate is reasonable for the orbit appears to be of order half an upstream Larmor gyration (fig.6.9).

The distribution in the foot is illustrated in Fig. 11.9, as contours of constant f_i over $\underline{V}_1$.

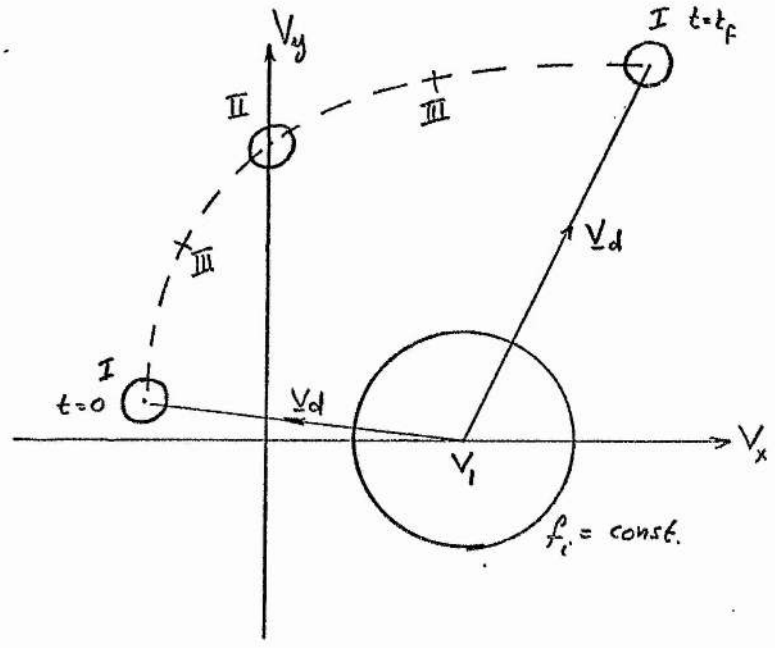

FIG 11.9

At the front of the resistive rise, the distribution has the double tail labelled at I-I; at the leading edge of the foot where the ions reach their turning point, $v_x=0$ and the "tail" is at II; in the foot, the double tail is at some intermediate position III-III. Slowing of the beams is along the direction of $\underline{V}_d$, simultaneously, ignoring the interaction between the tails. (Here the equal beam growth rates will apply, but the low density of the beams significantly reduces ω_{pe}^2/Ω_e^2 and so γ_m is lower; also ε_F drops by the density ratio of tail to main beam).

In parallel with equation (11.9), the dispersion relation pertinent to I, above, has been solved in the present work. This is

$$\frac{1}{\omega^2} + \frac{\varepsilon}{(\omega - kx_1)^2} + \frac{\varepsilon}{(\omega + kx_2)^2} = \frac{1}{\omega_o^2} \qquad (11.16)$$

$$X_1 = u_1 \text{ Cos } \theta + v_1 \text{ Sin } \theta$$
$$X_2 = u_1 \text{ Cos } \theta - v_1 \text{ Sin } \theta \quad ,$$

for equal minor beams of density $n=\varepsilon N_1$ arranged as in Fig. 11.10.

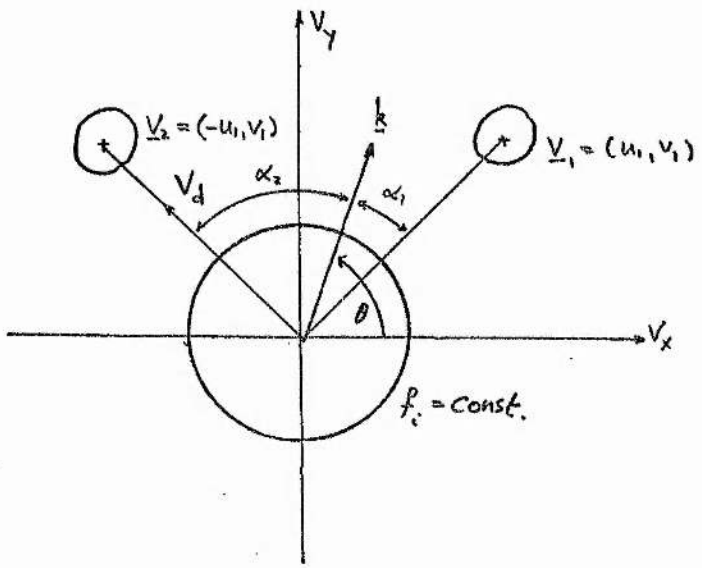

FIG 11.10

There is a net ion current to V_y, unlike (11.9), while it must be indicated that in (11.16) the ions are unmagnetized; this is suitable for the main beam; but not for the heavily gyrating reflected ions, and is the curious situation of a search for linear instabilities inside what is essentially a trapping process. Thus only times short with the reflection time should be considered.

Equation (11.9) has been extended to allow different beams. Then with $V_d=1$, $\varepsilon=0.1$, and $\alpha^2 \sim 140$, the growth rates are shown in Fig. 11.11.

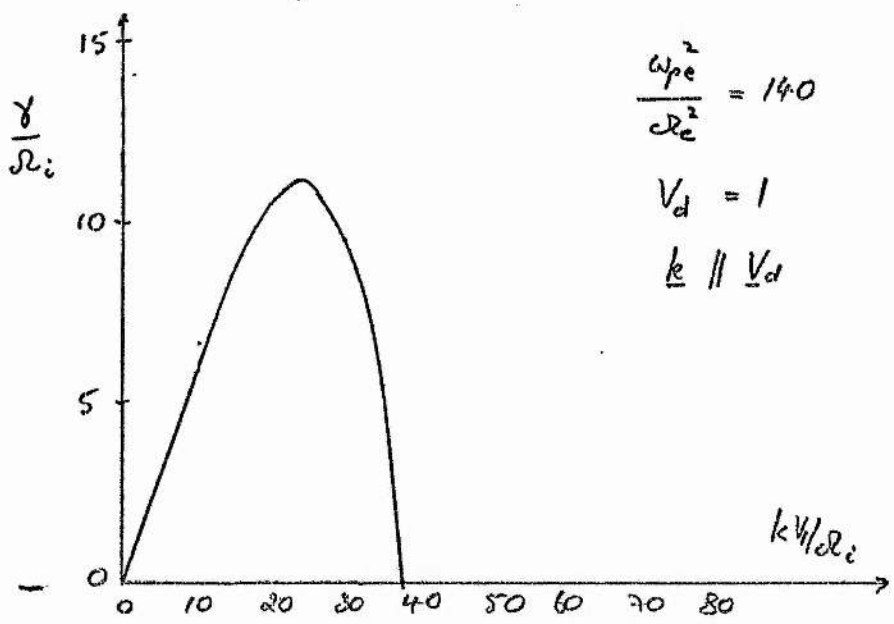

FIG 11.11

Normalized in the usual fashion, γ/Ω_i is plotted against $k V_1/\Omega_i$.

At the same parameters, Fig. 11.12 shows the growth rates along (either) drift $\underline{V}_d$ at $\theta = \pi/4$ (or $\theta = 3\pi/4$).

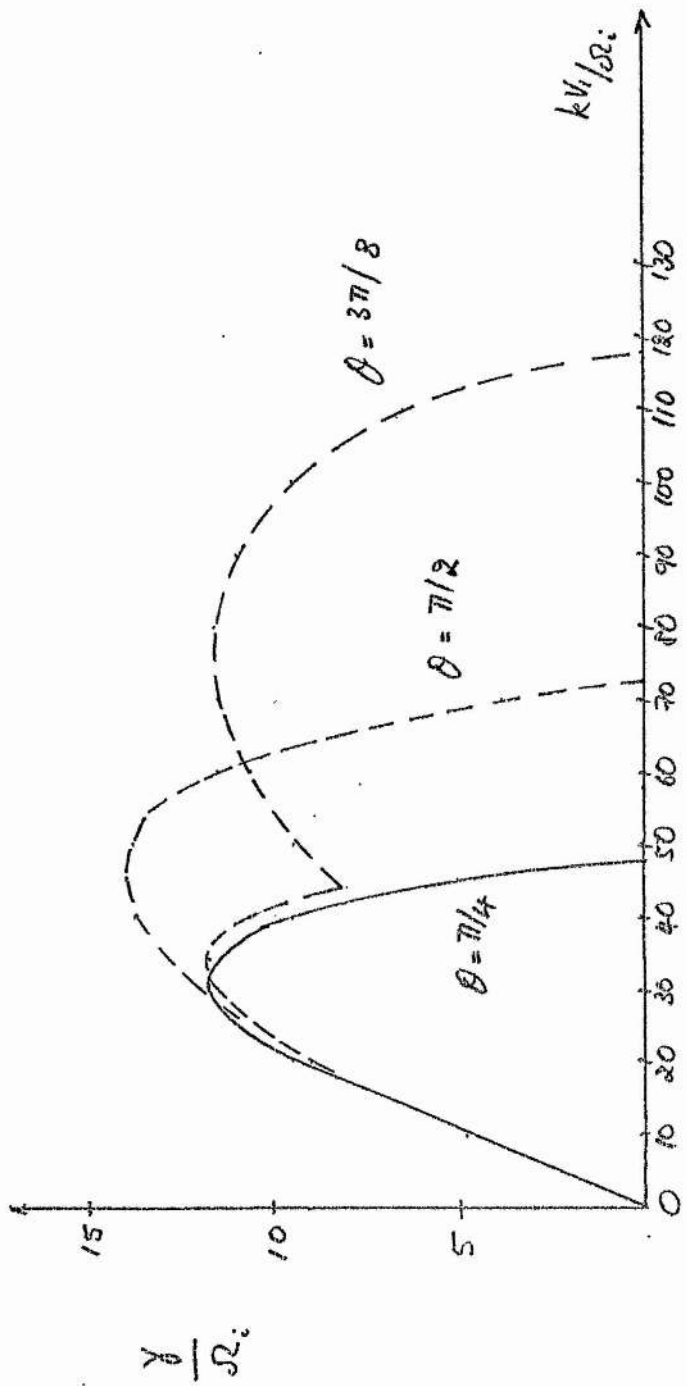
$\frac{\gamma}{\Omega_i}$
15
10
5
0
10
20
30
40
50
60
70
80
90
100
110
120
130
kV_1/Ω_i
$\theta = 3\pi/8$
$\theta = \pi/2$
$\theta = \pi/4$

FIG 11.12

Then γ_m is not significantly changed, and this configuration will not alter the slowing of the reflected beam. At $\theta = \pi/2$, there is an augmented growth rate (this is typical of the instability, with peak γ_m occurring for $\underline{k}$ off the drift $\underline{V}_d$; this has no effect on slowing the beam . At $\theta = 3\pi/8$, the general lack of interaction between the two beams is clear. It is noted that in (11.9), k appears only in the product kV_d. For off-$\underline{V}_d$ propagation, k will be larger for smaller V_d to give the same growth rate for a given (kV_d). The same is found for Fig. 11.12. If now the values $(k\ V_d \cos \alpha_{1,2})$ along either beam are fixed for peak growth γ_m, then $\alpha_1 < \alpha_2 \Rightarrow k_{m1} < k_{m2}$. The growth rate at some point is merely the growth of the most unstable wave.

There is thus some support for using the growth rate of (11.9). Their saturation and transit times in the foot are at worst and best

$$.3 \lesssim \tau_s \Omega_i \lesssim 46 \quad , \quad t_f \sim 0.5/\Omega_i$$

for

$$21\ \Omega_i \gtrsim \gamma_m \gtrsim 1.5\ \Omega_i \quad , \quad \gamma_m \tau_s \sim 7 \qquad (11.17)$$

The high-$\mathcal{M}^2$ instability can then saturate in the foot. The time to saturation is $\sim t_f$ so that some acceleration of the reflected ions can occur (their numbers correspond to the laminar model, if ϕ is unchanged). Fig. 11.5 shows that at about $\frac{1}{2}\tau_s$, the beams have only slowed by $\sim$10%, while in the constant electric field $(E_y = \frac{1}{C} V_1 B_1)$ they have gained about $\frac{1}{4}$ of the final laminar heating level. The slowing will cause a decrease in the

displacement Δy_i, diminished t_f, and lower heating compatible with the demands of the $\beta>\beta^*$ region. Such behaviour may account for the loss of foot structure in the high-β experiments reported here. At Garching $\alpha^2 \sim 10^4$ and high γ_m may be expected. For unequal beams ($\sim$10%) it has been estimated that γ_m reduces to $\sim$60%[18]. This gives $\gamma_m \sim 12\frac{1}{2} \cdot \Omega_i$, with $\tau_s \sim t_f$ and again the instability can saturate. But further consideration is necessary.

The instability above has been used for it gives the largest growth rates of unstable two-stream waves for perpendicular propagation. But it is a strictly electrostatic study, with a cool electron background $T_e << M_i V_d^2$. The ions are cold while even in the simulations, $v_i << V_d$, or $T_e \gtrsim T_i$. This is an unrealistic situation for $\beta>\beta^*$ shocks (with $T_e=T_i$ as usual). The exclusion of electromagnetic modes was shown valid only for $M_A^2(\tau)<4\ (1+\beta(x))$, $\beta \lesssim 1$, $\alpha^2 \gtrsim 1$[19]. This translates to $M \leq 2.1$, rather close to M^* and the loss of reflection dynamics.

The extension to electromagnetic modes and hot species has been studied by Auer et al.[18] and the effect is always to reduce the growth rates. It is further a consequence of this new approximation that peak growth rates do not occur along the drift direction. Thus slowing of the fast beam is in all respects less efficient.

Their particular aim was a study at the hot, $\beta>\beta^*$, Bow Shock parameters $\beta_e \sim 1$, $\beta_i \sim 0.5$, $M \sim 5$ and where Montgomery et al.[21] had measured an $\sim$10% tail. Numerical solution of the full dispersion relation, at the Bow Shock, was performed with three values of T_i/T_e, for equal beams. At $T_i/T_e=.0028$, the growth rate was comparable with the cold ion electrostatic

result. A thermalization time of $5\text{-}10/\gamma_m$ was assumed, but gave an ion thermalization length small compared with observation. Thus growth rates were too high. At $T_e/T_i \sim 0.28$, γ_m was strongly reduced by two orders of magnitude, and proper thermalization length was found. At $T_e/T_i \sim 0.56$, γ_m was again reduced, approaching Ω_i and the limits of the unmagnetized ion theory. While (11.9) gives $\gamma_m \sim 0.35\ \omega_{pi}$, Auer et al. find $\gamma_m \sim .31\ \omega_{pi}$, $2.5*10^{-3}\ \omega_{pi}$, $1.1*10^{-3}\ \omega_{pi}$, respectively.

For unequal beams, these growth rates were reduced (at $T_i/T_e \sim .05$) to about 60%. They further correspond to peak growth rates occuring at $\sim 4^o$, $\sim 35^o$, $\sim 40^o$, off the drift direction. At $T_e/T_i = 0.28$, electrostatic modes along $\underline{V}_d$ are stabilized, while electromagnetic growths there are ignorable.

Now the strong indication is that even quite cool equal ion beams in a hot electron plasma will cause growth rates considerably reduced from the electrostatic level. Differing beam densities will further reduce growth, although the dependence on the temperature of each beam is not clear. The model suggests that the temperature of the minor beam can be considerable. It has been shown that the incoming Maxwellian will not be significantly affected by the foot, or turbulence in L_s. Then temperature can be estimated from the upstream cut in f_1, effected by a potential, $\phi \sim \phi^*$ (sufficient to slow a cold beam of ions). This is shown in Fig. 11.13.

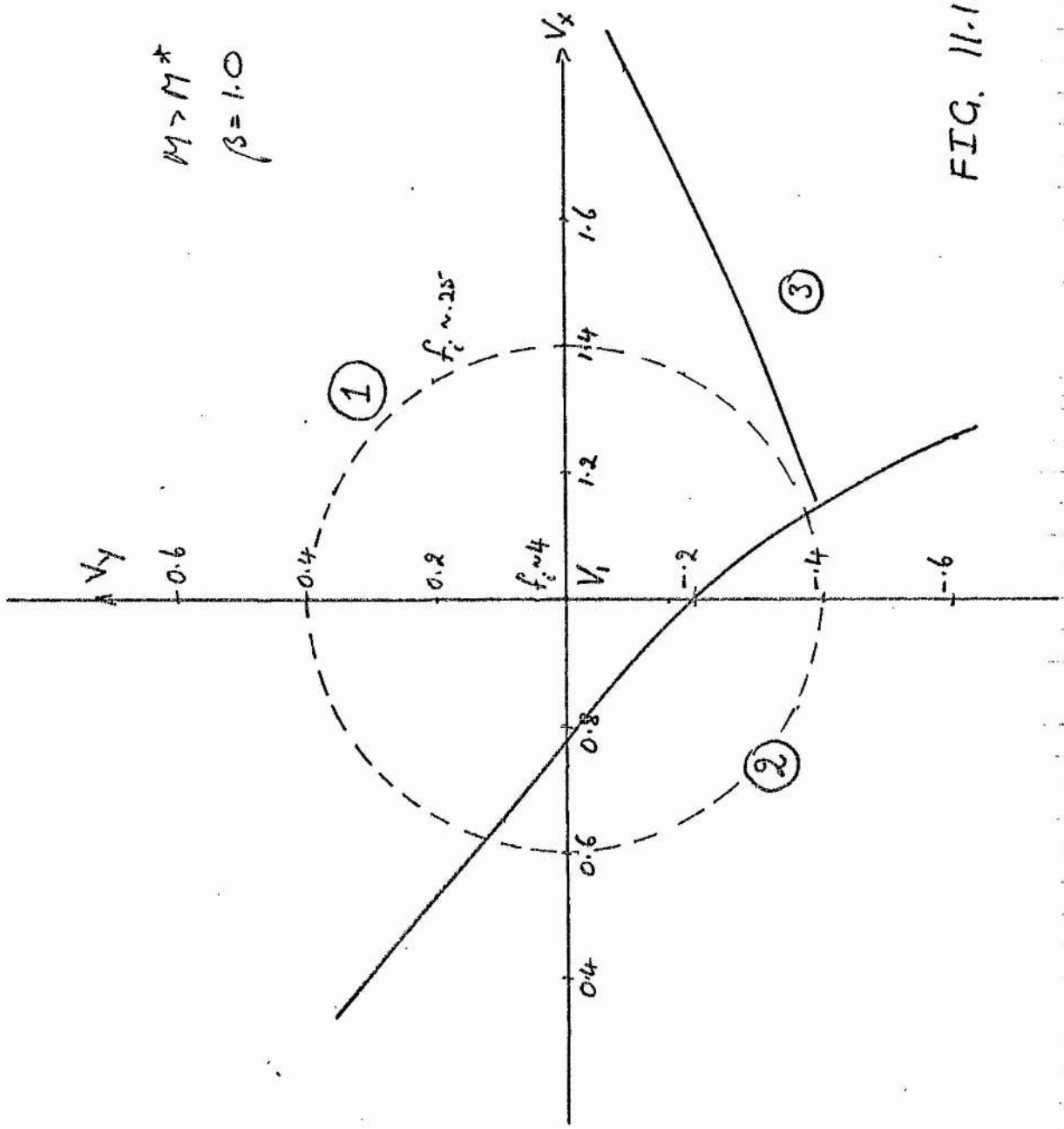

FIG. II.13

Here $\beta=1$, $T_{el}=T_{il}$. The regions are 1) ions to be transmitted, 2) to be reflected, 3) ions which spend some time downstream but return to the shock (their effect is small as they carry small f_i). At this reasonable potential (no measure of potential at high β is known) the thermal spread of a highly anisotropic minor beam can match that of the main beam, so that $T_e/T_i \gtrsim .5$ can be expected, and low maximum growth rates are likely, at large angles to V_d. The temperature of the main beam can of course increase to $T_e/T_i \sim 1$, while it has been shown that γ_m decreases with decreasing beam density. It is noted that at $\beta=0.3$, M=2.4, the model gives a minor beam density of $\sim 6\frac{1}{2}\%$, with excess heating, and with "thermal" energy, relative to its own drift, of about 10% of that of the main beam; so $T_i/T_e \sim .1$ at worst, on $\beta > \beta^*$.

It is then probable that for $\beta \gtrsim \beta^*$, $T_{el} \sim T_{il}$, and with no binary collisions, that the instability can be unimportant in the foot. It was noted by Auer that electron heating takes place on a very short scale, L_s, so that T_i/T_e is decreased there. Eselevich has measured a resistive preheating of electrons in the leading edge of L_s. But it is a contribution of this thesis that the instability must occur in the foot (at least at $\beta \gtrsim \beta^*$), where these considerations do not apply.

There is experimental evidence to support this. The foot appears to be a quite stable structure on large scales, while no increase of ion temperature has ever been observed there[7,43]; the foot length corresponds to the orbit of a laminar ion[28]. These points apply to low and high β shocks.

Indeed, the foot might be susceptible to cold ion two-stream instability. But this is just the criterion that no reflections occur at all!

The curious situation of a hot $\beta > \beta^*$ shock, where no collisions occur, and no turbulence, is found in the Bow Shock (the solar wind can have a mean time path approaching that of the Earth-Sun distance, while L_s ~few kilometers[40]!)

Auer's ion simulations were run on the Bow Shock data of Montgomery et. al.[21] Fig.11.14 shows the observable portion of a set of remarkable ion distributions, taken just before the resistive rise.

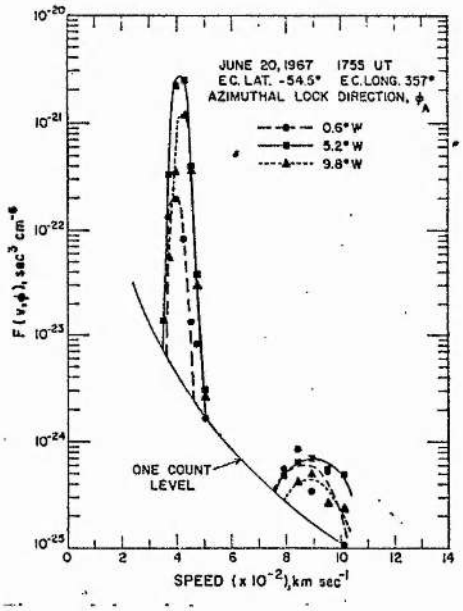

FIG 11.14

Clearly no thermalization is taking place in the foot, where low field fluctuations and small electron heating are sometimes observed. This may be compared with a downstream distribution (Fig. 11.15) where the coalescing of the two beams is apparent, and so some ion trapping is taking place.

The time of observation is 104 seconds past the resistive potential jump L_s, and should be compared with the $\lesssim 3$ second thermalization time of the electrons (which defines the jump).

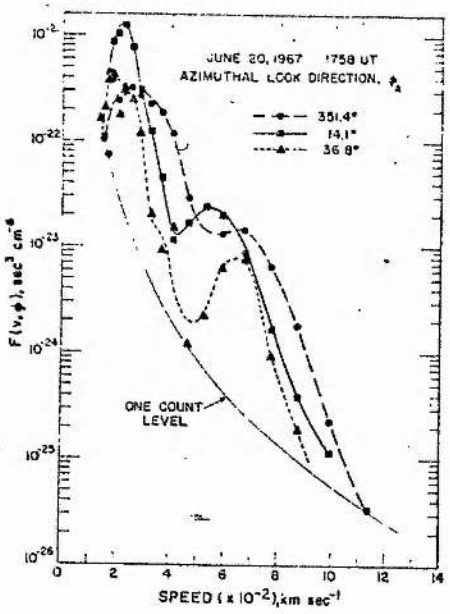

FIG 11.15

There is then no attenuation of the fast beam in or before L_s. There are no collisions. Thus laminar ions are expected again.

This shock shows the following peculiarities:

i) The jump B_2/B_1 has been measured by Fredricks et al.[44] to be ~ 4 on a thickness $L_s \sim C/\omega_{pe}$. Figs. 11.14, 15 show $V_1/V_2 \sim 1.3$ across L_s, while $N_2/N_1 \sim 3$. There is then apparent violation of flux and charge neutrality requirements. The condition $B_2/B_1 > N_2/N_1$ is typical of shock propagating

oblique to the magnetic field, but flux should be conserved. This seems to be an experimental shock (on the scale of L_s) behaving as the $\beta > \beta^*$ model! The electrons are slowed with the main bulk of ions. The deflection of $\underline{V}$ across this shock could not be determined.

ii) The thickness $L_s \sim C/\omega_{pe}$ is unusually thin compared with laboratory shocks where $L_s \sim$ few C/ω_{pe}. Auer has proposed the electrostatic Buneman electron-ion drift instability, which is effective on $\lesssim C/\omega_{pe}$ scales and which is typified by $\beta_e \sim 1$ as observed. Subsequently Wu and Fredricks[42] have shown that the electrostatic limit is inappropriate with Buneman modes being much lower, or even damped, in a complete treatment. They propose the electron-cyclotron drift instability unstable on $\leq C/\omega_{pe}$ lengths, and operating at $T_e \sim T_i$. It does not have time to saturate but is chosen because it can explain observed discrete frequency bands at harmonics of Ω_e, in wave fluctuations in the foot and in L_s. The electron behaviour is fairly well understood. It is noted that the work of Wu and Fredricks, supporting the loss of $T_e >> T_i$ -type electron instabilities, is further argument in favour of slow ion two-stream growth rates.

iii) Fig. 11.15 shows a secondary peak of $\sim$10% the number of main beam ions, upstream. A precursor is then expected and Neugebaur[43] has sometimes detected slowing of the ions there, but no ion heating.

Now if this shock is oblique, it cannot be properly modelled as above. Certainly the peculiar jumps observed obscure its proper nature. But oblique ($B_x \neq 0$) or not ($B_x = 0$), the same ambient constant electric field $E_y = \frac{1}{C} V_1 B_1 = - \frac{1}{C} V_{z1} B_{x1}$ is found, so that the acceleration in the

foot takes place in essentially the same direction. If $\underline{V}_1=(V_x,0,-V_z)$ is non-dimensionalized with respect to $|\underline{V}|$, then a roughly similar problem to that of the perpendicular shock occurs. This can be judged by the relative velocity of main beam and fast tail, and from Fig. 11.14 this is seen to be $\sim V_1$ as predicted by the model. Oblique shocks show large amplitude whistler precursors, but it has been shown by Biskamp and Welter[46] that for $M_A \gtrsim 6$, the fast beam is unaffected. Since $M_A \sim 8$[21], it seems reasonable to test the model against the Bow Shock.

Now $L_s \sim C/\omega_{pe} \sim \frac{1}{42} C/\omega_{pi} \sim \frac{1}{42M_A} \cdot V_1/\Omega_i$ is very thin in units of V_1/Ω_i and is approximated by an $L_s=0$ model, and is used in the following way.

If ϕ is chosen so that $V_1/V_2 \sim 1.3$ across L_s as observed, then $\phi=\phi_R \sim 0.2$, a jump too small to reflect any ions (at observed β_i, β_e). The main beam passes through ϕ and shows $T_{i2}/T_{i1} \sim 1.4$ with $T_{i2}/T_{iad} \sim 1$.

If on the other hand ϕ is chosen so that a 10% tail density results, then $\phi \gtrsim 0.46$. (Since $\beta > \beta^*$ no slowing of the ions is expected, and $v_2=.35>V_2^{RH}=.3$). But now the ions are found to have $T_{i2}/T_{i1} \gtrsim 26$ and at the model density ($n_2=2.8$), $T_{i2}/T_{iad} \gtrsim 9.3$. The observed Bow Shock data is

$$T_{i2}/T_{i1} \sim 27 \ , \ \frac{n_2}{n_1} \sim 3 \ , \ T_{i2}/T_{iad} \sim 9 \ ,$$

with $\gamma_i=2$! A further check is supplied by translating model heating into three degrees of freedom; then $T_{e2}/T_{e1} \sim 4.2$, while $T_{e2}/T_{e1} \sim 4.4$ experimentally, and so the perpendicular R-H relations applied to observed initial conditions give good agreement with the Bow Shock. (At least as regards temperature).

A simulation on this shock by Auer[18] showed a fluctuating resistive potential jump of mean magnitude $\sim\frac{1}{4}\ MV_1^2 \sim .25$ (with some precursor structure), a level insufficient to reflect ions electrostatically. They noted that only fine scale velocity space diffusion of reflected ions occured, due to two-stream instability.

But they propose that these gyrating ions cause a net current in the y-direction, on the scale of the gyro-radius r_i. This is consistent with violation of $V_1B_1=V_2B_2$ downstream, (also in the model) and with the $L_s=0$ approximation which gives a positive current downstream. Then from the x-component of electron momentum balance, and eliminating electron drifts by Ampère's Law, they find

$$e\phi\ (x) = \int \frac{1}{n}\ \frac{d}{dx}\ (P_e + \frac{B^2}{8\pi}\ )\ dx + \frac{e}{c}\int u_y\ B\ dx \qquad (11.18)$$

where u_y is the total ion drift in the +y-direction. The first term is the resistive potential jump, on scales of C/ω_{pe}, and refers to electron heating only. The second is scaled on r_i, and is due to laminar ion gyration. In the Bow Shock they show the first gives a jump of 100-200 eV on a length of $\sim$2 Km, while the second gives the same jump on scales from several hundred kilometers upstream to $\sim$100 Km downstream.

Now the laminar model, together with the simulation[18], suggests the following shock profile; from Fig. 6.9, and equation (11.18), it is shown in Fig. 11.16.

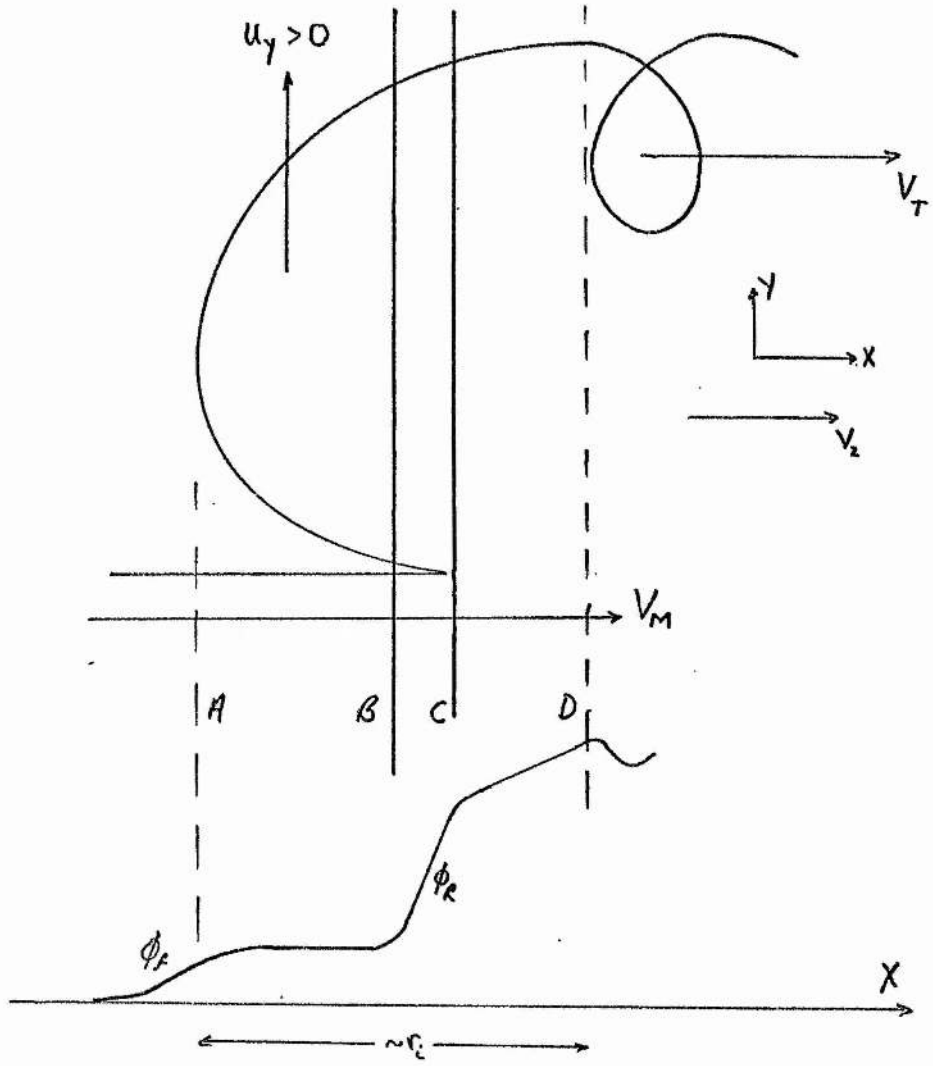

FIG 11.16

The total jump A to C must give observed 10% reflection, and is $\phi \sim 0.46$. The jump B to C must give observed slowing, $V_2/V_1 \sim .77$, so $\phi_R \sim 0.2$ (simulation gives $\sim .25$). But a strong foot structure must be proposed, $\phi_f \sim .26$; this is not found significantly in[18], but is in the simulations seen in[7]. The ratio $\phi_f/\phi \sim .56$ ($\beta \sim 1.5$) can be compared with Culham ($\beta \sim 0.1$) $\sim .25$, and Phillips and Robson[14]

$\sim$.55 ($\beta \sim 0.17$). This picture can explain ion heating. It predicts a slowing overall of $v_2 = .35 > V_2^{RH} = .3$, but it is noted that on the scale r_i, now, the main beam may displace significantly to -y under a Lorentz force, emerging downstream with a reduced x-velocity component and proper conservation.

The behaviour of the magnetic field due to this ion current is more complicated. The increase in $\underline{B}$, observed in the foot, while $dB/dx = -J_y^i < 0$, shows that electron and ion interactions must be considered. But $\underline{B}$ has the same form as ϕ_f when simultaneously observed in the foot.

It is noted too, that the fast ions will continue to gyrate at the ion cyclotron frequency downstream, and that currents can persist, averaging about a mean in long times. Thus an open orbit (of localised fast ions) sketched in Fig. 11.17 would give the field response shown.

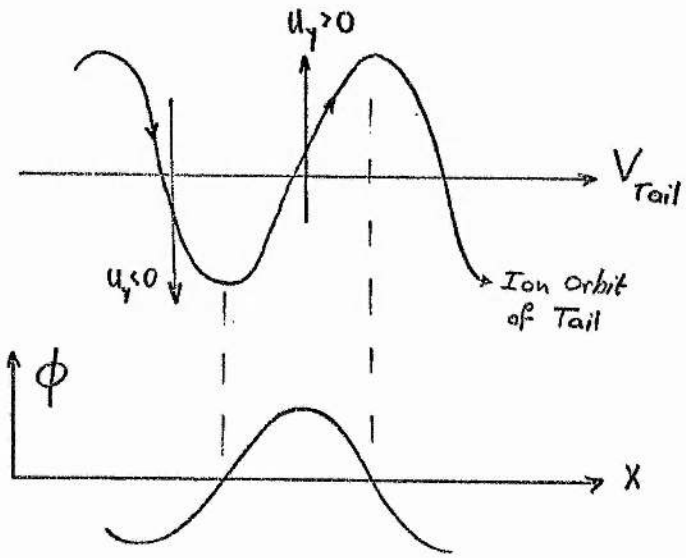

FIG 11.17

Electron density fluctuations at Ω_i could be expected, with electrons congregating in potential troughs.

The model of this thesis has been used above, by a method which copies known parameters. It has been principally concerned with laminar ion heating. Thus the Bow Shock is copied by the requirements of an $\sim$10% tail density, and the slowing of ions by the resistive potential. The proper heating is then found, with the relative velocity of beam and tail comparable with experiment. To this extent the model is applicable to the Bow Shock. There is strong likelihood that laminar ion heating explains the observed heating, but it is not certain that the potential profile of Fig. 11.16 is relevant. Thus this static potential rise can be replaced by a fast-fluctuating potential, with ions reflecting (and not trapping) off the first potential maximum. But since it is fairly clear that a $\beta > \beta^*$ experiment can be constructed without collisions or ion turbulence, increased emphasis is again placed on the laminar model; since $\beta > \beta^*$ is defined by reflecting ions (as experimentally observed in the Bow Shock), the decoupling of ion scales ($\sim r_i$) and electron scales ($\sim C/\omega_{pe}$) due to different spatial distributions of species current, is reasonable. Equation (11.18) shows the total potential jump is additive so that the ions can be slowed by a large potential jump which yet allows a decreasing resistive rise with falling electron heating. Since T_2^{RH} is fixed for some (M,β), and $M > M^*$ implies ion heating, electron heating must reduce.

It is interesting to once again consider the implications for shock thickness. Section §7 has already shown how positive (negative) ion currents can occur as L_s=0 (L_s sufficiently large).

In Fig. 11.18 a plot is given for the first time of ion flux (proportional to ion current), with L_s. At M=6, β=0.3< β*, the ion heating is a reasonable proportion of the R-H levels ($T_e/T_i \sim 3$), significant reflected ion flux occurs (and computer time is not excessive). Then comparison with experiment seems valid.

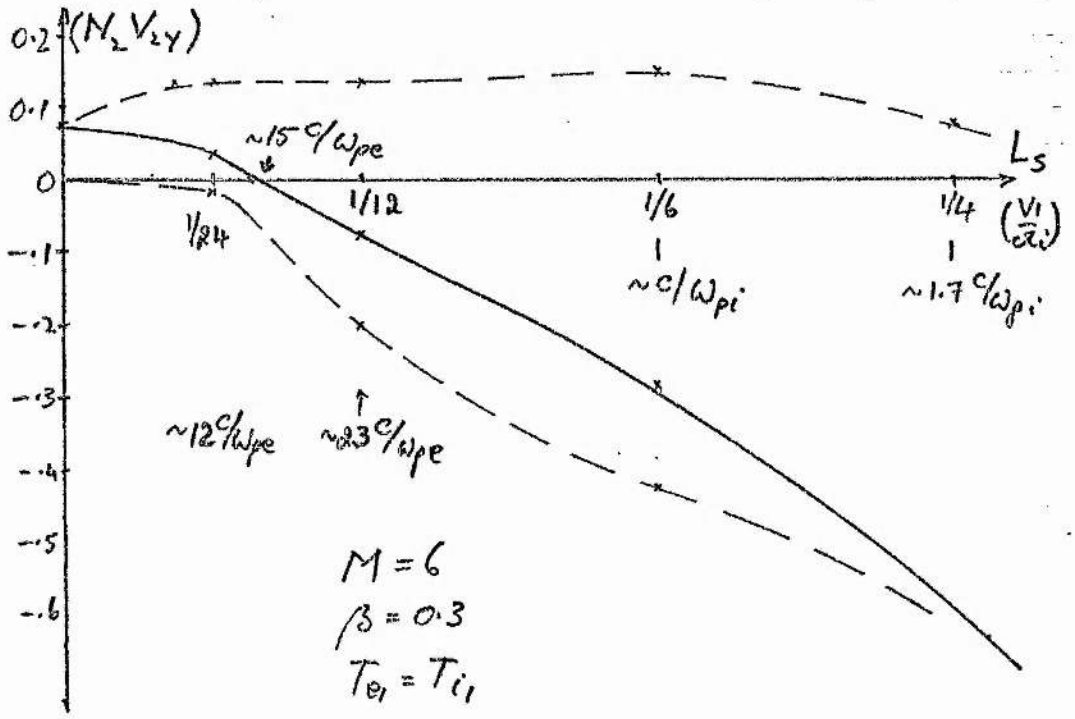

FIG 11.18

A self-consistent shock

width of $L_s \sim 15\ c/\omega_{pe}$ results. This may be compared with L_s=10 c/ω_{pe} at Culham ($\beta \sim 0.1$, $M \sim 3.5$) or with L_s=20 c/ω_{pe} due to Hintz (β=0.6, $M \sim 7.1$).

At β=0.1, the model has found small dependence of this length with M. This comparison is reasonable if inclusion of foot dynamics (on the main beam) has small effect; further this length will operate only if it is less than electron heating lengths. When no ion dynamics occurs (M<M*), $L_s \sim 5\text{-}10\ C/\omega_{pe}$ even at high β[10], in experiment. At $M \gtrsim M^*$, with ion heating, electron dynamics may play a reduced role (dependent of the relative levels of total and ion heating) as in Fig. 8.20; at M>>M* laminar ion heating reduces again. Thus it seems likely that electron heating requires a length at $M \gtrsim M^*$, of $L_s \sim 5\text{-}10\ C/\omega_{pe}$, still. Theoretical estimates have been summarized by Biskamp[9], but remain crude at $\gtrsim$ few C/ω_{pe}; also since $L_s \propto \nu^*$ (anomalous collision frequency) the resistive L_s can decrease with decreasing electron heating. Broadening of resistive L_s at M>M* has been observed in most experiments[1,7,10], and it is possible that a laminar decoupling of electron and ion lengths is taking place. The length L_s is taken from magnetic field profiles, and the response of B(x) to the ion current, especially in and behind L_s, remains undetermined. High resolution profiles would be of great interest, for both electric potential and magnetic field. The length decoupling is of interest as regards electron heating in the Garching shocks[5]; this is perhaps the only shock where the nature of electron heating is not understood. Thus no known universal instability can be found operative, where $T_i \geq T_e$ always ($T_{el} \sim T_{il}$)[9], and the electron drifts as calculated from Ampere's Law, $dB/dx = \frac{4\pi}{c} N e V_y^{(e)}$, are too low; $V_y^{(e)} \sim 3C_s$. A thick $\sim 30\ C/\omega_{pe}$ shock is found. But anomalous resistivity and the form of the turbulence spectrum is similar to those of the low-β, $T_e >> T_i$, shocks[9]. If

then $V_d = 3V_y^{(e)} \sim 9C_s \sim 0.21\ V_e$ for $L \sim 10\ C/\omega_{pe} \sim \frac{1}{3} L_s$, and $T_e > T_i$ somewhere in the shock, then electron cyclotron instability can occur[7]. It is further not without interest that the (non-self-consistent) model runs at Garching parameters give no net ion currents downstream, while the same applies for the $\beta < \beta^*$ Culham example.

Thus a consideration of the $\beta > \beta^*$ region has been performed. Binary collisions are important in laboratory shocks, while some "cool" shocks might show turbulent slowing of the ion beam. Generally, this latter is not expected, and the Bow Shock shows a laminar ion heating on scales much larger than the electrons. It has been assumed that only small perturbations of the initial plasma occur. The Bow Shock often shows quite violent behaviour while there are examples of laboratory shocks (Culham $\beta \sim 0.2 < \beta^*$, $M_A \sim 6.3$[1], Hintz $\beta \sim 1 > \beta^*$, $M_A \sim 8.4$[10]), also strongly turbulent. The source of this turbulence is difficult to determine, and may be a necessary non-laminar process at high $\beta > \beta^*$ given sufficient perturbation of the initial plasma. At Culham the thickness is so large that cylindrical effects are important. The turbulence is carried downstream into the plasma "piston" and the jump conditions become indeterminate. If it is driven by the two-beam instability then it is expected to occur at moderate $M \gtrsim M^*$. It is further possible that no adequate electron heating mechanism due to small perturbations can occur at $M >> M^*$, to substitute the vanishing laminar ion heating (Fig. 8.20). This occurs for all β. It has been suggested above that the $L_s \sim$ few C/ω_{pe} scaling leads to strong gradients in profiles as $M \to \infty$ ($L_s \to 0$ in units of V_1/Ω_i). The implied large electron drifts might be

sufficient to heat the electrons. Experimental study of the high M>>M* shocks would be of interest, especially for a determination of the electron heating length.

The collisionless shock wave is an enormously complex event and far beyond any detailed over-all theoretical study. Here a simple model has been investigated yielding a rare view of the shock on all scales. Of importance has been the ability of the various forms of "laminar distortion heating" to predict the correct order of magnitude for ion heating. But perhaps equally important is the resilience of the notion of laminar ion dynamics; thus in the presence of strong collisions, Kornherr[8] has found the ions possess two degrees of freedom perpendicular to the magnetic field, with non-adiabatic heating; while two-stream ion turbulence is not noticeably present in the region L_s, in the hot $\beta > \beta^*$ Bow Shock. The results of the run at the Culham $M \sim 3.5$, $\beta \sim 0.1$ shock are encouraging; thus some ion heating is measured comparable with the experiment, which in an energy balance

$$\tfrac{1}{2}MV_1^2 = \tfrac{1}{2}MV_2^2 + e\phi + \text{ion heating} ,$$

predicts ϕ such that $R_\phi = {}^{2e\phi}/_{M(V_1^2 - V_2^2)} \simeq 0.85$. This is not comparable with experiment, which finds $R_\phi \sim 1$. There is thus evidence that ion reflection forces an increase in total ϕ. The model's solutions for ϕ are an important contribution. Finally, the graphic displays of the downstream ion distribution represent new information on shock structure. Suggestions for further

analysis of their instabilities are clear - for example the $T_\perp \neq T_\parallel$ instability of Harris[45] (which is stable for perpendicular propagation and so will not have any effect on beam slowing) is predicted for both $M \gtrless M^*$ shocks, and extension to $T_x \neq T_y \neq T_z$ is suggested; while the slow two-ion-stream growth rates $\gamma_m \sim \Omega_i$, suggest a study of instabilities on times $t > \Omega_i^{-1}$ (where the equilibrium ion distribution is now time dependent). These displays show that significant ion currents in the plane of the shock, perpendicular to $\underline{B}$ can occur downstream. Maxwell's equations in the time independent, plane, shock give $dB/dx = \frac{-4\pi}{C}(J_y^i + J_y^e)$ Profiles can now vary on the spatial scales $L \sim r_i, \sim C/\omega_{pe}$ of J_y^i, J_y^e simultaneously, these also being the scales of the ion and electron heating mechanisms.

REFERENCES

[1] PAUL, J.W.M., HOLMES, L.S., PARKINSON, M.J., SHEFFIELD, J., Nature 208 (1965) 133.

[2] PAUL, J.W.M., GOLDENBAUM, G.C., ILLYOSHI, A., HOLMES,L.S., HARDCASTLE, R.A., Nature 216 (1967) 363.

[3] DAUGHNEY, C.C., HOLMES, L.S., PAUL, J.W.M., Phys. Rev. Lett. 25 (1970) 497.

[4] RYE, B.J., TAYLOR, J.C., (Editors), "Physics of Hot Plasmas", (Oliver and Boyd, Edinburgh), (1970), p.302.

[5] CHODURA, R., KEILHACKER, M., KORNHERR, M., NIEDERMEYER, H., Plasma Physics and Controlled Nuclear Fusion Research (Proc. 3rd Int. Conf. Novosibirsk, 1968) 1, IAEA, Vienna (1969) 143.

[6] KEILHACKER, M., KORNHERR, M., STEUER, K.-H., Z Physik 223 (1969) 385.

[7] KEILHACKER, M., KORNHERR, M., NIEDERMEYER, H., STEUER, K.-H., CHODURA, R., Plasma Physics and Controlled Nuclear Fusion Research (Proc. 4th Int. Conf. Madison, 1971) 3, IAEA, VIENNA (1971) 265.

[8] KORNHERR, M., Z Physik 233 (1970) 37.

[9] BISKAMP, D., Nuclear Fusion 13 (1973) 719.

[10] HINTZ, E., Plasma Physics and Controlled Nuclear Fusion Research (Proc. 3rd Int. Conf. Novosibirsk, 1968) 1, IAEA, Vienna (1969) 69.

[11] ESELEVICH, V.G., ESKOV, A.G., KURTMULLAEV, R.Kh., MALYUTIN, A.I., Sov. Phys. - JETP 33 (1971) 1120.

[12] ESELEVICH, V.G., ESKOV, A.G., KURTMULLAEV, R.Kh., MALYUTIN, A.I., Sov. Phys.- JETP 33 (1971) 898.

[13] TAYLOR, R.J., BAKER, D.R., IKEZI, H., Phys. Rev. Lett. 24 (1970) 206.

[14] PHILLIPS, P.E., ROBSON, A.E., Phys. Rev. Lett. 29 (1972) 154.

[15] HAIN, K., HAIN, G., ROBERTS, K.V., ROBERTS, S.J., KOPPENDORFER, W., Z. Nat., 15 (1960).

[16] KADOMTSEV. P. R., "Plasma Turbulence" (Academic Press) (1965)

[17] CAIRNS, R.A., J. Plasma Physics 6 (1971) 443.

[18] AUER, P.L., KILB, R.W., CREVIER, W.F., J. Geophys. Res. 76 (1971) 2927.

[19] PAPADOPOULOS, K., DAVIDSON, R.C., DAWSON, J.M., HABER, I., HAMMER, D.A., KRALL, N.A., SHANNY, R., Phys. Fluids 14 (1971) 849.

[20] BISKAMP, D., WELTER, H., Nuclear Fusion 12 (1970) 663.

[21] MONTGOMERY, M.D., ASBRIDGE, J.R., BAME, S.J., J. Geophys. Res. 75 (1970) 1217.

[22] SAGDEEV, R.Z., Rev. Plasma Physics 4 (1966) 23.

[23] COURANT, R., HILBERT, D., "Methods of Mathematical Physics" (Interscience Publishers, Inc., New York) (1953) Vol. I, p.164.

[24] SCHUMACHER, N., Plasma Physics and Controlled Nuclear Fusion Research (Proc. 3rd Int. Conf. Novosibirsk, 1968) 1, IAEA, Vienna (1969) 93.

[25] HARRIS, E.G., J. Nucl. Energy, Part c, 2 (1961) 138.

[26] PFIRSCH, D., SCHINDLER, K., J. Plasma Physics 5 (1971) 123.

[27] BORGES, J.L., "A Universal History of Infamy" (Penguin Books) (1975).

[28] ROBSON, A.E., SHEFFIELD, J., Plasma Physics and Controlled Nuclear Fusion Research (Proc. 3rd Int. Conf. Novosibirsk, 1968) 1, IAEA, Vienna (1969) 119.

[29] WOODS, L.C., Plasma Physics 11 (1969) 967.

[30] MORSE, D.L., (Private communication to R.A. Cairns)

[31] CAIRNS, R.A., Physics Letters 38A (1972) 445.

[32] SANDERSON, J.J., (to be published).

[33] MORSE, D.L., DESTLER, W.W., Plasma Physics 14 (1972) 153.

[34] BUNEMAN, O., Phys. Rev. 503 (1959) 115.

[35] CHODURA, R., KEILHACKER, M., KORNHERR, M., NIEDERMEYER, H., As in [5]

[36] TIDMAN, D.A., KRALL, N.A., "Shock Waves in Collisionless Plasmas" (Wiley-Interscience) (1971).

[37] RYE, B.J., TAYLOR, J.C., (Editors) "Physics of Hot Plasmas", (Oliver and Boyd, Edinburgh) (1970) p.276.

[38] STRINGER, T.E., Plasma Phys., 6 (1964) 267.

[39] BERTOTTI, B., BISKAMP, D., ESRIN, Frascati, Italy, ESRO. Spec. Pap. SP-51, (1969) 41.

[40] RYE, B.J., TAYLOR, J.C., (Editors) "Physics of Hot Plasmas", (Oliver and Boyd, Edinburgh) (1970) 278.

[41] ASBRIDGE, J.R., BAME, S.J., STRONG, I.B., J. Geophys. Res. 73 (1968) 5777.

[42] Wu, C.S., FREDRICKS, R.W., J. Geophys Res. 77 (1972) 5585.

[43] NEUGEBAUER, M., J. Geophys. Res. 75 (1970) 717.

[44] FREDRICKS, R.W., CROOK, G.M., KENNEL, C.F., GREEN, I.M., J. Geophys. Res. 75 (1970) 3751.

[45] HARRIS, E.G., See 25 .

[46] BISKAMP, D., WELTER, H., J. Geophys Res. 77 (1972) 6052.

[47] ZEEMAN, E.C., Breaking of Waves, D. Chillingworth (ed.) Symposium on Differential Equations and Dynamical Systems, Springer Notes 206 (1971) 2.